NASA/TM—1998-208509

ARL-TR-1804

Engine Gaseous, Aerosol Precursor and Particulate at Simulated Flight Altitude Conditions

C. C. Wey
Lewis Research Center, Cleveland, Ohio

C. Wey, D.J. Dicki, K.H. Loos, and D.E.Noss
Dynacs, Brook Park, Ohio

D.E. Hagen, P.D. Whitefield, M.B. Trueblood, M.E. Wilson, and D. Olson
University of Missouri at Rolla, Rolla, Missouri

J.O. Ballenthin, T.M. Miller, and A.A. Viggiano
Hanscom Air Force Base, Bedford, Massachusetts

J. Wormhoudt, T. Berkoff, and R. C. Miake-Lye
Aerodyne Research, Inc., Billerica, Massachusetts

National Aeronautics and
Space Administration

Lewis Research Center

October 1998

Available from:

NASA Center for Aerospace Information
7121 Standard Drive
Hanover, MD 21076
Price Code: A09

National Technical Information Service
5287 Port Royal Road
Springfield, VA 22100
Price Code: A09

Contents

Preface

The work reported herein was sponsored by National Aeronautics and Space Administration (NASA) Atmospheric Effects of Aviation Project (AEAP), and managed through the sub-element Emission Characterization at NASA Lewis Research Center (LeRC) by Mr. Richard Niedzwiecki, NASA, and Dr. Chowen Chou Wey, Army Research Laboratory (ARL). The engine test was conducted at NASA LeRC, Cleveland, OH. It was accomplished by the team efforts of many engineers and scientists from government and private organizations including NASA LeRC, Dynacs Engineering Company, Inc. (Dynacs), Pratt & Whitney (P&W), Aerodyne Research Inc. (ARI), Air Force Research Laboratory (AFRL), and University of Missouri-Rolla (UMR).

The main objective of this report is to document the results of a set of parametric studies of the effect of the fuel sulfur content on particulate emissions. The primary authors were:

Dr. John O. Ballenthin	AFRL
Mr. Dennis Dicki	Dynacs/NASA LeRC
Dr. Donald E. Hagen	UMR
Dr. Richard C. Miake-Lye	ARI
Dr. Thomas M. Miller	AFRL
Dr. A. A. Viggiano	AFRL
Dr. Changlie Wey	Dynacs/NASA LeRC
Dr. Chowen Chou Wey	ARL/NASA LeRC
Dr. Philip D. Whitefield	UMR
Dr. Joda C. Wormhoudt	ARI

This task is an accumulation of contributions from individuals acknowledged below and other persons too numerous to list. Although participants worked as a team with contributions beyond individual responsibilities, primary functions associated with each were:

Project Management	Mr. Richard W. Niedzwiecki	NASA LeRC
	Dr. Chowen Chou Wey	ARL/NASA LeRC
Principal Investigator	Dr. Chowen Chou Wey	ARL/NASA LeRC

MASS Team	Dr. Donald E. Hagen	UMR
	Mr. Max B. Trueblood	UMR
	Dr. Philip D. Whitefield	UMR
	Ms. Melissa Wilson	UMR
TDL Team	Dr. Richard C. Miake-Lye	ARI
	Dr. Joda C. Wormhoudt	ARI
	Mr. Tim Berkoff	ARI
CIMS Team	Dr. John O. Ballenthin	AFRL
	Dr. Thomas M. Miller	AFRL
	Dr. A. A. Viggiano	AFRL
Test Facility Team	Mr. Richard DelRoso	NASA LeRC
	Mr. Dennis Dicki	Dynacs/NASA LeRC
	Mr. Richard Sorge	NASA LeRC
	Mr. Quito Thomas	ARL/NASA LeRC
	Mr. Roger Werner	NASA LeRC
Gas Sampling Team	Mr. Kurt Loos	Dynacs/NASA LeRC
	Ms. Dawn Noss	Dynacs/NASA LeRC
	Dr. Changlie Wey	Dynacs/NASA LeRC

1. INTRODUCTION

The overall objective of the NASA Atmospheric Effects of Aviation Project (AEAP) is to develop scientific bases for assessing atmospheric impacts of the exhaust emissions by both current and future fleets of subsonic and supersonic aircraft. Among the six primary elements of the AEAP is Emissions Characterization. The objective of the Emission Characterization effort is to determine the exhaust emission constituents and concentrations at the engine exit plane.

In light of the recently obtained in-flight measurements of the composition of the plume of a Concorde aircraft, as described in a paper by Fahey et al. (1995) and in NASA's AESA report (Stolarski et al., 1995), the potentially important role of aerosol and aerosol precursor emissions is recognized. The particulate measurements obtained in these flight measurements indicate a high degree of sulfur dioxide (SO_2) oxidation to condensed sulfate. The data also suggest that SO_2 oxidation by hydroxyl radicals (OH) is not the dominant cause of the conversion.

Particulates directly emitted by jet aircraft are mostly soot with traces of heavy unburned hydrocarbons. Volatile aerosols are thought to be formed in the exhaust of the engines as a result of emissions related to the sulfur impurity in aviation fuel. Sulfur-containing aerosols are directly involved in the partitioning of reactive species controlling the abundance of ozone in the stratosphere where supersonic aircraft principally operate. This impact is maximized if the sulfate is formed within the exhaust plume. In the troposphere, subsonic emissions can cause the formation of contrails that, in turn, can also cause changes in background aerosol properties which may affect cloud cover and cloud optical properties. Changes in ozone and cloud properties are both elements of climate change and hence can influence the environment on long time scales.

Although the importance of aerosols and their precursors is now well recognized, the characterization of current subsonic engines for these emissions is far from complete. Furthermore, since the relationship of engine operating parameters to aerosol emissions is not known, extrapolation to untested and unbuilt engines necessarily remains highly uncertain. This engine test, as well as a parallel flight measurement, attempts to address both issues by expanding measurements of aerosols and aerosol precursors with fuels containing different levels of fuel sulfur content. Aviation fuels with a range of fuel sulfur were procured for both sampling venues.

The specific objective of this engine test is to obtain a database of sulfur oxides emissions as well as the non-volatile particulate emission properties as a function of fuel sulfur and engine operating conditions. The database of the non-volatile particulates emission properties is to be used as a comparative baseline with subsequent flight measurement. A database of volatile and non-volatile particulates and sulfur oxides is needed to validate engine and exhaust plume models.

2. TEST FACILITY

The engine used in this test was a Pratt & Whitney F100-200E turbofan engine. The normally variable convergent-divergent type exhaust nozzle was mechanically locked into position so that a throat area of 0.2787 m^2 (3.0 ft^2) would be maintained throughout the entire envelope of test

conditions. The fan bypass air is combined with the engine core flow upstream of the exhaust nozzle, with no intentional mixing of the two streams of air being performed before the gases exit the nozzle. The engine is representative of commercial type engines in the 89 - 133 KN (20,000 - 30,000 lbf) thrust class. It has an engine pressure ratio of 25 with a bypass ratio of 0.75. Test conditions ranged from idle to military power settings at altitudes from sea level up to 16,764m (55,000ft). The augmentor was locked out during the entire test. The simulated flight Mach number was 0.0 at sea level and 0.8 for all other altitude conditions. Aviation fuels that met or exceeded standard specification were used throughout the test.

As shown in Figure 1, the engine was installed into the NASA LeRC PSL-4 test cell on a multi-directional thrust measuring stand. Air is supplied to the engine through 0.8826 m (34.75 in) diameter inlet ducts which are directly connected to the front of the engine. Before the air enters the engine, the pressure and temperature are set to match the conditions that the engine would see at the desired altitude and flight Mach number. Downstream of the engine exhaust nozzle is the gas sampling rake followed by the 1.83m (72 in) diameter, water cooled exhaust collector. A circular cooling air torus is located in the forward portion of the test cell and provided 9.09 to 13.64 kg/sec (20 to 30 lb/sec) of cooling air maintaining a temperature below 37.8 °C (100 °F).

In order to protect the engine and test cell, the sea level static test points were run at total temperatures and total pressures equal to a normal day at sea level, but the altitude tank was at a pressure equivalent to an altitude of 3,048 m (10,000 ft). These types of conditions will yield engine performance very similar to those at a true static sea level condition.

The system used on this program to provide a hot, pressurized exhaust gas sample to the gas and particle analyzers consisted of a cruciform type rake located behind the engine exhaust nozzle, which held the sampling probes, a distribution box and a pump box. The vertical arms of the cruciform rake contain only gas sampling probes. The horizontal arms contain alternating Mach Number/Flow Angularity (MFA), stagnation temperature, and gas sampling probes. The gas sampling probes were designed to meet emissions certification test requirements. They were spaced equally across the arm, and could be ganged (valved to a common line) or sampled individually. Individual probe sampling allows spatial mapping of engine exit plane core, bypass, and intermediate mixed flow regimes.

The rake system was mounted on a support structure positioned between the engine exhaust nozzle and the inlet to the exhaust collector. The tips of the sampling probes were positioned 0.2144 m downstream of the exhaust nozzle exit plane. Details of the sampling rake along with the sampling probe design is described in Appendix A.

3. TEST PARAMETERS

Aviation fuel (Jet A) with a range of fuel sulfur was procured. Low and high sulfur values are limited by commercially available fuels and by fuel specification limits of 0.3% by weight. Low-sulfur fuel used had a sulfur content of approximately 18 parts per million (ppm), and the high-sulfur fuel of 1113 ppm. An intermediate level, 152 ppm, was set by mixing the low and the high sulfur fuels. A military fuel JP-8 + 100 with 336 ppm sulfur was also tested. Fuel samples were sent to both Wright Patterson AFB and a private laboratory to be comprehensively analyzed for each batch. Details of these analyses are listed in Tables 1 and 2. Sample #1 is the low sulfur fuel with corrosion inhibitor. Sample #2 is the low sulfur fuel with corrosion inhibitor, conductivity

additive, and icing inhibitor. Sample #3 is the high sulfur fuel with corrosion inhibitor. Sample #4 is the mixed medium sulfur fuel with corrosion inhibitor, conductivity additive, and icing inhibitor. Sample #5 is the JP8+100. Fuel additives used in this test series are listed in Table 3.

For the first 2 nights of the test program, the gas samples were drawn from individual sample probes in order to determine the distribution of the exhaust emissions across the engine exit plane. This also provided an opportunity to calibrate all the emission measurement systems. Individual samples were drawn from the vertical rake the first night, then the horizontal rake the second night. Figures 2 and 3 show the CO_2 measured from individual probes as a typical emission distribution.

Based on these distributions, the 3 inner most sampling probes from the engine centerline of each arm were ganged together for each measurement system for the third and subsequent test nights. Both of the horizontal arms are ganged together for the LeRC system. The bottom vertical rake was dedicated to the UMR/MASS system. The top vertical rake was dedicated to the AFRL/CIMS system.

Table 4 listed the test matrix which was set by parametrically varying the combustor inlet temperature (T_3) between idle and maximum power setting at simulated SLS and up to five other altitudes for each fuel. Figure 4 graphically illustrates the test conditions as a function of combustor pressure and temperature.

4. EMISSION MEASUREMENT SYSTEMS

Four diagnostic systems, extractive and non-intrusive (optical), were assembled for the gaseous and particulate emissions characterization measurements study. These systems are briefly described below. Details of the respective techniques and database established from this test are described in the appendices.

4.1 NASA Extractive Gaseous Emission Measurement System and Smoke Meter

The extractive gaseous emissions measurement system contains an array of analyzers dedicated to examining the concentrations of specific gases and a standard SAE smoke meter. This system is essentially identical to systems used for commercial aircraft engine emissions certification testing, except that probes are equally spaced in the present study, affecting the spatial averages of the exhaust. The gaseous emissions system includes analyzers for measurement of CO, CO_2, NO, NO_x, O_2, total unburnt hydrocarbons (THC), and SO_2. Details of each analyzer are described in Appendix B.

Spatial profiles were obtained by sampling individual probes of each arm of the rake system. Comparisons of vertical and horizontal species concentration and temperature profiles from the first two days of test series confirmed symmetry and gave confidence in representative sampling from either arm. Three inner-most probes from both horizontal arms were ganged for this system.

4.2 UMR Extractive Particulate Measurement System

Appendix C contains details on the particulates and aerosols characterization system employed in this study - the University of Missouri-Rolla Mobile Aerosol Sampling System (MASS). A brief overview of the system is given here. For this test the UMR trailer-based MASS facility was employed. The trailer was located immediately adjacent to the NASA LERC PSL building and was connected to the altitude chamber through 30m long heated sample and diluent lines. Particulate concentrations from single and ganged (multiple) probe sources and were monitored in real time, with typically a 1 Hz sampling frequency, using commercially available condensation nucleus counters (CNC's) (TSI and Met-One models: 3025 and 1105-5, respectively). Size distributions were determined both in real time and from sample tanks for particulate diameters ranging from 7 - 250 nm using differential mobility analysis. Hydration properties (e.g. soluble mass fraction) were derived from tank samples using a tandem differential mobility analysis system. A needle to grid electrostatic precipitator was used to collect particulate samples on electron microscope grids. Comprehensive data presented in Appendix D are summarized in section 5.3.

4.3 AFRL Extractive Sulfur Oxides Measurement System

A chemical ionization mass spectrometer (CIMS) from the Air Force Research Laboratory at Hanscom AFB was used to measure levels of SO_2 and HNO_3 in the F-100 jet engine exhaust. Exhaust gases were sampled through three extractor probes on the upper part of the vertical rake, 26 cm beyond the exit plane of the engine. The inlet lines were joined at a point 1 m from the probes, where the sampled gases entered an 0.64-cm OD, 7.3-m long stainless steel line which transported the exhaust effluent to the flow tube of the CIMS. The sampling line was heated to 150 °C to prevent condensables from adhering to the walls of the sampling line. The stainless steel lines (including the three probe lines) were coated with siloxane-covered glass to minimize sticking of HNO_3 to the walls. The exhaust effluent entered the CIMS flow tube through a 0.32-cm OD, 7.5-cm long capillary, which restricted the effluent flow to 4-15 slm (standard liters per minute). The flow tube utilized a fast flow (120 slm) of N_2 gas at 37 Torr pressure, diluting the engine effluent by typically a factor of 6.

Detection of the trace gases in the engine effluent was made by reacting the diluted engine effluent with CO_3^- ions in the flow tube over a path length of 2.5 cm. The chemistry involved in detecting SO_2 and HNO_3 is:

$$CO_3^- + SO_2 \rightarrow SO_3^- + CO_2,$$

followed in less than a microsecond by:

$$SO_3^- + O_2 + M \rightarrow SO_5^- + M,$$

where M is a third body (N_2 or O_2). Thus, the appearance of ion signal at 112 amu (SO_5^-) signifies the presence of SO_2 in the engine exhaust. Similarly,

$$CO_3^- + HNO_3 + M \rightarrow CO_3^-(HNO_3) + M,$$

and thus, appearance of ion signal at 123 amu [$CO_3^-(HNO_3)$] signifies the presence of HNO_3 in the engine exhaust. Known flow rates of calibration gases (SO_2 and HNO_3) were periodically added during each engine test condition (altitude, power level, and fuel type). Tests were carried out to determine loss rates in the sampling line, by injecting calibrant gases consecutively at four points along the line (see Appendix E). The combination of calibrant ion signal, calibrant flow rate, engine exhaust ion signal, and total engine effluent flow rate, give the mixing ratio (fractional concentration of SO_2 or HNO_3) in the engine exhaust. Emission indices (grams of SO_2 or NO_2 equivalent per kilogram of fuel, respectively) were evaluated from the respective mixing ratios using NASA's data for the percentage of CO_2 combustion product in the exhaust. Details of the method, instrument, and data analysis are given in Appendix E.

4.4 ARI Non-Intrusive Gaseous Emissions Measurement System

Aerodyne Research, Inc. (ARI) used infrared tunable diode laser (IR-TDL) absorption to measure SO_2, SO_3, NO, H_2O and CO_2 along an optical path through the center of the plume. Two lasers were operated simultaneously, with the two spatially coincident beams focused on the same detector. Multiplex detection was achieved by turning off each laser while the other laser was being spectrally scanned. The data acquisition rate resulted in accumulation of spectra from both lasers at a 600 Hz rate. The laser beams entered and exited the test cell through a calcium fluoride window with a 1-deg wedge to suppress interference fringes. The optical system inside the test cell allowed for either 14 passes through the exhaust, using multi-pass mirrors inside purged protective boxes, or two passes, using a retro-reflector. Some readjustment of the optical system during the test was required, due to motion of the test cell with changes in simulated altitude. During early test days, spectra were taken of several NO and CO_2 lines, in both two-pass and multi-pass configurations. For some low sulfur cases, and for all observations of fuels with higher sulfur loadings, the two spectral regions observed contained lines of SO_2 and SO_3, respectively. Both regions also contained H_2O lines, allowing direct calculation of sulfur oxide emission indices using the known water emission index. The spectral data, analysis procedures, and results are presented in Appendix F.

5. SUMMARY OF RESULTS

5.1. Gaseous Emission Data

Multiple data points acquired during steady-state conditions were relatively constant over time and were therefore averaged and reported as a single value. Dates and clock times are included in the table to document approximate duration per each steady-state test condition, and to correlate with data from other measurement systems. The full set of data, including engine parameters, smoke number and gaseous emissions, is listed and discussed in Appendix C.

5.2. Comparison of Extractive and Non-Intrusive Sulfur Oxides Data

SO_2 emissions were measured by three different techniques: extractive sampling using UV absorption (LeRC) and CIMS (AFRL) as well as non-intrusive *in situ* infrared TDL absorption (ARI). The SO_2 emissions indices for all three techniques agree within their respective uncertainty estimates. Emission indices averaged over all T_3 values are plotted in Figure 5 as a function of altitude for the three highest fuel sulfur loadings and all three measurement techniques. Table 5 gives emission indices averaged over all altitudes and power settings, Figure 5 shows that within the error limits, there is no trend with altitude. A similar lack of any discernible trend applies to plots as a function of T_3. Consideration of any column in Table 5 might suggest a trend with sulfur loading for a particular measurement technique, but a comparison among all three techniques indicates that no trend exists within the uncertainty limits. The differences in sulfur conversion with different sulfur content are most likely due to systematic errors in the measurements, not to a significant change in sulfur chemistry over the range of sulfur loadings. It can be seen from Table 5 that for all three fuels, the SO_2 emission indices or sulfur conversion fractions from the three techniques agree within the standard deviations of their data sets, even without considering any estimates of systematic errors.

The overall result of all three measurement techniques is that the measured SO_2 emission represents the majority of the fuel sulfur content (see Table 5). Measurements using the TDL technique provided an upper limit for emitted SO_3 concentrations, as the SO_3 emissions were below the detection sensitivity. This upper limit is sufficiently constraining for the high sulfur fuel to verify the conclusion that most of the emitted sulfur is in the form of SO_2.

5.3. Particulate Data

The UMR MASS was employed to characterize the particulate emissions over the range of engine flight conditions and fuel types described in this report. The data characterize the particulates generated in the engine and that continue to exist 12 cm downstream of the exit plane of the engine exhaust nozzle. This is the first database of its kind providing particulate characterization (i.e. total concentration, particulate number- and mass-based emission indices, soot volume fraction, total particulate size distributions) as a function of engine operating parameters and fuel formulation. A separate study of JP8+100 fuel was also performed and the results of this study are also presented here.A complete description of the measurement system, results and conclusions for the particulate data are presented in Appendix D.

6. CONCLUSIONS

A comprehensive set of data, including gaseous, particulate precursor, and particulate emissions, has been acquired at simulated sea-level-static and altitude conditions for four different fuels. Three JP-8 fuels with varying sulfur content from very low (less than 20 ppmm) through intermediate (152 ppmm) to high (1113 ppmm) sulfur were tested, with the lowest sulfur fuel

using two sets of additives. An additional, advanced fuel, JP-8+100 with a fuel sulfur content of 336 ppmm, was also tested. This database provides valuable information for the atmospheric assessment of aerosol and aerosol precursor emissions from aircraft engines.

SO_2 emission indices were measured by three different techniques, two extractive and one non-intrusive. Extractive samples were analyzed by ultraviolet absorption (gas analysis system) and chemical ionization mass spectrometry. In situ measurements were performed with infrared absorption using a tunable diode laser. The SO_2 emissions indices for all three techniques agree within their respective uncertainty estimates. The measured SO_2 emission represents the majority of the fuel sulfur content for all of the fuels used under all engine and altitude conditions.

Gaseous emissions data were acquired by the extractive engine exhaust analysis system at all test conditions. In part of the testing period, the CO_2 analyzer mal-functioned. On those occasions, emission indices were calculated by O_2 measurements. The emission indices of NO_x have stronger dependency on combustor inlet temperature (T_3) and pressure (P_3), weaker dependency on fuel flow and no dependency on fuel sulfur content. No SO_2 data were obtained during the low sulfur fuel test since the concentrations are below the detection limit of this system. Emission indices of SO_2 showed no dependency on T_3.

The CIMS system provided a comprehensive database on SO_2 for all fuels. The emission indices for SO_2 are essentially independent of engine exhaust temperature and altitude. It is the first time that a HNO_3 database has been obtained for engine emissions at the exit plane. Within the uncertainties in the data, the emission indices for HNO_3 are independent of the sulfur level in the fuel. The HNO_3 level decreases with temperature, presumably because HNO_3 is not stable at high temperatures. No CIMS measurements of SO_3 were obtained, due to losses in the sampling line.

The TDL system performed reliably throughout the test period, making measurements in both double-pass and multi-pass configurations. During most of the test, SO_2 and SO_3 spectral regions were measured, each of which also contained several H_2O lines which were used as reference lines for emission index calculations. For the lowest sulfur fuel case, when the SO_2 levels were below the detection sensitivity, NO and CO_2 absorption was measured. SO_2 emission indices were obtained for all engine power conditions at altitudes of 9,144m (30,000 ft) and above for all but the lowest sulfur fuel. SO_3 was always below the detection sensitivity of the instrument but, for the high sulfur fuel case, the measurements allow an upper bound for the SO_3 level to be obtained. This upper bound is consistent with the level of sulfur emission present as SO_2.

The MASS system provided a comprehensive database on particulates. For the total concentration, no strong dependence of emission index on T_3 or altitude is observed. In some cases a weak dependence is observed where the EI appears to peak at T_3's around 600-700 °K. The mean emission indices for the high and medium sulfur cases are comparable. The mean emission index for the low sulfur case studied was significantly lower (by a factor of between 3 to 4) than that for the high and medium sulfur cases. However, each fuel had a different additive package. The mean number-based emission index for the JP8+100 fuel case was $(2.0 \pm 0.4) \times 10^{14}$ particles/kg fuel burned. This result is comparable to the emission indices measured for the medium and high sulfur cases. In this case, however, yet a different additive package is present in a different baseline fuel.

An analysis of the particle mass distributions indicated >90% of the particle mass fell within the measurement regime of the DMA (10 - 300 nm) and thus the estimation of mass-based emission indices from the mean volume diameter of the distributions and an assumed density for the particles was valid.

For all fuels and test conditions studied the size distributions are of a log-normal type with mean diameters in the range 50-65 nm. In the case of the medium sulfur fuel study, data were acquired for the same engine operating conditions at different times when test conditions were repeated with the same fuel on different days.These data provide an opportunity to explore the engine performance issue of particulate emission stability between subsequent measurements at equivalent test conditions. The emissions reproducibility is good. The standard deviation in the mean diameters was 1.5% and that of the half widths of the distribution was 3%.

REFERENCES

1. D. W. Fahey, et al., "In Situ Observations In Aircraft Exhaust Plumes In the Lower Stratosphere at Midlatitudes", in *Journal of Geophysical Research*, Vol. 100, No. D2, pp. 3065-3074 (1995)

2. D. W. Fahey, et al., "Emission Measurement of the Concord Supersonic Aircraft in the Lower Stratosphere", *Science*, Vol. 270, pp. 70-74 (1995)

3. R.. S. Stolarski et al., "1995 Scientific Assessment of the Atmospheric Effects of Stratospheric Aircraft", NASA Reference Publication 1381

Table 1.—Wright-Patterson Laboratory Fuel Analysis

TEST	METHOD	LIMITS MIN	LIMITS MAX	Sample #1	Sample #2	Sample #3	Sample #4	Sample #5
Total Acid Number, mg KOH/g	D974		0.1	0.0	0.0	0.0	0.0	0.008
Aromatics, % vol	D1319		22	15	17	10	15	9.7
Aromatics, %	HPLC			14.9	20.8	18.2	20.1	14.1
Olefins, %vol			5.0					1.0
Mercaptan Sulfur, % wt	D3227		0.003	0.000	0.000	0.000	0.000	0.000
Total Sulfur, % wt	D4294		0.3	0.0	0.0	0.1	0.0	0.03
Sulfur Content, ppm	ASTM3120			<1				
Sulfur Content, ppm	x-ray fluorescence			~0	~0	1113	152	336
Distillation	D86							
IBP, °C			Report					161
10% recovered, °C			205	161	162	184	162	176
20% recovered, °C								182
50% Recovered, °C			Report	179	180	214	184	197
90% recovered, °C			Report	228	229	243	236	234
FBP, °C			300	270	273	270	272	263
Residue, % vol			1.5	1.2	1.2	1.2	1.2	1.2
Loss, % vol			1.5	1.3	1.4	1.1	1.1	1.3
Flash Point, °C	D56	38		39	38	51	40	45
Density at 15 °C, kg/cu meter	D1298	775	840	791	792	812	795	46
Freezing Point, IC	D2386		-40	-52	-51	-41	-51	-56
Viscosity @ -20 °C cSt	D445		8	3.1	3.1	5.7	3.4	3.3
Hydorgen Content, %wt	D3343	13.4		14.0	13.9	14.0	14.0	14.2
Smoke Point, mm	D1322	25		24##	24##	24##	24#	24.0##
Copper Corrosion	D130		1	1a	1a	1a	1a	1a
Thermal Stability	D3241							
Tube Rating Visual			<3	1	4##	1	4##	1
Change in Press., mm of Hg			25	0	1	0	3	0
Existent Gum, mg/ 100mL	D381		7	3	3	2	2	3
Water Reaction	D1094		1B	1	1	2#	1	2##
Conductivity, pS/m	D2624	200	600	0##	892##	0##	860##	450
FSII	D5006	0.10	0.15	0.00##	0.11	0.00##	0.14	0.13
Net Heat of Combustion, MJ/kg	D3338	42.8		43.4	43.3	43.3	43.3	43.4
Lubricity (BOCLE)	D5001		Report	0.55	0.50	0.65	0.5	0.55

—out of range

Table 2.—Martel Laboratory Fuel Analysis

Analytical Parameter	Method	#1	#2	#3	#4	#5	Units
Filtration Time	ASTM SPEC	33.3	33.1	48.7	32.3	39.4	sec/l
Particulate Contamination	ASTM D5452	0.2	0.1	0.4	0.2	0.1	mg/l
Appearance / Workmanship	ASTM D4176	bright clear	light yellow	yellow	light yellow	light yellow	
Water Reaction	ASTM D1094	1.5	1	0	0	2	ml
Water Reaction - Interface	ASTM D1094	2	2	2	2	2	ml
Water Reaction - Separation	ASTM D1094	3	3	3	3	3	ml
Conductivity of Aviation Fuels	ASTM D2624	106	850	12	670	402	pS/m
Hydrogen Content of Aviation Fuels	ASTM D3343	13.94	13.89	13.82	13.86	14.02	% wt
Determination of Fuel Icing Inhibitors	ASTM D5006	<0.01	0.11		0.11	0.12	%
Hydrocarbon Constituents by FIA:	ASTM D1319						
Aromatics	ASTM D1319	16.1	17.1	16.2	17.4	11	
Olefins	ASTM D1319	1	1.2	1.5	1	1.2	
Saturates	ASTM D1319	82.9	81.7	82.3	81.6	87.8	
Smoke Point of Aviation Fuels	ASTM D1322	21	22.2	22.6	23	21	mm
Jet Fuel Thermal Oxidation Test (JFTOT)	ASTM D3241	0.1	0	0	0	0	mmHg
Color Deposit Rating	ASTM D3241	<1	<1	<1	<2	<1	
Existent Gum in Fuels by Jet Evaporation	ASTM D381	<1.0	1a	<1	<1.0	<1.0	sh
Corrosion (Copper Strip Test)	ASTM D130	1 a	<1.0	1a	1a	1a	
Distillation of Petroleum Products	ASTM D86						
Initial Boiling Point	ASTM D86	302	306	328	308	322	°F
10% Recovered	ASTM D86	318	318	364	322	344	°F
20% Recovered	ASTM D86	324	326	378	330	354	°F
30% Recovered	ASTM D86	332	340	390	346	364	°F
40% Recovered	ASTM D86	340	340	402	346	372	°F
50% Recovered	ASTM D86	350	350	414	356	380	°F
60% Recovered	ASTM D86	360	362	430	370	390	°F
70% Recovered	ASTM D86	376	378	446	390	400	°F
80% Recovered	ASTM D86	400	400	466	418	418	°F
90% Recovered	ASTM D86	440	440	488	458	446	°F
End Point	ASTM D86	518	524	526	526	508	°F
Recovery	ASTM D86	99	99	99	99	99	%
Residue	ASTM D86	1	1	1	1	1	%
Loss	ASTM D86	0	0	0	0	0	%
Flash Point (Pensky-Martens closed cup)	ASTM D93	95	100	97	90	105	°F
Freezing Point	ASTM D2386	<-50	<-50	<-50	<-50	<-50	°F
Gravity, API (Hydrometer)	ASTM D287	47.5	47.1	42.8	46.2	46	@60degAPI
Kinematic Viscosity @ -20 deg C	ASTM D445	3.1	2.9	5.5	3.4	4.2	cSt
Heat of Combustion (Lower Heating Value)	ASTM D240	18690	18720	18730	18610	18740	BTU/lb
Total Acid Number	ASTM D664	0.01	0.01	0.01	0.01	0.01	mgKOH/g
Mercaptan Sulfur	ASTM D3227	<0.001	<0.001	0.002	<0.001	<0.001	%
Sulfur Non-dispersive X-Ray Spectrometry	ASTM D4294	<0.01	<0.01	0.1	0.02	0.03	Mass %
Sulfur	ASTM D4951	<0.01	<0.01	0.11	0.02	0.03	%
Iron	EPA 200.7	<1	<1	<1	<1	<1	ppm
Copper	EPA 200.7	<1	<1	<1	<1	<1	ppm
Zinc	EPA 200.7	<10	<10	<10	<10	<10	ppm

Table 3.—Fuel Additives

Product	Company	Quantity	Components
Corrosion Inhibitor	Octel America	9 - 22.5 g/m^3 fuel	70-80% NJ Trade Secret Registry #00850201001-5000P, 20-30% Xylene, 0-5% Ethylbenzene, <250ppm Benzene
Conductivity Additive	Octel America	1.5 ppm by weight	50-60% Toluene, 5-10% Mixed Aromatic Solvents C9-16, 0-5% Isopropyl Alcohol, 1-10% NJ Trade Secret Registry # 00850201001-5457P, 1-10% Dodecyl Benzene Sulfonic Acid, 10-20% NJ Trade Secret Registry #00850201001-5037P, <595ppm Benzene
Icing Inhibitor	Aldrich Chemical	0.12% by volume	Diethylene Glycol Methyl Ether

Table 4.—Test Matrix

Date	Altitude	T_3	Fuel
8/11/97 & 8/12/97	9,144m (30,000ft)	443°C (830°F)	Low sulfur Jet A (~18ppm) with Corrosion Inhibitor
8/14/97 & 8/15/97	SLS	idle (~224°C/435°F), 343°C(650°F), 399°C(750°F), 443°C(830°F), mil(~522°C/972°F)	Low sulfur Jet A (~18ppm)with Corrosion Inhibitor
	9,144m (30,000ft)	idle(~226°C/435°F), 343°C(650°F), 399°C(750°F), 443°C(830°F), mil(~486°C/907°F)	
	12,192m (40,000ft)	idle(~260°C/500°F), 343°C(650°F), 399°C(750°F), mil(~447°C/836°F)	
	15,240m (50,000ft)	idle(~349°C/660°F), 399°C(750°F), mil(~438°C/821°F)	
	16,764m (55,000ft)	idle(~410°C/769°F), mil(~451°C/843°F)	
8/21/97	SLS	idle (~218°C/425°F), 343°C(650°F), 399°C(750°F), 443°C(830°F), mil(~515°C/959°F)	Low sulfur Jet A (~18ppm) with Corrosion Inhibitor, Conductivity Additive, & Icing Inhibitor
	9,144m (30,000ft)	idle(~228°C/443°F), 343°C(650°F), 399°C(750°F), 443°C(830°F), mil(~486°C/907°F)	
	12,192m (40,000ft)	idle(~264°C/507°F), 343°C(650°F), 399°C(750°F), mil(~437°C/818°F)	
	15,240m (50,000ft)	idle(~354°C/670°F), 399°C(750°F), mil(~443°C/829°F)	
	16,764m (55,000ft)	mil(~442°C/828°F)	
8/25/97 & 8/26/97	SLS	idle (~221°C/430°F), 288oC(550°F), 343°C(650°F), 399°C(750°F), 443°C(830°F), mil(~516°C/960°F)	High sulfur Jet A (1113ppm) with Corrosion Inhibitor
	9,144m (30,000ft)	idle(~228°C/443°F), 343°C(650°F), 399°C(750°F), 443°C(830°F), mil(~488°C/910°F)	
	10,668m (35,000ft)	idle(~228°C/443°F), 343°C(650°F), 399°C(750°F), 443°C(830°F), mil(~447°C/837°F)	
	12,192m (40,000ft)	idle(~262°C/504°F), 343°C(650°F), 399°C(750°F), mil(~442°C/827°F)	

Table 4.—Test Matrix (Continued)

	15,240m (50,000ft)	idle(~357°C/674°F), 399°C(750°F), mil(~443°C/829°F)	
	16,764m (55,000ft)	idle(~423°C/775°F), mil(~446°C/834°F)	
8/28/97 & 9/2/97	SLS	idle (~227°C/440°F), 343°C(650°F), 399°C(750°F), 443°C(830°F), mil(~515°C/959°F)	Medium sulfur Jet A (152ppm) with Corrosion Inhibitor, Conductivity Additive, & Icing Inhibitor
	9,144m (30,000ft)	idle(~228°C/443°F), 343°C(650°F), 399°C(750°F), 443°C(830°F), mil(~492°C/917°F)	
	10,668m (35,000ft)	idle(~229°C/445°F), 343°C(650°F), 399°C(750°F), 443°C(830°F), mil(~452°C/846°F)	
	12,192m (40,000ft)	idle(~269°C/517°F), 343°C(650°F), 399°C(750°F), mil(~444°C/831°F)	
	15,240m (50,000ft)	idle(~355°C/670°F), 399°C(750°F), mil(~447°C/838°F)	
	16,764m (55,000ft)	idle(~421°C/790°F), mil(~451°C/843°F)	
9/4/97 & 9/5/97	SLS	idle (~221°C/430°F), 343°C(650°F), 399°C(750°F), 443°C(830°F), mil(~514°C/958°F)	JP8+100 (336ppm)
	9,144m (30,000ft)	idle(~233°C/452°F), 343°C(650°F), 399°C(750°F), 443°C(830°F), mil(~497°C/926°F)	
	10,668m (35,000ft)	idle(~233°C/451°F), 343°C(650°F), 399°C(750°F), 443°C(830°F), mil(~453°C/848°F)	
	12,192m (40,000ft)	idle(~269°C/517°F), 343°C(650°F), 399°C(750°F), mil(~443°C/830°F)	
	13,716m (45,000ft)	idle(~310°C/590°F), 399°C(750°F), mil(~445°C/833°F)	
	15,240m (50,000ft)	idle(~352°C/666°F), 399°C(750°F), mil(~442°C/828°F)	
	16,764m (55,000ft)	idle(~417°C/782°F), mil(~454°C/849°F)	

Table 5.—Sulfur dioxide Emission Indices and Exhaust SO2 Fractions of Fuel Sulfur, Averaged Over All Altitudes and Power Settings

Fuel	LeRC Sampling	AFRL CIMS	ARI TDL
High Sulfur Fuel	2.01 ! 0.18	2.49 ! 0.62	1.63 ! 0.22
JP-8 + 100	0.53 ! 0.08	0.57 ! 0.09	0.56 ! 0.10
Mixed Sulfur Fuel	0.31 ! 0.065	0.34 ! 0.07	0.26 ! 0.08

Sulfur Dioxide Emission Indices Averaged Over Altitude/Power Settings
(Error limits do not include estimates of systematic errors, but are simply standard deviations)

Fuel	LeRC Sampling	AFRL CIMS	ARI TDL
High Sulfur Fuel	0.90 ! 0.08	1.19 ! 0.28	0.73 ! 0.19
JP-8 + 100	0.78 ! 0.11	0.85 ! 0.13	0.83 ! 0.22
Mixed Sulfur Fuel	1.02 ! 0.21	1.11 ! 0.22	0.87 ! 0.30

Fraction of Fuel Sulfur in Exhaust in the Form of Sulfur Dioxide
(ARI error limits include estimates of systematic errors, added in quadrature to standard deviations formed from repeated measurements)

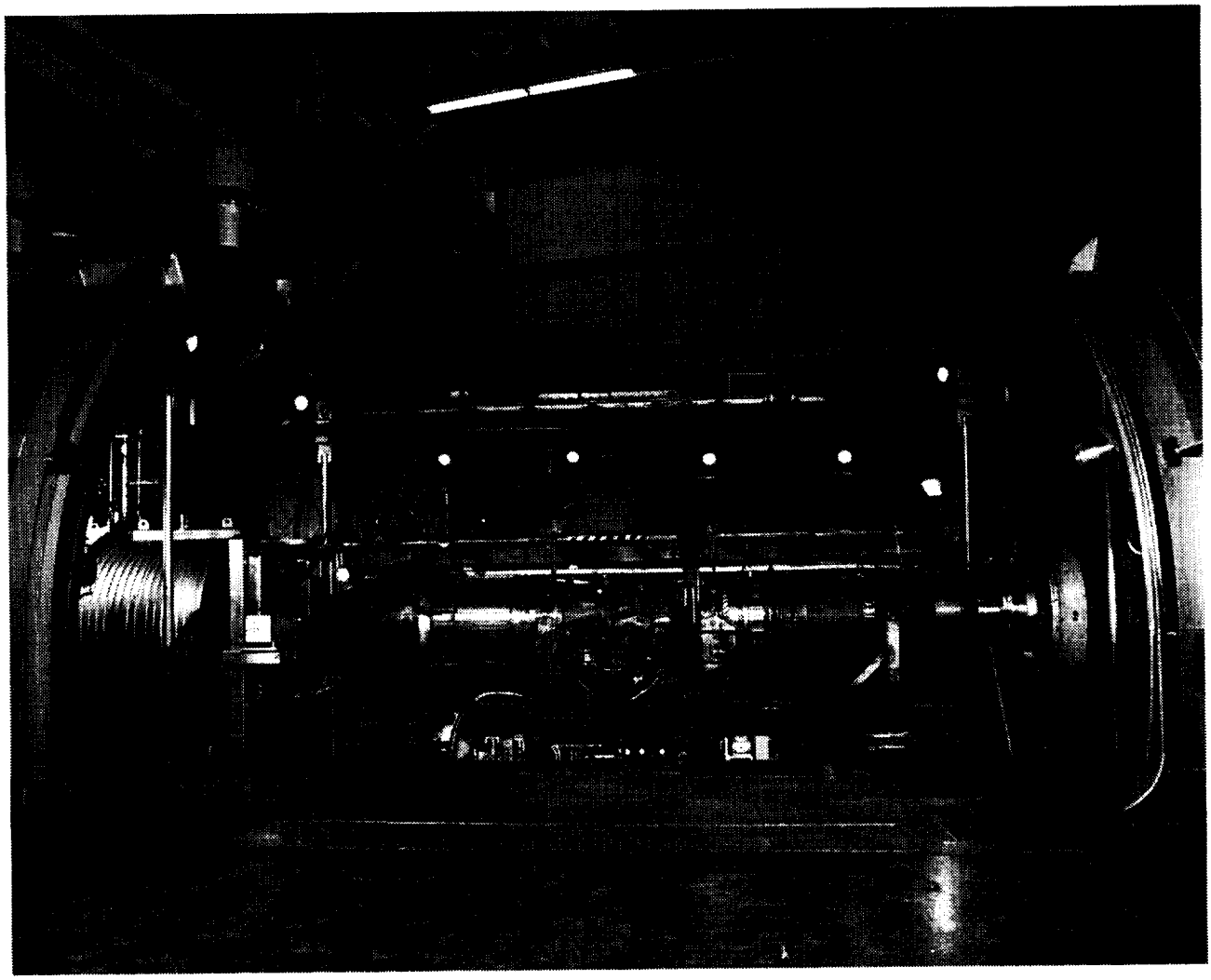

Figure 1.—PSL4 Facility of NASA Lewis Research Center

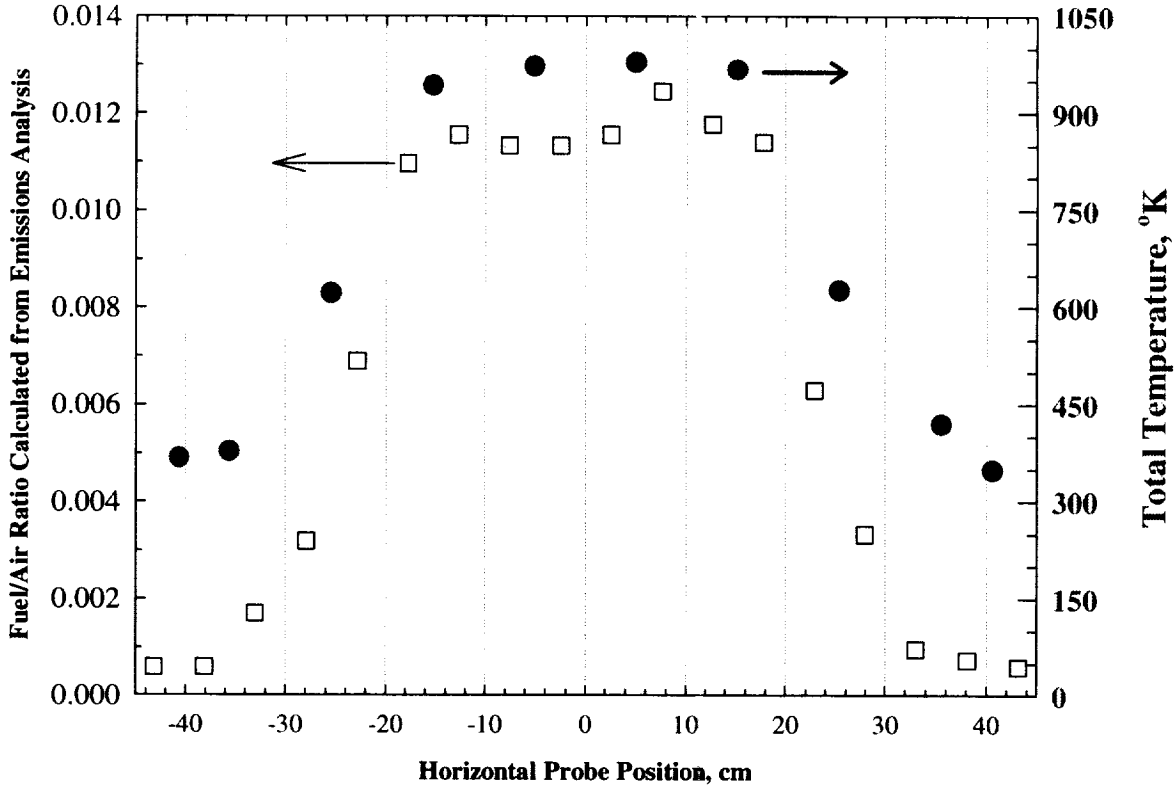

Figure 2.—Horizontal probe distributions of emissions fuel/air ratio ant total temperature

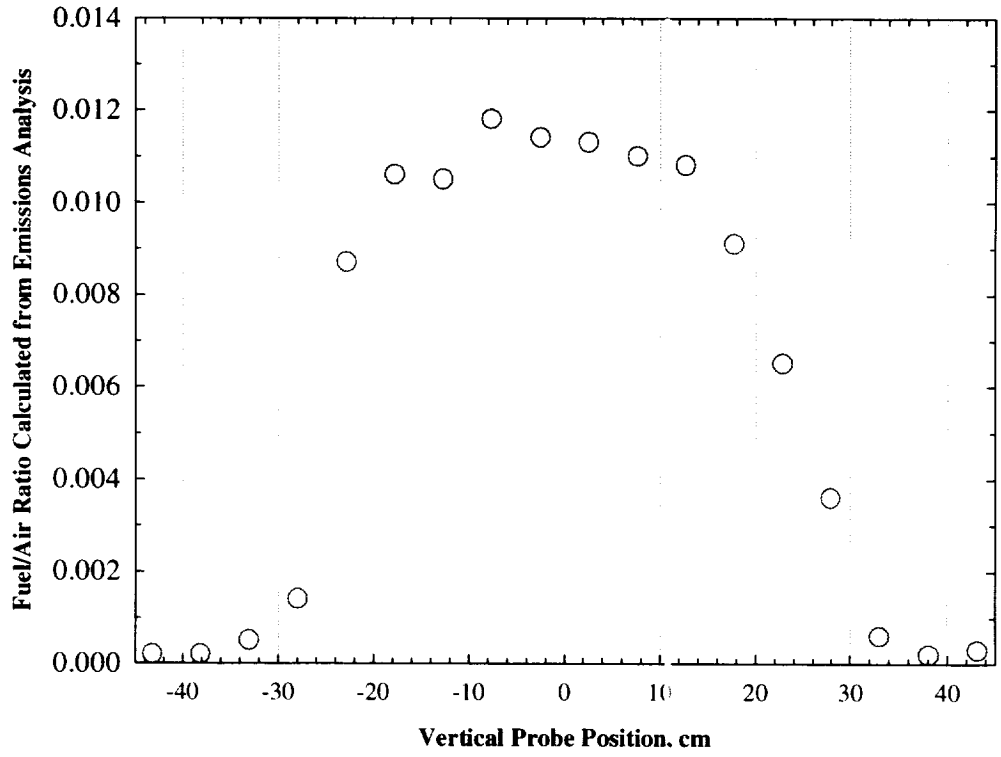

Figure 3.—Vertical probe distribution of emissions fuel/air ratio

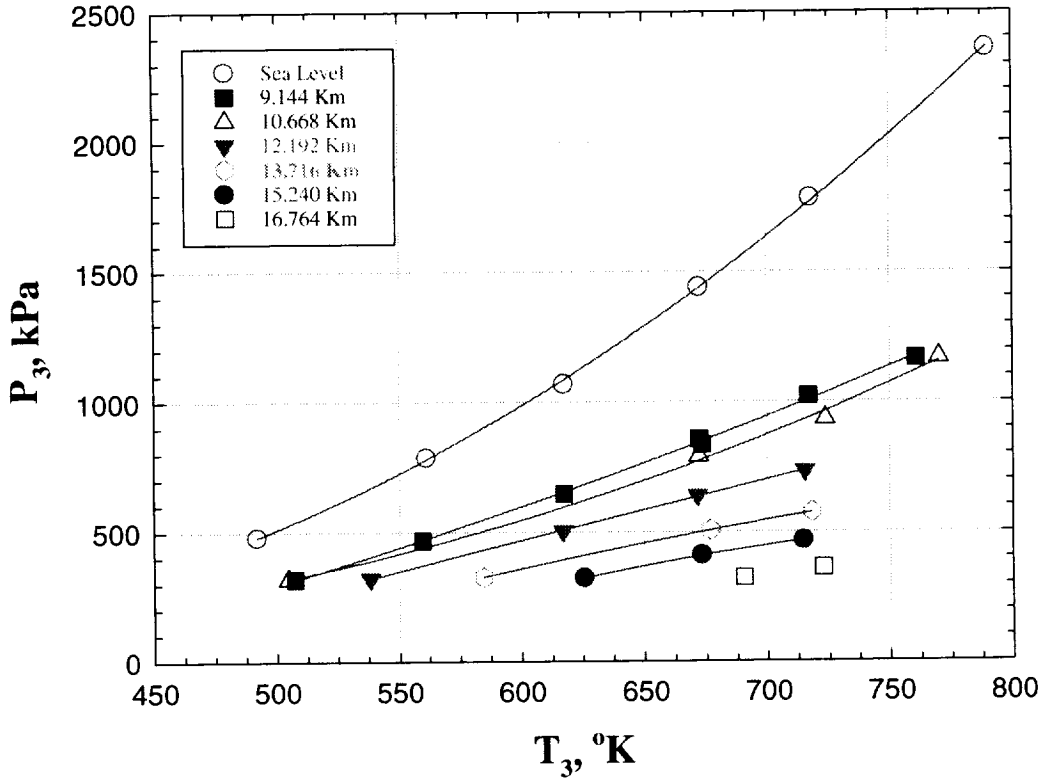

Figure 4.—P_3 vs T_3 of All Test Conditions

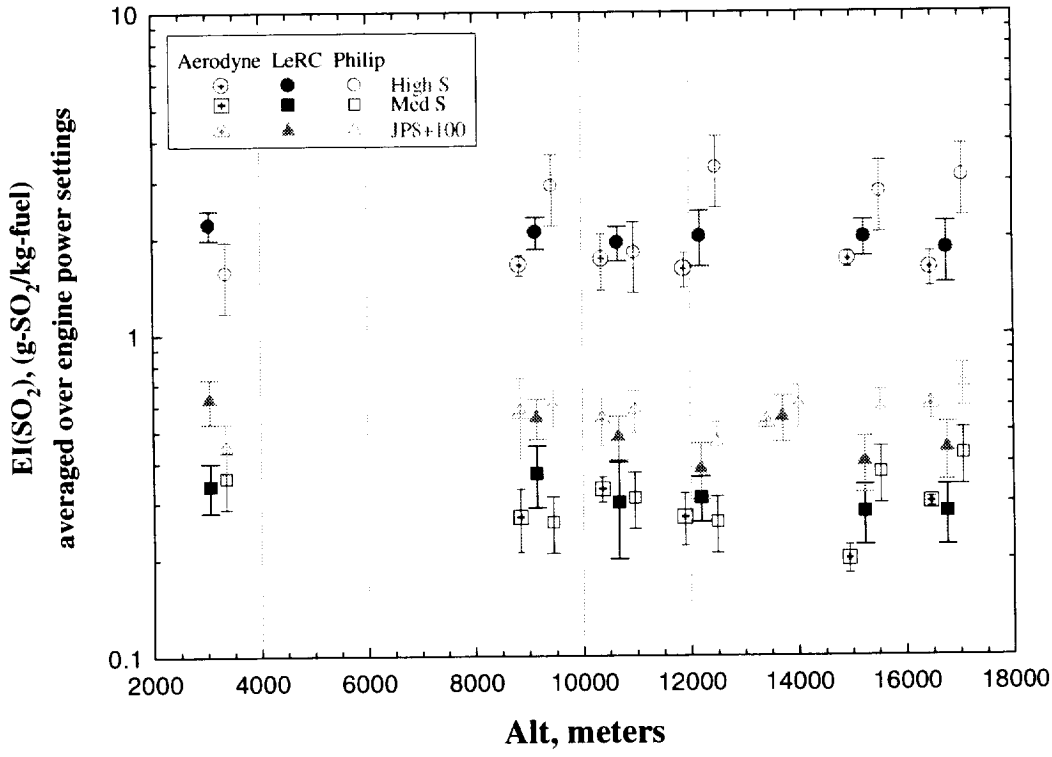

Figure 5.—Comparisons of $EI(SO_2)$

APPENDIX A
Sampling Probe Rake System

Dennis Dicki
Dynacs Engineering Company, Inc.

A.1. INTRODUCTION

The exhaust gas sampling rake used to draw off a sample was a cruciform type rake which was designed and fabricated by AEDC and used in the previous 1995 engine emissions program[1]. The rake assembly consists of a solid strut extending across the entire back of the exhaust nozzle on the horizontal centerline, with two additional struts located on the vertical centerline which are supported on the rake support structure and extend into the exhaust plume to a point just above or below the center of the horizontal strut. This is shown in Figures A-1 and A-2. The horizontal strut consists of alternating Mach number/flow angularity probes and static temperature probes between the gas sample probes which are located on 5.08 cm centerlines. There are a total of 7 Mach number/flow angularity probes, 10 static temperature probes and 18 gas sampling probes on this rake. The tips of the sampling probes were positioned 21.44 cm (8.44 in) downstream of the exhaust nozzle exit plane. The bottom half of the vertical rake contains 9 standard gas sampling probes. The top half of the vertical rake contains 9 open-ended 0.635 cm O.D. glass lined tubes.

The rakes were all mounted on a support structure made of 15.24 cm square structural tubing. The structure was positioned between the engine exhaust nozzle and the inlet to the exhaust collector, then welded to the floor. Also mounted on this structure were the mirror tables used for the Aerodyne analyzer.

The sample probe tips on the rakes in the bottom vertical and both horizontal quadrants are shown in Figure A-3 and were designed to meet the SAE standards for emission instrumentation. The probes on the top vertical rake consisted of a 0.635 cm glass lined tube which was pressed into 0.794 cm tube and both were chamfered to an angle of 45°. See Figure A-4 for details. The Mach Number/flow angularity probes consisted of single, centered total pressure tap, surrounded by 4 static type taps slightly downstream of the probe tip, on the tapered portion of the tip. This probe was designed to provide Mach Number and swirl characteristics of the exhaust plume (Figure A-5). The static temperature was measured with thermocouple probes as shown in Figure A-6.

The sample flowed through smooth bore, thin wall stainless steel tubes between the rakes and the various pieces of equipment. The tubes were electrically heated and insulated either individually or in bundles of 3. Each individual assembly (hose) had a separate temperature controller in order to maintain a minimum temperature of 176.7 °C (350°F). The valve and pump box were also regulated to maintain the temperature at 176.7 °C (350°F).

For the first 2 nights of the test program the gas samples were drawn from the exhaust plume using individual sample probes, which went from the sample rake through individual electrically heated stainless steel tubes to a valve switching box, through a heated pumping box and then to the analyzers. The valve switching box is a piece of AEDC hardware that has the capability of drawing from individual probes or ganged samples from the rake. It is shown schematically in Figure A-7. Individual samples were drawn from the vertical rake the first night, then the horizontal rake the second night in order to map the size of the exhaust plume. The pump box was used to increase the sample gas pressure to some value higher than atmospheric which is required to get it through the bank of NASA gas analyzers.

For the third and subsequent test nights, the sample extraction tubing on the horizontal rake was reconfigured so that the sample from each of the 3 inner most sample probes from the engine centerline, were ganged together and the sample sent through electrically heated stainless steel tubes to the heated pump box then to the LeRC analyzers. See Figure A-8 for schematic. The bottom vertical rake was dedicated to UMR, which used the 3 inner most gas sampling probes. The top vertical rake was dedicated to AFRL. The 3 innermost probe tubes were ganged together at the base of the rake and connected to glass lined, electrically heated hoses which brought the sample outside of the test cell to the analyzer.

REFERENCES

1. R. P. Howard et al "Experimental Characterization of Gas Turbine Emissions at Simulated Flight Altitude Conditions"AEDC-TR-96-3, September 1996.

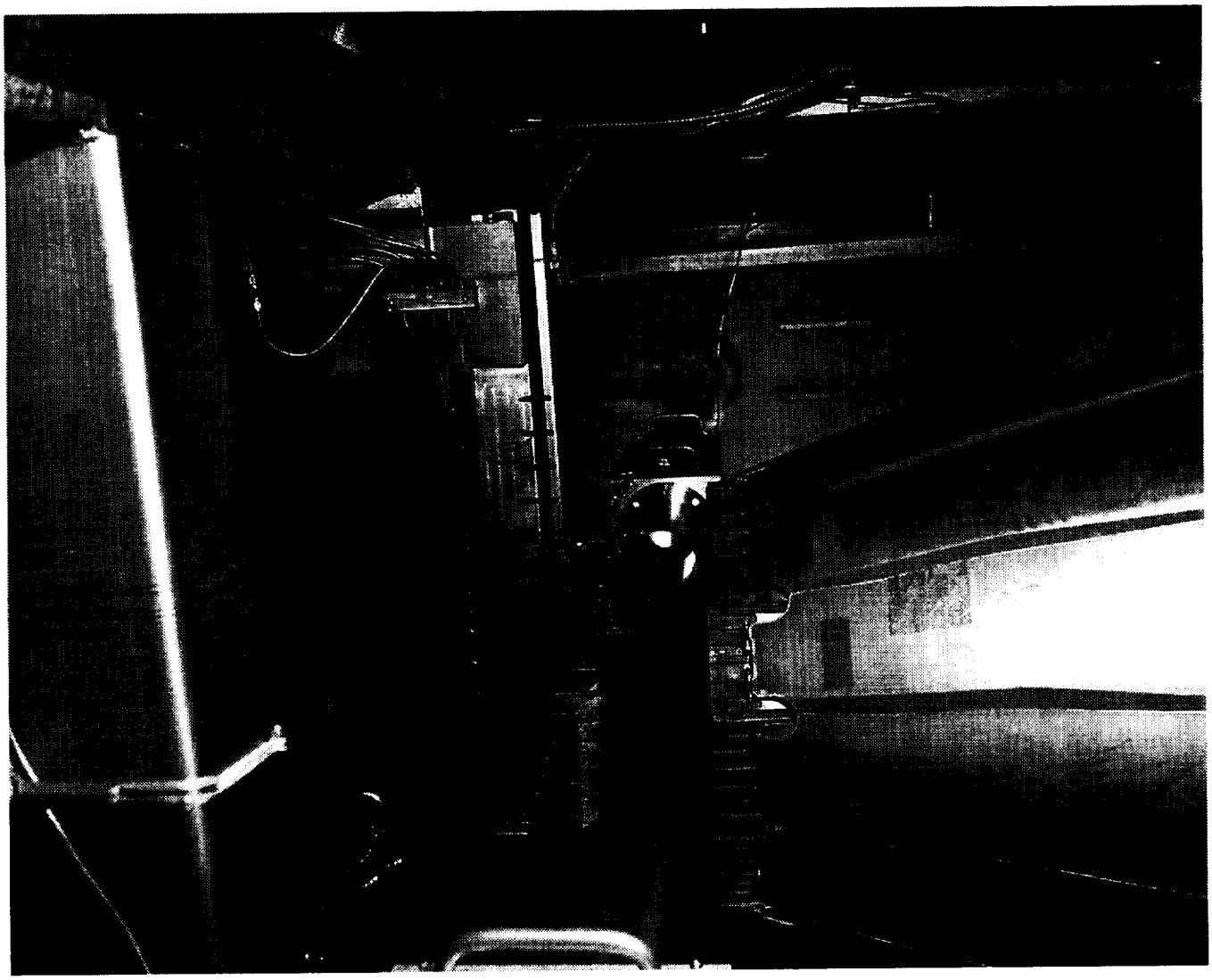

Figure A-1.—Side-view of sampling probe rake and engine nozzle exit

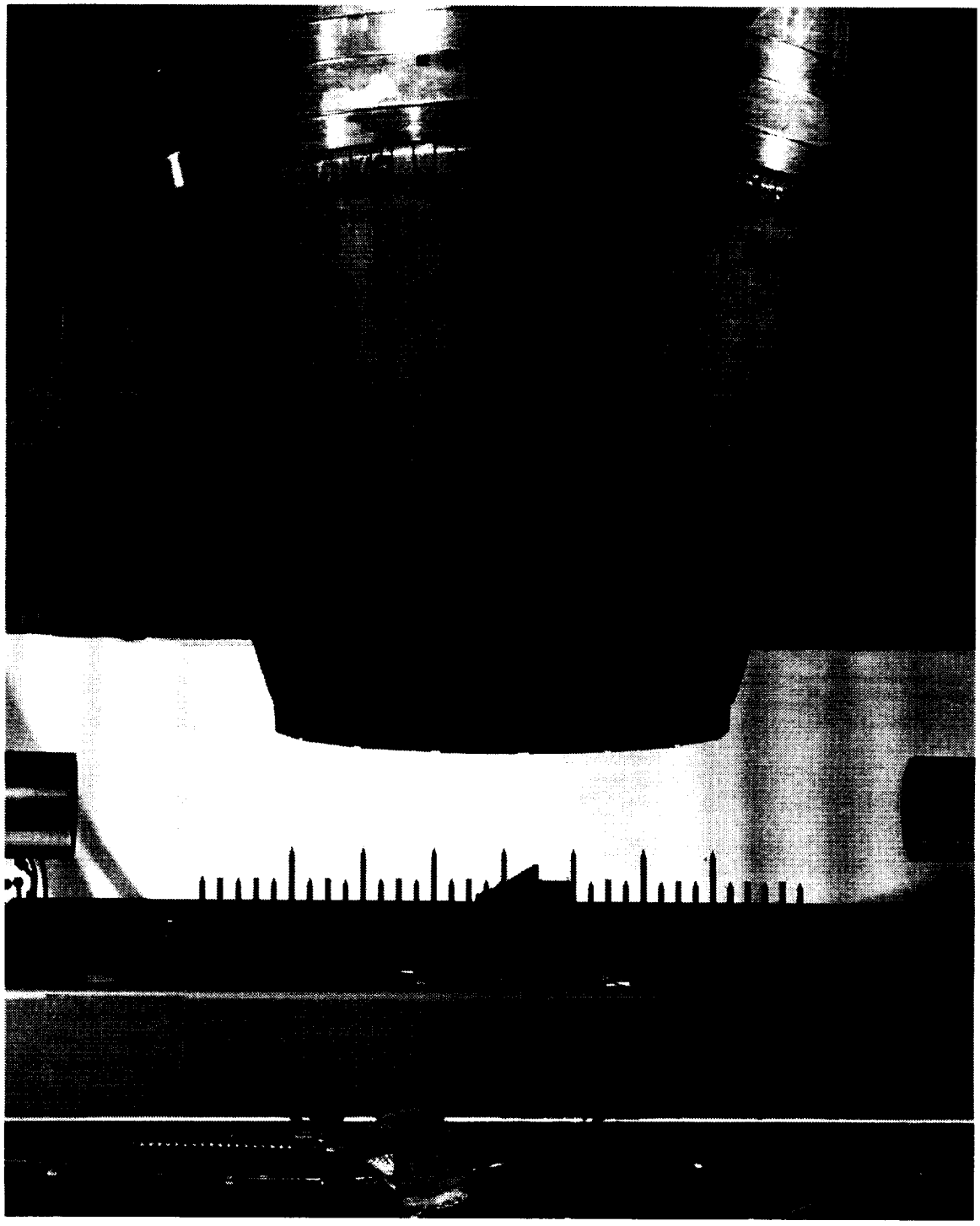

Figure A-2.—Top-view of sampling probe rake and engine nozzle exit

Figure A-3.—Standard Sampling Probe

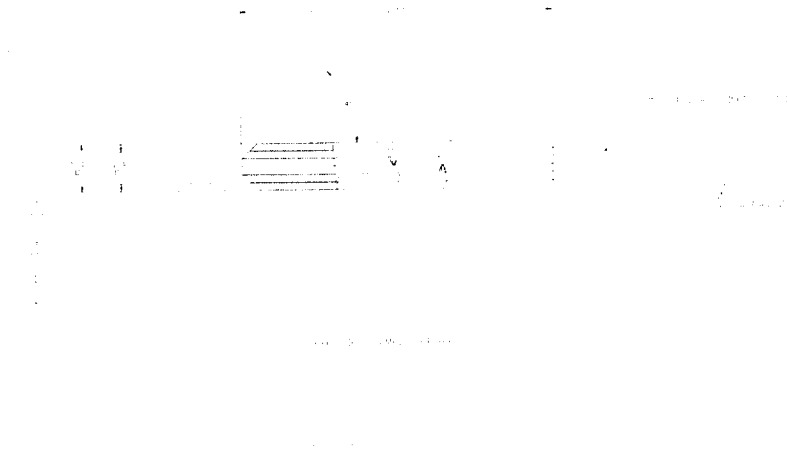

Figure A-4. —Philips Sample Probe

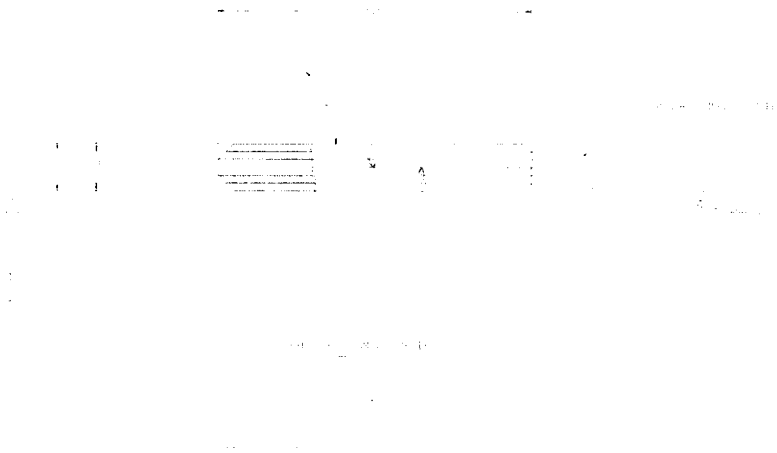

Figure A-5.—Mach/Flow Angularity Probe

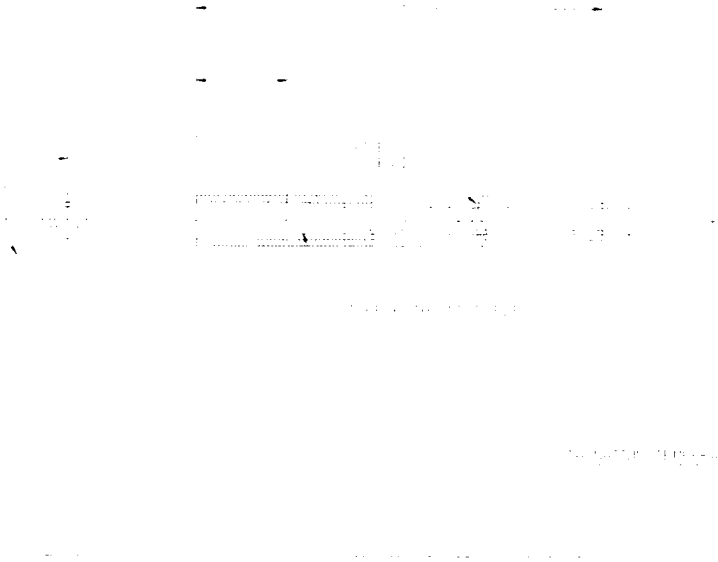

Figure A-6.—Stagnation Temperature Probe

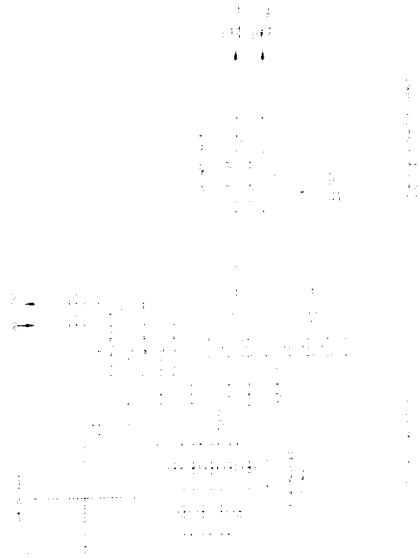

Figure A-7.—Sample Gas Extraction Schematic for Runs 1 & 2

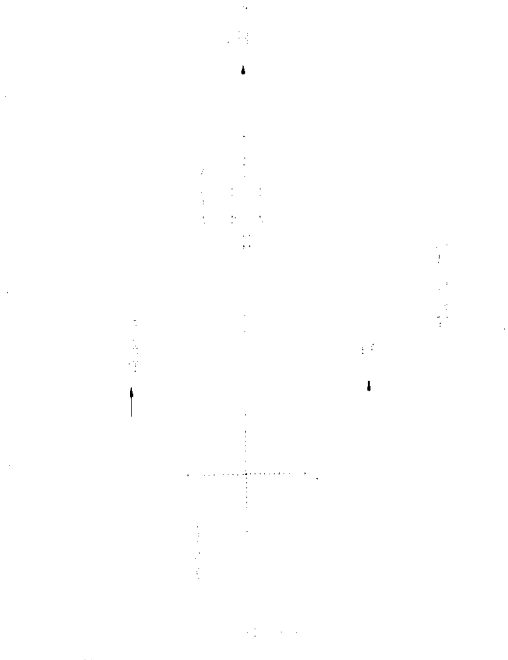

Figure A-8.—Sample Gas Extraction Schematic for Runs 3-14

APPENDIX B
Extractive Gas Sampling System and Smoke Meter

Kurt Loos and Dawn Noss
Dynac Engineering Company, Inc.

B.1. INTRODUCTION

Exhaust gases drawn through the sampling rakes were diverted to a gas bench containing an array of analyzers dedicated to examining the concentrations of specific gases contained in the sample stream. Similarly, smoke number values were acquired using a standard smoke meter.

B.2. INSTRUMENTATION

Extracted products of combustion were analyzed for levels of carbon dioxide (CO_2), carbon monoxide (CO), oxygen (O_2), nitric oxide (NO), oxides of nitrogen (NO_X), sulfur dioxide (SO_2), and unburned hydrocarbons (THC) as detected by a rack of gas analyzers. Provided by Rosemount Analytical, Inc. of La Habra, California, the Rosemount System consisted of seven individual instruments feeding from a single sample input line. Internal solenoid valves tied into a control panel and programmable logic controller served to distribute the flow through the necessary sample conditioning paths appropriate for each apparatus. Hot, wet, samples were directed to both the chemiluminescence analyzers for NO and NO_X detection and the THC analyzer that used flame ionization technology. For the remaining systems, the incoming sample was sent first through a refrigeration bath of a glycol / water mixture to lower the sample dew point to below 4.4 °C (40 °F). CO_2 and CO levels were determined through employing dedicated non-dispersive infrared systems while O_2 was measured using a paramagnetic detector system.

Prior to each test period, the Rosemount System was calibrated through the steady state data acquisition system, ESCORT. Using a direct connection which bypassed the sample line, nitrogen gas was passed through the entire gas bench for a period of six minutes to purge the lines of any residual gases and to serve as a zero gas for the analyzers. This process was repeated for all active ranges associated with each apparatus. Similarly, span gases of known species concentration were introduced for an up scale value. All gas concentrations were traceable to the National Institute of Standards and Technology (NIST) except for those used in calibrating the THC and SO_2 analyzers. No NIST certified standard gases were obtainable for this purpose. In lieu of standard information, the calibration gas supplier's statement of concentration was used for set-up purposes.

Four sampling rakes (see Appendix A) were each connected to individual electrically heated sampling lines of 0.635 cm diameter stainless steel maintained at 160 °C (320 °F) and plumbed to a heated valve and pump enclosure (HVPE). The HVPE contained directional valving and an array of five pumps (see Figure A-9).

To ensure that proper sample conditions were maintained for analyzer accuracy, pressure, temperature, and flow information were monitored through ESCORT. Temperature instrumentation existed at the exit of each sampling probe, at each junction of two heated lines, throughout the HVPE, and at the input location for both the Rosemount system and the smoke meter. The amount of sample gas received by the analyzers was displayed on meters within the control room. If the flow was insufficient for the entire gas bench to be run as a unit, sampling through the Rosemount System was taken by an appropriate combination of individual analyzers.

B.3. DATA ACQUISITION

Initially each probe was sampled to determine whether the engine emissions profile would prove to be symmetrical. Once symmetry was determined, the four arms were individually assigned to each research group. This allowed parallel sampling of the emissions. At no time was the sample gas shared by any of the analysis centers.

Species level output was sent from the individual Rosemount analyzers to the data system, ESCORT, where it was converted from milli-volts to appropriate engineering units based upon the calibration information specific to that test period. Real time updates of concentration values were displayed once per second for preliminary review. Additionally, a data reduction routine was incorporated into the ESCORT programming. Emission indices were also calculated

The gas sampling system used was designed and built by Rosemount Analytical, Inc. to continuously monitor aircraft turbine engine exhaust. The analyzers used in the system and their range capabilities were:

Analyzer	Operable Ranges	Calibration Concentrations	Calibration Gas Constituents	Analyzer Technology
CO_2-Rosemount Model 880	0-2500ppm	2000ppm	CO_2 in N_2	Non-Dispersive IR
	0-5%	4%		
	0-15%	12.90%		
CO-Rosemount Model 880	0-1%	0.79%	CO in N_2	Non-Dispersive IR
	0-5%	2.03%		
	0-10%	8.50%		
O_2-Rosemount Model 755	0-25%	20.90%	Air	Paramagnetic
NO_X-Rosemount Model 955	0-100ppm	92.3ppm	NO_X in N_2	Chemiluminescence
	0-1000ppm	764ppm		
NO-Rosemount Model 955	0-100ppm	92.2ppm	NO in N_2	Chemiluminescence
	0-1000ppm	763ppm		
SO_2-Rosemount Model ETL 9100	0-10ppm	7.28ppm	SO_2 in N_2	Electro-Optic Etalon
	0-100ppm			
THC-Rosemount Model 404	0-250ppm	70ppm	C_3H_8 in Air	Flame Ionization

The gas samples were passed through heated, smooth bore, stainless steel hoses to the sample distribution system. The sample distribution system was previously used at Arnold Engineering Development Center for the Atmospheric Effects of Aviation Project, and allows any combination of probe samples to be directed to the gas analyzer system. NASA's distribution system included five individually controlled vacuum pumps which raised the sample pressure above atmospheric. The pumps allowed the samples to be drawn into the analyzers from the test section.

The samples directed to the oxygen, oxides of carbon, and sulfur dioxide analyzers were sent through a glycol/water refrigeration bath where condensibles were removed and the sample dew point was lowered below 4.44 °C (40°F). The temperature and humidity of the samples directed to the oxides of nitrogen and hydrocarbon analyzers were maintained.

An SAE smoke meter was used as a qualitative measure of particles in the exhaust. The measurement was reported as smoke number.

APPENDIX C
NASA Engine Parameters and Emission Data

Changlie Wey
Dynacs Engineering Company, Inc.

Chowen Chou Wey
Army Research Lab./NASA LeRC

C.1. INTRODUCTION

Emissions measurements were performed in the mixed stream of engine core flow and fan by-pass air using a cruciform type sampling rake described in Appendix A. The tips of the sampling probes were 0.214 meter behind the engine exhaust nozzle. There are total of 36 gas sampling probes, 9 for each arm. Figure C-1 shows the position of the sampling probes relative to the engine exhaust nozzle. Heated stainless steel sampling tubes connect sampling probes to the heated pump box, which is located outside the chamber. The temperature of all the components of the sampling system downstream of the sampling probe was maintained at or above 176 °C.

Gaseous emissions in the engine exhaust were measured by an aircraft turbine engine exhaust analysis system. The system, described in Appendix B, is similar to a system that would be used for commercial aircraft engine emissions certification testing and therefore should provide reliable data for this study. Operation of the system followed the ICAO regulations[1].

Concentrations of CO_2, CO, O_2, NO, NO_x, SO_2, and total unburned hydrocarbon were measured. Fuel/air ratio, combustion efficiency and emission indices were calculated from the measured concentrations per the SAE ARP1533[2].

A smoke meter (ROSECO 473B) was used to measure smoke per ICAO standard. The reflectances of sampled filter paper were measured by a reflection densitometer and the result was recorded as smoke number.

Emissions data were obtained for all test conditions with engine power level ranging from idle to takeoff and altitudes ranging from sea level to 15 Km. The spatial profiles of the emissions were determined by drawing the gas samples from individual sample probes on the first two days. Based on the distributions, the three innermost sample probes from the engine centerline of each horizontal arm were ganged together for the gas analysis system for the rest of test.

---

[1] ICAO International and Recommended Practices ANNEX 16 as "Environmental Protection", Volume II – "Aircraft Engine Emissions", 1993

[2] SAE Aerospace Recommended Practice ARP1533, " Procedure for the Calculation of Gaseous Emissions from Aircraft Turbine Engines", 1996

C.2. RESULT

All emission data along with the engine parameters are presented in Tables C-1 through C-5. Operation parameters listed in these tables include simulated altitude (ALT), engine inlet pressure (PS1), dew point of inlet air (Dewp), combustor inlet pressure (P3) and temperature (T3), engine air flow rate (WA1), combustor air flow rate (WABURN), fuel flow rate (WFT). Fuel/Air ratio is determined from measured air flow and fuel flow. Concentrations of gaseous species and emissions indices (EI) are also listed.

NO and NO_x emission indices are plotted in Figures C-2 through C-7 for respective altitudes and displayed as functions of combustor inlet temperature, T_3. Figures C-8 through C-13 contain the same information as functions of combustor inlet pressure, P_3. It is obvious that NO_x emission indices have no dependency on fuel sulfur contents.

Figures C-14 through C-18 show the NO_x emission indices as a function of fuel flow for each fuel. Figures C-19 and C-20 show the NO_x emission indices as a function of T_3 and P_3 respectively in case of the high sulfur fuel. Compare these 2 plots with Figure C-15, one can conclude that NO_x emission indices have stronger dependency on T_3 and P_3 than that of fuel flow. Figure C-21 shows a typical comparison of the calculated fuel-air ratio by using emissions measurements and by using fuel flow measurements.

There are no SO_2 data obtained during the low sulfur fuel tests since the concentrations are below the detection limit. EI (SO_2) values are plotted in Figures C-22 through C-24 for respective fuels and displayed as functions of combustor inlet temperature, T_3. It shows no dependency on T_3.

Figure C-25 shows the smoke number versus altitude at a constant combustor inlet temperature. It shows that the smoke number decreases as the altitude increases. It can also be considered as the smoke number increases as the combustor inlet pressure increases.

Table C-1.—Summary of Fuel 1† Test Result

rdg	Date	Time	ALT	PlaPos	PS1	Dewp	P3	T3	WA1	WAb	WFT	FAR	CO2	CO	O2	NO_x	HC	NO	SO2	EICO	EIHC	EINOx	EINO	η_h%	SN
			m		kPa	°K	kPa	°K	kg/sec	kg/sec	kg/hr		%	%	%	ppm	ppm	ppm	ppm	SAE ARP1533					
404	8/15	3:18	9093	18.9	44.2	233.5	318.0	514.7	23.43	8.57	337.2	0.011	1.891	0.013	18.4	26.5	13.5	14.6	n/a	13.9	0.8	4.8	2.6	99.59	
408	8/15	4:12	16786	85.0	11.4	231.5	363.1	724.1	15.39	7.35	717.1	0.027	3.863	0.015	15.2	167.4	0.6	150.2	n/a	7.6	0.0	14.9	13.4	99.82	
409	8/15	4:14	16775	85.0	11.3	231.9	362.5	723.9	15.37	7.34	715.2	0.027	3.863	0.015	15.2	167.4	0.6	150.2	n/a	7.6	0.0	14.9	13.4	99.82	
412	8/15	4:26	15271	19.1	15.6	232.0	318.3	623.3	16.06	7.17	510.3	0.020	2.975	0.008	16.6	85.1	0.6	70.3	n/a	5.6	0.0	9.8	8.1	99.87	
413	8/15	4:27	15281	19.1	15.4	231.9	317.5	625.3	15.98	7.13	514.0	0.020	2.975	0.008	16.6	85.1	0.6	70.3	n/a	5.6	0.0	9.8	8.1	99.87	
418	8/15	4:47	15251	67.3	14.8	231.3	406.4	673.0	18.61	8.62	726.8	0.023	3.420	0.006	15.9	133.8	0.5	113.7	n/a	3.6	0.0	13.4	11.4	99.91	
419	8/15	4:48	15247	67.3	14.9	231.4	403.1	671.6	18.64	8.58	720.3	0.023	3.420	0.006	15.9	133.8	0.5	113.7	n/a	3.6	0.0	13.4	11.4	99.91	
422	8/15	5:02	15229	85.1	14.4	231.4	457.6	711.7	19.62	9.36	874.5	0.026	3.716	0.006	15.4	176.0	0.4	152.3	n/a	3.1	0.0	16.3	14.1	99.93	
423	8/15	5:03	15218	85.1	14.5	231.5	459.4	711.6	19.73	9.41	878.1	0.026	3.716	0.006	15.4	176.0	0.4	152.3	n/a	3.1	0.0	16.3	14.1	99.93	
427	8/15	5:24	12207	19.0	26.6	230.7	317.0	532.9	19.69	8.02	403.0	0.014	2.227	0.009	17.8	40.0	3.6	26.4	n/a	8.0	0.2	6.1	4.0	99.79	
428	8/15	5:25	12203	19.1	26.6	231.0	316.9	533.6	19.68	8.02	402.1	0.014	2.227	0.009	17.8	40.0	3.6	26.4	n/a	8.0	0.2	6.1	4.0	99.79	
432	8/15	5:41	12194	54.2	25.1	231.0	504.4	617.3	25.95	11.39	786.7	0.019	2.878	n/a	16.8	96.5	0.4	78.4	n/a	n/a	0.0	11.5	9.3	n/a	
433	8/15	5:49	12197	53.0	25.6	231.1	501.2	617.4	25.85	11.37	771.9	0.019	2.849	n/a	16.8	94.5	0.4	76.3	n/a	n/a	0.0	11.4	9.2	n/a	
436	8/15	5:57	12195	66.3	24.0	230.6	644.5	672.4	29.90	13.75	1107.7	0.022	3.332	n/a	16.0	158.1	0.4	133.1	n/a	n/a	0.0	16.3	13.7	n/a	
437	8/15	6:02	12199	65.6	24.1	230.2	633.3	671.8	29.45	13.55	1079.3	0.022	3.312	n/a	16.1	156.5	0.4	130.7	n/a	n/a	0.0	16.2	13.6	n/a	
439	8/15	6:17	12187	84.9	23.3	230.8	739.5	719.6	31.74	15.12	1373.0	0.025	3.661	n/a	15.5	227.9	0.8	187.5	n/a	n/a	0.0	21.5	17.7	n/a	
440	8/15	6:21	12180	84.8	23.2	230.2	737.4	719.7	31.57	15.08	1366.0	0.025	3.663	n/a	15.5	227.2	0.8	186.9	n/a	n/a	0.0	21.4	17.6	n/a	
447	8/16	2:22	9106	18.9	43.6	264.2	317.8	556.9	22.30	8.26	351.8	0.012	2.080	0.011	18.1	29.1	3.1	24.4	n/a	11.0	0.2	4.8	4.0	99.72	
451	8/16	2:54	3157	19.1	99.0	264.1	486.6	496.6	40.92	13.59	460.3	0.009	1.601	0.020	18.9	20.3	26.0	9.1	n/a	24.6	1.9	4.3	1.9	99.23	
452	8/16	2:59	3163	19.1	98.7	264.0	482.9	497.5	40.71	13.48	461.4	0.010	1.618	0.019	18.8	20.6	25.3	7.8	n/a	24.2	1.8	4.3	1.6	99.25	2.3
453	8/16	3:04	3157	19.1	98.9	264.2	482.2	498.6	40.42	13.49	463.0	0.010	1.622	0.019	18.8	20.5	24.8	7.7	n/a	23.6	1.8	4.3	1.6	99.27	

† Fuel 1: low sulfer fuel with corrosion inhibitor

Table C-1.—Summary of Fuel 1† Test Result (Continued)

454	8/16	3:11	3152	36.4	95.7	264.1	1039.7	618.0	61.70	24.93	1347.1	0.015	2.280	0.002	17.8	81.0	1.8	72.1	n/a	1.6	0.1	12.2	10.8	99.95	
455	8/16	3:18	3155	36.4	95.5	264.1	1044.1	619.2	61.77	25.05	1343.7	0.015	2.342	0.003	17.6	80.3	0.8	68.9	n/a	2.5	0.0	11.7	10.1	99.94	
456	8/16	3:22	3150	36.4	95.5	264.2	1043.5	619.5	61.60	25.07	1342.7	0.015	2.341	0.002	17.7	80.9	0.7	69.1	n/a	1.3	0.0	11.8	10.1	99.97	
457	8/16	3:24	3154	45.7	93.1	264.1	1368.9	672.4	72.41	30.88	2015.9	0.018	2.690	0.003	17.1	100.3	0.8	97.9	n/a	2.0	0.0	12.8	12.5	99.95	12.9
458	8/16	3:29	3157	45.7	93.5	264.2	1379.6	672.7	72.78	31.13	2024.3	0.018	2.774	0.002	16.9	159.6	0.7	140.9	n/a	1.6	0.0	19.8	17.4	99.96	
459	8/16	3:35	3157	45.7	93.2	264.1	1375.7	673.2	72.44	31.05	2020.7	0.018	2.768	0.003	17.0	159.8	0.6	139.0	n/a	2.3	0.0	19.8	17.2	99.94	
460	8/16	3:40	3164	56.9	90.6	264.2	1699.8	716.9	82.51	36.59	2758.6	0.021	3.159	0.003	16.3	269.7	0.7	229.9	n/a	1.9	0.0	29.4	25.0	99.95	
463	8/16	3:52	3159	56.9	90.5	264.3	1694.1	717.3	82.16	36.47	2747.1	0.021	3.154	0.001	16.3	272.3	0.6	240.4	n/a	0.9	0.0	29.7	26.2	99.98	
464	8/16	3:59	3160	56.9	90.6	264.1	1696.6	717.7	82.38	36.47	2751.4	0.021	3.162	0.002	16.3	270.7	0.6	237.8	n/a	1.1	0.0	29.5	25.9	99.97	
465	8/16	4:04	3149	85.1	84.5	264.3	2311.2	795.5	98.89	46.23	4376.3	0.026	3.894	0.002	15.1	484.6	0.8	414.8	n/a	1.0	0.0	43.1	36.9	99.97	
466	8/16	4:12	3163	85.1	84.4	264.3	2306.4	795.8	98.87	46.16	4367.3	0.026	3.891	0.004	15.1	485.4	0.9	410.3	n/a	2.0	0.0	43.2	36.5	99.95	
467	8/16	4:22	3161	19.2	98.8	264.4	483.8	503.7	40.36	13.45	464.7	0.010	1.646	0.018	18.8	20.2	22.0	9.1	n/a	22.5	1.6	4.2	1.9	99.31	
470	8/16	5:53	9103	19.3	43.8	264.8	318.4	499.8	23.76	8.75	335.6	0.011	1.787	0.022	18.5	20.4	24.0	11.0	n/a	24.4	1.6	3.9	2.1	99.27	
472	8/16	5:58	9105	19.3	43.6	264.8	317.2	499.0	23.69	8.73	335.6	0.011	1.790	0.023	18.5	20.0	24.0	9.8	n/a	26.4	1.6	3.8	1.9	99.22	
473	8/16	6:04	9104	45.7	41.4	265.0	656.5	616.9	35.72	15.31	956.1	0.017	2.703	0.005	17.1	90.9	0.7	77.1	n/a	3.4	0.0	11.6	9.8	99.92	
474	8/16	6:14	9103	45.8	41.3	265.3	657.3	615.3	35.72	15.33	951.4	0.017	2.720	0.006	17.0	89.5	1.1	75.4	n/a	4.2	0.1	11.3	9.6	99.90	
475	8/16	6:24	9109	57.4	39.4	265.0	857.9	671.1	41.83	18.79	1396.5	0.021	3.243	0.004	16.2	163.4	0.4	141.7	n/a	2.3	0.0	17.4	15.1	99.95	
476	8/16	6:25	9110	57.7	39.4	265.1	863.0	671.9	41.97	18.87	1405.8	0.021	3.243	0.004	16.2	163.4	0.4	141.7	n/a	2.3	0.0	17.4	15.1	99.95	
477	8/16	6:32	9104	67.5	37.9	265.2	1036.8	716.5	46.69	21.70	1834.3	0.024	3.482	0.003	15.8	244.1	0.4	208.1	n/a	1.8	0.0	24.3	20.7	99.96	
478	8/16	6:35	9107	67.5	37.8	265.1	1038.0	717.3	46.64	21.74	1837.4	0.024	3.482	0.004	15.8	243.3	1.5	212.0	n/a	2.3	0.1	24.2	21.1	99.94	
479	8/16	6:39	9102	66.5	37.9	265.3	1023.1	717.6	46.23	21.41	1804.6	0.023	3.477	0.003	15.8	241.5	0.6	209.5	n/a	1.6	0.0	24.1	20.9	99.96	
480	8/16	6:42	9103	85.0	36.8	265.3	1163.0	759.1	48.90	23.43	2205.1	0.026	3.841	0.005	15.2	321.4	0.6	278.9	n/a	2.4	0.0	29.1	25.2	99.94	
481	8/16	6:49	9102	85.0	36.7	265.2	1158.1	757.8	48.83	23.39	2192.9	0.026	3.826	0.005	15.2	320.5	0.6	275.9	n/a	2.4	0.0	29.1	25.1	99.94	
482	8/16	6:54	9112	44.9	41.4	265.3	642.8	616.2	35.04	14.98	912.0	0.017	2.612	0.005	17.2	86.2	0.4	71.7	N/a	3.7	0.0	11.4	9.5	99.91	

Fuel 1: low sulfer fuel with corrosion inhibitor

Table C-2.—Summary of Fuel 2‡ Test Result

rdg	Date	Time	ALT	PlaPos	PS1	Dewp	P3	T3	WA1	WAb	WFT	FAR	CO2	CO	O2	NO_x	HC	NO	SO2	EICO	EIHC	EINOx	EINO	η_b,%	SN
			m		kPa	°K	kPa	°K	kg/sec	kg/sec	kg/hr		%	%	%	ppm	ppm	ppm	ppm	SAE ARP1533					
500	8/22	0:44	12230	19.2	26.9	234.2	321.4	536.0	19.92	8.01	409.9	0.014	1.999	0.007	17.4	34.4	6.1	26.8	0.03	7.2	0.4	5.9	4.6	99.79	
502	8/22	0:52	12227	54.8	25.1	233.6	510.6	615.9	26.10	11.36	796.6	0.020	2.791	0.003	16.3	94.1	3.2	80.6	0.04	2.1	0.1	11.5	9.9	99.94	
503	8/22	1:09	12226	53.6	25.3	233.5	504.9	617.2	25.88	11.27	779.1	0.019	2.773	0.003	16.4	90.4	3.1	76.7	0.07	2.1	0.1	11.2	9.5	99.94	
506	8/22	1:18	12237	67.1	23.7	233.3	646.4	672.4	29.83	13.58	1111.5	0.023	3.207	0.002	15.8	148.1	3.1	130.8	0.13	1.5	0.1	15.9	14.0	99.95	
507	8/22	1:27	12222	67.1	23.7	233.1	647.8	672.1	29.92	13.62	1113.3	0.023	3.223	0.002	15.8	149.8	3.0	131.8	0.00	1.5	0.1	16.0	14.0	99.95	
508	8/22	1:32	12245	85.4	23.0	233.1	729.1	709.9	31.47	14.80	1338.4	0.025	3.604	0.003	15.2	206.9	3.0	179.6	0.01	1.5	0.1	19.8	17.2	99.95	
509	8/22	1:45	12237	85.4	23.1	232.6	731.8	709.7	31.62	14.85	1340.0	0.025	3.621	0.003	15.2	207.5	3.0	178.4	0.00	1.5	0.1	19.7	17.0	99.95	
513	8/22	2:05	15196	19.2	15.9	232.5	318.2	625.9	16.16	7.05	518.9	0.020	2.628	0.005	16.6	77.5	3.5	65.9	0.11	3.8	0.2	10.1	8.6	99.90	
515	8/22	2:25	15191	65.5	15.4	232.2	405.8	671.5	18.82	8.52	718.8	0.023	3.005	0.004	16.1	116.4	3.5	100.1	0.15	2.8	0.1	13.3	11.4	99.92	
517	8/22	2:34	15172	65.8	15.1	231.9	402.7	672.3	18.62	8.45	713.1	0.023	3.000	0.004	16.1	115.1	3.5	98.6	0.08	2.7	0.1	13.2	11.3	99.92	
518	8/22	2:38	15184	85.3	14.6	231.8	465.1	715.8	19.83	9.33	888.5	0.026	3.483	0.005	15.4	165.4	3.1	144.1	0.02	2.9	0.1	16.3	14.2	99.92	
519	8/22	2:45	15185	85.3	14.6	231.9	464.6	715.6	19.80	9.34	885.1	0.026	3.477	0.005	15.4	166.3	3.1	144.5	0.00	2.8	0.1	16.4	14.3	99.92	
520	8/22	2:56	16775	84.6	11.6	231.5	369.2	714.5	15.72	7.38	724.9	0.027	3.149	0.006	15.9	131.7	3.5	114.2	0.00	4.1	0.1	14.3	12.4	99.89	
522	8/22	3:00	16824	84.6	11.2	231.5	357.5	716.2	15.18	7.16	700.5	0.027	3.086	0.006	16.0	129.9	3.5	113.0	0.00	4.2	0.1	14.4	12.6	99.89	
525	8/22	3:23	9105	18.7	43.6	231.9	317.2	502.6	23.56	8.50	332.1	0.011	1.469	0.010	18.2	18.2	20.5	10.4	0.00	13.9	1.7	4.2	2.4	99.51	
526	8/22	3:32	9107	18.6	43.5	231.7	317.1	501.2	23.56	8.51	332.7	0.011	1.539	0.011	18.2	18.8	22.4	9.3	0.03	14.0	1.7	4.1	2.1	99.50	
527	8/22	3:36	9105	18.6	43.5	231.9	317.3	501.4	23.64	8.49	333.7	0.011	1.540	0.011	18.2	18.8	22.8	9.1	0.00	14.1	1.8	4.1	2.0	99.49	
528	8/22	3:45	9101	46.1	41.3	231.4	661.9	618.5	35.55	15.01	965.3	0.018	2.670	0.002	16.6	96.0	3.2	77.7	0.00	1.6	0.1	12.3	10.0	99.95	
529	8/22	3:49	9104	45.1	41.4	231.2	643.8	616.4	34.84	14.66	927.2	0.018	2.607	0.002	16.7	89.4	3.2	72.2	0.00	1.8	0.2	11.7	9.5	99.94	
530	8/22	3:58	9104	57.0	39.6	231.7	852.1	672.5	41.45	18.22	1381.6	0.021	3.112	0.002	16.0	167.7	3.1	136.7	n/a	1.2	0.1	18.5	15.1	99.96	
531	8/22	3:59	9106	57.1	39.6	231.6	852.9	672.8	41.41	18.22	1383.0	0.021	3.118	0.002	16.0	167.7	3.1	137.5	n/a	1.2	0.1	18.5	15.1	99.96	
532	8/22	4:02	9099	57.1	39.5	231.1	854.4	673.6	41.44	18.26	1388.1	0.021	3.117	0.002	16.0	168.9	3.1	138.1	n/a	1.1	0.1	18.6	15.2	99.96	

Fuel 2 : low sulfur fuel with corrosion inhibitor, conductivity additive and icing inhibitor

Table C-2.—Summary of Fuel 2‡ Test Result (Continued)

533	8/22	4:07	9116	66.7	37.8	231.5	1020.8	716.7	45.97	20.91	1802.0	0.024	3.526	0.002	15.4	243.3	3.1	200.8	n/a	1.0	0.1	23.7	19.6	99.97
534	8/22	4:18	9110	66.6	37.8	231.0	1022.2	716.7	45.90	20.91	1798.8	0.024	3.512	0.002	15.4	243.8	3.0	200.0	n/a	1.0	0.1	23.9	19.6	99.97
535	8/22	4:24	9103	85.0	37.0	231.2	1169.2	759.4	49.07	23.06	2208.1	0.027	3.891	0.002	14.8	324.5	3.0	265.1	0.00	1.1	0.1	28.8	23.5	99.96
536	8/22	4:29	9110	85.0	37.0	231.2	1169.4	759.0	49.10	23.05	2207.8	0.027	3.885	0.002	14.8	330.4	3.0	280.9	0.00	1.1	0.1	29.3	24.9	99.97
537	8/22	4:35	9107	85.0	36.9	230.8	1166.8	759.0	48.97	23.00	2199.7	0.027	3.879	0.002	14.8	324.6	3.0	279.9	n/a	1.1	0.1	28.9	24.9	99.96
542	8/22	5:23	3172	19.2	98.5	227.9	482.9	489.6	40.42	13.13	446.7	0.009	1.406	0.012	18.3	18.4	32.4	8.2	0.03	17.7	2.7	4.4	2.0	99.31
544	8/22	5:34	3160	19.3	99.0	227.1	482.1	460.8	40.74	13.55	459.2	0.009	1.432	0.011	18.3	19.2	29.8	6.4	0.00	16.2	2.5	4.5	1.5	99.37
545	8/22	5:40	3161	19.3	99.0	226.9	480.9	468.3	40.87	13.48	460.3	0.010	1.443	0.011	18.3	19.2	30.7	6.2	0.03	16.1	2.5	4.5	1.5	99.37
546	8/22	5:45	3145	36.9	95.2	226.7	1075.2	616.6	63.60	25.28	1396.3	0.015	2.276	0.002	17.1	83.4	3.6	70.9	0.04	1.4	0.2	12.5	10.6	99.95
549	8/22	5:56	3164	37.2	95.2	226.7	1086.6	616.9	63.95	25.49	1407.5	0.015	2.314	0.002	17.1	84.6	3.2	71.0	0.00	1.3	0.2	12.5	10.5	99.95
550	8/22	6:01	3161	47.8	92.3	226.9	1456.3	672.1	76.17	32.07	2174.6	0.019	2.790	0.001	16.4	174.3	3.2	151.1	0.09	0.9	0.1	21.4	18.5	99.97
551	8/22	6:09	3158	47.8	92.4	227.2	1460.6	671.8	76.15	32.16	2178.6	0.019	2.777	0.001	16.4	173.3	3.1	149.8	0.01	0.9	0.1	21.4	18.5	99.97
552	8/22	6:12	3157	59.0	89.2	227.3	1804.0	717.3	87.08	37.95	3000.2	0.022	3.223	0.001	15.7	288.5	3.3	255.4	n/a	0.7	0.1	30.7	27.2	99.97
553	8/22	6:22	3161	58.7	89.2	227.3	1802.4	716.3	86.88	37.93	2987.1	0.022	3.212	0.001	15.7	286.6	3.4	254.5	n/a	0.8	0.1	30.6	27.2	99.97
554	8/22	6:27	3161	85.1	83.4	227.2	2366.6	787.9	101.40	46.68	4518.4	0.027	3.922	0.002	14.6	485.9	3.6	430.5	n/a	0.8	0.1	42.8	37.9	99.97
555	8/22	6:31	3164	85.1	83.5	227.2	2369.3	788.2	101.51	46.81	4524.3	0.027	3.929	0.001	14.6	489.5	3.6	431.6	0.01	0.7	0.1	43.0	37.9	99.97

Fuel 2 : low sulfur fuel with corrosion inhibitor, conductivity additive and icing inhibitor

Table C-3.—Summary of Fuel 3* Test Result

rdg	Date	Time	ALT	Pla_Pos	PS1	Dewp	P3	T3	WA1	WA36	WFT	FAR	CO2	CO	O2	NO_x	HC	NO	SO2	EICO	EIHC	EINOx	EINO	η_b,%	EISO2	SN
			m		kPa	°K	kPa	°K	kg/sec	kg/sec	kg/hr		%	%	%	ppm	ppm	ppm	ppm	SAE ARP1533						
569	8/25	23:45	12197	19.2	26.8	235.7	318.8	537.1	19.71	7.95	398.4	0.014	1.688	0.008	18.0	28.5	4.2	21.5	7.65	9.5	0.3	5.7	4.3	99.75	2.16	
572	8/26	0:02	12215	19.2	26.6	235.1	319.3	534.6	19.79	7.98	400.8	0.014	1.687	0.008	18.0	28.4	4.7	20.7	6.75	9.7	0.3	5.7	4.2	99.74	1.91	
573	8/26	0:13	12202	54.0	25.3	235.0	508.3	617.7	26.06	11.40	772.9	0.019	2.512	0.004	16.8	84.6	1.0	73.3	11.13	3.5	0.1	11.5	10.0	99.91	2.11	
574	8/26	0:22	12205	53.9	25.1	234.7	503.4	616.6	25.80	11.28	761.6	0.019	2.494	0.004	16.8	82.8	1.1	71.2	11.22	3.5	0.1	11.4	9.8	99.91	2.15	
575	8/26	0:30	12213	53.9	25.3	234.3	506.0	615.8	26.03	11.38	766.2	0.019	2.497	0.004	16.8	82.5	1.2	70.7	11.30	3.4	0.1	11.3	9.7	99.91	2.16	
576	8/26	0:37	12208	66.7	23.8	234.2	646.8	673.0	30.00	13.65	1090.5	0.022	2.926	0.004	16.2	135.1	1.1	122.0	12.67	2.6	0.0	15.8	14.3	99.94	2.06	
577	8/26	0:40	12214	67.3	23.7	234.2	648.7	673.2	30.04	13.71	1095.7	0.022	2.904	0.004	16.2	134.4	1.1	120.8	13.02	2.6	0.1	15.9	14.2	99.93	2.13	
579	8/26	0:54	12213	65.9	24.0	234.1	638.9	671.8	29.72	13.51	1072.3	0.022	3.013	0.004	16.1	139.5	0.7	123.2	10.36	2.6	0.0	15.9	14.0	99.94	1.64	
580	8/26	1:00	12202	84.8	23.1	233.8	734.2	715.4	31.58	14.92	1325.3	0.025	3.482	0.004	15.4	198.7	0.5	182.5	14.87	2.4	0.0	19.6	18.0	99.94	2.04	
581	8/26	1:07	12204	84.9	23.1	233.9	734.8	714.7	31.59	14.94	1324.5	0.025	3.473	0.004	15.4	201.3	0.5	182.8	14.55	2.4	0.0	19.9	18.1	99.94	2.01	
582	8/26	1:09	12214	84.9	23.2	233.9	737.6	714.3	31.71	15.00	1326.2	0.025	3.483	0.004	15.4	201.0	0.5	182.1	14.58	2.4	0.0	19.8	18.0	99.94	2.00	
583	8/26	1:17	12201	19.0	26.6	233.8	318.0	541.1	19.54	7.90	394.2	0.014	1.750	0.008	17.9	29.3	4.4	23.1	6.91	9.3	0.3	5.7	4.5	99.75	1.88	
585	8/26	1:30	15174	19.0	15.8	233.3	322.6	629.8	16.32	7.14	520.5	0.020	2.187	0.005	17.3	67.2	1.6	57.8	8.24	5.0	0.1	10.5	9.0	99.87	1.79	
587	8/26	1:36	15188	19.0	15.9	233.3	324.5	630.4	16.34	7.17	521.9	0.020	2.037	0.005	17.5	59.7	1.0	52.4	9.02	5.0	0.1	10.0	8.8	99.88	2.10	
588	8/26	1:47	15171	66.4	15.1	233.3	405.5	674.1	18.70	8.55	708.6	0.023	2.409	0.005	17.0	92.9	0.9	82.8	9.10	4.1	0.0	13.2	11.7	99.90	1.80	
590	8/26	1:53	15174	65.8	15.2	233.1	403.8	672.5	18.68	8.52	701.9	0.023	2.378	0.005	17.0	90.3	1.0	80.7	9.17	4.0	0.1	13.0	11.6	99.90	1.83	
591	8/26	1:57	15173	85.0	14.6	233.0	465.3	716.1	19.86	9.39	875.5	0.026	2.989	0.006	16.1	140.3	0.8	126.7	11.31	3.9	0.0	16.1	14.5	99.91	1.80	
592	8/26	2:02	15194	85.0	14.6	232.9	466.2	716.2	19.90	9.43	873.5	0.026	2.993	0.006	16.1	141.3	0.9	127.5	10.83	3.8	0.0	16.2	14.6	99.91	1.72	
593	8/26	2:04	15195	85.0	14.6	233.0	465.0	716.0	19.80	9.39	869.8	0.026	2.839	0.005	16.3	127.9	1.0	118.2	13.13	3.8	0.0	15.4	14.3	99.91	2.20	
594	8/26	2:14	16766	85.0	11.5	232.7	367.0	718.8	15.58	7.38	710.8	0.027	2.652	0.007	16.6	108.5	1.0	99.4	9.60	5.2	0.0	14.0	12.8	99.87	1.72	
596	8/26	2:20	16743	85.0	11.2	232.5	357.9	719.1	15.15	7.20	689.8	0.027	2.721	0.007	16.5	111.1	1.0	103.4	11.13	5.2	0.0	14.0	13.0	99.87	1.95	

Fuel 3: high sulfur fuel with corrosion inhibitor

Table C-3.—Summary of Fuel 3* Test Result (Continued)

598	8/26	2:54	9117	18.8	43.9	232.7	319.8	500.7	23.85	8.64	329.4	0.011	1.427	0.011	18.3	17.3	20.4	11.5	5.87	15.7	1.7	4.1	2.7	99.46	1.95	
599	8/26	2:56	9117	18.8	43.9	232.6	320.0	500.7	23.87	8.63	330.4	0.011	1.423	0.011	18.3	17.8	22.3	10.3	4.99	16.0	1.9	4.2	2.4	99.44	1.66	
600	8/26	3:05	9115	45.4	41.9	232.4	657.1	616.6	35.62	15.04	929.4	0.017	2.544	0.004	16.8	85.2	0.8	74.6	10.61	2.9	0.0	11.5	10.0	99.93	1.98	
601	8/26	3:10	9124	45.4	41.7	232.5	655.7	616.8	35.47	14.99	924.8	0.017	2.544	0.004	16.8	84.9	0.7	73.8	10.49	3.0	0.0	11.4	9.9	99.93	1.96	
602	8/26	3:14	9118	45.4	41.6	232.6	653.6	616.7	35.38	14.95	924.3	0.017	2.539	0.004	16.8	84.3	0.6	73.2	10.42	2.9	0.0	11.4	9.9	99.93	1.96	
603	8/26	3:18	9118	56.9	39.8	232.3	856.5	672.2	41.66	18.39	1364.5	0.021	3.067	0.003	16.0	161.5	0.6	144.3	14.33	2.1	0.0	18.1	16.1	99.95	2.23	
605	8/26	3:29	9114	57.4	39.7	232.1	863.3	673.0	41.90	18.54	1376.5	0.021	3.070	0.003	16.0	162.4	0.5	144.6	14.70	2.1	0.0	18.1	16.2	99.95	2.29	
606	8/26	3:44	9120	67.0	38.1	232.1	1033.5	717.0	46.49	21.28	1783.6	0.023	3.448	0.003	15.4	236.9	0.5	212.9	16.29	1.8	0.0	23.6	21.2	99.96	2.26	
607	8/26	3:52	9117	67.0	38.1	232.3	1034.2	717.5	46.51	21.27	1782.7	0.023	3.450	0.003	15.4	227.4	0.4	212.3	15.84	1.8	0.0	22.7	21.2	99.96	2.20	
608	8/26	3:57	9118	67.0	38.1	232.0	1035.7	718.0	46.54	21.32	1783.6	0.023	3.449	0.003	15.4	218.6	0.4	212.1	15.56	1.9	0.0	21.8	21.1	99.95	2.16	
609	8/26	4:04	9122	85.2	37.0	232.2	1167.8	760.8	48.94	23.14	2161.9	0.026	3.125	0.003	15.6	544.7	0.1	726.1	12.67	2.0	0.0	59.8	79.7	99.95	1.94	
611	8/26	4:15	9121	85.2	36.9	231.9	1166.7	760.6	49.01	23.15	2160.4	0.026	3.877	0.004	14.8	325.7	0.3	294.9	17.10	1.8	0.0	29.0	26.2	99.96	2.12	
613	8/26	4:22	9121	85.2	36.9	231.7	1167.4	761.3	48.92	23.13	2161.5	0.026	3.871	0.004	14.8	329.8	0.3	292.9	16.67	1.8	0.0	29.4	26.1	99.96	2.06	
622	8/26	23:44	3196	19.0	97.4	256.2	475.8	494.4	40.29	13.08	449.6	0.010	1.438	0.010	18.3	19.5	27.9	8.8	6.20	14.3	2.3	4.6	2.1	99.43	2.03	0.0
623	8/26	23:53	3202	19.0	99.0	256.5	481.6	493.8	40.93	13.28	450.8	0.009	1.470	0.010	18.4	19.4	29.5	8.1	6.17	14.0	2.4	4.5	1.9	99.43	1.99	0.0
624	8/26	23:57	3191	29.6	97.1	256.6	797.3	564.0	53.94	20.08	879.8	0.012	1.844	0.002	17.8	40.8	4.1	33.2	8.48	2.6	0.3	7.6	6.2	99.91	2.18	
625	8/27	0:03	3193	29.4	97.1	256.7	781.4	560.0	53.41	19.76	853.0	0.012	1.823	0.002	17.8	39.9	3.8	31.3	8.56	2.7	0.3	7.5	5.9	99.91	2.22	
627	8/27	0:07	3200	29.4	97.2	256.7	782.4	560.0	53.48	19.79	853.4	0.012	1.809	0.003	17.8	40.0	3.8	31.5	8.46	2.8	0.3	7.6	6.0	99.91	2.22	
628	8/27	0:13	3220	37.1	95.4	257.0	1075.2	616.3	63.41	25.37	1362.4	0.015	2.231	0.001	17.1	80.6	2.0	70.9	10.79	0.9	0.1	12.4	10.9	99.97	2.30	
629	8/27	0:17	3198	37.1	95.4	257.1	1084.1	616.8	63.84	25.50	1375.7	0.015	2.228	0.001	17.1	81.4	2.0	71.4	11.07	0.9	0.1	12.5	11.0	99.97	2.36	
630	8/27	0:20	3208	37.1	95.4	257.1	1082.8	616.7	63.60	25.47	1374.3	0.015	2.221	0.001	17.1	81.5	1.9	71.3	11.18	0.9	0.1	12.6	11.0	99.97	2.40	
631	8/27	0:33	3174	48.0	92.5	257.5	1462.7	673.2	76.34	32.24	2136.9	0.018	2.808	0.001	16.4	172.1	1.7	155.9	13.62	0.4	0.1	21.0	19.1	99.98	2.31	20.6
632	8/27	0:34	3217	48.0	92.5	257.4	1464.1	673.3	76.42	32.29	2137.7	0.018	2.810	0.001	16.4	171.5	1.7	155.6	13.57	0.5	0.1	20.9	19.0	99.98	2.31	
633	8/27	0:36	3211	59.3	89.4	257.5	1807.6	717.9	86.83	38.02	2928.4	0.021	3.233	0.001	15.8	286.7	1.8	259.6	15.31	0.4	0.1	30.5	27.6	99.98	2.26	

Fuel 3: high sulfur fuel with corrosion inhibitor

Table C-3.—Summary of Fuel 3* Test Result (Continued)

635	8/27	0:45	3180	58.7	89.5	257.6	1794.3	716.8	86.54	37.85	2894.4	0.021	3.199	0.001	15.8	284.2	1.8	257.0	15.39	0.4	0.1	30.6	27.6	99.98	2.31	20.6
636	8/27	0:52	3220	85.1	83.5	257.9	2366.6	787.6	101.16	46.80	4397.7	0.026	3.939	0.001	14.7	470.4	2.0	428.5	16.80	0.5	0.1	41.3	37.6	99.98	2.05	
637	8/27	0:54	3171	85.0	84.1	257.8	2371.9	789.3	101.73	47.13	4407.6	0.026	3.946	0.001	14.6	476.0	2.4	433.0	16.06	0.5	0.1	41.7	37.9	99.98	1.96	
640	8/27	2:33	10618	19.1	34.6	234.1	318.8	502.3	22.07	8.43	356.1	0.012	1.696	0.009	17.7	19.8	19.5	13.5	6.53	10.6	1.4	4.0	2.7	99.62	1.82	
642	8/27	2:47	10630	19.1	34.7	233.9	318.2	501.5	22.10	8.43	355.7	0.012	1.529	0.009	18.2	19.5	20.8	11.4	6.27	11.9	1.6	4.3	2.5	99.56	1.94	8.8
643	8/27	2:53	10614	65.0	30.6	233.9	797.3	673.3	37.31	16.94	1324.7	0.022	3.231	0.002	15.9	164.6	2.5	144.3	13.90	1.0	0.1	17.5	15.3	99.97	2.05	
645	8/27	3:01	10616	64.9	30.5	233.9	793.7	673.6	37.03	16.84	1315.9	0.022	3.033	0.002	16.0	163.3	2.0	143.0	13.07	1.1	0.1	18.5	16.2	99.97	2.07	14.9
646	8/27	3:05	10646	84.9	29.4	232.8	931.1	721.0	40.00	18.92	1676.9	0.025	3.614	0.002	15.1	245.1	1.9	213.6	14.14	1.0	0.1	23.4	20.4	99.97	1.87	
648	8/27	3:11	10618	84.9	29.4	233.1	931.2	720.2	40.07	18.92	1671.5	0.025	3.659	0.002	15.1	244.1	1.9	211.4	13.77	1.0	0.1	23.0	19.9	99.97	1.80	
650	8/27	3:29	15180	18.9	16.1	232.8	324.3	625.7	16.48	7.23	519.3	0.020	2.200	0.004	17.2	65.3	3.0	55.3	9.82	3.2	0.2	10.1	8.6	99.91	2.13	
652	8/27	3:39	15173	18.9	16.1	232.7	325.1	618.6	16.62	7.29	514.9	0.020	2.238	0.004	17.3	60.9	2.8	51.4	9.54	3.2	0.2	9.3	7.8	99.91	2.03	
653	8/27	3:42	15174	68.0	15.2	232.1	419.5	672.5	19.30	8.83	741.2	0.023	2.501	0.003	16.8	99.3	2.8	87.0	11.32	2.5	0.1	13.6	11.9	99.93	2.15	
655	8/27	3:53	15208	68.1	15.4	232.1	426.6	675.8	19.53	8.98	749.8	0.023	2.573	0.003	16.6	105.6	2.4	92.3	11.94	2.4	0.1	14.0	12.3	99.93	2.21	4.5
656	8/27	3:56	15168	84.9	14.9	231.4	473.4	709.8	20.39	9.62	885.0	0.026	2.847	0.004	16.2	136.6	2.3	120.2	12.45	2.5	0.1	16.4	14.5	99.93	2.08	
658	8/27	4:01	15167	84.9	14.9	232.2	473.7	710.6	20.33	9.59	886.3	0.026	2.781	0.004	16.2	136.3	2.3	121.3	12.87	2.6	0.1	16.8	14.9	99.93	2.20	
659	8/27	4:04	15159	84.9	15.1	232.0	480.3	710.2	20.62	9.77	890.5	0.025	2.924	0.003	16.2	137.7	2.4	122.0	12.83	2.4	0.1	16.1	14.3	99.93	2.10	
660	8/27	4:13	16795	18.8	11.4	232.3	325.8	685.3	14.65	6.77	599.2	0.025	2.322	0.004	17.0	84.7	2.3	73.8	10.42	3.6	0.1	12.5	10.9	99.90	2.14	
661	8/27	4:15	16788	18.8	11.4	232.0	325.5	686.0	14.62	6.76	600.1	0.025	2.299	0.004	17.1	82.6	2.6	73.0	8.92	3.5	0.1	12.3	10.9	99.90	1.85	
662	8/27	4:16	16822	18.8	11.4	232.1	326.0	686.0	14.62	6.78	598.7	0.025	2.309	0.004	17.1	82.6	2.6	73.0	8.20	3.5	0.1	12.2	10.8	99.90	1.68	
664	8/27	4:22	16801	18.8	11.4	231.6	327.2	685.8	14.63	6.79	599.6	0.025	2.407	0.005	17.0	82.6	2.6	73.2	9.23	3.8	0.1	11.7	10.4	99.90	1.83	
665	8/27	4:23	16824	18.8	11.4	231.6	327.4	685.6	14.66	6.80	598.7	0.025	2.407	0.005	17.0	82.6	2.6	73.2	9.61	3.8	0.1	11.7	10.4	99.90	1.90	

Fuel 3: high sulfur fuel with corrosion inhibitor

Table C-4.—Summary of Fuel 4[1] Test Result

rdg	Date	Time	ALT	Pla_Pos	PS1	Dewp	P3	T3	WA1	WA36	WFT	FAR	CO2	CO	O2	NO_x	HC	NO	SO2	EICO	EIHC	EINOx	EINO	η_b %	EISO2	SN
			m		kPa	°K	kPa	°K	kg/sec	kg/sec	kg/hr		%	%	%	ppm	ppm	ppm	ppm	SAE ARP1533						
673	8/28	23:54	12207	19.3	26.6	233.8	322.2	542.7	19.80	7.96	417.2	0.015	1.668	0.005	18.0	29.1	2.8	24.3	1.24	6.2	0.2	5.9	5.0	99.83	0.35	
674	8/28	23:55	12222	19.3	26.6	233.6	322.2	542.5	19.83	7.95	418.1	0.015	1.665	0.005	18.0	29.1	2.7	23.8	1.12	6.3	0.2	6.0	4.9	99.83	0.32	
675	8/29	0:01	12187	53.3	25.1	233.5	495.6	616.1	25.55	11.06	768.5	0.019	2.385	0.003	16.9	78.9	0.9	69.8	2.00	2.6	0.0	11.3	10.0	99.94	0.40	
676	8/29	0:05	12204	53.3	25.2	233.7	497.1	615.4	25.61	11.10	768.4	0.019	2.359	0.002	17.0	79.2	0.9	69.4	1.65	2.1	0.1	11.5	10.1	99.95	0.33	
677	8/29	0:11	12209	53.3	25.2	233.5	497.5	618.8	25.59	11.11	772.0	0.019	2.384	0.002	16.9	82.3	0.8	71.8	1.69	2.0	0.0	11.8	10.3	99.95	0.34	
681	8/29	0:27	12178	65.8	23.9	233.3	631.4	671.6	29.41	13.32	1077.6	0.023	2.809	0.002	16.4	129.3	0.5	115.4	1.84	1.5	0.0	15.8	14.1	99.96	0.31	
683	8/29	0:31	12190	85.3	23.0	233.2	729.5	717.0	31.32	14.72	1348.4	0.025	3.513	0.003	15.4	205.3	0.2	181.5	1.92	1.4	0.0	20.1	17.8	99.97	0.26	
686	8/29	0:38	12194	85.4	23.0	232.9	729.8	716.9	31.41	14.76	1350.5	0.025	3.467	0.002	15.4	206.5	0.2	180.4	1.78	1.4	0.0	20.5	17.9	99.97	0.25	
688	8/29	0:58	15273	19.0	15.9	232.6	324.9	627.9	16.41	7.16	532.9	0.021	2.613	0.003	16.6	61.4	0.6	52.9	1.30	2.6	0.0	8.0	6.9	99.94	0.24	
690	8/29	1:03	15260	19.0	15.9	232.4	323.9	629.4	16.37	7.15	530.2	0.021	2.248	0.003	17.2	61.4	0.6	52.6	1.15	3.0	0.0	9.3	8.0	99.93	0.24	
692	8/29	1:17	15260	65.7	15.1	232.1	400.5	674.2	18.57	8.39	711.7	0.024	2.485	0.003	16.8	90.5	0.6	79.4	1.46	2.4	0.0	12.5	10.9	99.94	0.28	8.8
694	8/29	1:23	15256	65.5	15.2	232.3	399.4	673.0	18.58	8.39	708.3	0.024	2.343	0.003	17.0	88.8	0.7	77.7	1.40	2.6	0.0	13.0	11.3	99.94	0.28	
696	8/29	1:28	15256	85.2	14.7	232.1	466.5	720.6	19.88	9.35	895.7	0.027	2.867	0.004	16.2	139.4	0.7	125.0	1.76	2.7	0.0	16.7	14.9	99.93	0.29	
698	8/29	1:35	15259	85.2	14.5	232.2	462.2	721.6	19.72	9.24	892.0	0.027	2.750	0.004	16.5	139.4	0.7	125.7	1.61	2.8	0.0	17.4	15.7	99.93	0.28	
704	8/29	2:02	16734	85.3	11.3	232.0	361.7	724.7	15.31	7.21	718.1	0.028	2.718	0.005	16.7	110.1	0.7	98.1	1.30	3.7	0.0	13.9	12.4	99.91	0.23	
705	8/29	2:07	16798	85.3	11.4	231.5	363.5	724.1	15.38	7.24	718.6	0.028	2.672	0.005	16.6	114.0	0.7	101.2	1.28	3.8	0.0	14.6	13.0	99.91	0.23	
708	8/29	2:28	9145	19.0	44.0	231.8	317.9	503.0	23.81	8.52	335.0	0.011	1.503	0.009	18.2	17.9	18.0	9.7	0.95	12.2	1.4	4.0	2.2	99.57	0.30	
709	8/29	2:31	9140	19.1	43.9	231.9	318.4	500.9	23.86	8.54	336.0	0.011	1.454	0.009	18.3	17.7	19.0	9.3	0.91	12.8	1.6	4.1	2.2	99.55	0.30	
711	8/29	2:37	9137	44.7	41.6	231.8	636.5	617.6	34.80	14.51	918.8	0.018	2.682	0.002	16.7	91.3	0.7	77.4	1.60	1.5	0.0	11.7	9.9	99.96	0.28	
712	8/29	2:43	9127	44.6	41.9	231.8	641.2	617.6	34.98	14.63	917.1	0.017	2.661	0.002	16.7	89.9	0.4	74.9	1.73	1.5	0.0	11.6	9.6	99.96	0.31	
714	8/29	2:56	9132	56.5	39.7	231.5	846.0	672.5	41.25	18.10	1369.2	0.021	3.138	0.001	16.0	161.5	0.3	141.1	2.91	0.9	0.0	17.7	15.4	99.98	0.44	14.9

Fuel 4: mixed medium sulfur fuel with corrosion inhibitor, conductivity additive and icing inhibitor

Table C-4.—Summary of Fuel 4[1] Test Result (Continued)

715	8/29	2:58	9105	56.5	40.2	231.5	856.4	672.7	41.80	18.32	1384.1	0.021	3.141	0.001	16.1	165.0	0.2	141.6	2.42	0.9	0.0	18.0	15.5	99.98	0.37	
716	8/29	3:02	9158	66.2	38.2	231.5	1016.8	717.2	46.01	20.84	1788.4	0.024	3.554	0.002	15.5	236.4	0.3	210.2	3.05	0.9	0.0	22.9	20.4	99.98	0.41	
717	8/29	3:10	9132	66.2	38.2	231.4	1015.2	717.2	46.02	20.82	1782.4	0.024	3.591	0.002	15.5	240.3	0.2	207.2	2.88	0.9	0.0	23.0	19.9	99.98	0.38	
718	8/29	3:13	9147	84.8	37.0	231.6	1167.7	764.0	49.00	22.93	2216.2	0.027	4.148	0.002	14.8	337.8	0.2	287.0	2.78	0.9	0.0	28.2	23.9	99.98	0.32	
719	8/29	3:19	9123	84.9	37.0	231.4	1166.8	764.6	48.93	22.94	2212.9	0.027	4.191	0.002	14.7	340.5	0.1	287.2	2.64	0.9	0.0	28.1	23.7	99.98	0.30	
720	8/29	3:25	9144	84.9	36.8	231.3	1161.8	764.7	48.71	22.84	2205.3	0.027	4.174	0.002	14.8	322.0	0.1	285.6	2.62	0.9	0.0	26.7	23.7	99.98	0.30	
722	8/29	3:37	9131	35.0	43.0	231.3	466.7	559.2	29.14	11.44	577.7	0.014	2.128	0.004	17.5	43.2	1.1	32.6	2.08	3.4	0.1	6.9	5.2	99.92	0.47	2.3
725	8/29	3:45	9137	35.0	42.9	231.3	465.7	559.6	29.09	11.44	580.7	0.014	2.000	0.004	17.5	42.9	1.1	32.7	2.03	3.6	0.1	7.3	5.6	99.91	0.48	
726	8/29	3:50	9136	35.0	42.9	231.1	467.0	560.0	29.22	11.49	583.6	0.014	1.989	0.003	17.5	42.9	1.0	32.6	2.05	3.5	0.1	7.4	5.6	99.91	0.49	
740	9/2	22:51	3192	19.1	98.9	255.7	480.9	499.2	40.72	13.07	465.9	0.010	1.403	0.009	18.2	22.3	19.9	14.0	0.95	12.9	1.7	5.4	3.4	99.53	0.32	0.0
741	9/2	22:53	3196	19.1	98.9	255.9	480.4	498.3	40.53	13.10	465.0	0.010	1.406	0.009	18.3	22.1	21.4	12.3	0.87	13.1	1.8	5.3	3.0	99.51	0.29	
742	9/2	22:57	3225	36.8	95.4	256.1	1052.1	618.5	62.57	24.66	1377.2	0.016	2.342	0.001	17.2	82.5	0.8	78.7	1.51	1.0	0.0	12.1	11.5	99.97	0.31	
746	9/2	23:05	3196	36.8	95.3	256.7	1055.5	617.1	62.74	24.76	1378.5	0.016	2.336	0.001	17.2	81.9	0.4	88.9	1.84	0.9	0.0	12.0	13.0	99.98	0.37	
747	9/2	23:09	3198	36.8	95.3	256.9	1056.2	616.5	62.71	24.77	1375.6	0.015	2.388	0.001	17.2	81.8	0.4	74.5	1.74	0.9	0.0	11.7	10.7	99.98	0.35	
748	9/2	23:17	3224	36.8	95.0	257.3	1054.7	615.7	62.67	24.75	1375.2	0.015	2.414	0.001	17.2	78.5	0.6	70.9	2.41	0.9	0.0	11.1	10.1	99.98	0.48	
749	9/2	23:21	3201	48.0	92.6	257.4	1443.3	673.4	75.72	31.69	2180.9	0.019	2.934	0.001	16.4	175.0	0.3	151.6	2.19	0.6	0.0	20.5	17.8	99.99	0.36	
751	9/2	23:31	3208	48.0	92.3	257.7	1440.5	672.3	75.44	31.65	2173.9	0.019	2.943	0.001	16.4	175.6	0.2	153.8	2.17	0.6	0.0	20.5	18.0	99.99	0.35	18.7
752	9/2	23:34	3215	59.4	89.2	257.9	1790.2	718.8	86.61	37.56	3005.7	0.022	3.381	0.001	15.8	294.9	0.3	252.6	2.31	0.4	0.0	30.0	25.7	99.99	0.33	
753	9/2	23:39	3213	59.4	89.1	258.1	1792.2	718.4	86.47	37.54	3006.6	0.022	3.430	0.001	15.8	294.6	0.3	268.3	2.34	0.4	0.0	29.6	27.0	99.99	0.33	
754	9/2	23:49	3206	59.4	89.2	258.2	1801.4	718.4	86.76	37.68	3013.7	0.022	3.469	0.001	15.8	294.8	0.3	264.4	2.40	0.4	0.0	29.3	26.3	99.99	0.33	
755	9/2	23:54	3246	85.1	83.7	258.4	2353.5	788.2	101.22	46.24	4515.5	0.027	4.199	0.001	14.7	483.9	0.5	438.0	2.24	0.4	0.0	39.9	36.1	99.99	0.26	
763	9/3	1:59	10594	19.0	34.7	234.4	317.8	505.7	22.22	8.32	367.3	0.012	1.528	0.008	18.2	19.7	13.7	12.6	0.76	10.2	1.1	4.4	2.8	99.66	0.23	
764	9/3	2:04	10541	64.3	31.1	234.4	791.7	671.0	37.67	16.77	1355.2	0.022	3.177	0.002	16.1	162.7	1.2	148.0	2.01	1.1	0.1	17.6	16.0	99.97	0.30	
766	9/3	2:11	10522	64.5	30.9	233.8	791.7	672.2	37.49	16.75	1350.0	0.022	3.158	0.002	16.0	159.0	0.7	148.6	2.71	1.1	0.0	17.3	16.2	99.97	0.41	

Fuel 4: mixed medium sulfur fuel with corrosion inhibitor, conductivity additive and icing inhibitor

Table C-4.—Summary of Fuel 4[1] Test Result

769	9/3	2:22	10498	85.3	29.7	233.9	936.7	725.3	40.52	18.85	1747.9	0.026	3.807	0.002	15.2	260.5	0.3	241.2	2.59	1.1	0.0	23.6	21.9	99.97	0.33	
770	9/3	2:27	10544	85.3	29.6	233.7	936.2	726.0	40.49	18.82	1747.4	0.026	3.805	0.002	15.1	258.9	0.2	246.1	2.60	1.0	0.0	23.5	22.3	99.98	0.33	
773	9/3	2:40	15183	19.4	16.2	233.2	320.1	624.8	16.41	7.08	525.0	0.021	2.176	0.003	17.5	60.7	1.0	51.2	1.54	3.2	0.1	9.5	8.0	99.92	0.34	
774	9/3	2:41	15175	19.4	16.2	233.2	320.1	624.1	16.41	7.09	523.0	0.021	2.188	0.004	17.5	60.7	1.0	51.2	1.47	3.3	0.1	9.5	8.0	99.92	0.32	
775	9/3	2:45	15167	19.4	16.2	233.2	320.5	624.3	16.43	7.10	524.1	0.021	2.231	0.003	17.4	61.7	0.6	52.4	1.51	3.1	0.0	9.5	8.0	99.92	0.32	
779	9/3	2:57	15200	66.1	15.4	233.3	410.0	673.1	19.09	8.60	738.1	0.024	2.521	0.003	17.0	97.1	0.7	82.3	1.77	2.4	0.0	13.2	11.2	99.94	0.33	3.0
780	9/3	3:00	15196	85.3	14.9	232.7	471.3	715.6	20.21	9.45	913.1	0.027	3.297	0.004	16.0	156.4	0.6	136.4	2.10	2.5	0.0	16.3	14.2	99.94	0.31	
783	9/3	3:12	15169	85.2	14.9	232.9	470.4	713.5	20.29	9.49	907.8	0.027	3.359	0.004	15.8	159.2	0.6	131.2	1.91	2.5	0.0	16.3	13.4	99.94	0.27	
786	9/3	3:35	16777	19.1	11.3	232.7	320.0	694.5	14.40	6.56	612.7	0.026	2.717	0.005	16.8	85.1	1.1	73.2	1.79	3.7	0.1	10.7	9.2	99.91	0.31	
789	9/3	3:42	16795	19.1	11.3	232.5	320.6	694.0	14.44	6.58	613.7	0.026	2.345	0.005	17.0	84.0	0.6	73.9	1.41	4.3	0.0	12.2	10.8	99.90	0.29	
791	9/3	3:47	16804	85.3	11.1	232.3	351.8	724.8	15.00	6.99	713.0	0.028	2.822	0.006	16.5	116.2	0.6	105.5	1.74	4.0	0.0	14.1	12.8	99.90	0.29	

[1] Fuel 4: mixed medium sulfur fuel with corrosion inhibitor, conductivity additive and icing inhibitor

Table C-5—Summary of Fuel 5[ϕ] Test Result

rdg	Date	Time	ALT	PlaPos	PS1	Dewp	P3	T3	WA1	WA36	WFT	FAR	CO2	CO	O2	NO_X	HC	NO	SO2	EICO	EIHC	EINOx	EINO	η_h%	EISO2	SN
			m		kPa	°K	kPa	°K	kg/sec	kg/sec	kg/hr		%	%	%	ppm	ppm	ppm	ppm	SAE ARP1533						
801	9/5	0:11	12190	18.7	26.6	233.5	326.9	538.7	20.00	8.12	411.4	0.014	1.627	0.005	17.9	28.2	6.2	20.8	n/a	6.7	0.5	5.9	4.4	99.80	n/a	
802	9/5	0:14	12190	18.7	26.8	232.9	326.1	542.9	19.90	8.08	412.4	0.014	1.651	0.005	18.0	28.8	5.2	21.3	n/a	6.4	0.4	5.9	4.4	99.81	n/a	
803	9/5	0:14	12183	18.7	26.8	232.9	326.1	543.2	19.89	8.07	412.4	0.014	1.660	0.005	18.0	29.1	5.1	21.5	n/a	6.3	0.4	6.0	4.4	99.82	n/a	
804	9/5	0:21	12174	53.4	25.2	232.5	500.7	617.5	25.72	11.23	757.6	0.019	2.584	0.003	16.8	84.0	2.4	70.6	1.37	2.0	0.1	11.1	9.4	99.94	0.25	
805	9/5	0:24	12177	53.4	25.3	233.1	503.7	619.0	25.80	11.28	763.1	0.019	2.581	0.003	16.7	84.9	2.0	71.4	1.70	2.0	0.1	11.3	9.5	99.94	0.31	
806	9/5	0:26	12156	53.4	25.5	232.5	506.1	618.7	25.84	11.35	761.7	0.019	2.582	0.003	16.7	84.7	1.9	71.2	1.76	2.0	0.1	11.2	9.4	99.94	0.33	
809	9/5	0:37	12187	65.7	23.9	232.3	634.7	670.0	29.49	13.48	1051.9	0.022	2.944	0.002	16.4	131.9	1.7	112.4	1.82	1.4	0.1	15.4	13.1	99.96	0.30	8.8
810	9/5	0:37	12158	65.7	23.9	231.9	632.8	669.9	29.50	13.46	1050.8	0.022	2.956	0.002	16.3	132.1	1.7	112.8	1.96	1.4	0.1	15.3	13.1	99.96	0.32	
811	9/5	0:40	12177	84.7	23.3	232.1	736.4	714.8	31.72	14.96	1325.6	0.025	3.671	0.003	15.3	204.0	1.2	174.1	2.24	1.4	0.0	19.1	16.3	99.96	0.29	
812	9/5	0:43	12190	84.7	23.1	231.9	731.5	716.5	31.38	14.89	1315.8	0.025	3.683	0.003	15.2	208.6	1.1	178.3	2.01	1.4	0.0	19.5	16.7	99.96	0.26	
813	9/5	0:49	12182	84.7	23.0	232.3	729.7	716.2	31.33	14.85	1310.6	0.025	3.775	0.003	15.2	209.3	0.9	178.0	2.09	1.3	0.0	19.1	16.3	99.97	0.27	
814	9/5	0:57	15255	18.9	15.6	232.0	319.1	625.4	16.02	7.08	501.7	0.020	2.216	0.004	17.4	61.3	1.0	50.9	1.73	3.3	0.1	9.5	7.8	99.92	0.37	
816	9/5	1:04	15259	18.9	15.5	232.1	318.7	625.9	16.02	7.08	503.4	0.020	2.342	0.004	17.2	56.2	1.0	53.9	1.90	3.3	0.1	8.2	7.9	99.92	0.39	
817	9/5	1:08	15254	18.9	15.5	231.6	319.0	625.7	16.03	7.08	502.7	0.020	2.348	0.004	17.2	50.2	0.9	54.1	1.97	3.2	0.1	7.3	7.9	99.92	0.40	
819	9/5	1:20	15258	67.2	14.8	231.5	403.9	676.9	18.45	8.49	700.6	0.023	2.517	0.003	17.0	93.5	1.3	79.9	2.29	2.6	0.1	12.7	10.9	99.93	0.43	2.3
821	9/5	1:22	15250	67.2	14.7	231.1	402.9	675.9	18.39	8.46	698.0	0.023	2.477	0.003	17.0	91.5	1.0	77.8	2.15	2.5	0.1	12.6	10.7	99.94	0.42	
822	9/5	1:25	15257	84.9	14.3	231.2	455.6	714.7	19.43	9.20	848.6	0.026	3.142	0.004	16.2	134.8	1.1	116.4	2.57	2.7	0.0	14.7	12.7	99.93	0.39	
823	9/5	1:30	15260	84.9	14.3	231.1	455.7	715.2	19.43	9.23	847.0	0.026	3.165	0.004	16.2	136.6	1.0	117.9	2.48	2.6	0.0	14.8	12.8	99.94	0.37	
824	9/5	1:33	15248	84.9	14.3	231.1	455.4	715.8	19.40	9.22	843.4	0.025	3.164	0.004	16.2	136.7	1.1	117.9	2.36	2.6	0.0	14.8	12.8	99.94	0.36	
825	9/5	1:41	16806	19.2	11.6	231.5	321.8	688.5	14.43	6.67	582.2	0.024	2.403	0.004	17.2	80.1	0.8	70.3	2.24	3.7	0.0	11.4	10.0	99.91	0.44	
826	9/5	1:46	16824	19.2	11.6	231.4	322.4	689.6	14.48	6.69	583.4	0.024	2.372	0.004	17.2	80.5	0.8	69.4	1.99	3.6	0.0	11.6	10.0	99.91	0.40	

Fuel 5: JP8 + 100

Table C-5—Summary of Fuel 5[$] Test Result (Continued)

827	9/5	1:52	16800	19.2	11.6	231.0	322.2	690.8	14.43	6.68	584.2	0.024	2.384	0.004	17.2	81.3	0.8	70.0	1.98	3.6	0.0	11.7	10.0	99.91	0.39	
828	9/5	1:56	16820	84.7	11.3	230.9	360.0	726.7	15.13	7.19	694.5	0.027	2.958	0.006	16.5	112.8	1.1	101.6	3.13	3.9	0.0	13.1	11.8	99.90	0.50	
829	9/5	2:01	16811	84.7	11.3	230.5	360.9	727.1	15.18	7.22	694.5	0.027	3.010	0.006	16.5	118.1	0.8	102.4	2.03	3.8	0.0	13.5	11.7	99.91	0.32	
833	9/5	2:29	9096	19.0	43.7	230.6	322.3	506.1	23.88	8.62	333.2	0.011	1.299	0.008	18.0	16.2	14.3	10.5	1.60	12.3	1.3	4.2	2.8	99.58	0.58	
834	9/5	2:34	9092	19.0	43.9	231.4	322.5	506.5	23.83	8.63	333.1	0.011	1.304	0.008	18.3	16.4	14.7	10.2	1.59	12.1	1.3	4.3	2.7	99.58	0.58	
835	9/5	2:34	9109	19.0	43.9	231.1	322.2	506.5	23.89	8.64	331.8	0.011	1.305	0.008	18.3	16.4	14.8	10.2	1.52	12.1	1.4	4.3	2.7	99.58	0.56	
836	9/5	2:44	9108	44.1	41.6	230.6	630.4	618.9	34.47	14.44	884.7	0.017	2.523	0.002	16.9	85.1	0.7	72.4	3.07	1.5	0.0	11.5	9.8	99.96	0.58	
837	9/5	2:47	9102	44.1	41.8	231.0	633.3	619.0	34.69	14.51	887.4	0.017	2.515	0.002	16.9	85.0	0.6	72.1	3.04	1.5	0.0	11.6	9.8	99.96	0.58	
839	9/5	2:55	9095	55.8	40.0	230.5	833.6	673.6	40.93	17.95	1312.7	0.020	3.079	0.001	16.1	160.3	0.4	139.7	3.75	0.9	0.0	17.9	15.6	99.98	0.58	10.9
840	9/5	2:58	9128	55.8	39.9	230.1	832.4	673.7	40.86	17.89	1315.0	0.020	3.111	0.001	16.1	161.4	0.4	139.0	3.79	0.9	0.0	17.8	15.3	99.98	0.58	
841	9/5	3:03	9130	65.2	38.3	231.1	1000.5	715.8	45.55	20.66	1704.0	0.023	3.463	0.001	15.5	228.1	0.4	203.2	4.59	0.8	0.0	22.7	20.2	99.98	0.63	
842	9/5	3:11	9100	65.1	38.4	230.3	1003.0	716.2	45.64	20.73	1703.6	0.023	3.486	0.002	15.5	231.6	0.4	203.7	4.47	0.9	0.0	22.9	20.1	99.98	0.61	
843	9/5	3:16	9111	65.1	38.3	230.2	1002.2	716.3	45.69	20.69	1706.8	0.023	3.488	0.001	15.5	232.8	0.3	204.2	4.38	0.8	0.0	23.0	20.1	99.98	0.60	
844	9/5	3:19	9092	85.0	36.9	230.0	1165.6	769.5	48.79	22.99	2165.1	0.026	4.057	0.002	14.7	339.5	0.3	286.4	3.57	0.9	0.0	28.9	24.4	99.98	0.42	
845	9/5	3:23	9126	85.0	37.0	230.0	1168.3	770.0	48.84	23.04	2167.7	0.026	4.054	0.002	14.7	343.0	0.3	288.4	3.44	0.9	0.0	29.2	24.6	99.98	0.41	
846	9/5	3:27	9089	85.0	36.9	229.9	1167.0	770.4	48.77	23.00	2162.8	0.026	4.062	0.002	14.7	341.0	0.3	287.8	3.52	1.0	0.0	29.1	24.5	99.98	0.42	
854	9/5	22:50	3128	18.8	98.9	255.2	476.0	494.3	40.28	13.14	435.5	0.009	1.343	0.010	19.9	20.3	23.9	9.3	1.27	15.0	2.1	5.1	2.4	99.44	0.45	2.3
855	9/5	22:53	3181	18.8	98.8	255.2	475.0	494.1	40.28	13.13	433.1	0.009	1.335	0.010	19.9	20.3	25.1	8.2	1.86	15.3	2.2	5.2	2.1	99.42	0.66	
856	9/5	22:55	3195	18.8	98.9	255.2	475.2	493.8	40.32	13.14	431.8	0.009	1.336	0.010	20.0	20.3	25.0	7.9	1.61	15.4	2.2	5.2	2.0	99.42	0.57	
857	9/5	22:58	3172	37.4	95.0	255.5	1072.6	619.7	63.08	25.31	1335.4	0.015	2.296	0.001	18.6	85.9	1.6	75.1	2.95	0.9	0.1	12.8	11.2	99.97	0.61	
858	9/5	23:05	3194	37.4	95.3	255.4	1081.7	618.7	63.71	25.55	1345.6	0.015	2.296	0.001	18.6	86.0	0.7	72.3	3.07	0.9	0.0	12.8	10.8	99.98	0.64	
859	9/5	23:07	3172	37.5	95.2	255.4	1082.0	618.3	63.49	25.54	1345.6	0.015	2.294	0.001	18.6	86.1	0.7	72.0	3.07	0.9	0.0	12.8	10.7	99.98	0.64	
861	9/5	23:17	3186	47.8	92.5	255.6	1447.8	671.5	75.75	32.15	2060.1	0.018	2.830	0.001	17.8	176.2	0.5	151.2	3.70	0.5	0.0	21.4	18.3	99.99	0.62	16.8
863	9/5	23:21	3196	47.8	92.5	255.5	1447.8	671.3	75.79	32.17	2061.7	0.018	2.835	0.001	17.8	176.4	0.5	150.8	3.72	0.5	0.0	21.4	18.3	99.99	0.63	

Fuel 5: JP8 + 100

Table C-5—Summary of Fuel 5[ϕ] Test Result (Continued)

864	9/5	23:27	3177	59.6	89.2	255.7	1817.2	719.0	86.91	38.42	2888.8	0.021	3.316	0.001	17.1	302.7	0.5	259.7	4.57	0.4	0.0	31.4	27.0	99.99	0.66	
865	9/5	23:33	3172	59.6	89.2	255.8	1820.2	718.9	87.10	38.45	2890.1	0.021	3.316	0.001	17.1	303.1	0.5	258.8	4.56	0.4	0.0	31.5	26.9	99.99	0.66	
867	9/5	23:40	3171	59.6	89.2	256.0	1823.6	719.0	87.30	38.53	2898.3	0.021	3.320	0.001	17.1	305.3	0.5	259.1	4.58	0.4	0.0	31.7	26.9	99.99	0.66	
868	9/5	23:49	3183	59.6	89.1	255.9	1823.5	718.9	87.15	38.51	2895.3	0.021	3.324	0.001	17.1	306.6	0.5	258.6	4.58	0.4	0.0	31.7	26.8	99.99	0.66	
869	9/5	23:53	3213	85.1	83.8	256.0	2370.9	787.7	101.25	47.09	4304.0	0.025	4.052	0.001	16.0	499.0	0.7	428.1	5.38	0.5	0.0	42.6	36.6	99.99	0.64	
871	9/5	23:57	3196	85.1	83.7	256.0	2375.7	787.7	101.33	47.21	4303.2	0.025	4.060	0.001	16.0	505.9	0.7	431.5	5.28	0.5	0.0	43.1	36.8	99.99	0.63	
874	9/6	1:20	13750	18.8	20.8	234.0	325.2	582.7	18.06	7.68	454.0	0.016	1.927	0.004	19.0	50.6	2.2	39.1	2.20	4.1	0.1	9.0	6.9	99.89	0.54	
875	9/6	1:21	13771	18.8	20.6	234.5	325.1	586.7	17.98	7.64	457.1	0.017	1.922	0.004	19.0	51.7	1.0	39.8	2.15	4.1	0.1	9.2	7.1	99.90	0.53	
878	9/6	1:32	13770	66.4	18.9	233.9	505.9	676.9	23.35	10.72	849.9	0.022	2.635	0.002	18.1	122.8	1.3	100.2	3.22	1.9	0.1	16.0	13.0	99.95	0.58	4.5
879	9/6	1:36	13775	66.4	18.7	233.9	503.0	677.0	23.19	10.66	843.1	0.022	2.638	0.002	18.1	122.3	1.3	99.0	3.17	1.9	0.1	15.9	12.9	99.95	0.57	
880	9/6	1:39	13753	84.9	18.0	234.0	573.4	718.6	24.46	11.65	1038.0	0.025	3.060	0.003	17.4	169.3	1.2	140.1	3.68	2.0	0.1	19.0	15.7	99.95	0.57	
881	9/6	1:47	13748	84.9	18.1	233.5	573.9	717.7	24.55	11.69	1035.2	0.025	3.215	0.003	17.2	179.7	1.0	147.2	3.59	1.9	0.0	19.2	15.7	99.95	0.53	
884	9/6	2:00	16848	18.7	11.6	233.2	323.0	691.8	14.47	6.62	606.4	0.026	2.422	0.005	18.5	94.4	1.3	81.4	2.84	3.8	0.1	13.3	11.5	99.90	0.56	
885	9/6	2:07	16872	18.7	11.4	232.8	321.2	692.0	14.37	6.57	606.4	0.026	2.436	0.006	18.3	91.6	0.9	77.8	2.02	4.7	0.0	12.9	10.9	99.89	0.39	
887	9/6	2:16	16869	85.0	11.3	232.8	359.8	724.3	15.21	7.16	718.5	0.028	2.804	0.006	17.8	120.9	1.0	106.8	3.01	4.1	0.0	14.8	13.0	99.90	0.51	
889	9/6	2:21	16843	85.0	11.3	232.8	361.1	724.1	15.25	7.17	718.0	0.028	2.756	0.005	17.9	118.5	0.9	104.8	2.74	4.0	0.0	14.7	13.0	99.90	0.47	
890	9/6	2:25	16846	85.0	11.3	232.8	360.2	723.8	15.21	7.17	716.6	0.028	2.734	0.005	17.9	117.5	0.9	103.1	2.47	4.0	0.0	14.7	12.9	99.90	0.43	
892	9/6	2:40	10615	18.8	34.7	232.0	316.4	506.1	21.86	8.25	361.0	0.012	1.401	0.008	19.9	20.1	12.5	12.9	1.46	11.2	1.1	4.9	3.1	99.63	0.49	
893	9/6	2:42	10612	18.8	34.7	232.5	317.1	506.8	21.86	8.26	360.1	0.012	1.415	0.008	19.9	20.2	12.4	12.8	1.31	11.1	1.0	4.9	3.1	99.63	0.44	
894	9/6	2:50	10616	18.8	34.8	232.1	316.9	506.9	21.85	8.26	361.6	0.012	1.425	0.008	19.8	20.5	13.1	12.4	1.31	11.0	1.1	4.9	3.0	99.63	0.44	
896	9/6	3:03	10626	63.7	30.9	232.4	781.7	672.0	36.71	16.52	1321.7	0.022	3.046	0.002	17.5	157.4	0.8	135.6	3.53	1.1	0.0	17.7	15.3	99.97	0.55	10.9
897	9/6	3:05	10631	63.7	30.8	232.1	780.4	671.7	36.63	16.49	1318.8	0.022	3.089	0.002	17.5	159.0	0.7	135.8	3.54	1.1	0.0	17.7	15.1	99.97	0.55	
898	9/6	3:12	10623	63.7	30.8	231.8	780.2	671.5	36.63	16.48	1316.7	0.022	3.137	0.002	17.4	159.9	0.6	135.3	3.44	1.1	0.0	17.5	14.8	99.97	0.53	
899	9/6	3:15	10649	84.9	29.5	232.4	931.6	726.4	39.89	18.67	1731.5	0.026	3.748	0.002	16.5	252.1	0.6	213.8	3.56	1.0	0.0	23.2	19.7	99.97	0.46	
900	9/6	3:20	10578	84.9	29.5	231.6	934.5	723.9	39.99	18.79	1725.9	0.026	3.733	0.002	16.5	250.9	0.5	211.3	3.43	1.0	0.0	23.2	19.5	99.97	0.44	
901	9/6	3:25	10619	84.9	29.6	231.8	936.3	723.1	40.13	18.83	1724.7	0.025	3.720	0.002	16.5	250.4	0.5	210.2	3.53	1.0	0.0	23.2	19.5	99.97	0.45	

[ϕ] Fuel 5: JP8 + 100

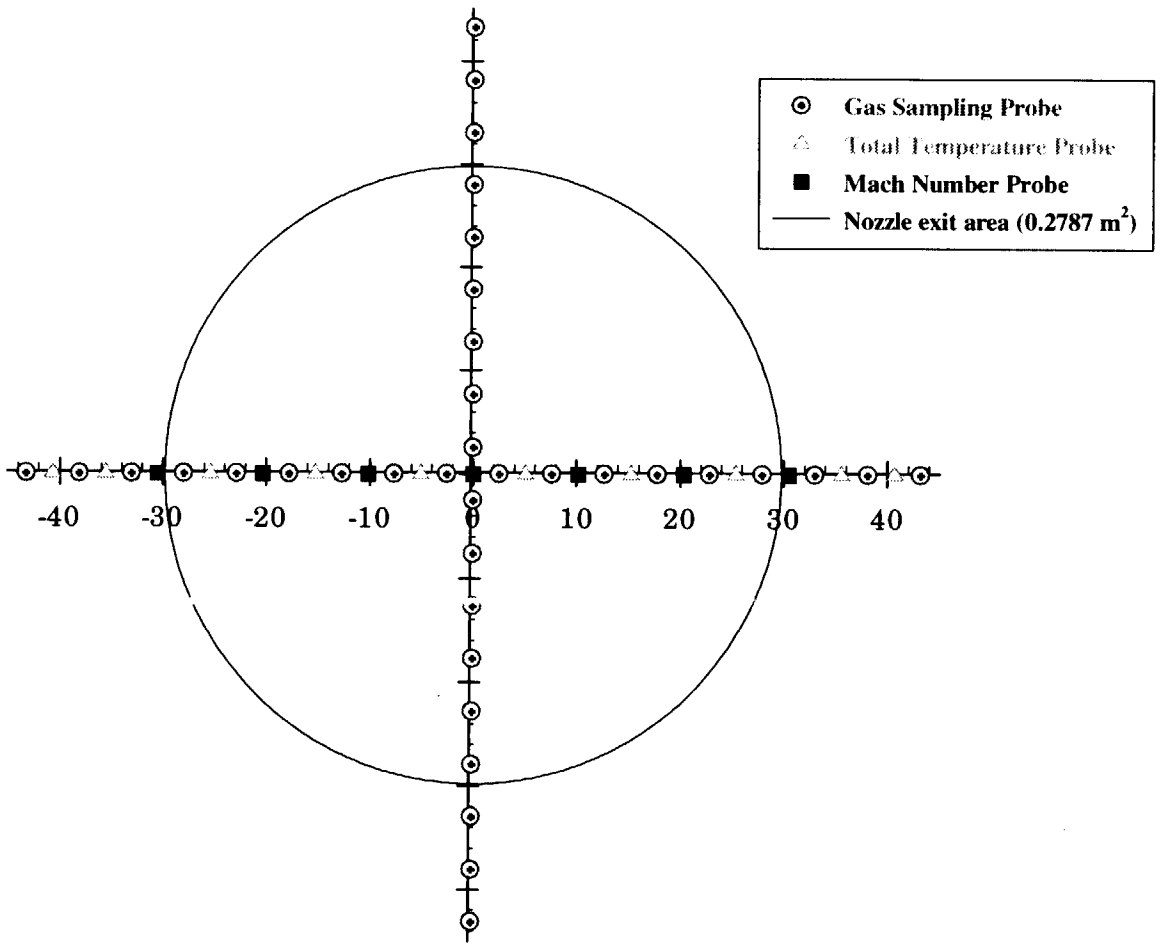

Figure C-1.—Sampling Probe Locations relative to the Engine Exit Plane

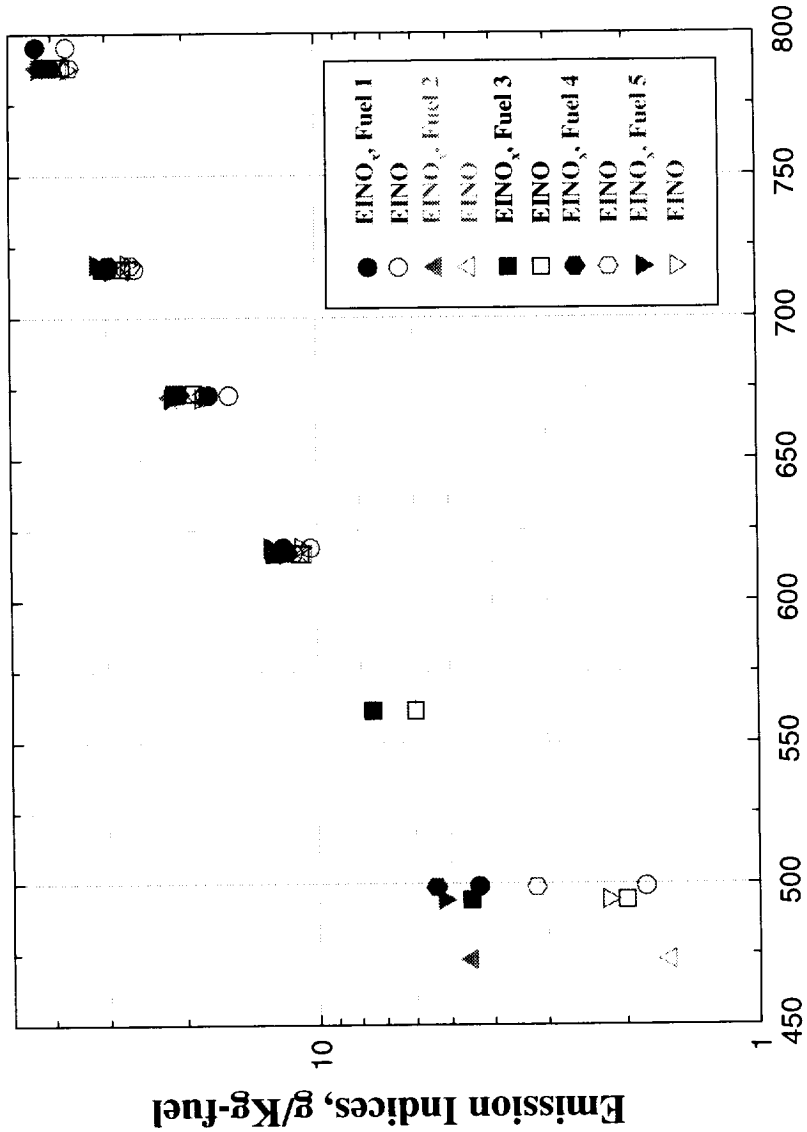

Figure C-2.—EI(NO) and EI(NO_x) vs. T_3 at Sea Level

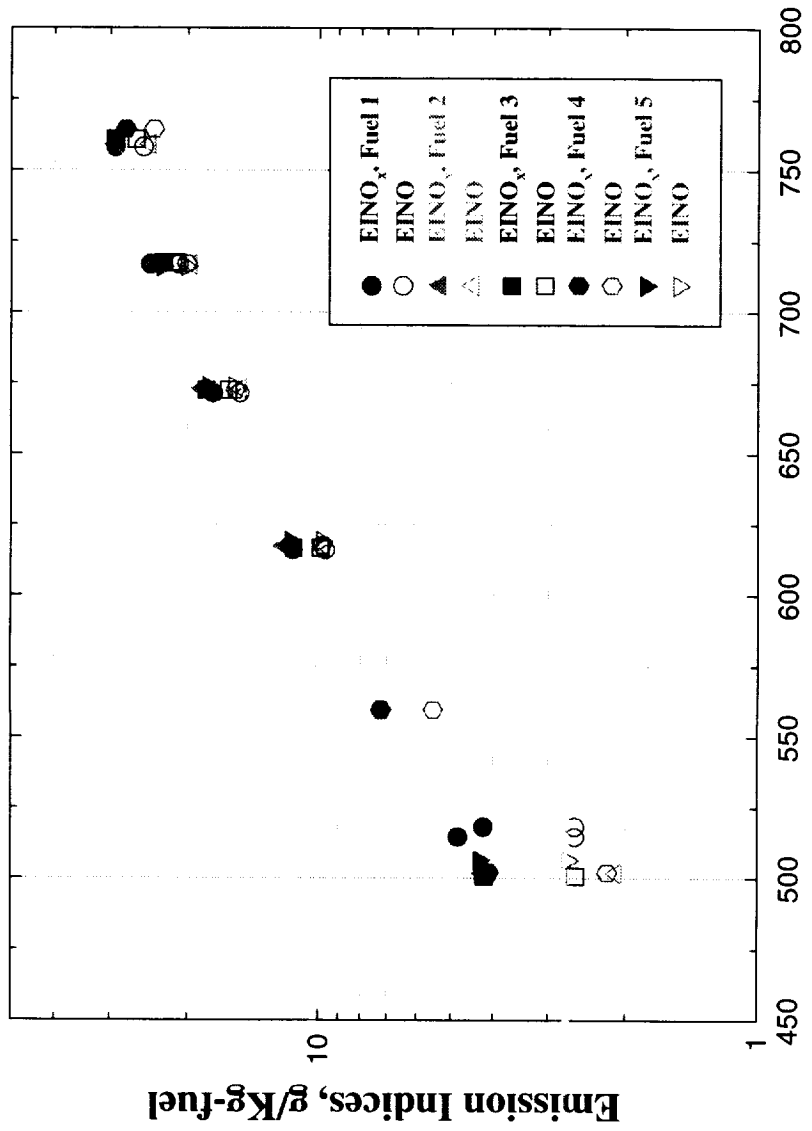

Figure C-3.—EI(NO) and EI(NO_x) vs. T_3 at 9.14 Km

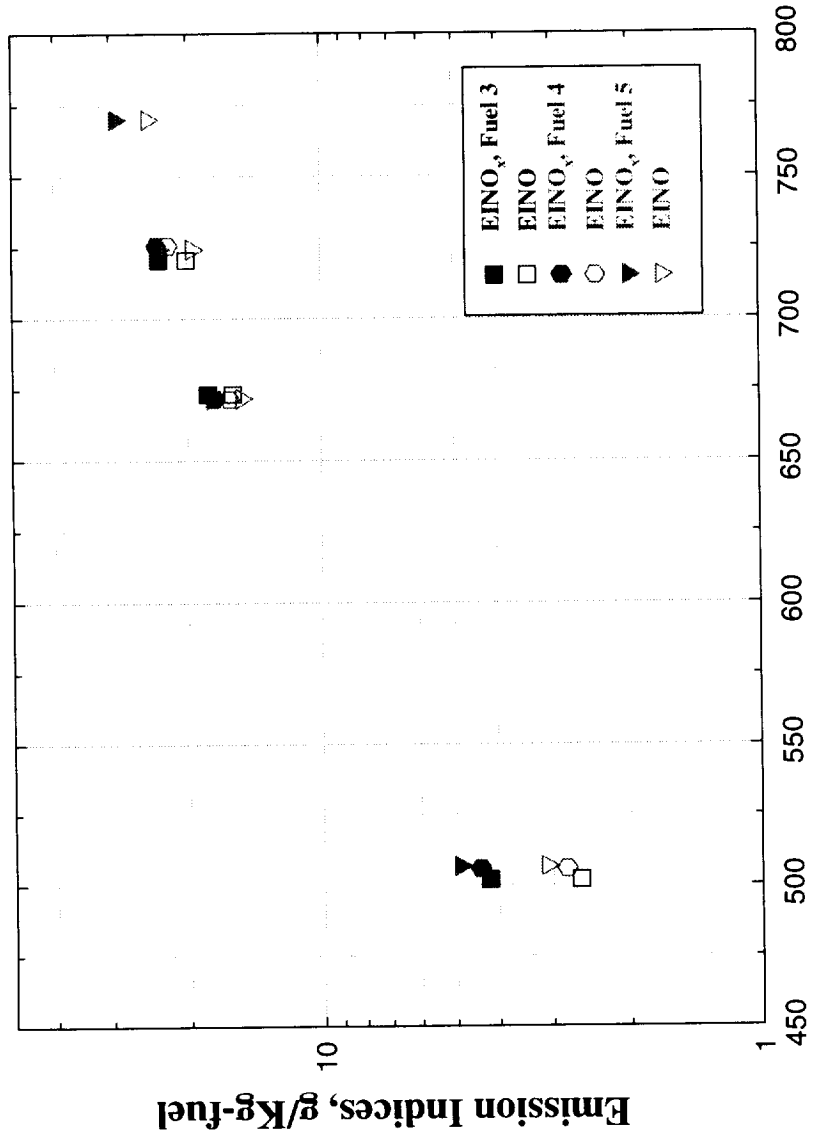

Figure C-4.—EI(NO) and EI(NO_x) vs. T_3 at 10.7 Km

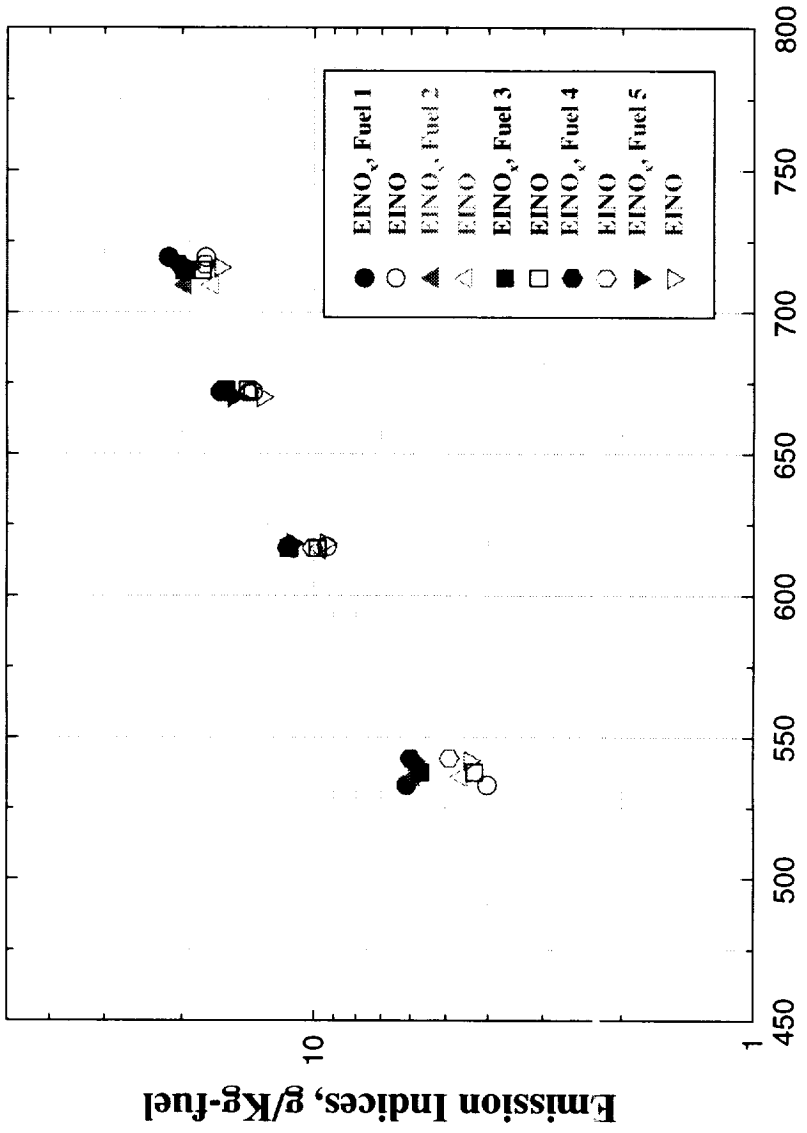

Figure C-5.—EI(NO) and EI(NO_x) vs. T_3 at 12.19 Km

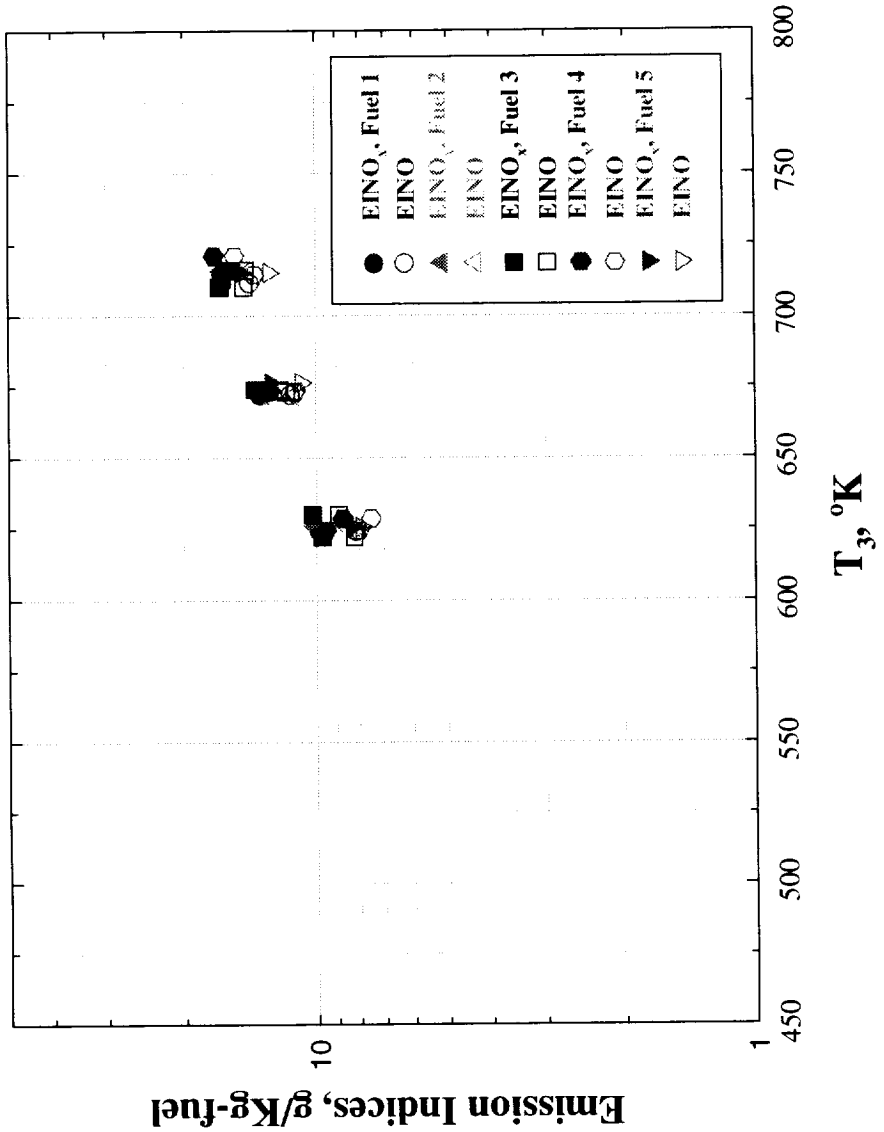

Figure C-6.—EI(NO) and EI(NO_x) vs. T_3 at 15.24 Km

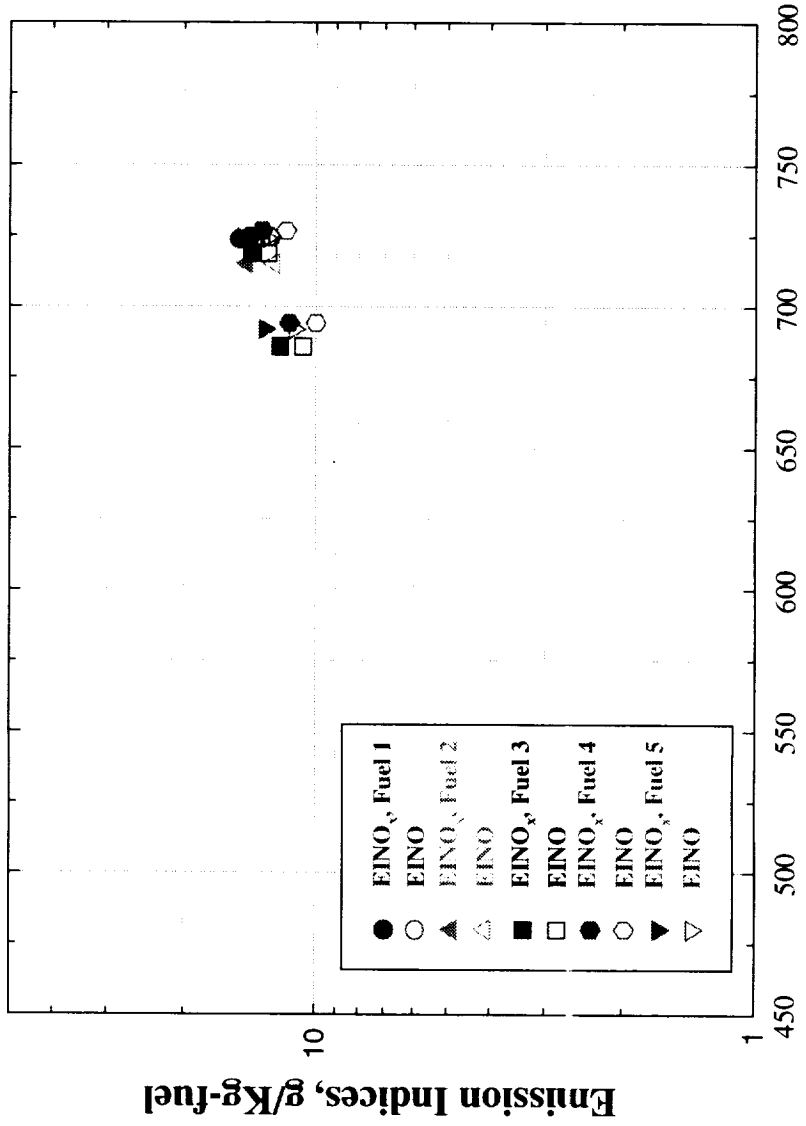

Figure C-7.—EI(NO) and EI(NO_x) vs. T_3 at 16.76 Km

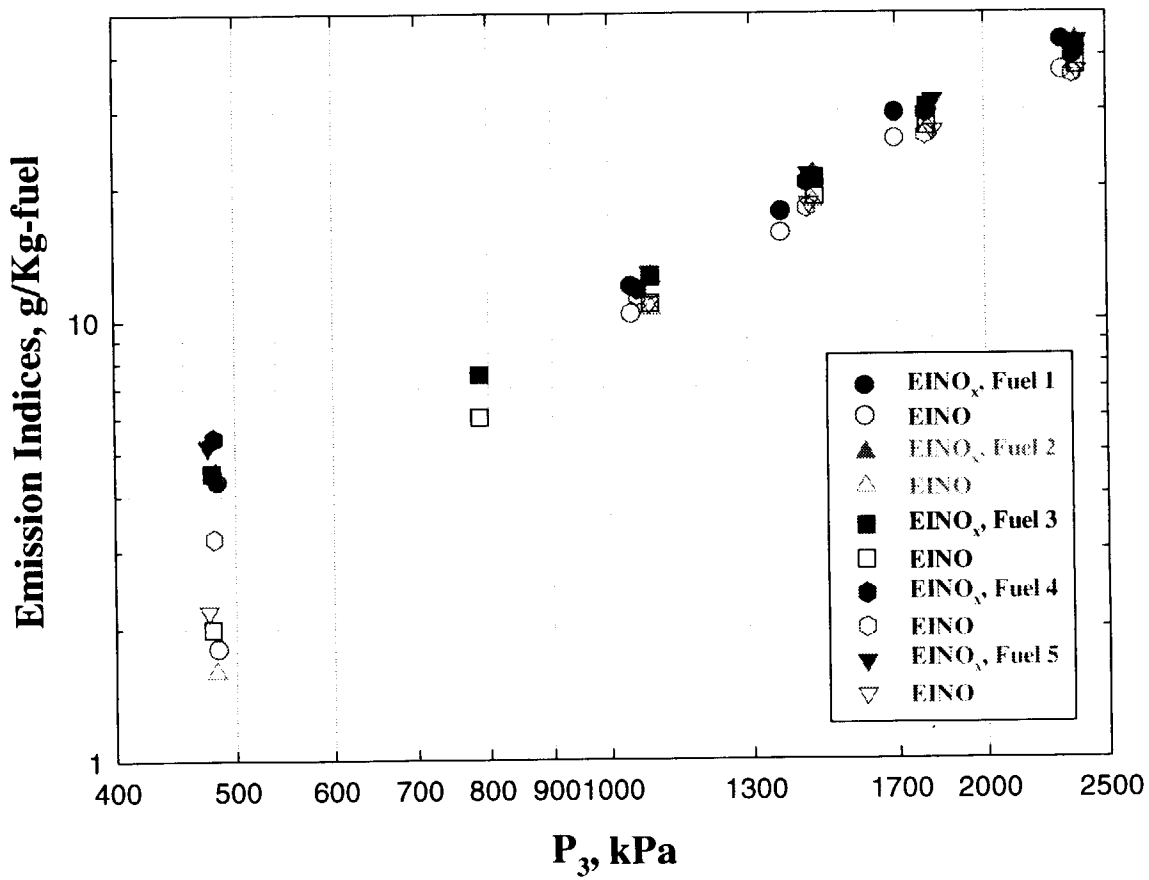

Figure C-8.—EI(NO) and EI(NO_x) vs. P_3 at Sea Level

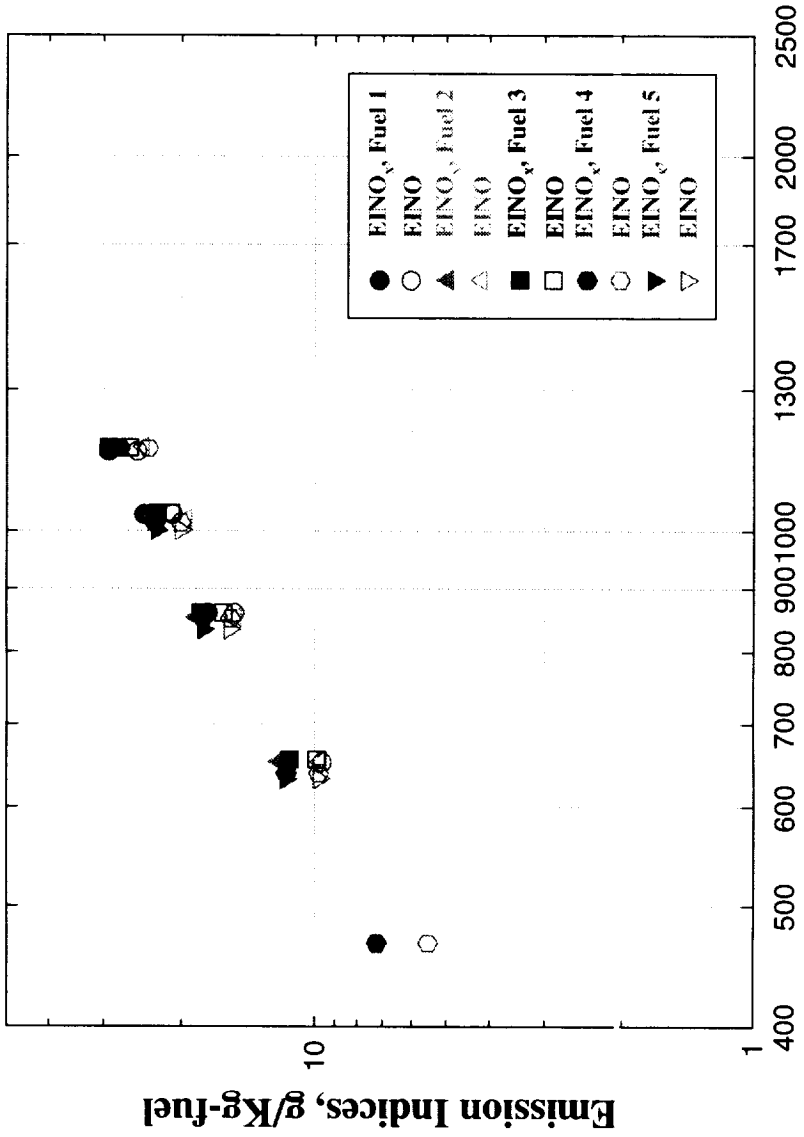

Figure C-9.—EI(NO) and EI(NO_x) vs. P_3 at 9.14 Km

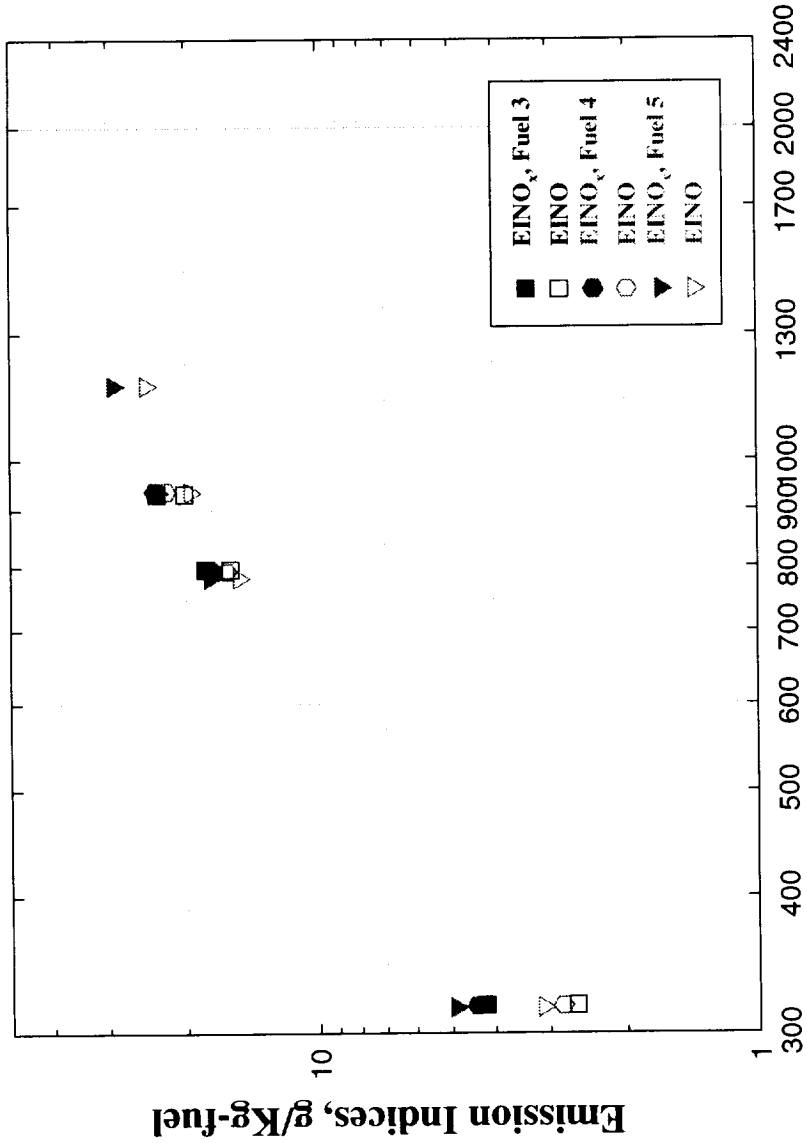

Figure C-10.—EI(NO) and EI(NO_x) vs. P_3 at 10.7 Km

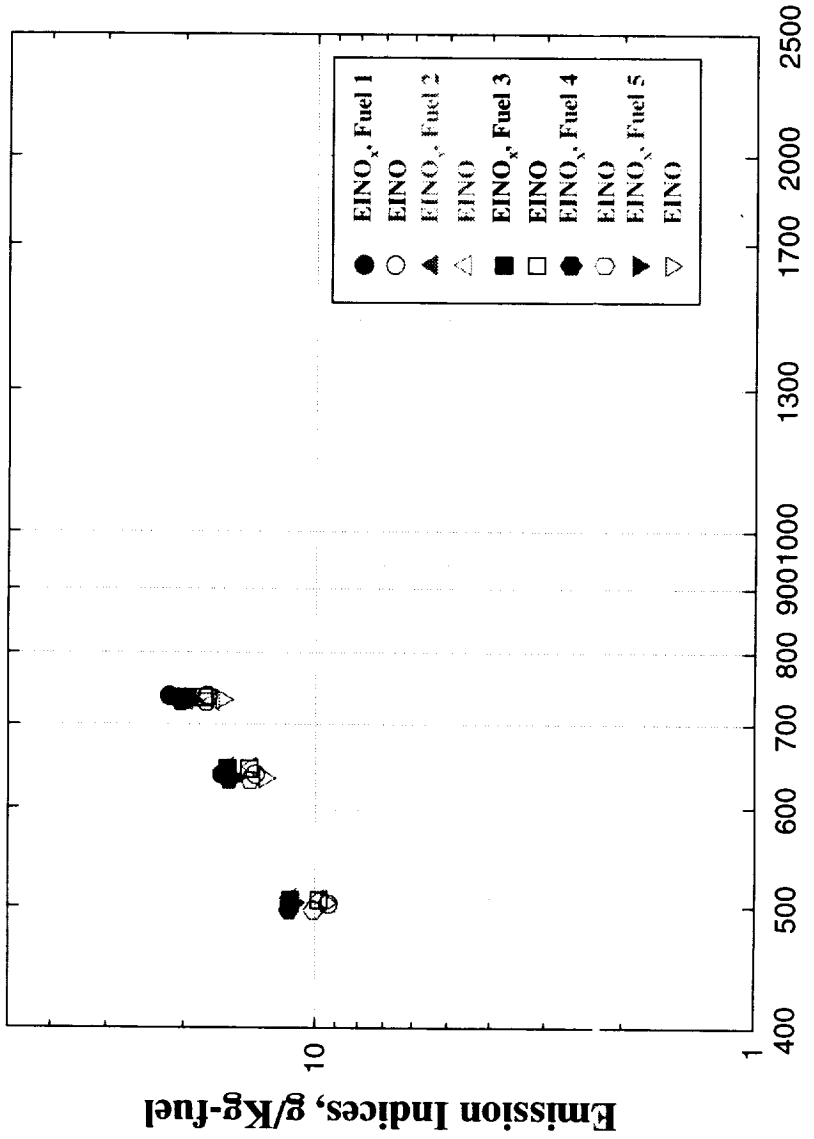

Figure C-11.—EI(NO) and EI(NO_x) vs. P_3 at 12.19 Km

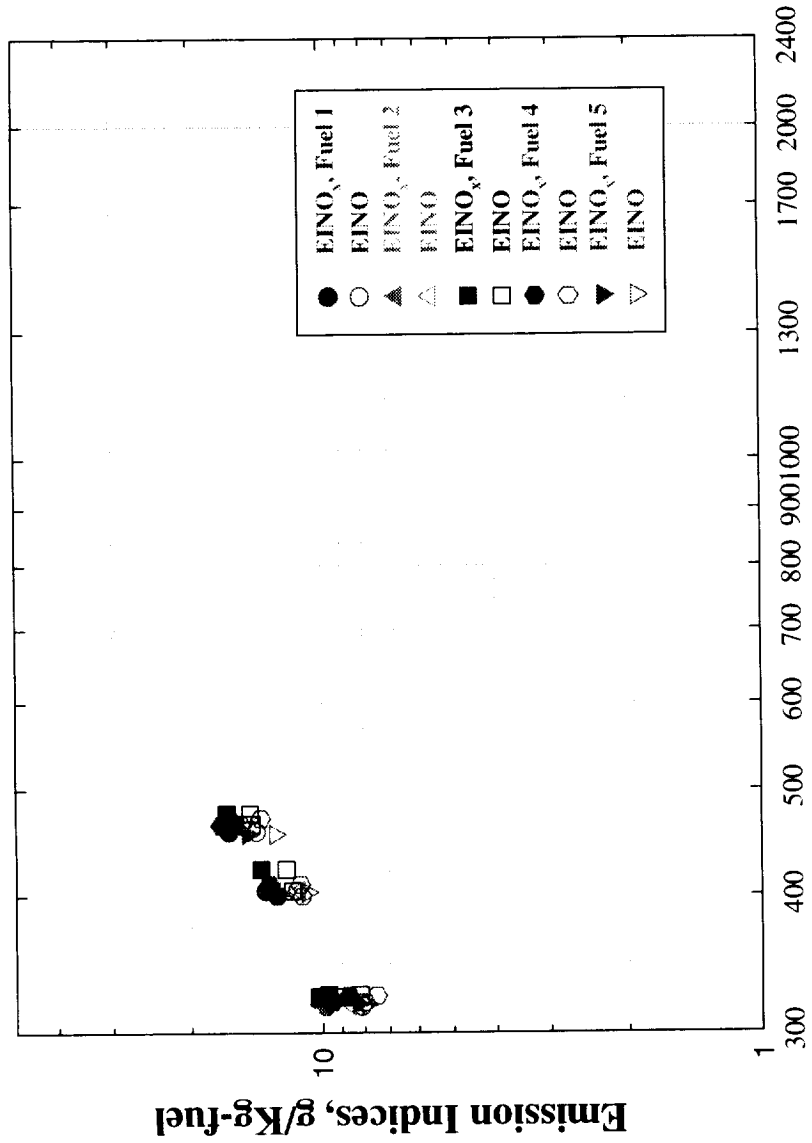

Figure C-12.—EI(NO) and EI(NO_x) vs. P_3 at 15.24 Km

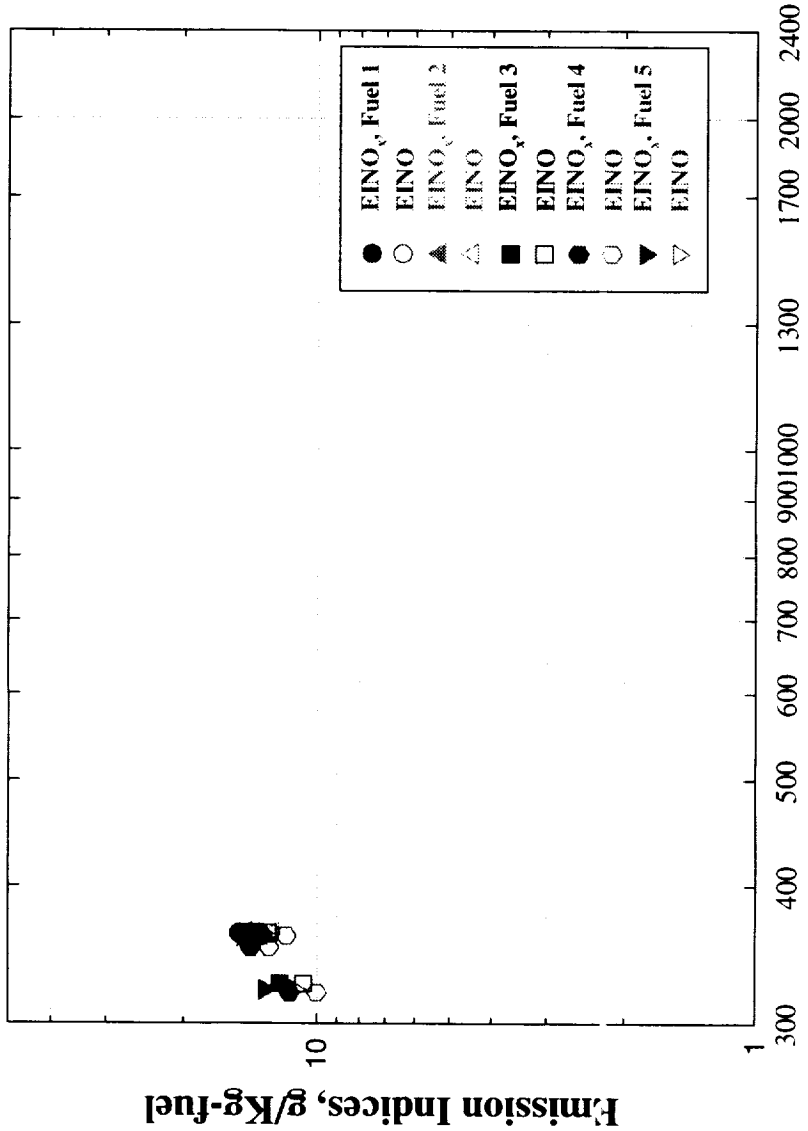

Figure C-13.—EI(NO) and EI(NO_x) vs. P_3 at 16.76 Km

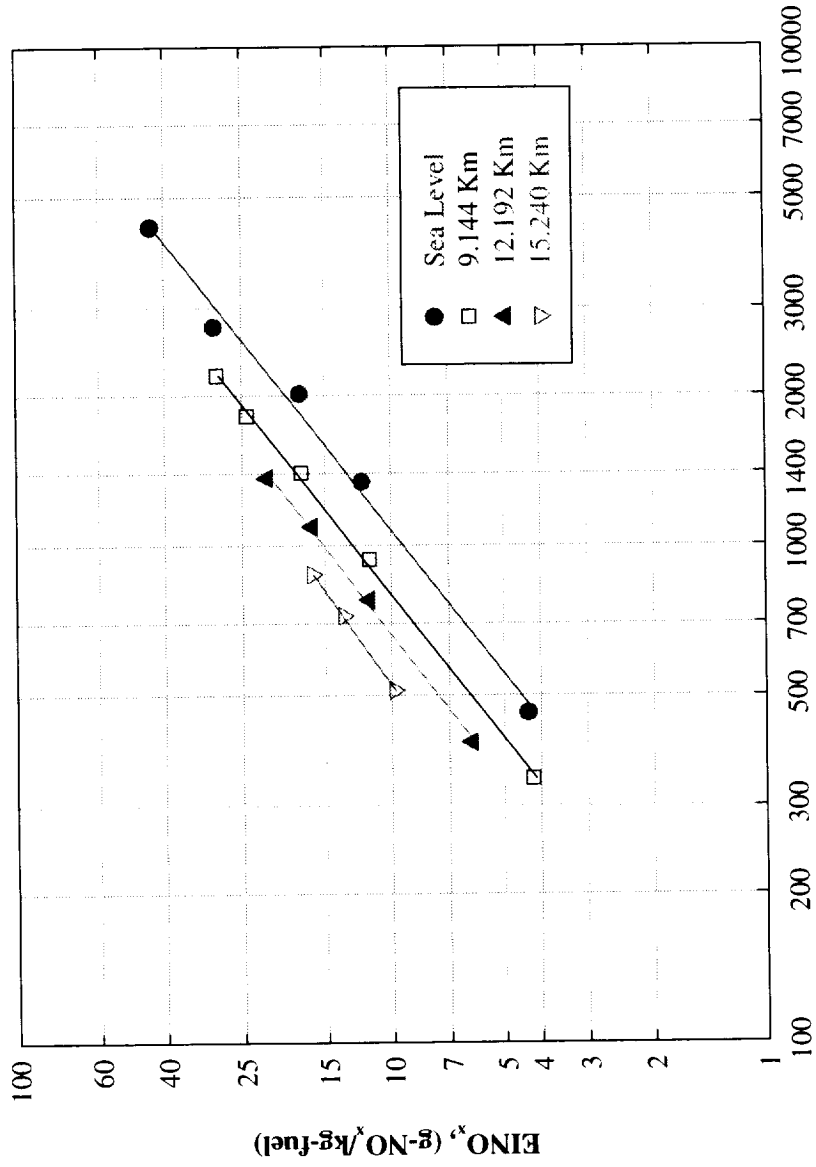

Figure C-14.—EI(NOx) vs. fuel flow for Fuel 1

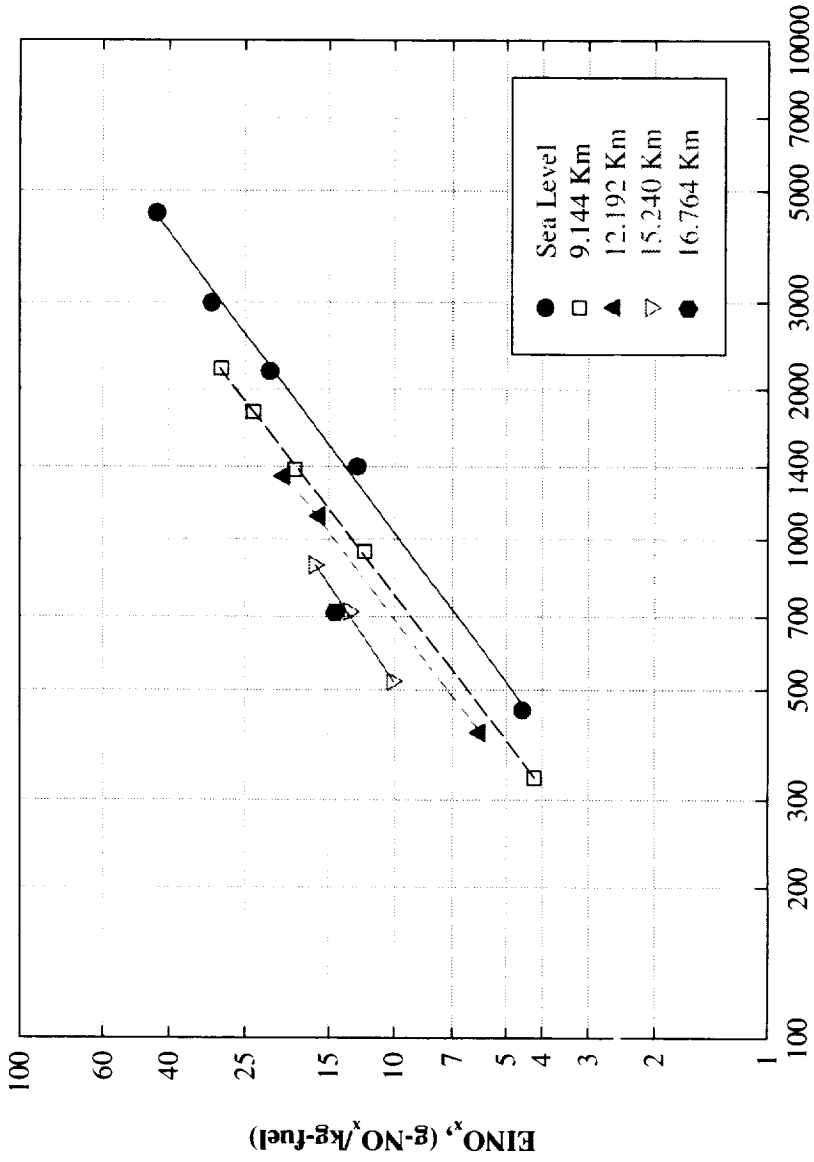

Figure C-15.—EI(NOx) vs. fuel flow for Fuel 2

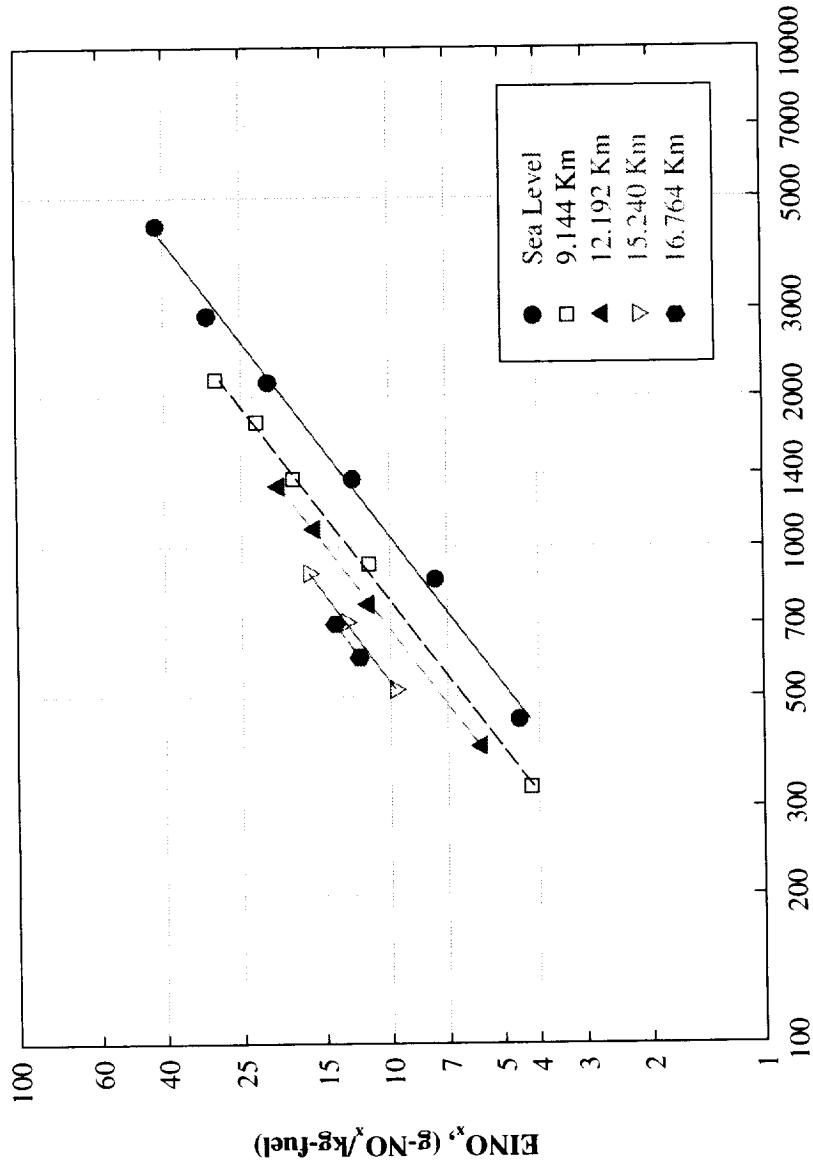

Figure C-16.—EI(NOx) vs. fuel flow for Fuel 3

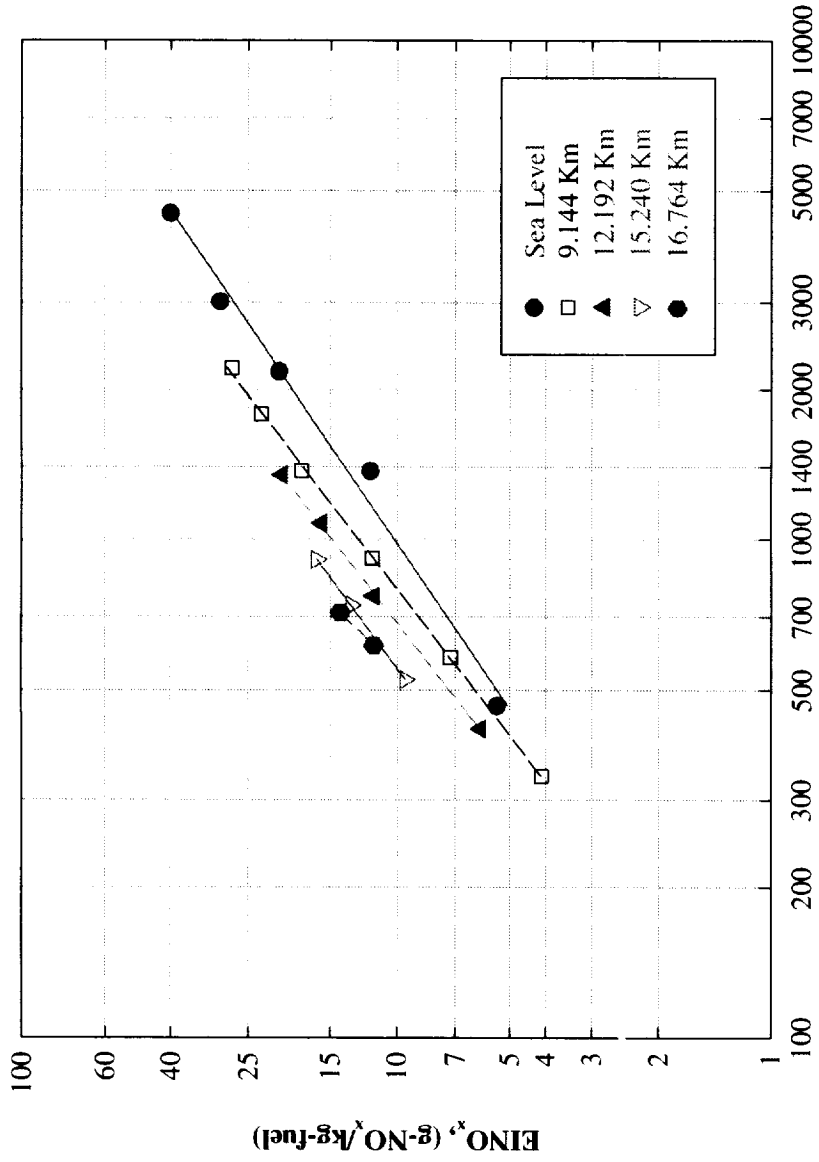

Figure C-17.—EI(NOx) vs. fuel flow for Fuel 4

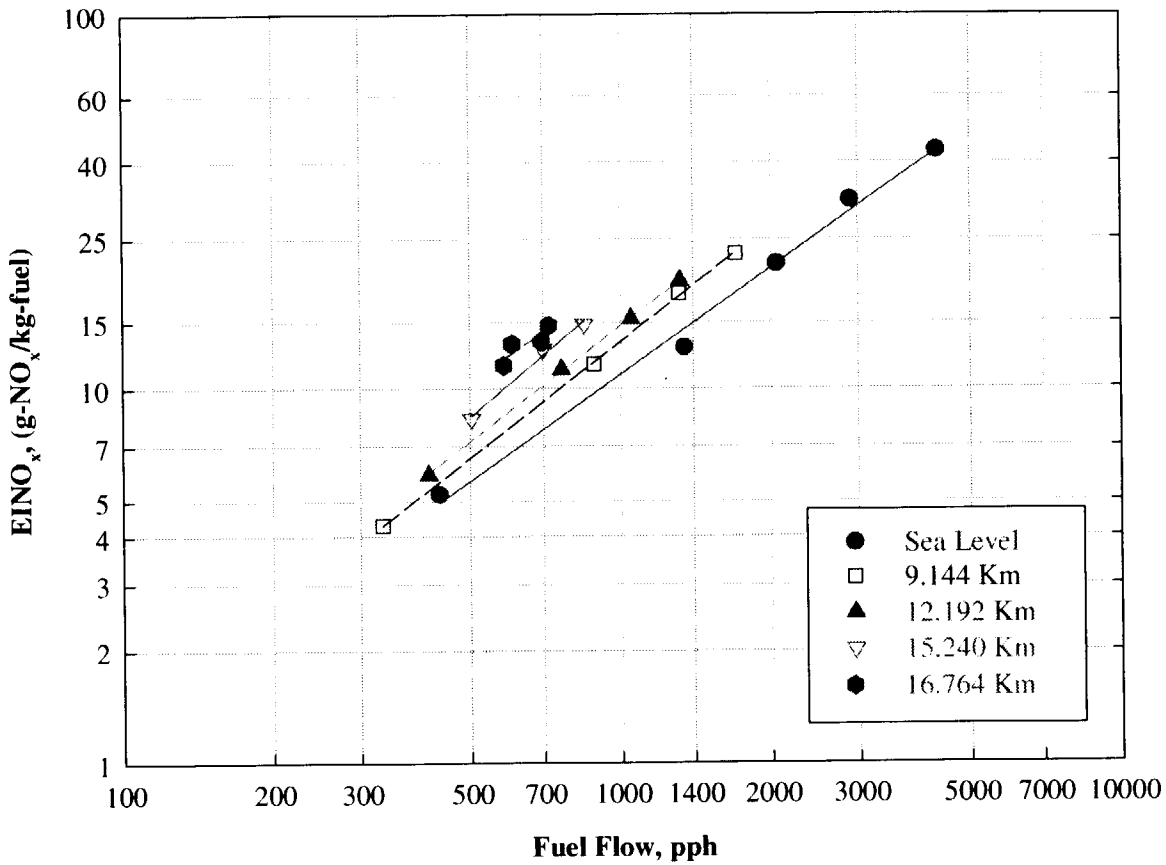

Figure C-18.—EI(NOx) vs. fuel flow for Fuel 5

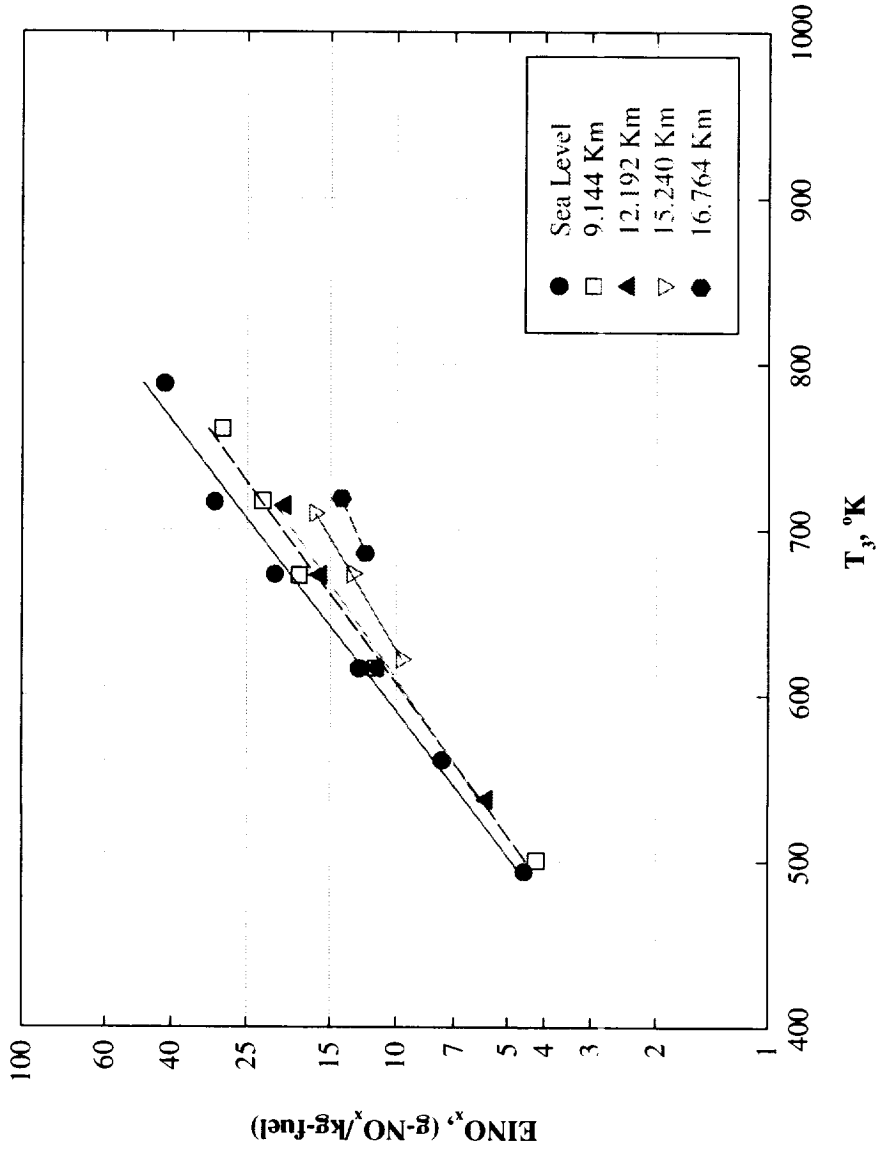

Figure C-19.—EI(NO_x) vs. combustor inlet temperature for Fuel 3

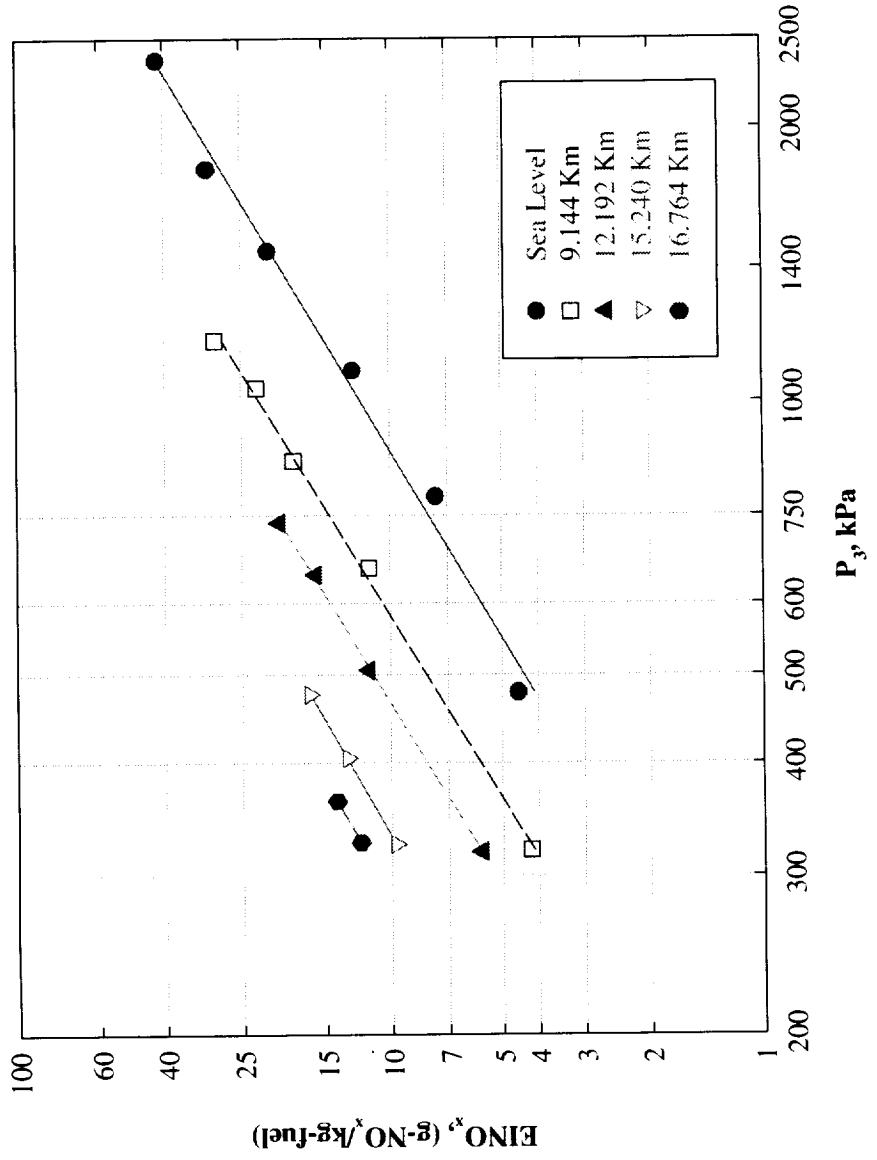

Figure C-20.—EI(NO_x) vs. combustor inlet pressure for Fuel 3

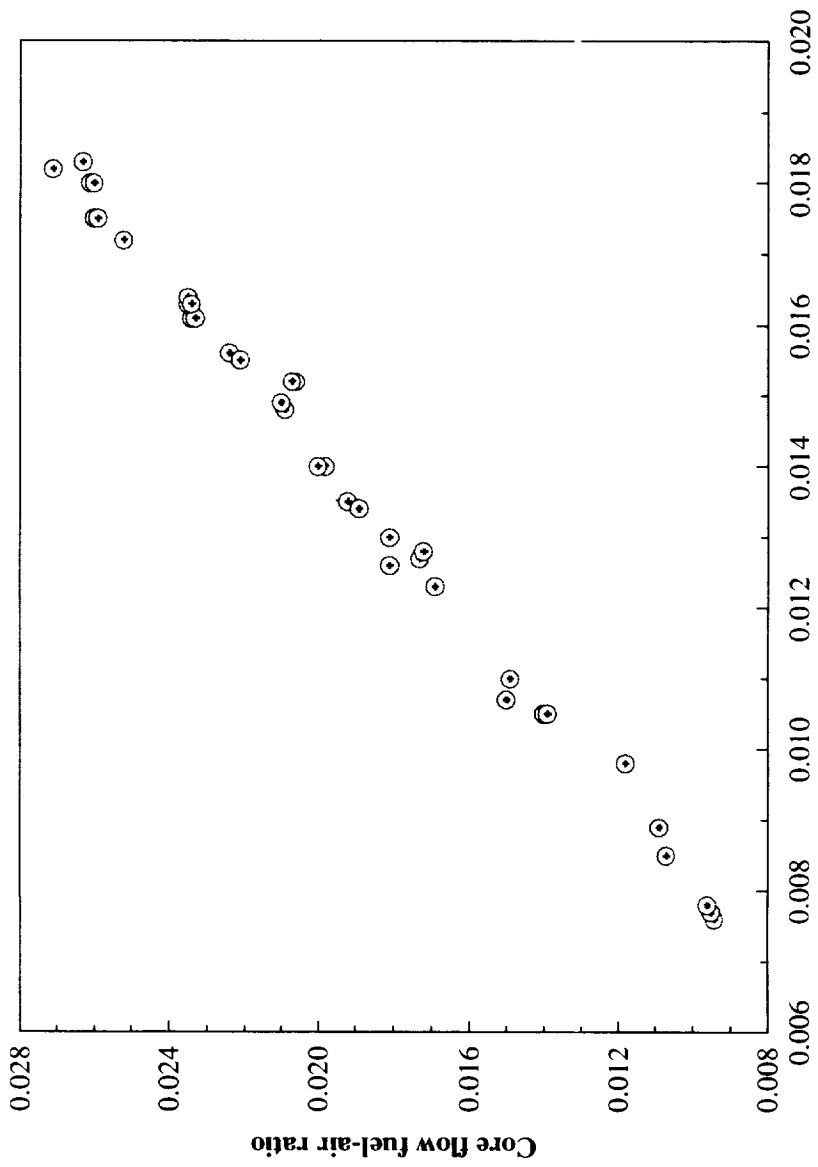

Figure C-21.—Comparisons of Fuel-Air Ratio

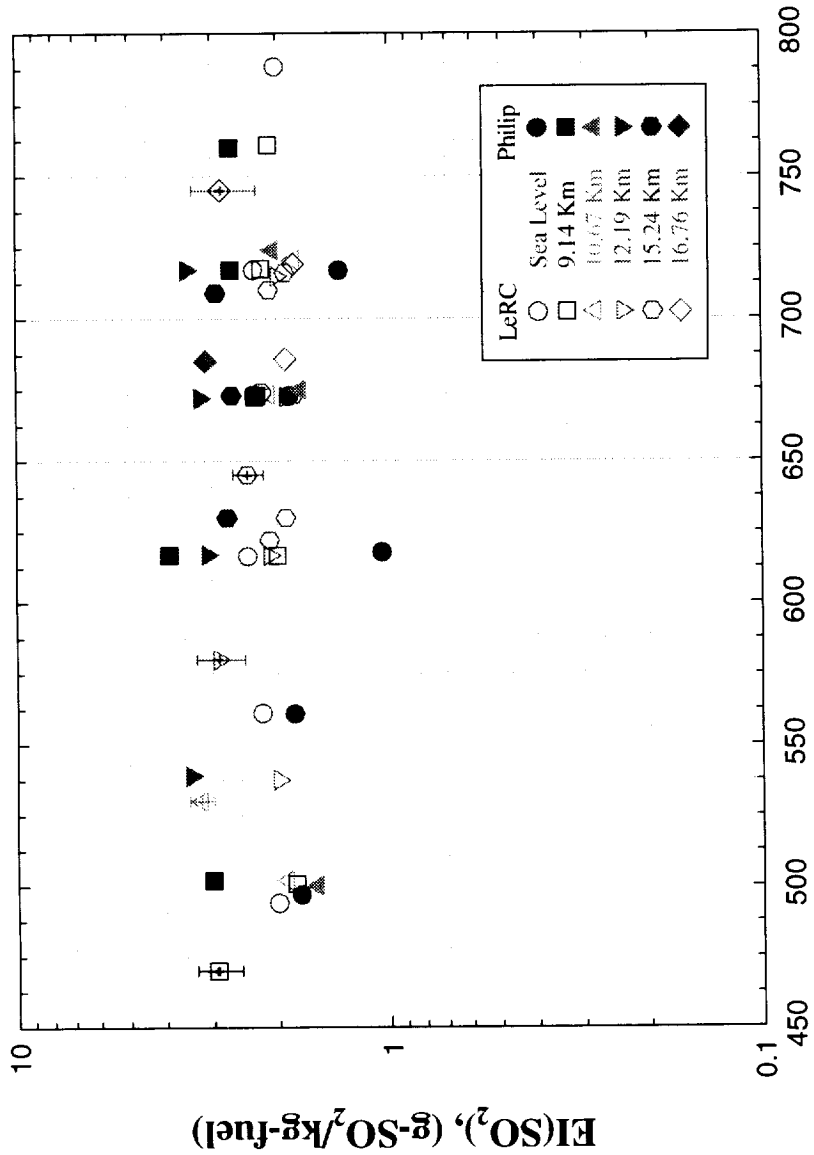

Figure C-22.—EI(SO_2) vs. T_3 for Fuel 3 (high sulfur fuel ~1113ppm)

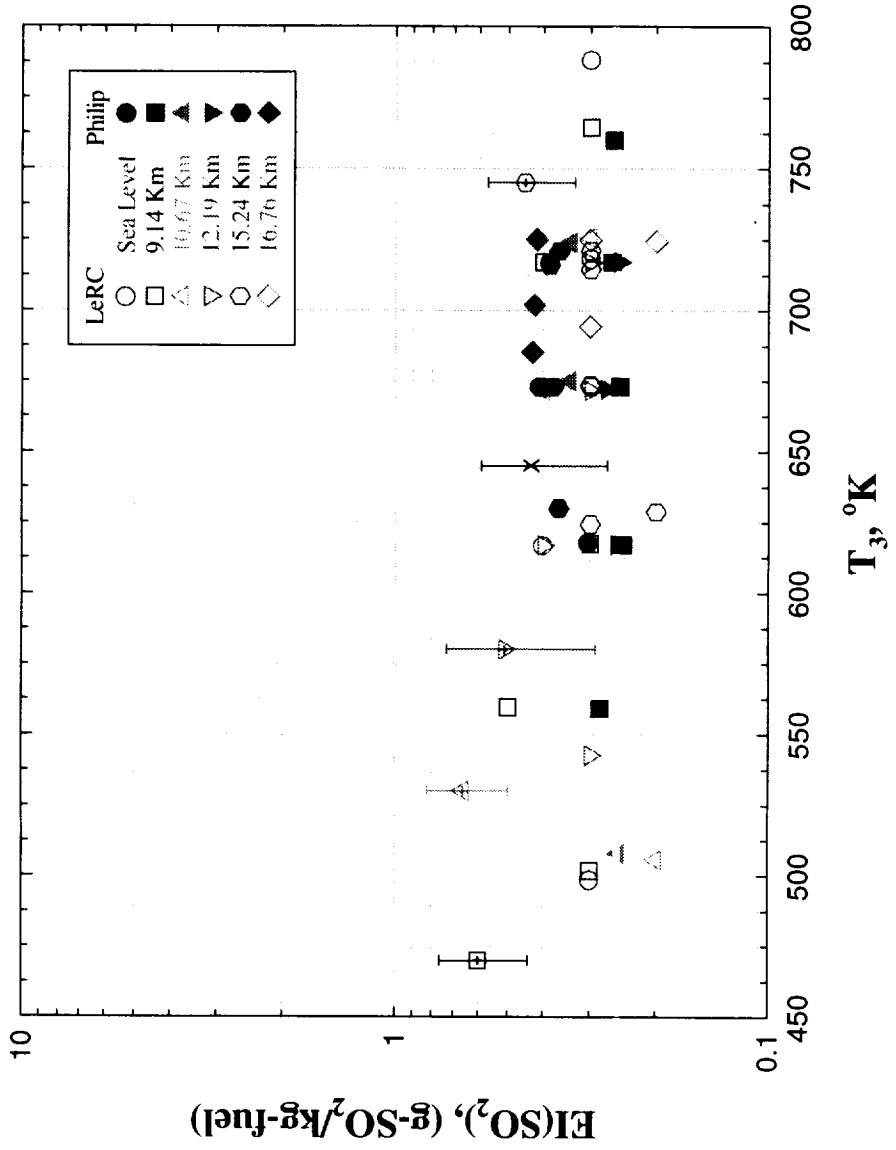

Figure C-23.—EI(SO_2) vs. T_3 for Fuel 4 (medium sulfur fuel ~152ppm)

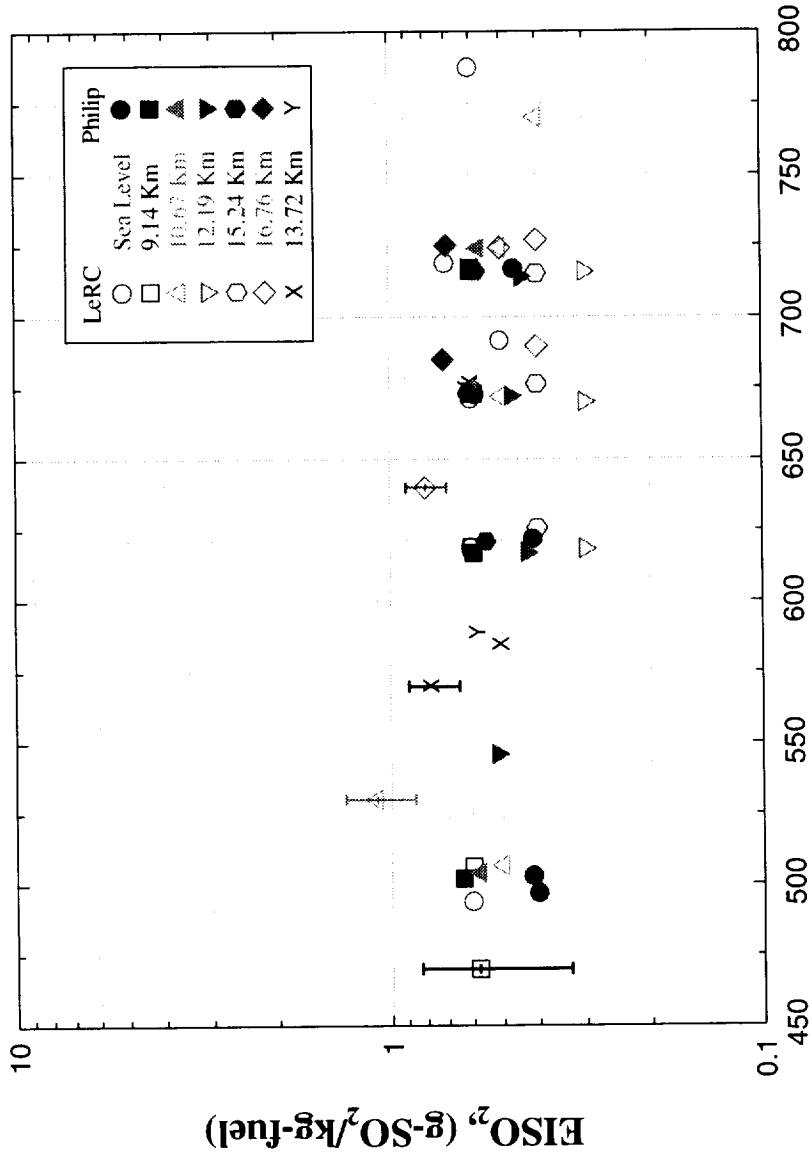

Figure C-24.—EI(SO_2) vs. T_3 for Fuel 5 (JP8+100 fuel ~336ppm S)

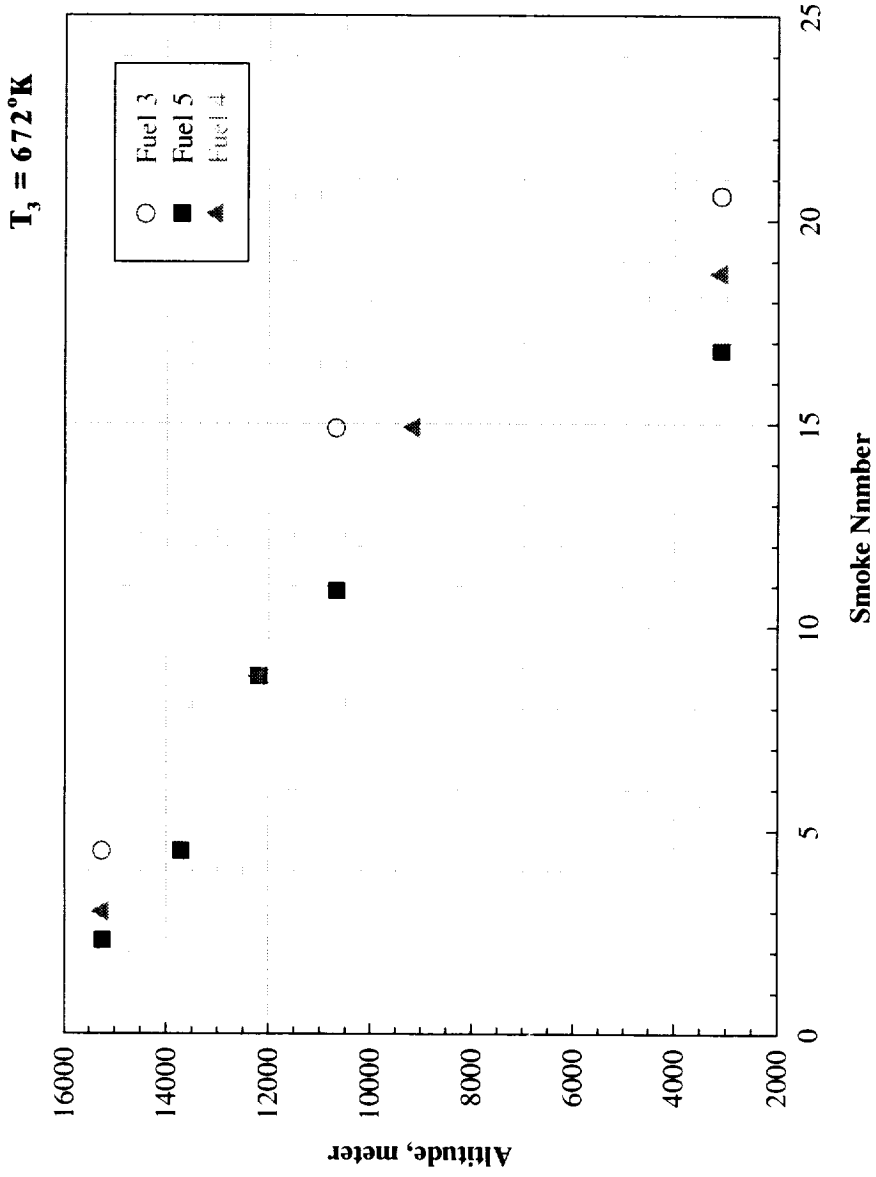

Figure C-25.—Smoke number vs. altitude at T_3 = 672°K

APPENDIX D
Particulate Sampling Measurements

D.E. Hagen, P.D. Whitefield, M.B. Trueblood, M.E. Wilson and D. Olson
Cloud and Aerosol Sciences Laboratory
University of Missouri-Rolla, Rolla MO 65401, USA

D.1. INTRODUCTION

The industry standard for particulate measurements is the smoke number. Smoke number although of considerable use for engine design considerations, does not provide the fundamental physical characterization of engine particulate emissions required to support models that explore the environmental impact of these emissions (Paladino 1997). These models require inputs on such particulate physical characteristics as: concentration, particulate number-based and mass-based particulate emission index, size distribution, hydration/growth potential (as described by measurements of particulate size dependent soluble mass fraction) and morphology. The University of Missouri-Rolla Mobile Aerosol Sampling System (UMRMASS) has been specifically designed to measure these desired physical characteristics and has been employed successfully in previous altitude chamber, ground test, combustor rig and in flight test environments (see.for example Howard et al 1996, Hagen et al 1992, 1993a, 1996, 1998 and Paladino 1998). In this appendix we describe the application of UMRMASS to characterize the particulate emissions of an F100-E200 series engine as a function of combustor inlet temperature (T_3), altitude and fuel formulation. This study also included the examination of the particulate emissions from the same engine burning JP8 with the +100 fuel additive.

D.2. EXPERIMENTAL APPROACH

A trailer-based UMRMASS was employed in this NASA Lewis sponsored F100 altitude chamber emissions study. The trailer was located adjacent to the NASA LeRC PSL facility and at a distance of approximately 30m from the engine test cell. Engine exhaust, extracted with the sampling probe rake was diluted with heated dry particle free air immediately downstream of the probe manifold assembly and the resulting dried and diluted exhaust sample was ducted to the trailer through a heated stainless steel sample line (0.0064 m o.d. at 423 °K). A schematic diagram of the UMRMASS configuration in the trailer is given in Figure D-1. The diluted sample arriving at the trailer was distributed to the following measurement stations:

(1) Total concentration - the total concentration was recorded in real time using a commercially available condensation nucleus counter (CNC) with a 1Hz sample frequency. Since CNC's will saturate at high particulate concentrations (Hagen et al. 1993b) further particulate dilution in the total concentration measurement line was achieved using needle filter diluters (Olson et al. 1996). The total concentration was monitored continuously throughout the test and was recorded as a function of time.

(2) Size distribution - size distributions were recorded using the differential mobility analysis technique (Howard et al. 1996). Diluted exhaust sample was either ducted directly to the differential mobility analyzer (DMA) and a size spectrum was recorded in real-time or the diluted sample was ducted to a 40 liter storage tank after which size spectra were recorded off-line but typically within a few minutes of storage.

Since the MASS methodology has been described extensively elsewhere (Hagen 1993a, Howard et al. 1996) no further discussion will be provided here.

D.3. PARTICULATE CHARACTERIZATION RESULTS

In this project the particulate physical characteristics, described in section D-2 were measured as a function of altitude and combustor inlet temperature (T_3) using JetA jet fuel with 3 sulfur contents defined as low, medium and high each including several different additives, and with JP8 with the +100 additive (see Tables 1-4). The data are all reported using the escort number for reference to the test matrix. The data presented below is based on the entire test program data set excluding test point periods 406-436 and 450-498.

Tables D-1 thru D-4 are compilations of the mean particulate number-based EI's, mean mass-based EI's, and particulate volume fractions for each test point with each table representing the data for a given fuel. The quoted uncertainty in all cases is based on the analysis of both statistical and systematic errors arising from the measurement methodologies. Table D-5 lists the mean particulate number-based EI's, mean mass-based EI's, and particulate volume fractions for all measurements on a given fuel. The mean mass-based EI's and particulate volume fractions are calculated using the measured size distribution and number-based EI's for each test condition. An analysis of the particle mass distributions indicated >90% of the particle mass fell within the measurement regime of the DMA (10-300nm), see Figures D-2 and D-3. Figures D-4 through D-7 plot the number-based EI's for all fuels as a function of T_3 for fixed altitudes. Associated with each escort number there are mean size distributions. These size distributions are plotted in Figures D-8 thru D-35. Table D-6 reports the average mean diameters for all size distributions measured at all engine operating conditions for each fuel studied. The quoted uncertainty is one standard deviation. Where more than one size distributions can be associated with a given test condition (as a result of returning at a later time to any given test condition) each distribution associated with the same test condition, and identified by its escort number is plotted on the same axis in Figure D-36. These data are presented to explore issues of the engines reproducibility of particulate emission characteristics for a given set of operational parameters.

D.4. CONCLUSIONS

The following conclusions can be drawn from particulate emissions measurements presented in section D-3.

Emission Indices:

- No strong dependence of EI on T_3 or altitude is observed. In some cases a weak dependence is observed where the EI appears to peak at T_3's around 600-700 ^{o}K (see Figures D-4 - D-7).

- The lack of any strong dependence of EI on T_3 or altitude justifies the representation of the fuel effect on particulate emissions using the mean value for all test conditions studied for a given fuel (Table D-5).

- The mean EIs for the high and medium sulfur cases are comparable. The mean EI for the low sulfur case studied was significantly lower (by a factor of between 3 to 4) than that for the high and medium sulfur cases. There were, however, several variables in the fuel formulation beyond that of sulfur content. The base fuel for the low sulfur case was hydrotreated and contained a different additive package to the high sulfur which had not been hydrotreated. The medium sulfur fuel was a blend of the high and low sulfur fuels providing the desired mid-range sulfur concentration. It is clear from these data that particulate emissions can be significantly affected through fuel formulation modification but it is not clear what facet of modification is responsible for observed emissions changes.

- The mean number -based EI for the JP8+100 fuel case was $(2.0 \pm 0.4) \times 10^{14}$ particles/kg fuel burned. This result is comparable to the EIs measured for the medium and high sulfur cases. In this case, however, yet a different additive package is present in a different baseline fuel.

- The mean mass-based EI's and particulate volume fractions, both of which are calculated using the measured size distribution and number-based EI's for each test condition, exhibit the same trends as a function of fuel formulation.

- An analysis of the particle mass distributions indicated >90% of the particle mass fell within the measurement regime of the DMA (10 - 300 nm) and thus the estimation of mass-based EI's from the mean volume diameter of the distributions and an assumed density for the particles was valid.

Size Distributions

- For all fuels and test conditions studied the size distributions are of a log-normal type with mean diameters in the range 50-65nm (see Table D-6).

In the case of the medium sulfur fuel study, data were acquired for the same engine operating conditions at different times when test conditions were repeated with the same

fuel on different days. These data provide an opportunity to explore the engine performance issue of particulate emission stability between subsequent measurements at equivalent test conditions. The emissions reproducibility is good. The standard deviation in the mean diameters was 1.5% and that of the half widths of the distribution was 3%.

REFERENCES

1. Alofs, D.J., C.K. Lutrus, D.E. Hagen, G.J. Sem, and J.L. Blesener, "Intercomparison between commercial condensation nucleus counters and an alternating temperature gradient cloud chamber", Aerosol Sci. & Techn. 23, 239-249 (1995).

2. Hagen, D.E., M.B. Trueblood, and P.D. Whitefield, "A field sampling of jet exhaust aerosols", Particle Sci. & Techn. 10, 53-63 (1992).

3. Hagen, D.E., P.D. Whitefield, M.B. Trueblood, and H.V. Lilenfeld, "Particulates and aerosols characterized in real time from harsh environments using the UMR mobile aerosol sampling system (MASS)", AIAA (Amer. Institute of Aeronautics and Astronautics) paper No. 93-2344 (1993a).

4. Hagen, D.E., C.K. Lutrus, M.B. Trueblood, P.D. Whitefield, D.J. Alofs, L.R. Dominguez-Sommer, and J.R.C. Futrell, "Use of an alternating gradient cloud chamber to measure the performance of a condensation nucleus counter", Proc. 39th meeting of the Institute of Env. Sci. 1, 319 (1993b).

5. Hagen, D.E., and P.D. Whitefield, "Particulate emissions in the exhaust plume from commercial jet aircraft under cruise conditions", J. Geophys. Res. Atmos. 101, 19551-19557 (1996).

6. Hagen, D., P. Whitefield, J. Paladino, M. Trueblood, and H. Lilenfeld, "Particulate sizing and emission indices for a jet engine exhaust sampled at cruise", Geophys. Res. Lett. 25, 1681- 1684 (1998).

7. Howard, R.P., "Experimantal characterization of gas turbine emissions at simulated flight altitude conditions", AEDC-TR-96-3, Arnold Engineering Development Center tech. report, NTIS, Sept. 1996.

8. Olson, D.D., M.B. Trueblood, and P.D. Whitefield, "The development of a novel dilution technique for sub-micron particulate characterization", OURE program report, University of Missouri- Rolla, 1996.

9. Paladino, J., P. Whitefield, D. Hagen, A.R. Hopkins, and M. Trueblood, "Particle concentration characterization for jet engine emissions under cruise conditions", Geophys. Res. Lett. 25, 1697- 1700 (1998).

ESP *	Alt *	T_3	Fuel	EI (n) *	EI(n) unc.	EI(m)*	EI(m) unc.	PVF *	PVF unc.
596	9	511	High	1.03E+14	+/- 2.07E+13	0.01	+/- 2.77E-03	1.66E-11	+/- 3.32E-12
599	9	616	High	2.99E+14	+/- 5.99E+13	0.11	+/- 2.22E-02	5.07E-10	+/- 1.01E-10
603	9	672	High	2.62E+14	+/- 5.25E+13	0.10	+/- 1.94E-02	6.31E-10	+/- 1.26E-10
607	9	716	High	1.02E+14	+/- 2.04E+13	0.08	+/- 1.60E-02	6.98E-10	+/- 1.40E-10
611	9	755	High	1.61E+14	+/- 3.22E+13	0.25	+/- 5.00E-02	2.73E-09	+/- 5.46E-10
569	12	537	High	1.59E+14	+/- 3.18E+13	0.03	+/- 5.43E-03	3.20E-11	+/- 6.41E-12
572	12	616	High	4.79E+14	+/- 9.59E+13	0.13	+/- 2.69E-02	3.09E-10	+/- 6.18E-11
575	12	671	High	5.66E+14	+/- 1.13E+14	0.32	+/- 6.44E-02	9.99E-10	+/- 2.00E-10
580	12	716	High	4.69E+14	+/- 9.38E+13	0.26	+/- 5.22E-02	1.11E-09	+/- 2.23E-10
584	15	628	High	1.25E+14	+/- 2.50E+13	0.05	+/- 9.83E-03	6.48E-11	+/- 1.30E-11
587	15	672	High	2.04E+14	+/- 4.08E+13	0.06	+/- 1.12E-02	9.21E-11	+/- 1.84E-11
591	15	716	High	2.12E+14	+/- 4.25E+13	0.11	+/- 2.10E-02	2.32E-10	+/- 4.64E-11
594	17	716	High	1.24E+14	+/- 2.47E+13	0.06	+/- 1.21E-02	9.72E-11	+/- 1.94E-11

*

ESP Escort parameter / number
Alt Altitude
EI (n) Number-based emission index
EI (m) Mass-based emission index
PVF Particle volume fraction
unc uncertainty (1s).

Table D-1: Emission Indices and Soot Volume Fractions as a Function of Altitude, T_3 and Fuel - High Sulfur

ESP *	Alt *	T_3	Fuel	EI (n) *	EI(n) unc.	EI(m)*	EI(m) unc.	PVF *	PVF unc.
857	3	616	JP8+100	1.56E+14	+/- 3.12E+13	0.07	+/- 1.32E-02	5.83E-10	+/- 1.17E-10
860	3	672	JP8+100	3.1E+14	+/- 6.19E+13	0.20	+/- 3.93E-02	1.27E-09	+/- 2.55E-10
863	3	716	JP8+100	3.03E+14	+/- 6.06E+13	0.21	+/- 4.21E-02	1.49E-09	+/- 2.98E-10
868	3	789	JP8+100	1.76E+14	+/- 3.53E+13	0.14	+/- 2.73E-02	1.16E-09	+/- 2.33E-10
835	9	616	JP8+100	2.85E+14	+/- 5.69E+13	0.10	+/- 2.02E-02	2.15E-10	+/- 4.29E-11
837	9	672	JP8+100	1.76E+14	+/- 3.53E+13	0.08	+/- 1.65E-02	4.24E-10	+/- 8.49E-11
840	9	716	JP8+100	1.3E+14	+/- 2.60E+13	0.07	+/- 1.43E-02	5.07E-10	+/- 1.01E-10
844	9	766	JP8+100	6.02E+13	+/- 1.20E+13	0.03	+/- 6.67E-03	3.63E-10	+/- 7.26E-11
890	11	505	JP8+100	3.48E+13	+/- 6.97E+12	0.00	+/- 6.47E-04	6.36E-12	+/- 1.27E-12
894	11	678	JP8+100	4.14E+14	+/- 8.28E+13	0.17	+/- 3.37E-02	3.97E-10	+/- 7.94E-11
899	11	728	JP8+100	1.39E+14	+/- 2.77E+13	0.07	+/- 1.42E-02	5.03E-10	+/- 1.01E-10
803	12	616	JP8+100	4.81E+14	+/- 9.63E+13	0.16	+/- 3.16E-02	2.16E-10	+/- 4.33E-11
806	12	672	JP8+100	3.09E+14	+/- 6.19E+13	0.16	+/- 3.22E-02	3.98E-10	+/- 7.96E-11
811	12	716	JP8+100	2.4E+14	+/- 4.81E+13	0.14	+/- 2.83E-02	5.50E-10	+/- 1.10E-10
871	14	589	JP8+100	6.36E+13	+/- 1.27E+13	0.01	+/- 2.34E-03	3.00E-11	+/- 6.00E-12
875	14	678	JP8+100	3.19E+14	+/- 6.38E+13	0.11	+/- 2.10E-02	1.55E-10	+/- 3.10E-11
879	14	718	JP8+100	2.59E+14	+/- 5.19E+13	0.12	+/- 2.41E-02	2.63E-10	+/- 5.26E-11
814	15	622	JP8+100	1.4E+14	+/- 2.80E+13	0.04	+/- 8.79E-03	5.20E-11	+/- 1.04E-11
817	15	672	JP8+100	2.26E+14	+/- 4.53E+13	0.09	+/- 1.82E-02	1.31E-10	+/- 2.63E-11
822	15	716	JP8+100	1.92E+14	+/- 3.84E+13	0.10	+/- 1.94E-02	1.97E-10	+/- 3.94E-11
824	17	689	JP8+100	6.92E+13	+/- 1.38E+13	0.02	+/- 4.66E-03	3.65E-11	+/- 7.30E-12
827	17	728	JP8+100	1.38E+14	+/- 2.77E+13	0.07	+/- 1.36E-02	8.50E-11	+/- 1.70E-11
882	17	689	JP8+100	5.53E+13	+/- 1.11E+13	0.02	+/- 3.31E-03	2.74E-11	+/- 5.48E-12
886	17	722	JP8+100	1.18E+14	+/- 2.36E+13	0.05	+/- 1.05E-02	8.05E-11	+/- 1.61E-11

*

ESP Escort parameter / number
Alt Altitude
EI (n) Number-based emission index
EI (m) Mass-based emission index
PVF Particle volume fraction
unc uncertainty (1s)

Table D-2: Emission Indices and Soot Volume Fractions as a Function of Altitude, T_3 and Fuel - JP8+100

ESP *	Alt *	T_3	Fuel	EI (n) *	EI(n) unc.	EI(m)*	EI(m) unc.	PVF *	PVF unc.
621	3	494	Mid S	1.80E+13	+/- 3.59E+12	0.01	+/- 2.81E-03	5.08E-11	+/- 1.02E-11
624	3	561	Mid S	5.76E+13	+/- 1.15E+13	0.01	+/- 2.93E-03	8.40E-11	+/- 1.68E-11
627	3	616	Mid S	4.10E+14	+/- 8.21E+13	0.24	+/- 4.70E-02	1.01E-09	+/- 2.02E-10
630	3	672	Mid S	3.86E+14	+/- 7.73E+13	0.26	+/- 5.20E-02	1.37E-09	+/- 2.74E-10
633	3	716	Mid S	2.74E+14	+/- 5.47E+13	0.22	+/- 4.36E-02	1.76E-09	+/- 3.52E-10
636	3	789	Mid S	1.57E+14	+/- 3.13E+13	0.13	+/- 2.62E-02	1.29E-09	+/- 2.58E-10
707	9	505	Mid S	6.56E+13	+/- 1.31E+13	0.01	+/- 1.26E-03	1.10E-11	+/- 2.21E-12
711	9	616	Mid S	1.42E+14	+/- 2.83E+13	0.07	+/- 1.47E-02	3.88E-10	+/- 7.75E-11
712	9	672	Mid S	1.93E+14	+/- 3.87E+13	0.09	+/- 1.72E-02	5.10E-10	+/- 1.02E-10
716	9	716	Mid S	9.84E+13	+/- 1.97E+13	0.06	+/- 1.12E-02	4.99E-10	+/- 9.98E-11
718	9	761	Mid S	7.94E+13	+/- 1.59E+13	0.05	+/- 9.93E-03	5.50E-10	+/- 1.10E-10
720	9	561	Mid S	2.71E+13	+/- 5.42E+12	0.01	+/- 1.44E-03	4.38E-11	+/- 8.77E-12
773	15	622	Mid S	1.60E+14	+/- 3.19E+13	0.05	+/- 1.03E-02	6.11E-11	+/- 1.22E-11
650	15	622	Mid S	1.58E+14	+/- 3.15E+13	0.07	+/- 1.49E-02	9.71E-11	+/- 1.94E-11
687	15	628	Mid S	1.97E+14	+/- 3.93E+13	0.07	+/- 1.35E-02	1.18E-10	+/- 2.36E-11
653	15	672	Mid S	1.58E+14	+/- 3.15E+13	0.07	+/- 1.49E-02	9.71E-11	+/- 1.94E-11
656	15	716	Mid S	3.02E+14	+/- 6.04E+13	0.19	+/- 3.82E-02	4.01E-10	+/- 8.02E-11
659	17	686	Mid S	1.80E+14	+/- 3.59E+13	0.09	+/- 1.72E-02	9.05E-11	+/- 1.81E-11
784	17	700	Mid S	7.20E+13	+/- 1.44E+13	0.03	+/- 5.75E-03	4.69E-11	+/- 9.38E-12
790	17	728	Mid S	1.23E+14	+/- 2.46E+13	0.07	+/- 1.32E-02	9.76E-11	+/- 1.95E-11
640	11	505	Mid S	9.18E+13	+/- 1.84E+13	0.02	+/- 4.15E-03	2.74E-11	+/- 5.47E-12
642	11	672	Mid S	3.23E+14	+/- 6.46E+13	0.17	+/- 3.33E-02	4.26E-10	+/- 8.52E-11
700	17	683	Mid S	1.88E+14	+/- 3.76E+13	0.06	+/- 1.26E-02	6.39E-11	+/- 1.28E-11
768	11	728	Mid S	2.39E+14	+/- 4.78E+13	0.13	+/- 2.70E-02	4.74E-10	+/- 9.49E-11
646	11	755	Mid S	2.15E+14	+/- 4.29E+13	0.13	+/- 2.62E-02	8.69E-10	+/- 1.74E-10
695	15	716	Mid S	5.01E+14	+/- 1.00E+14	0.242	+/- 4.84E-02	3.51E-10	+/- 7.01E-11
780	15	716	Mid S	2.00E+14	+/- 4.00E+13	0.112	+/- 2.24E-02	2.49E-10	+/- 4.97E-11
763	11	672	Mid S	6.12E+14	+/- 1.22E+14	0.295	+/- 5.90E-02	3.85E-10	+/- 7.71E-11

Table D-3: Emission Indices and Soot Volume Fractions as a Function of Altitude, T_3 and Fuel - Mid Sulfur

ESP *	Alt *	T_3	Fuel	EI (n) *	EI(n) unc.	EI(m)*	EI(m) unc.	PVF *	PVF unc.
542	3	505	Low S	1.131E+13	+/- 2.26E+12	0.00	+/- 9.29E-04	1.548E-11	+/- 3.10E-12
545	3	616	Low S	5.113E+13	+/- 1.02E+13	0.04	+/- 8.28E-03	2.236E-10	+/- 4.47E-11
549	3	672	Low S	6.091E+13	+/- 1.22E+13	0.08	+/- 1.56E-02	5.17E-10	+/- 1.03E-10
552	3	716	Low S	3.265E+13	+/- 6.53E+12	0.05	+/- 9.87E-03	3.77E-10	+/- 7.54E-11
554	3	794	Low S	1.344E+13	+/- 2.69E+12	0.02	+/- 4.63E-03	2.151E-10	+/- 4.30E-11
529	9	672	Low S	6.432E+13	+/- 1.29E+13	0.06	+/- 1.18E-02	3.515E-10	+/- 7.03E-11
532	9	716	Low S	3.924E+13	+/- 7.85E+12	0.05	+/- 9.79E-03	3.941E-10	+/- 7.88E-11
534	9	755	Low S	6.91E+12	+/- 4.82E-02	0.01	+/- 4.28E-10	8.558E-11	+/- 1.14E-10
527	9	616	Low S	8.755E+13	+/- 1.75E+13	0.06	+/- 1.13E-02	1.995E-10	+/- 3.99E-11
498	12	547	Low S	4.019E+13	+/- 8.04E+12	0.02	+/- 3.26E-03	3.124E-11	+/- 6.25E-12
505	12	672	Low S	3.808E+13	+/- 7.62E+12	0.02	+/- 4.93E-03	7.578E-11	+/- 1.52E-11
508	12	716	Low S	5.791E+13	+/- 1.16E+13	0.05	+/- 1.00E-02	1.734E-10	+/- 3.47E-11
513	15	622	Low S	9.876E+13	+/- 1.98E+13	0.06	+/- 1.30E-02	1.103E-10	+/- 2.21E-11
514	15	672	Low S	9.384E+13	+/- 1.88E+13	0.06	+/- 1.29E-02	1.25E-10	+/- 2.50E-11
517	15	716	Low S	2.928E+13	+/- 5.86E+12	0.02	+/- 3.20E-03	3.605E-11	+/- 7.21E-12

*

ESP Escort parameter / number
Alt Altitude
EI (n) Number-based emission index
EI (m) Mass-based emission index
PVF Particle volume fraction
unc uncertainty (1s)

Table D-4: Emission Indices and Soot Volume Fractions as a Function of Altitude, T3 and Fuel - Low Sulfur

Fuel	EI (n)	EI(n) unc.	EI(m)	EI(m) unc.	PVF	PVF unc.
Low S	4.84E+13	+/- 9.58E+12	0.04	+/- 7.97E-03	1.95E-10	+/- 4.55E-11
Med S	2.01E+14	+/- 4.02E+13	0.11	+/- 2.11E-02	4.08E-10	+/- 8.16E-11
High S	2.51E+14	+/- 5.03E+13	0.12	+/- 2.41E-02	5.79E-10	+/- 1.16E-10
JP8+100	2E+14	+/- 4.00E+13	0.09	+/- 1.86E-02	3.81E-10	+/- 7.62E-11

*

ESP Escort parameter / number
Alt Altitude
EI (n) Number-based emission index
EI (m) Mass-based emission index
PVF Particle volume fraction
unc uncertainty (1s)

Table D-5: Average Emission Indices and Soot Volume Fractions For All Data

Fuel	xbar(nm) *	unc
Low S	63.14	14.46
Med S	53.93	10.60
High S	55.86	13.88
JP8+100	57.75	7.08

*

xbar (nm) Average mean diameter
unc uncertainty (1s)

Table D-6: Average Mean Diameters For All Data

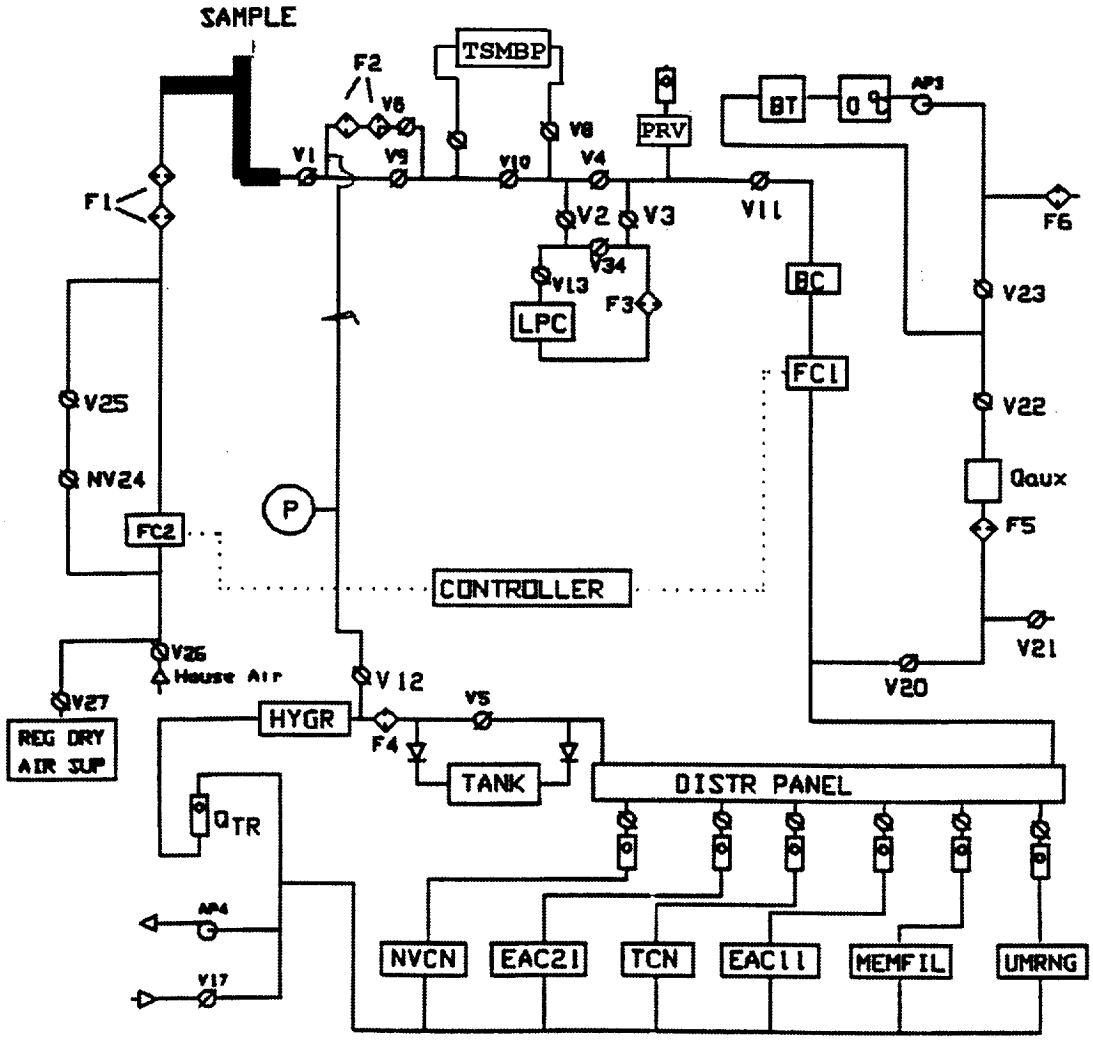

Figure D-1: Schematic of UMR - MASS System

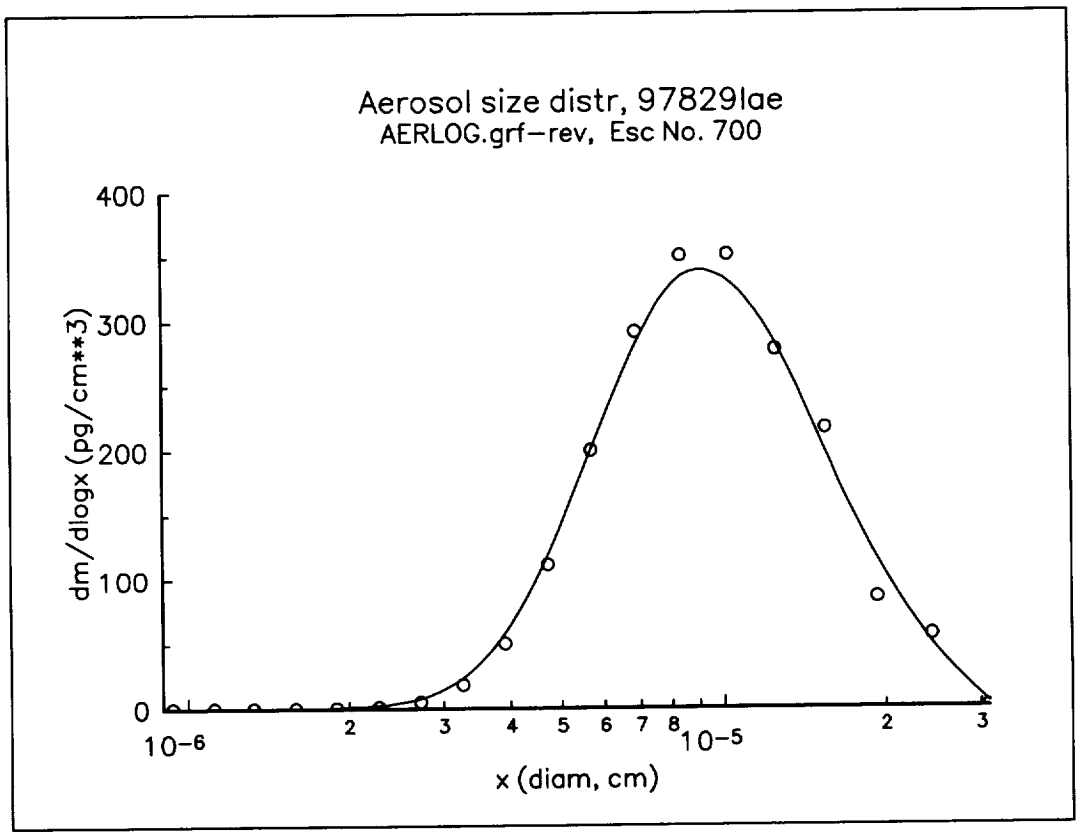

Figure D-2: Particle mass distributions showing > 90% of particle mass falls within measurement range from 10 nm to 300 nm particle diameter

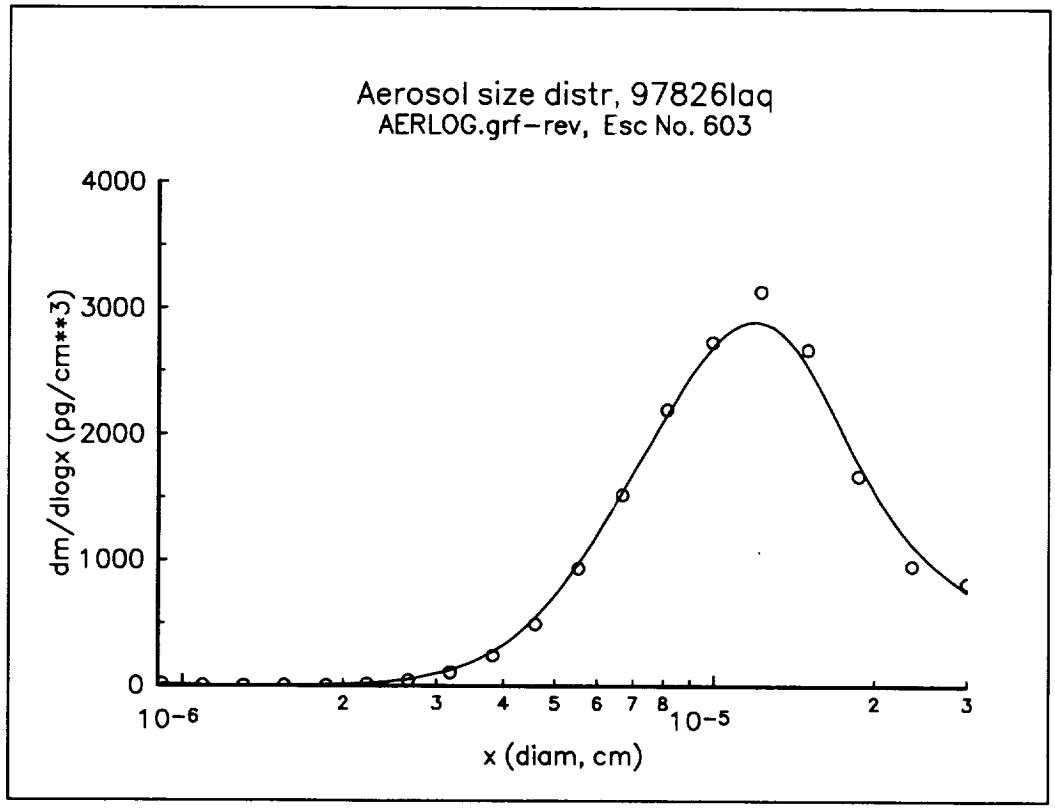

Figure D-3: Particle mass distributions showing > 90% of particle mass falls within measurement range from 10 nm to 300 nm particle diameter

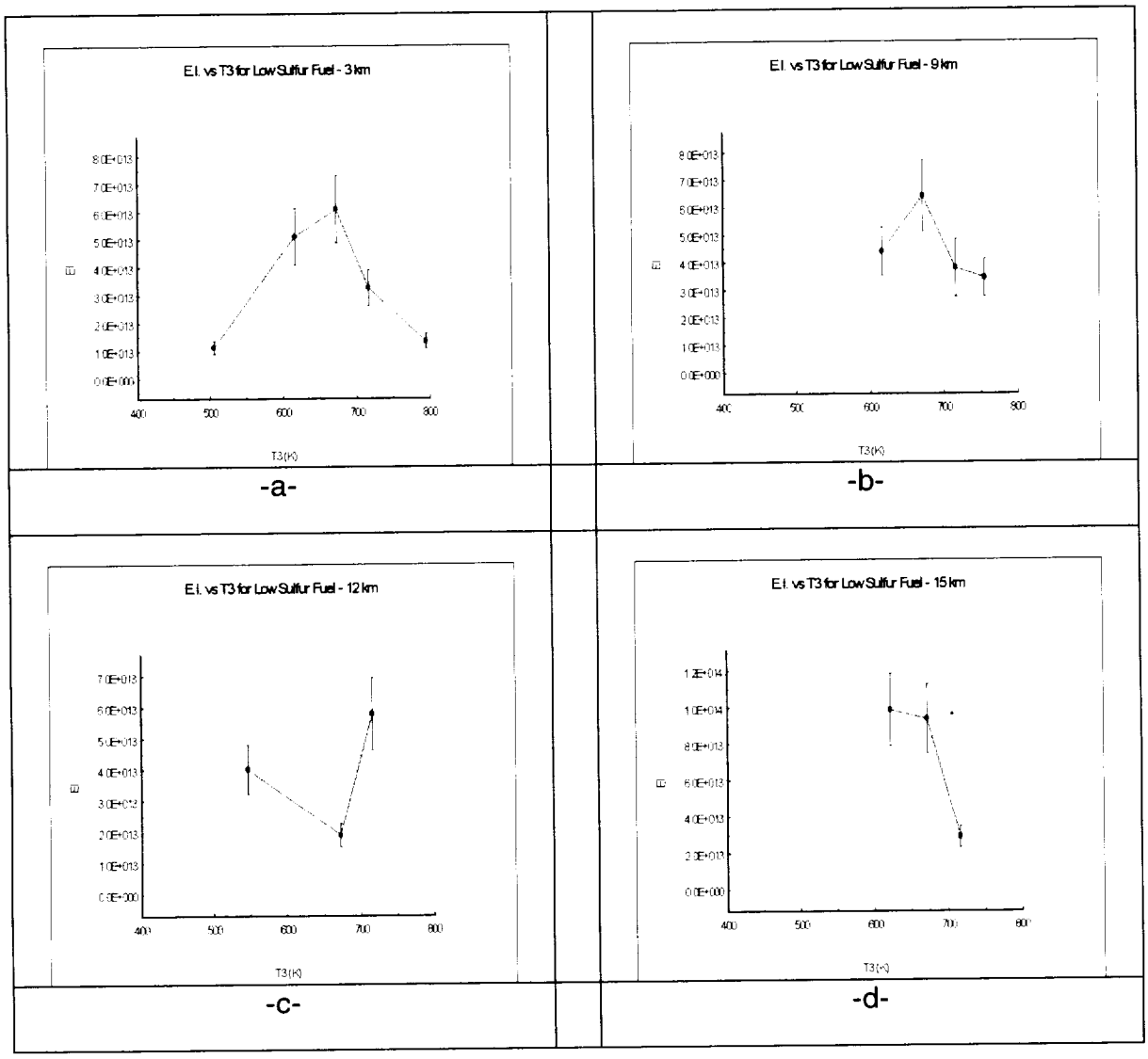

Figure D-4 a-d: EI vs T_3 for Low Sulfur Case at altitudes a=3km, b=9km, c=12km, d=15km

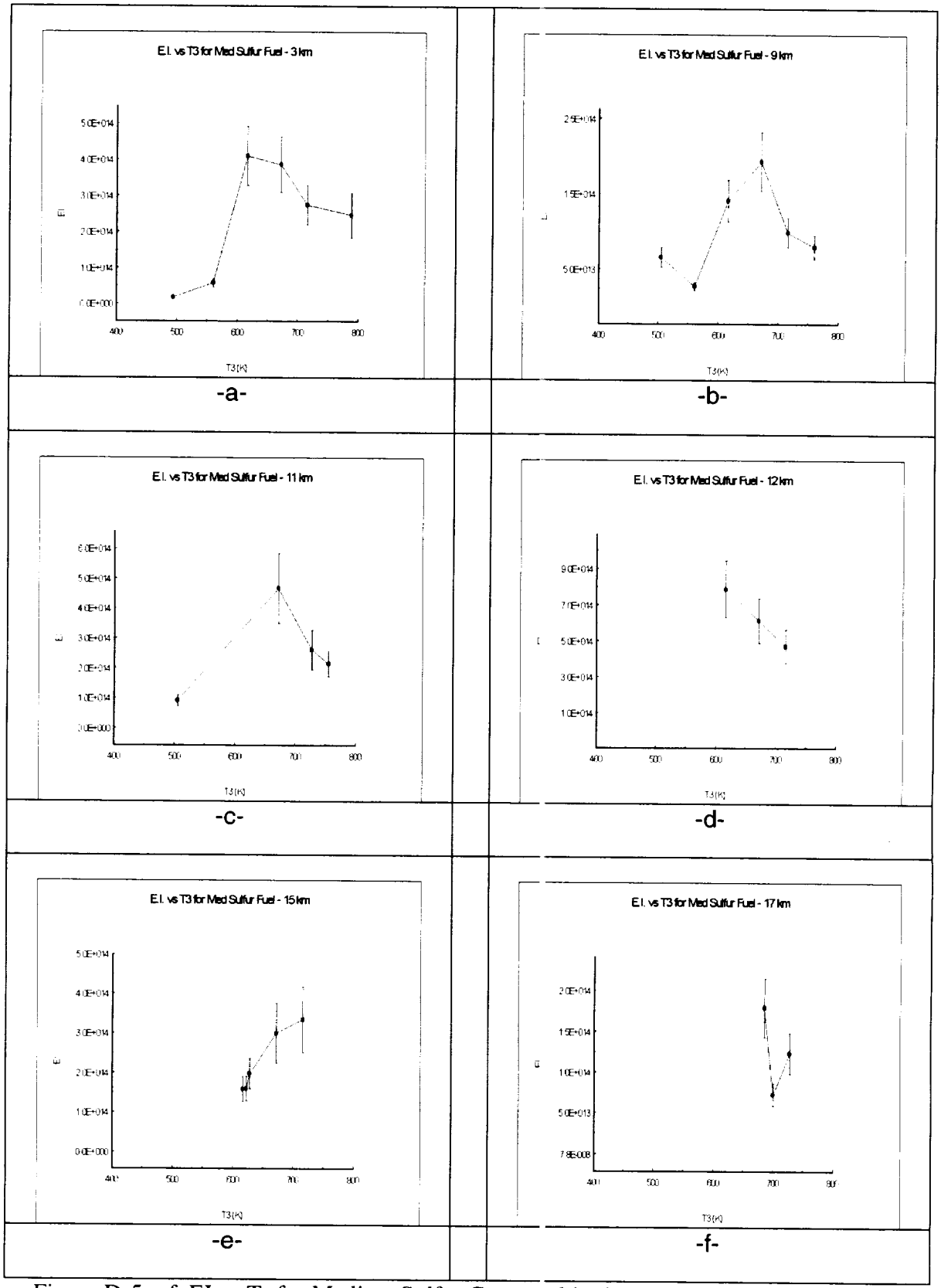

Figure D-5 a-f: EI vs T_3 for Medium Sulfur Case at altitudes a=3km, b=9km, c=11km, d=12km, e=15km, f=17km

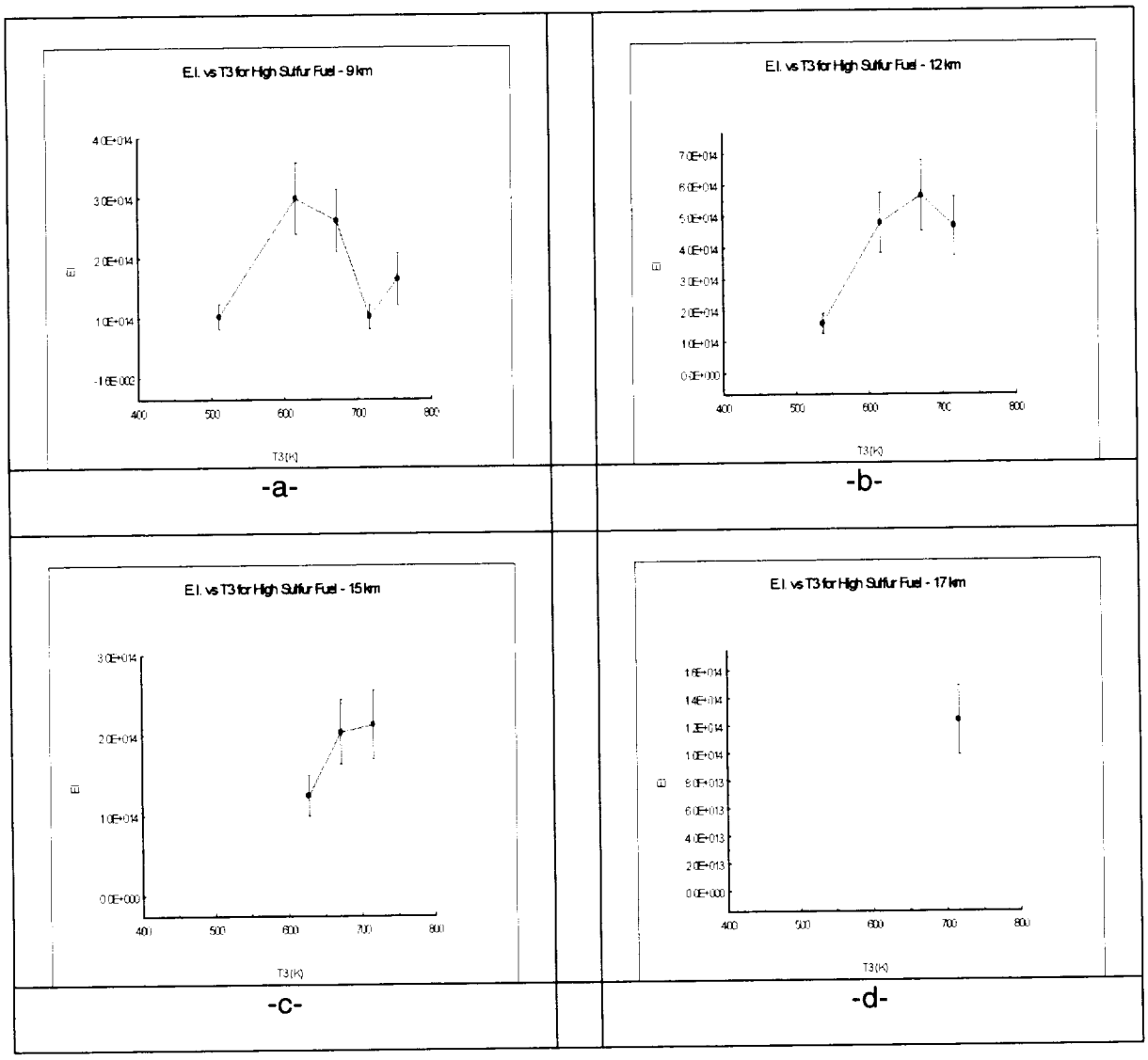

Figure D-6 a-d: EI vs T_3 for High Sulfur Case at altitudes a=3km, b=9km, c=12km, d=15km

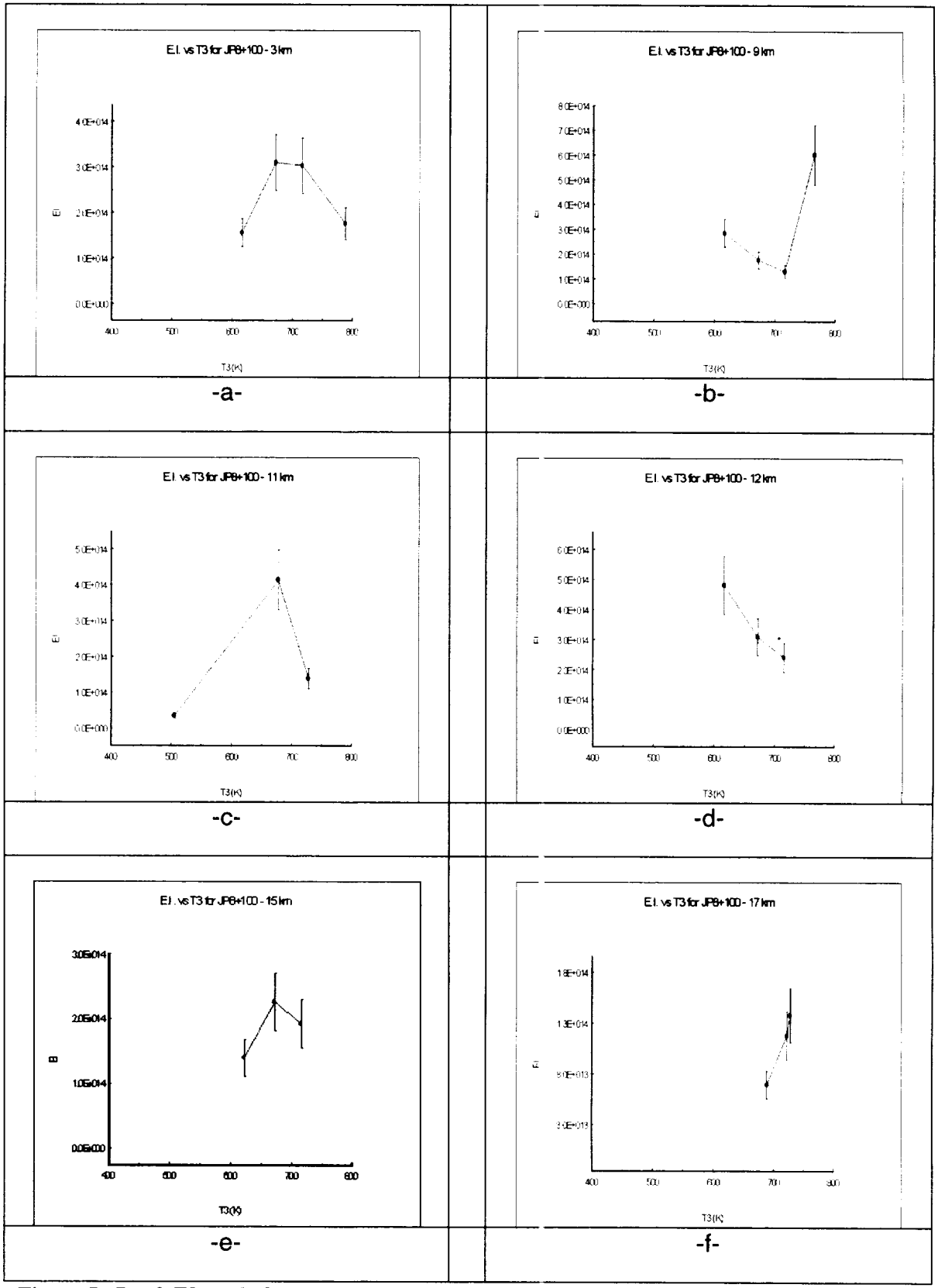

Figure D-7 a-f: EI vs T_3 for JP8+100 Case at altitudes a=3km, b=9km, c=11km, d=12km, e=15km, f=17km

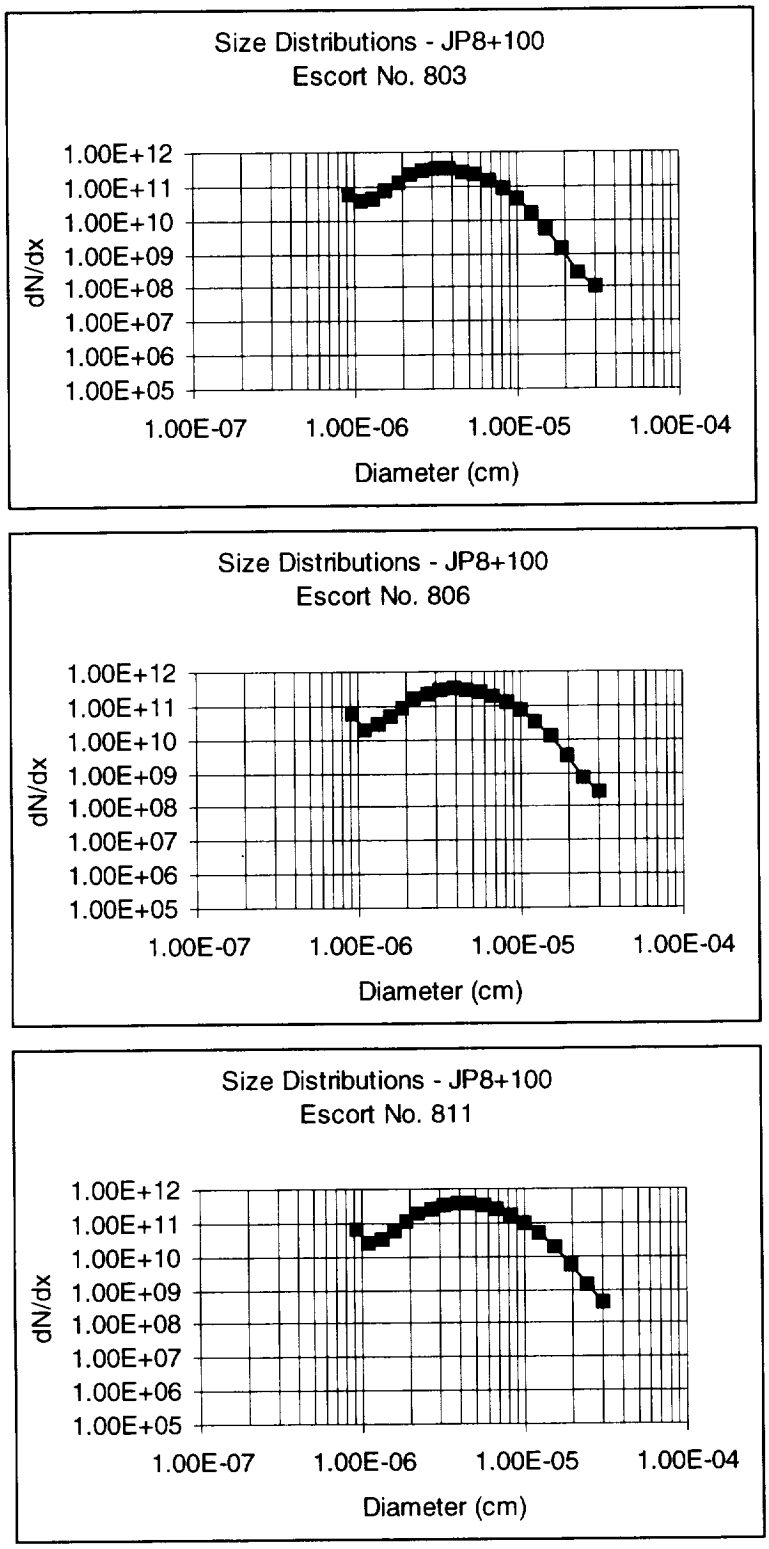

Figure D-8: Size distributions for escort numbers 803, 806, 811

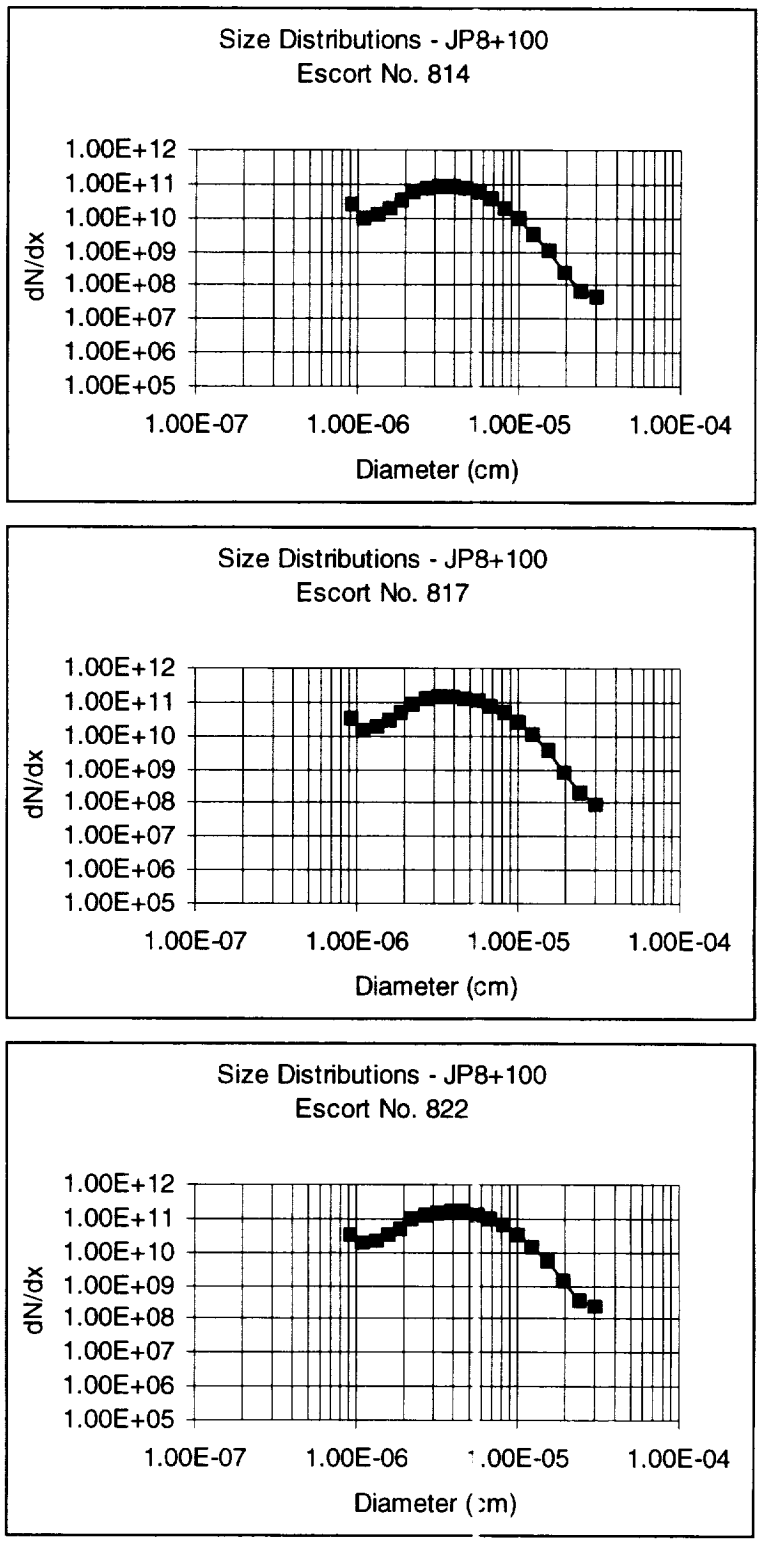

Figure D-9: Size distributions for escort numbers 814, 817, 822

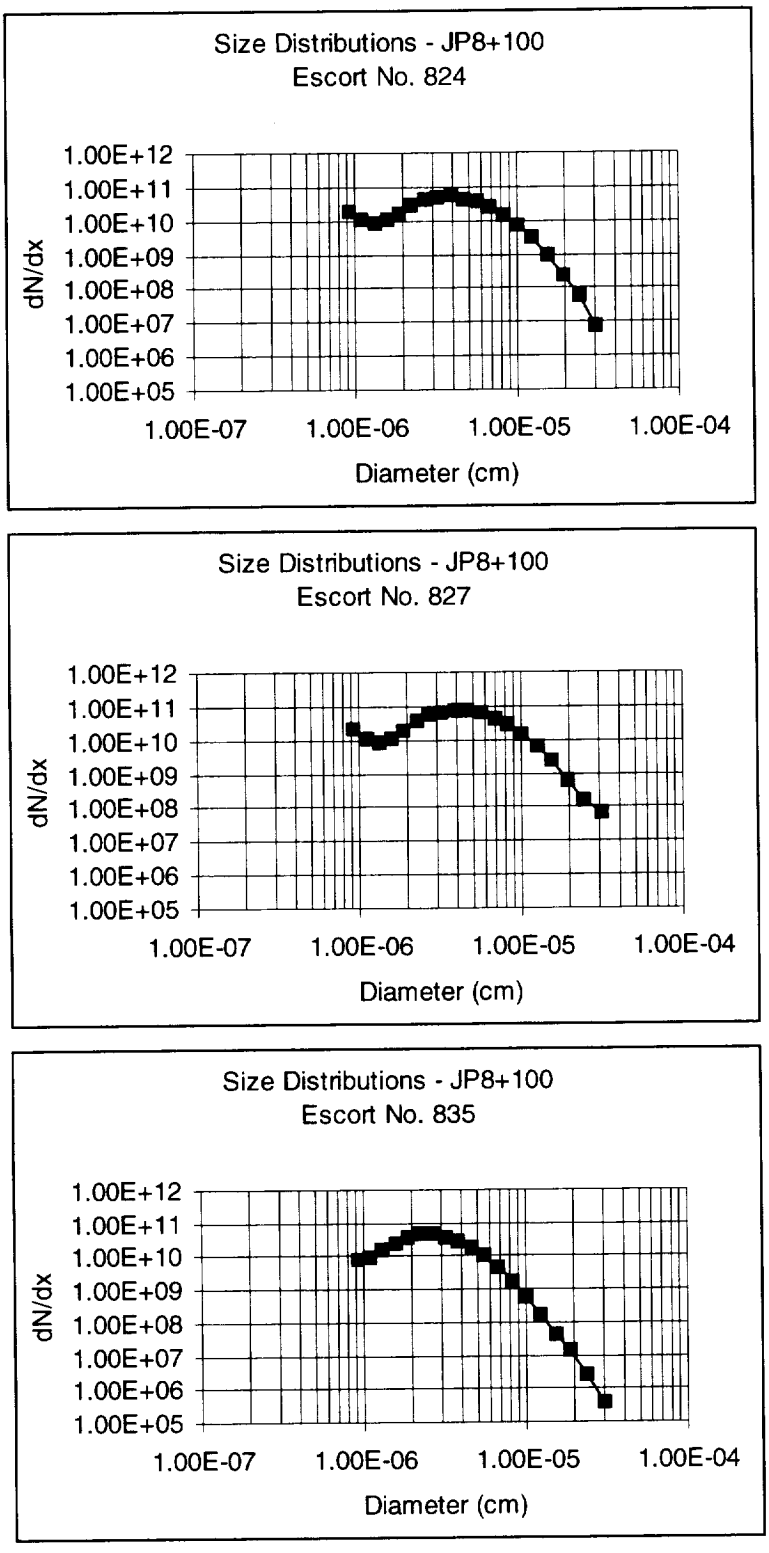

Figure D-10: Size distributions for escort numbers 824, 827, 835

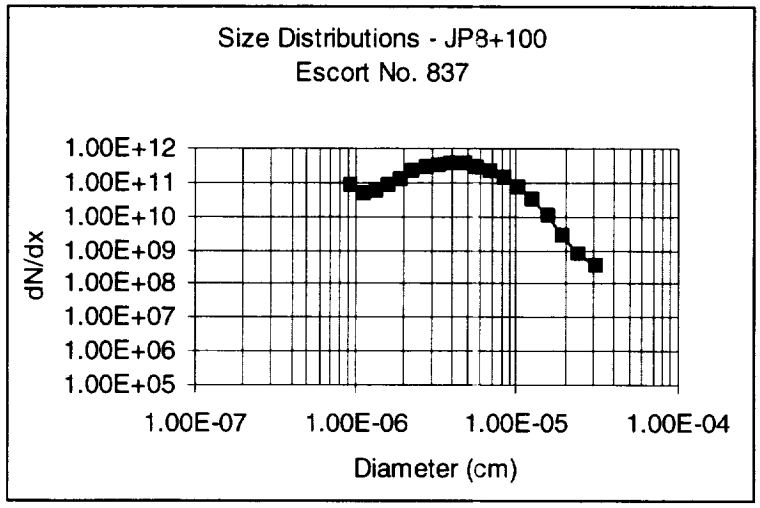

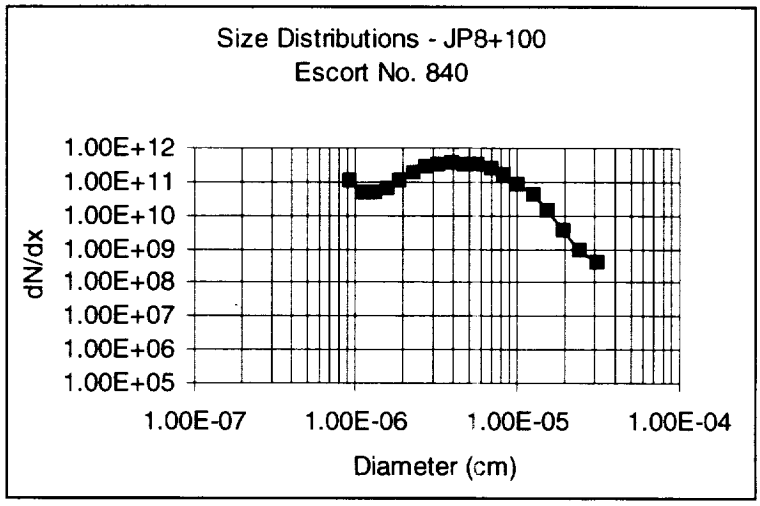

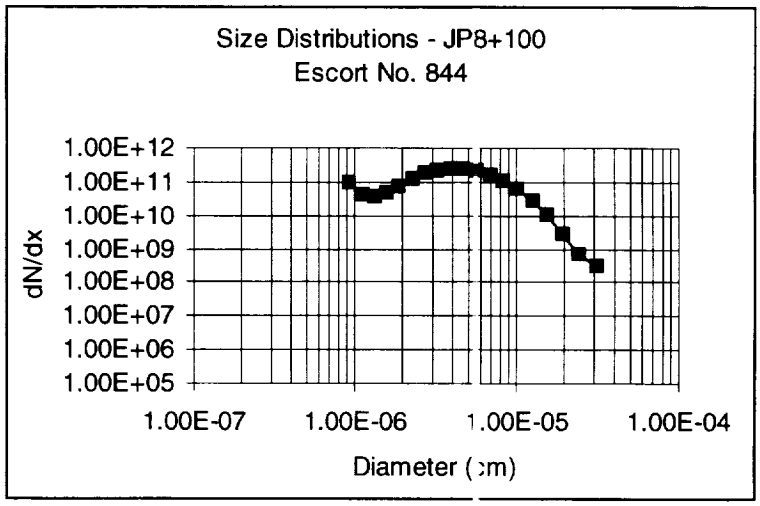

Figure D-11: Size distributions for escort numbers 837, 840, 844

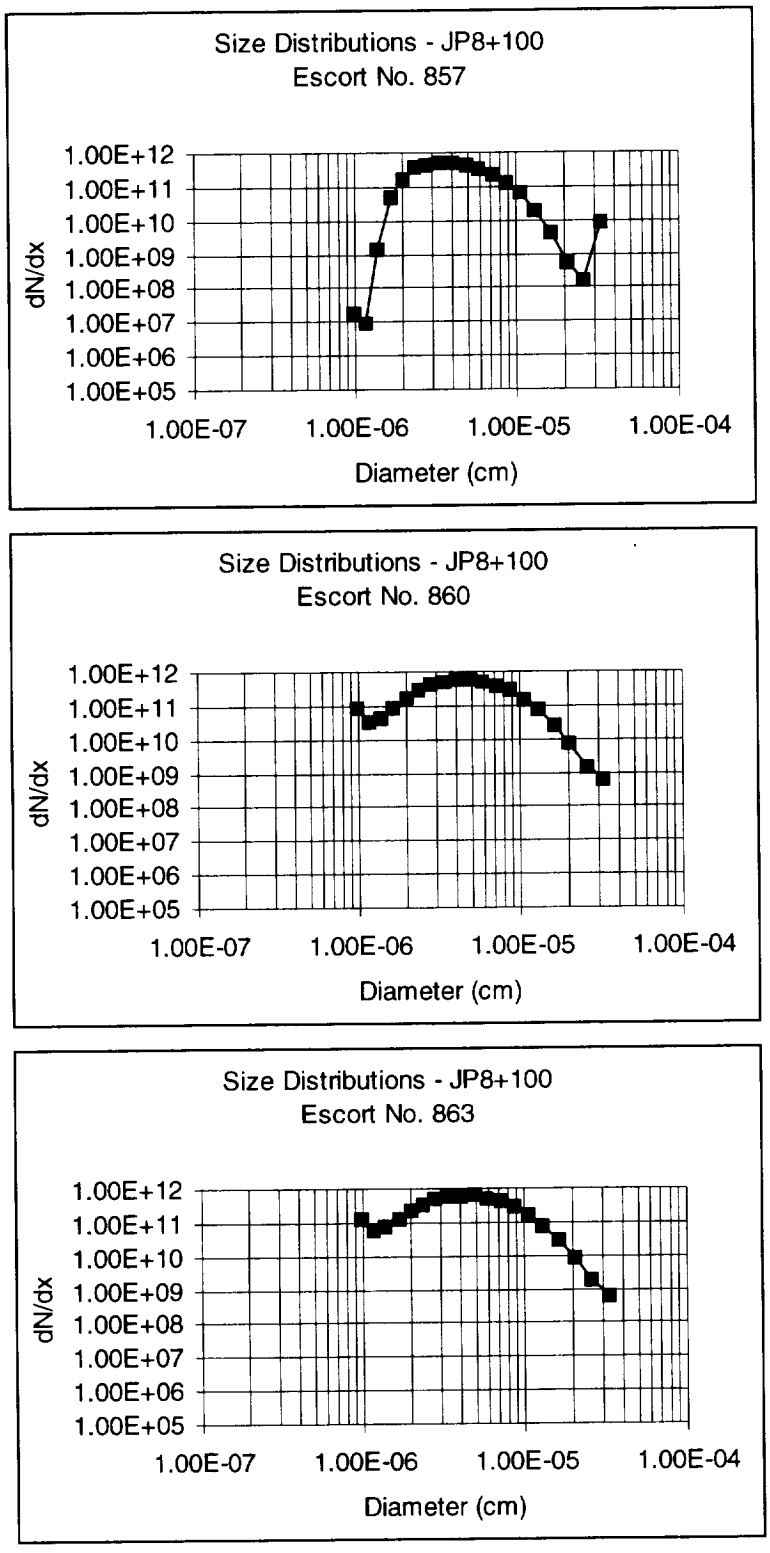

Figure D-12: Size distributions for escort numbers 857, 860, 863

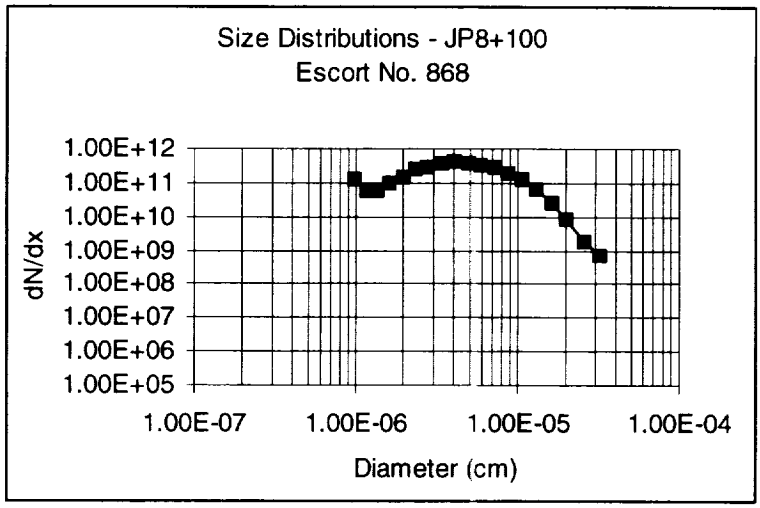

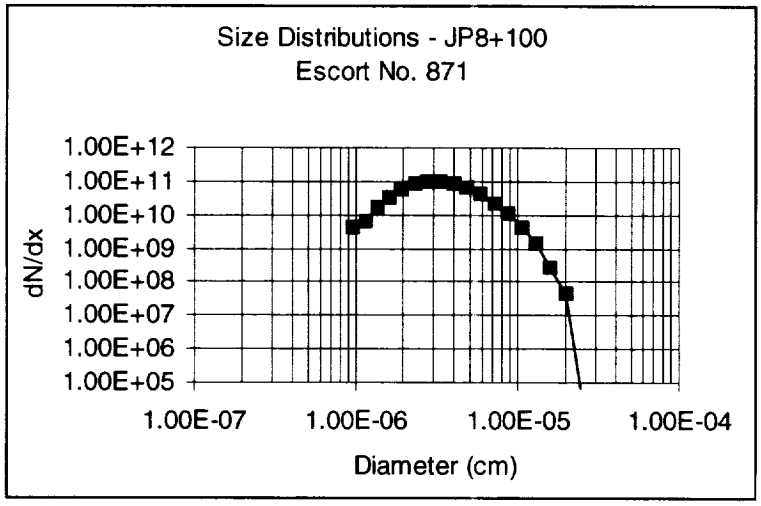

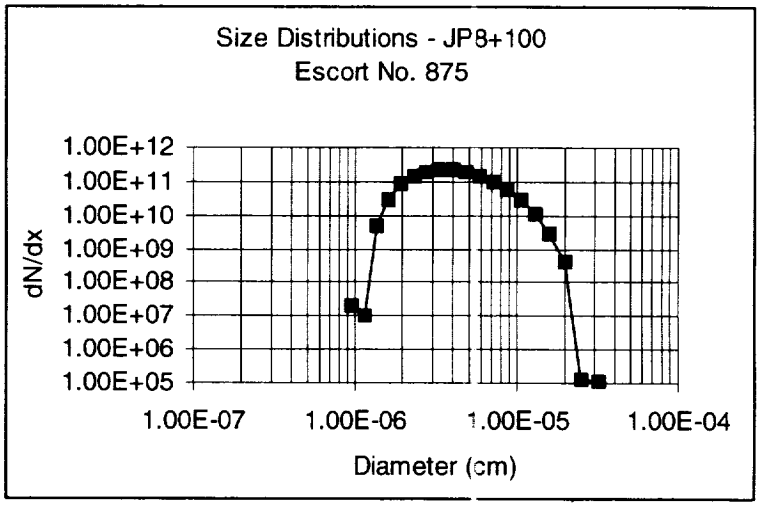

Figure D-13: Size distributions for escort numbers 868, 871, 875

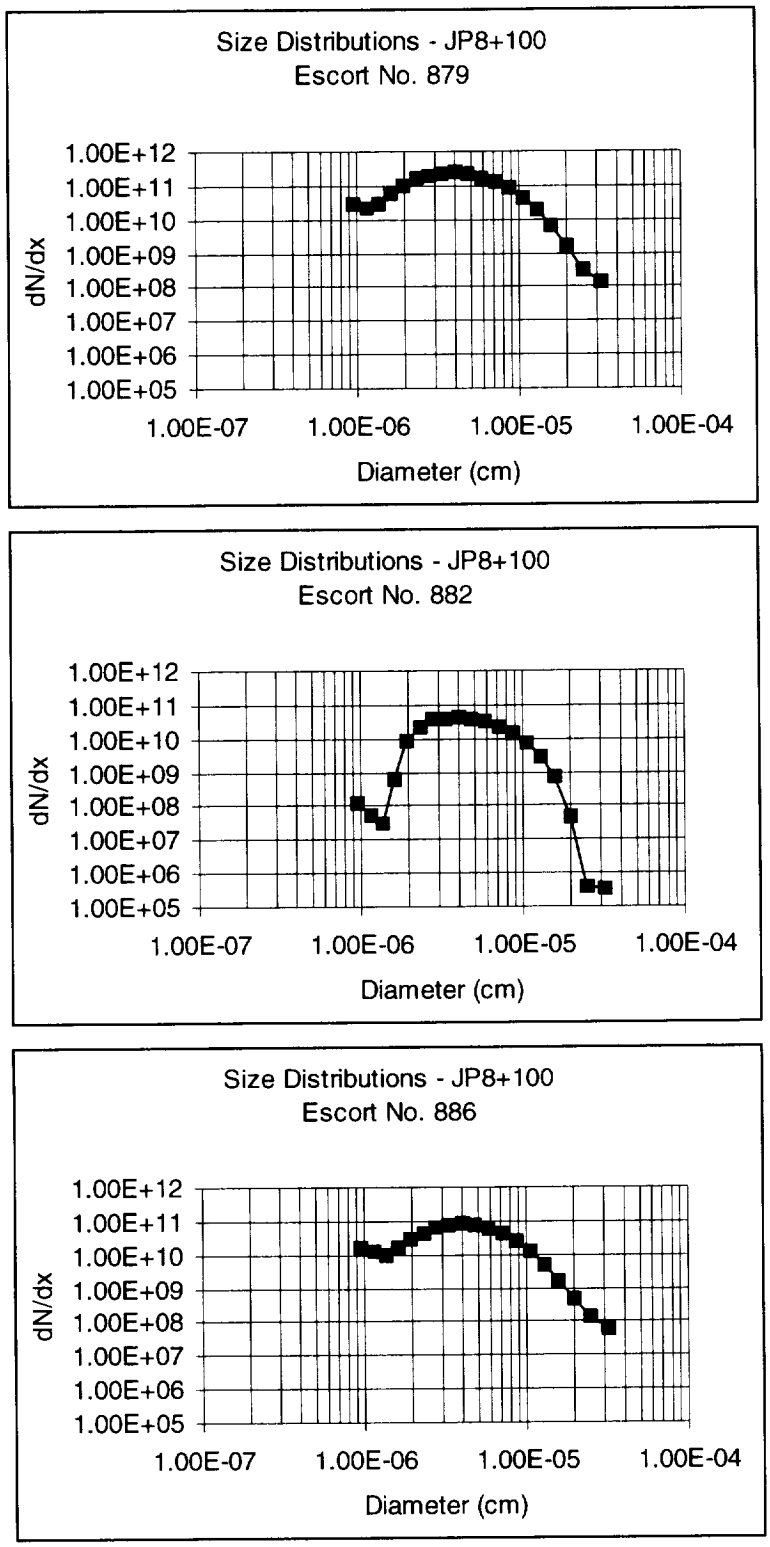

Figure D-14: Size distributions for escort numbers 879, 882, 886

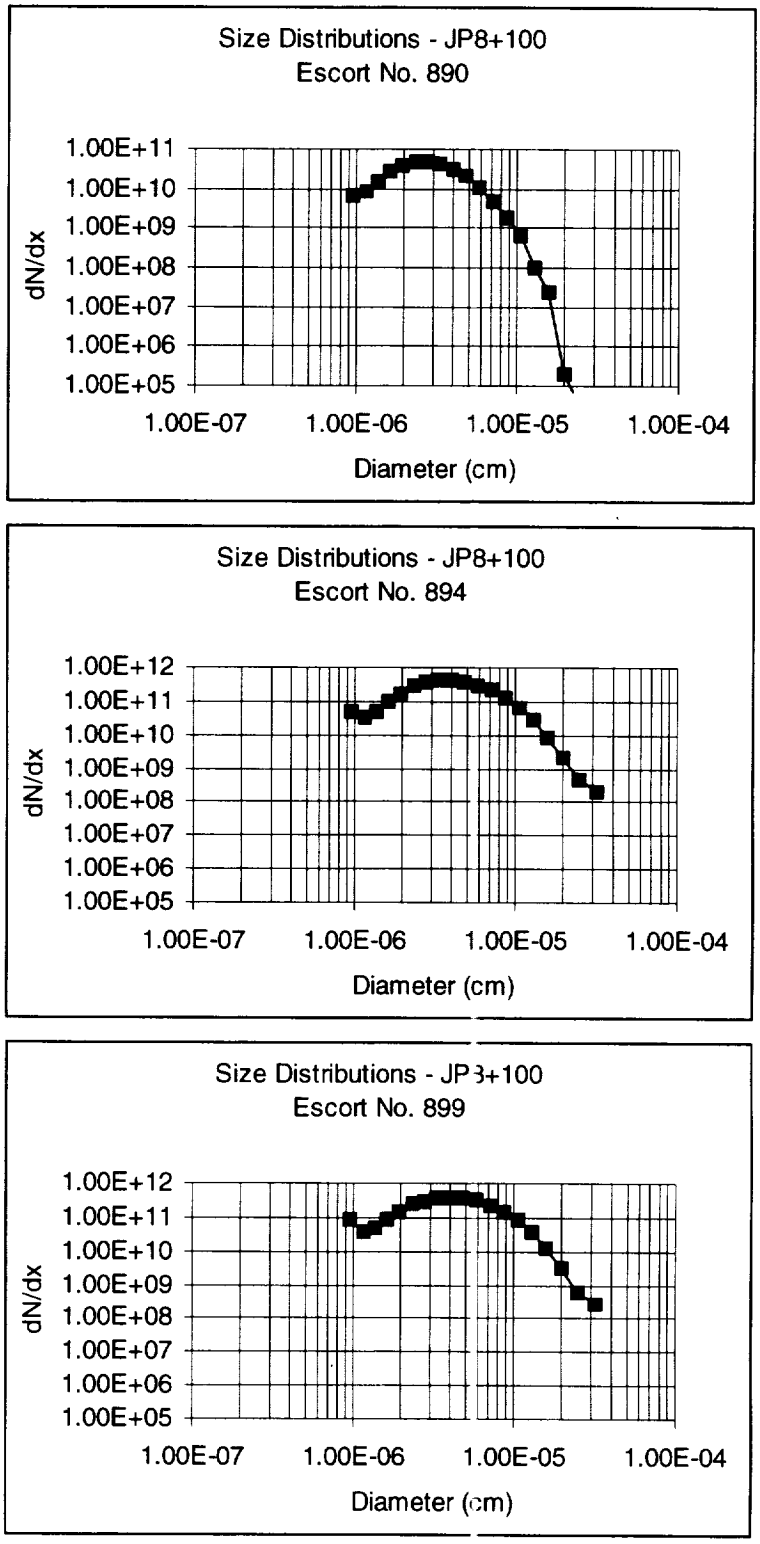

Figure D-15: Size distributions for escort numbers 890, 894, 899

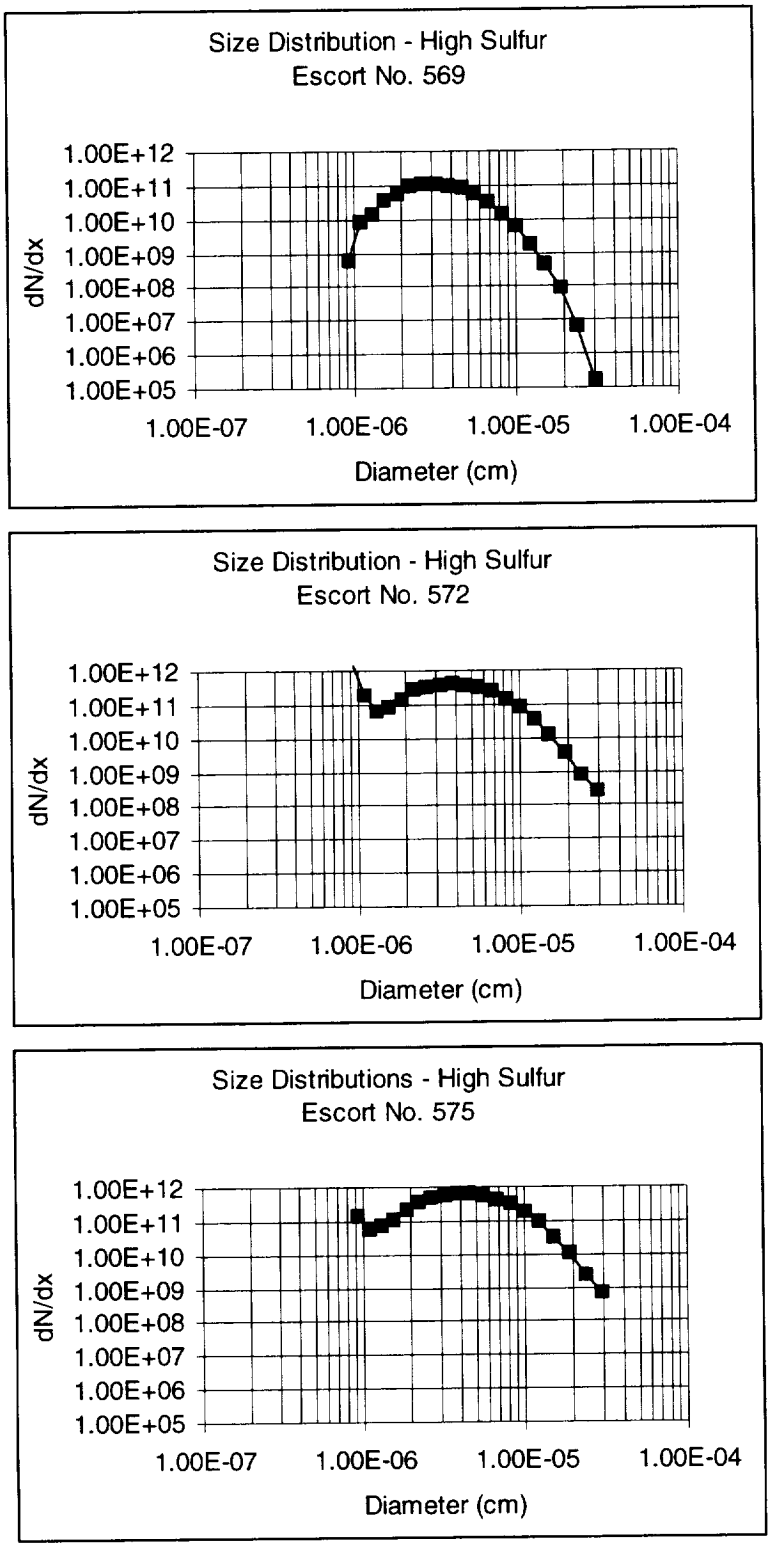

Figure D-16: Size distributions for escort numbers 569, 572, 575

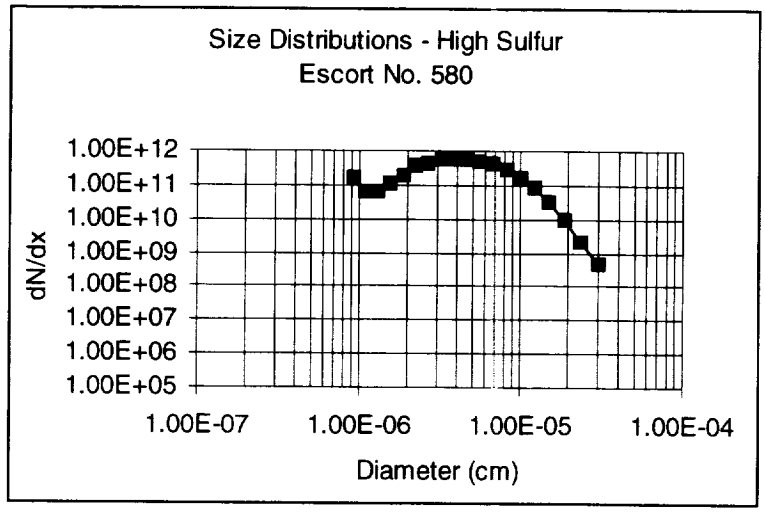

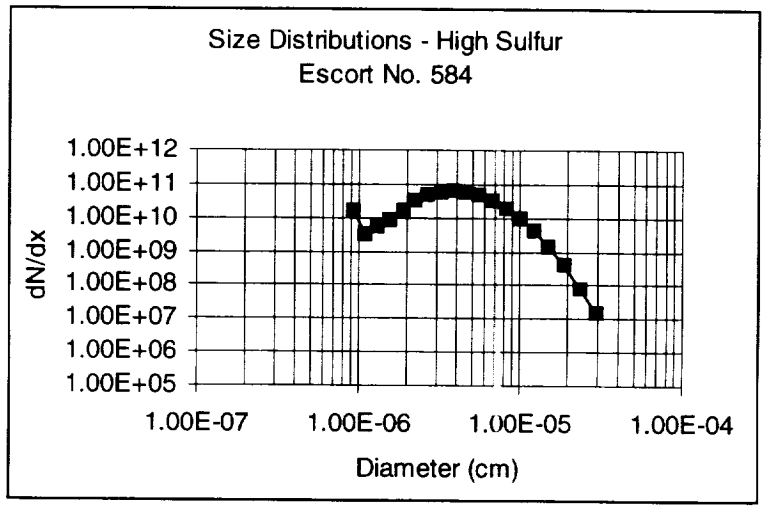

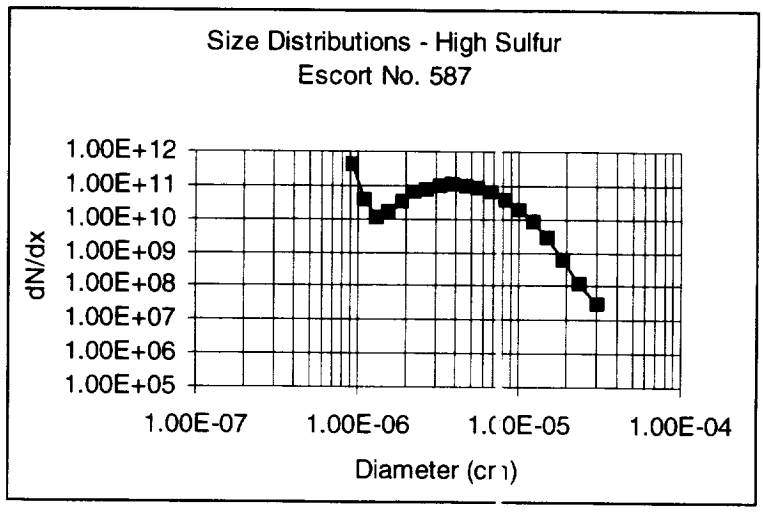

Figure D-17: Size distributions for escort numbers 580, 584, 587

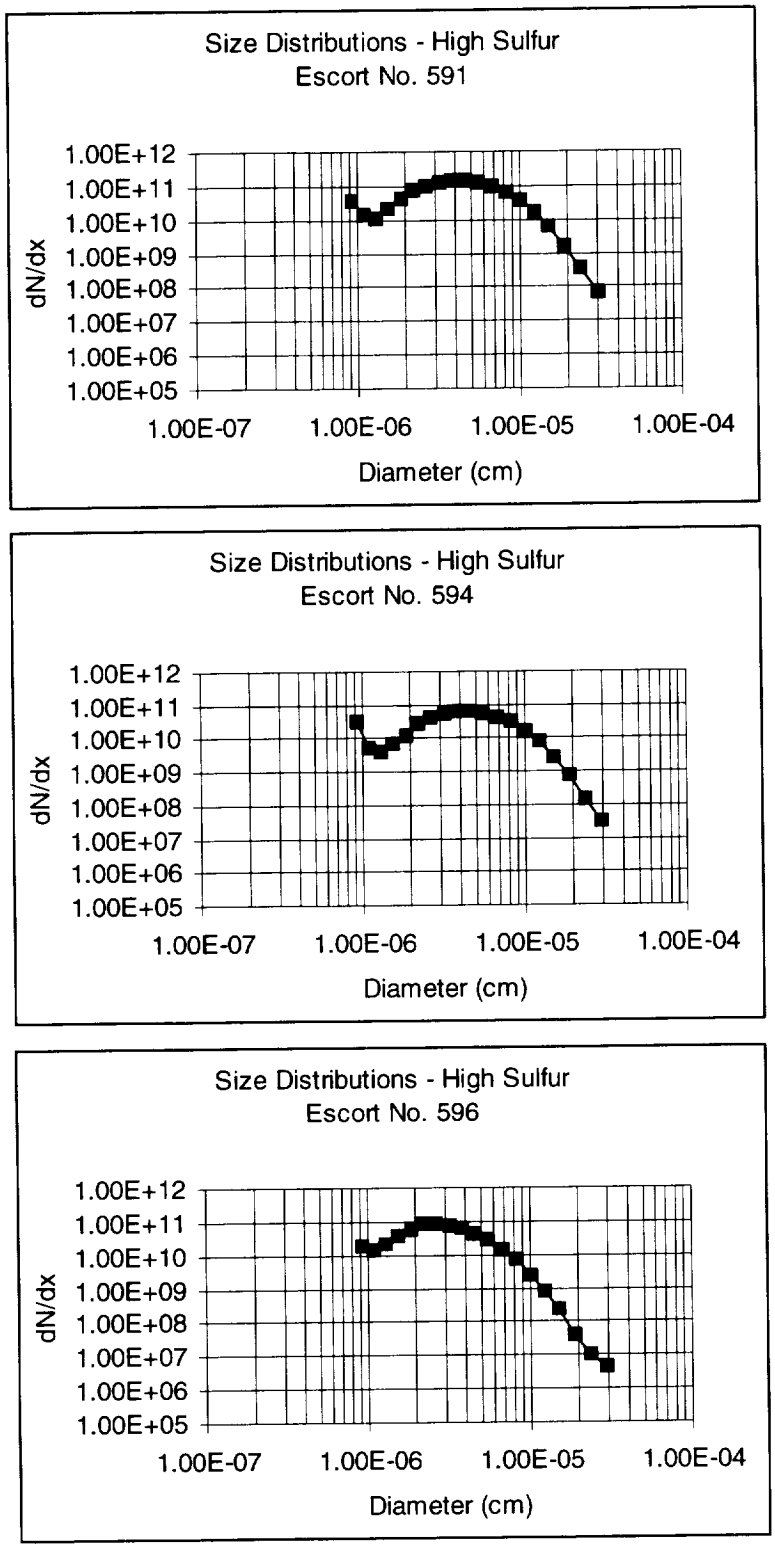

Figure D-18: Size distributions for escort numbers 591, 594, 596

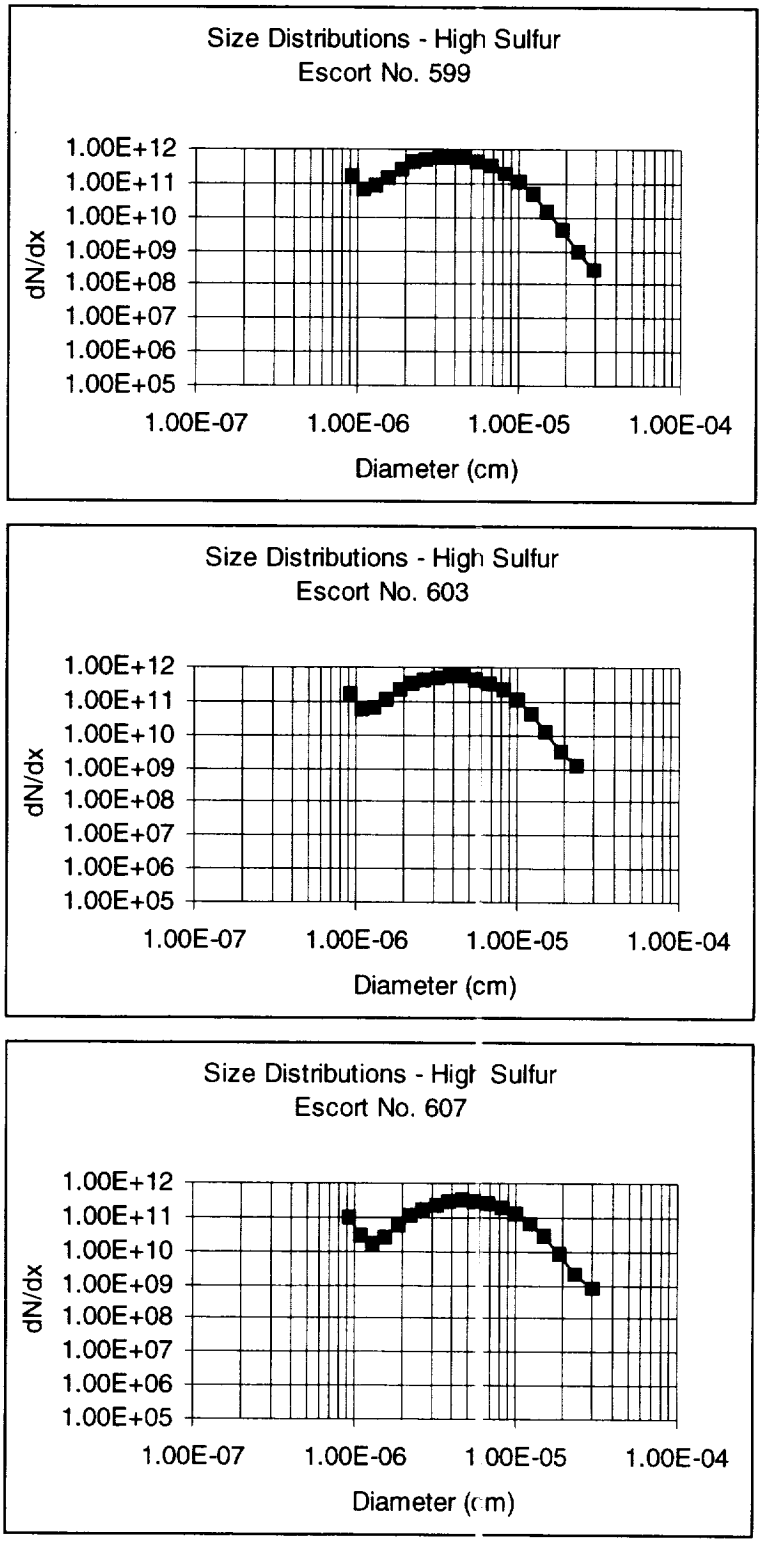

Figure D-19: Size distributions for escort numbers 599, 603, 607

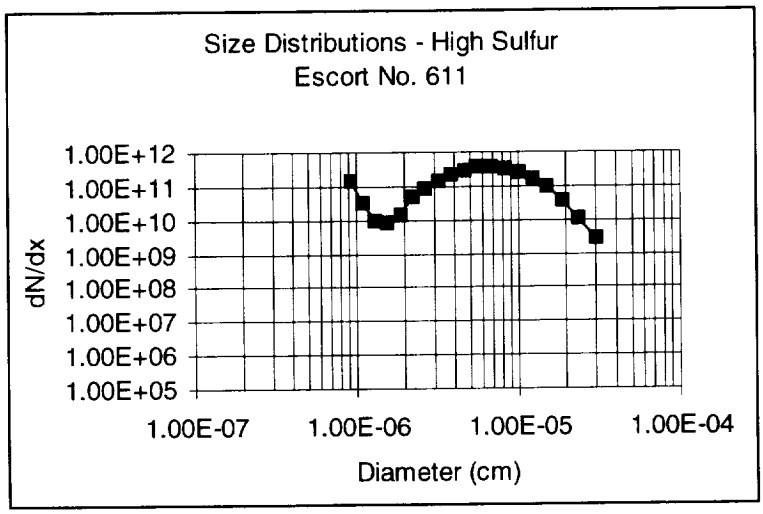

Figure D-20: Size distribution for escort number 611

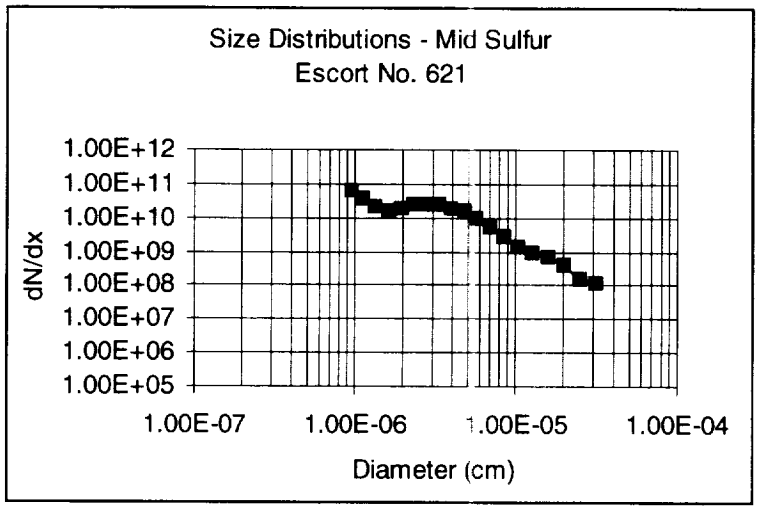

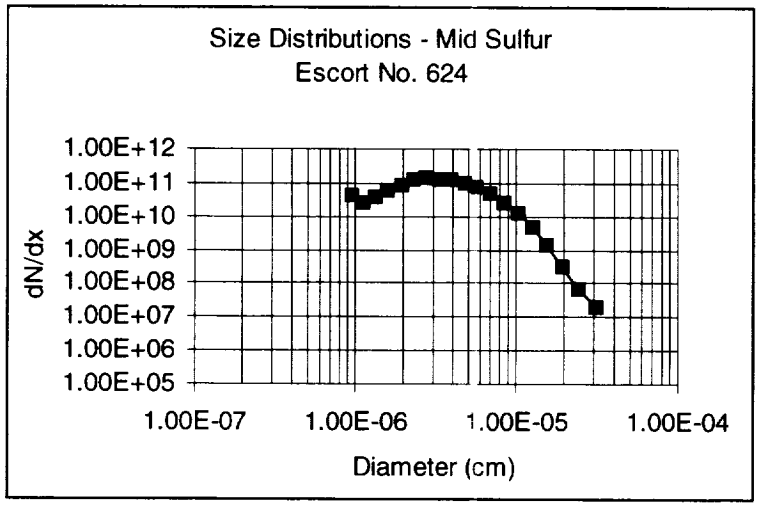

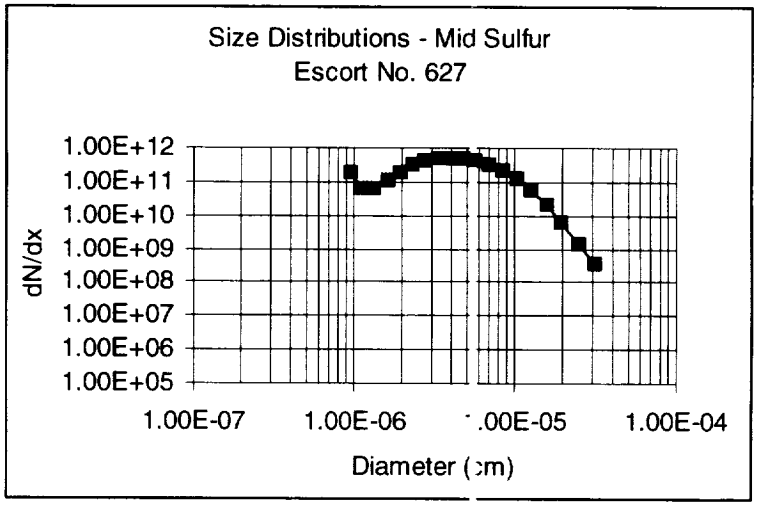

Figure D-21: Size distributions for escort numbers 621, 624, 627

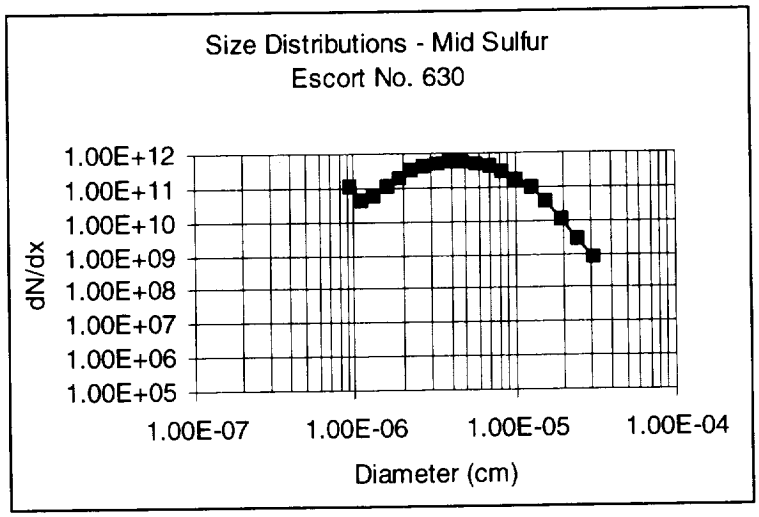

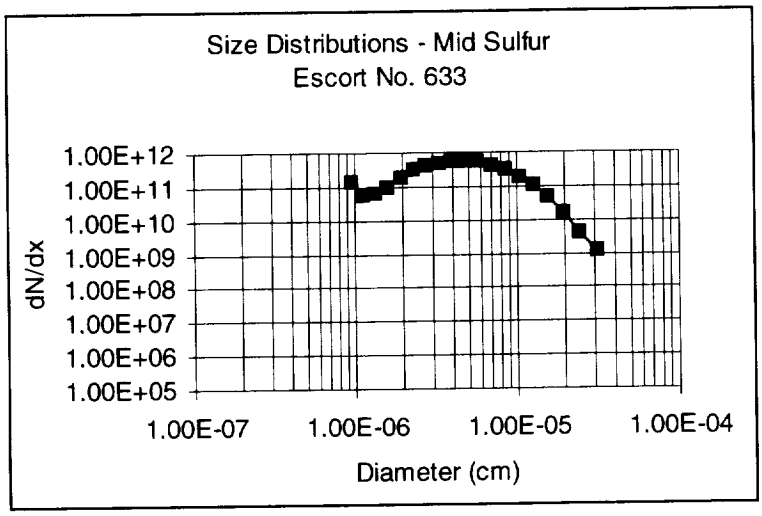

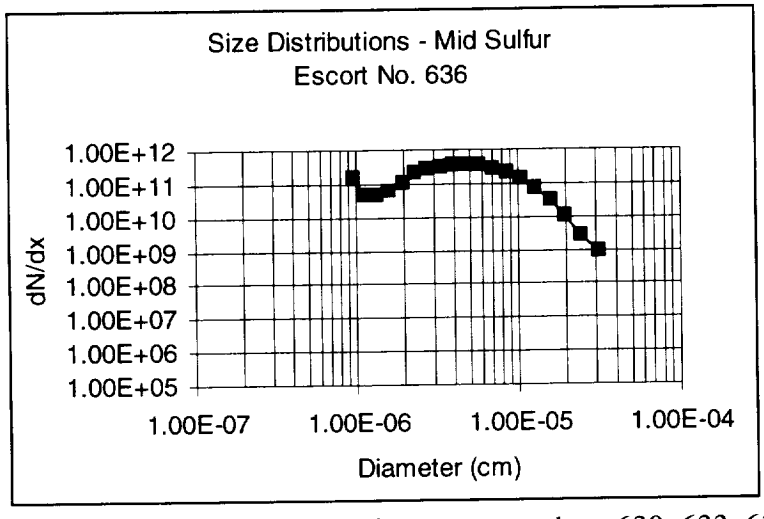

Figure D-22: Size distributions for escort numbers 630, 633, 636

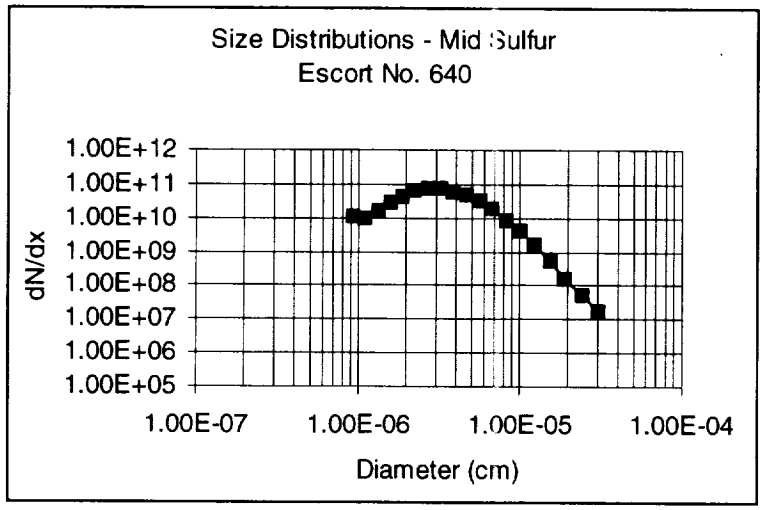

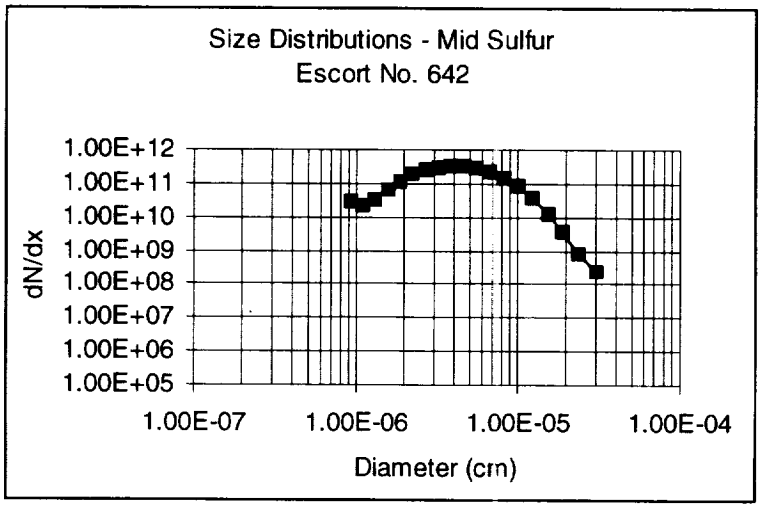

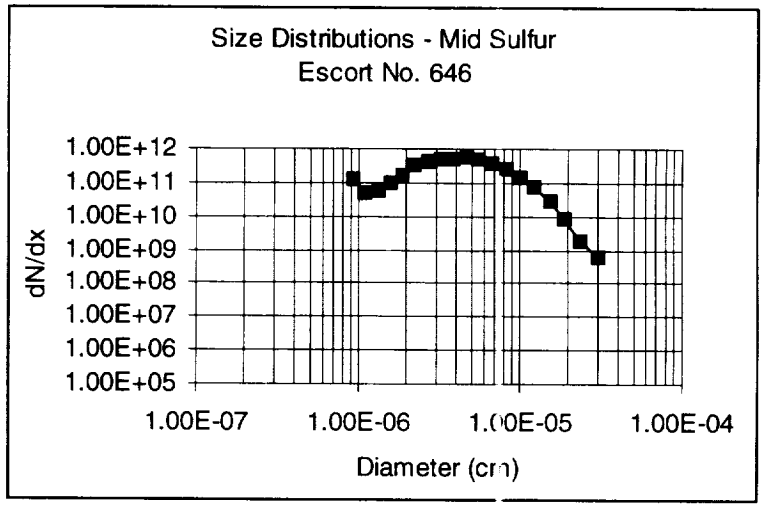

Figure D-23: Size distributions for escor numbers 640, 642, 646

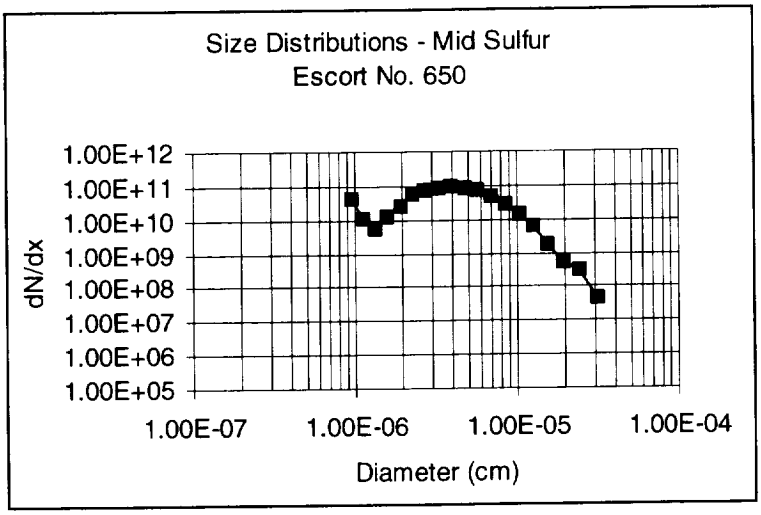

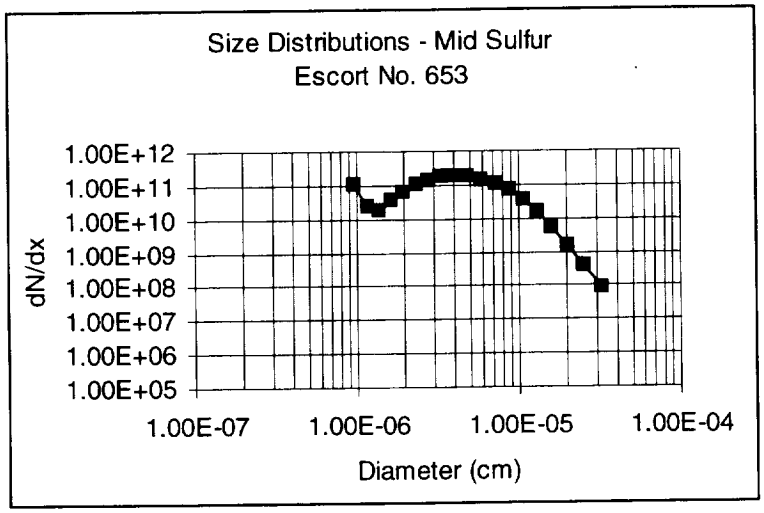

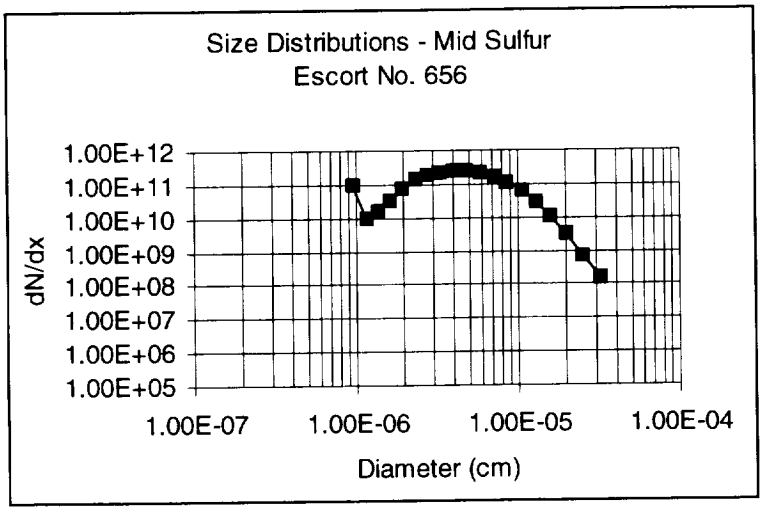

Figure D-24: Size distributions for escort numbers 650, 653, 656

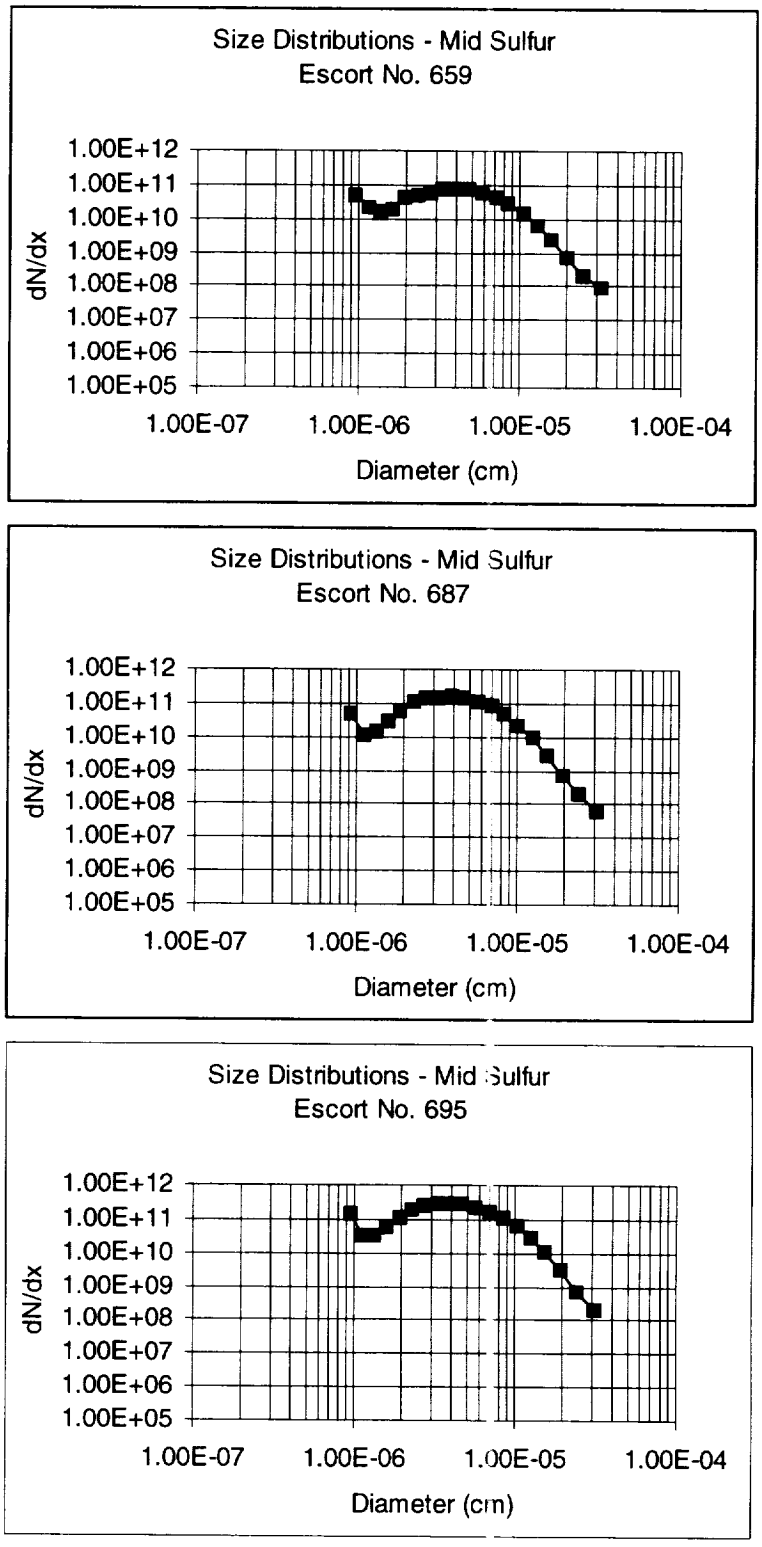

Figure D-25: Size distributions for escort numbers 659, 687, 695

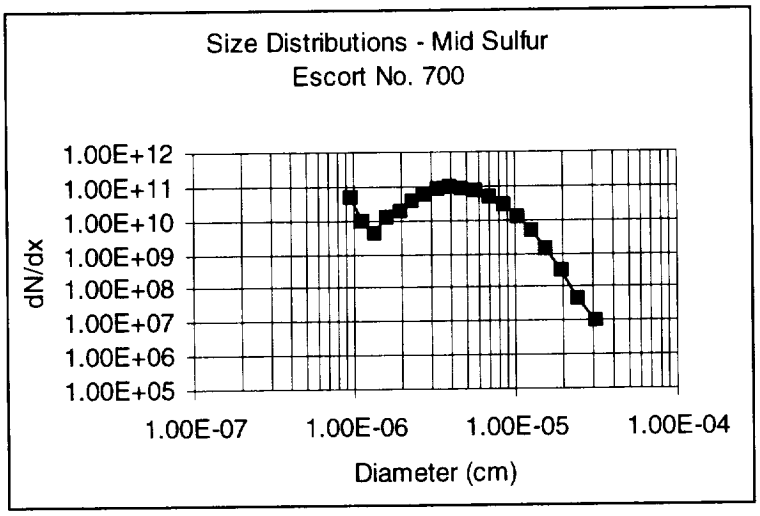

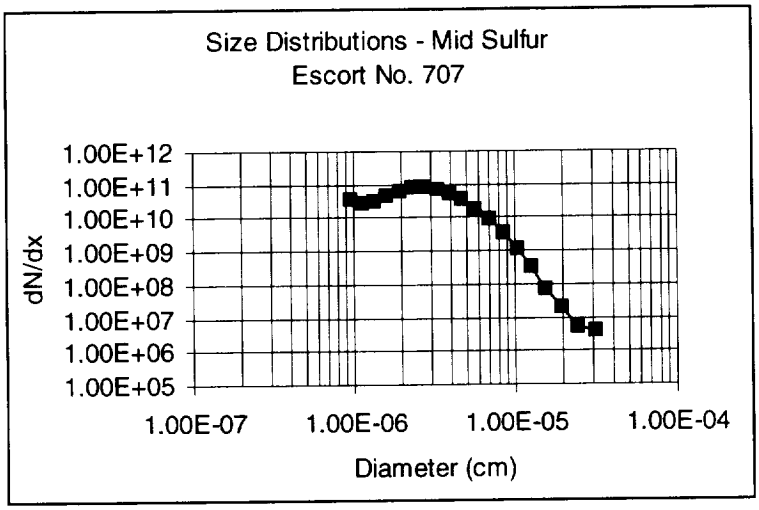

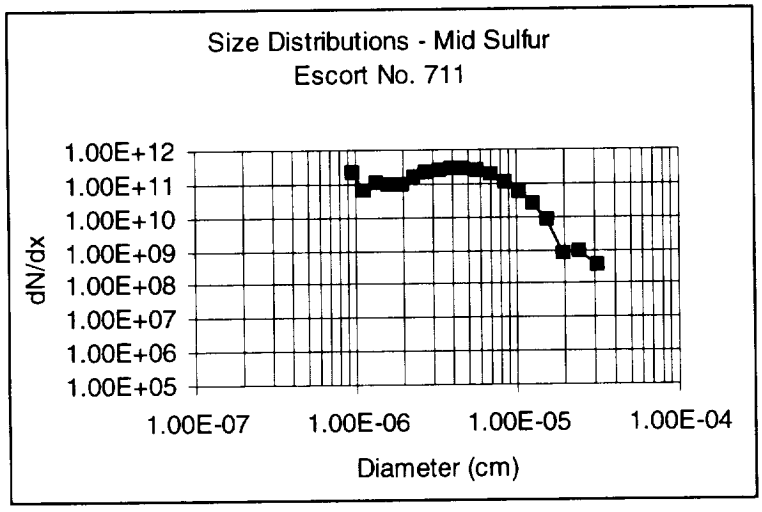

Figure D-26: Size distributions for escort numbers 700, 707, 711

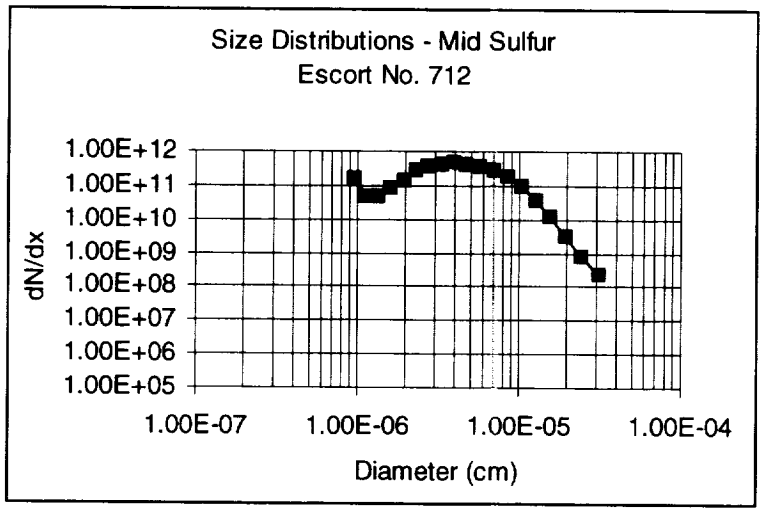

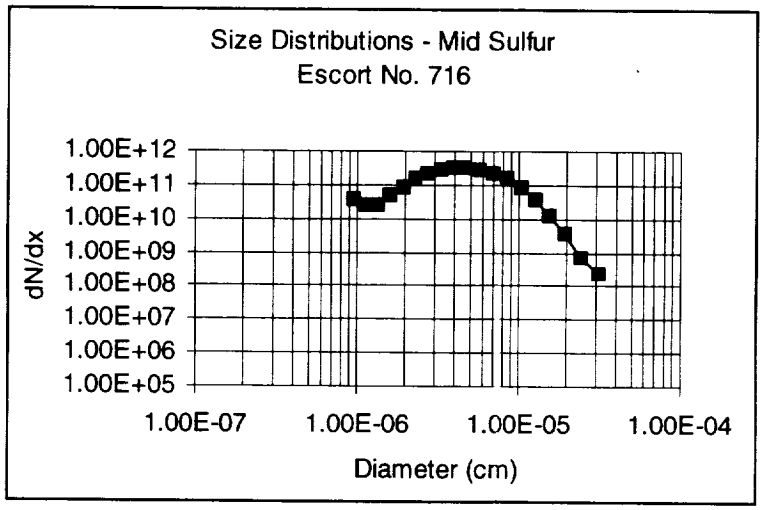

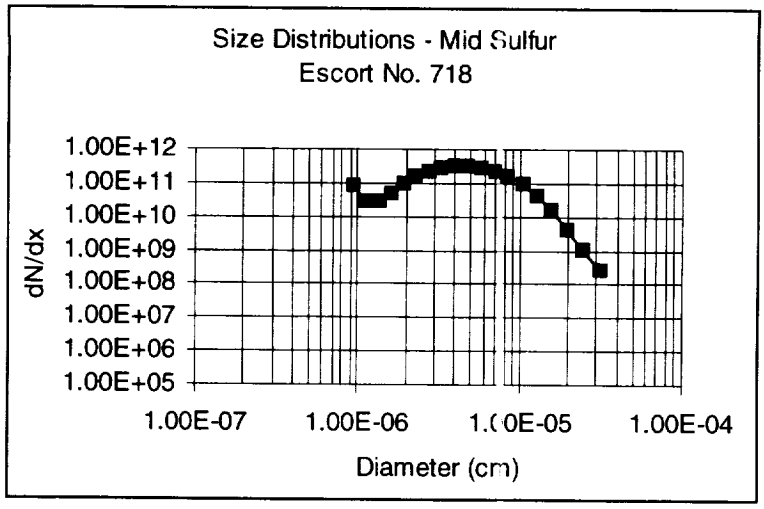

Figure D-27: Size distributions for escort numbers 712, 716, 718

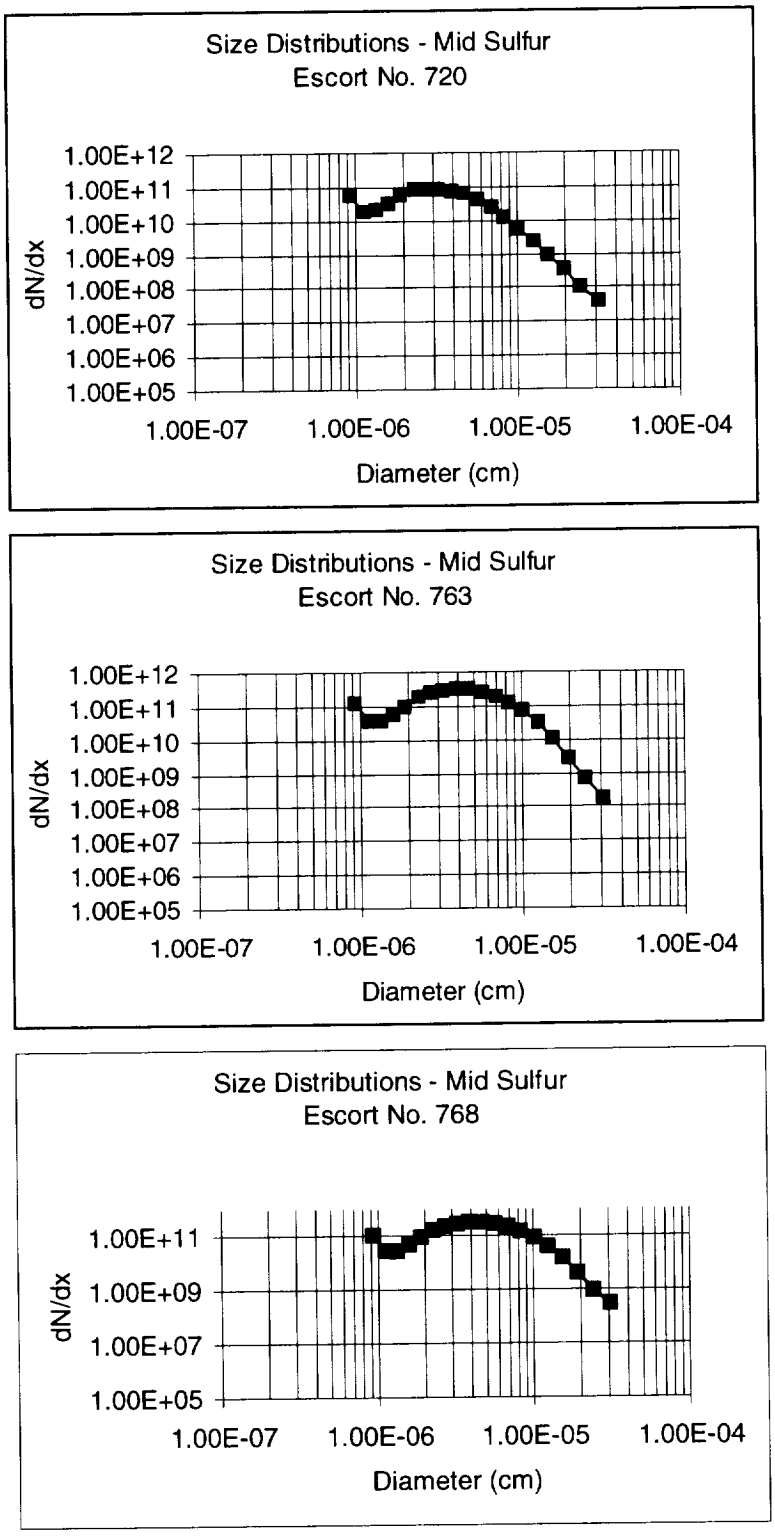

Figure D-28: Size distributions for escort numbers 720, 763, 768

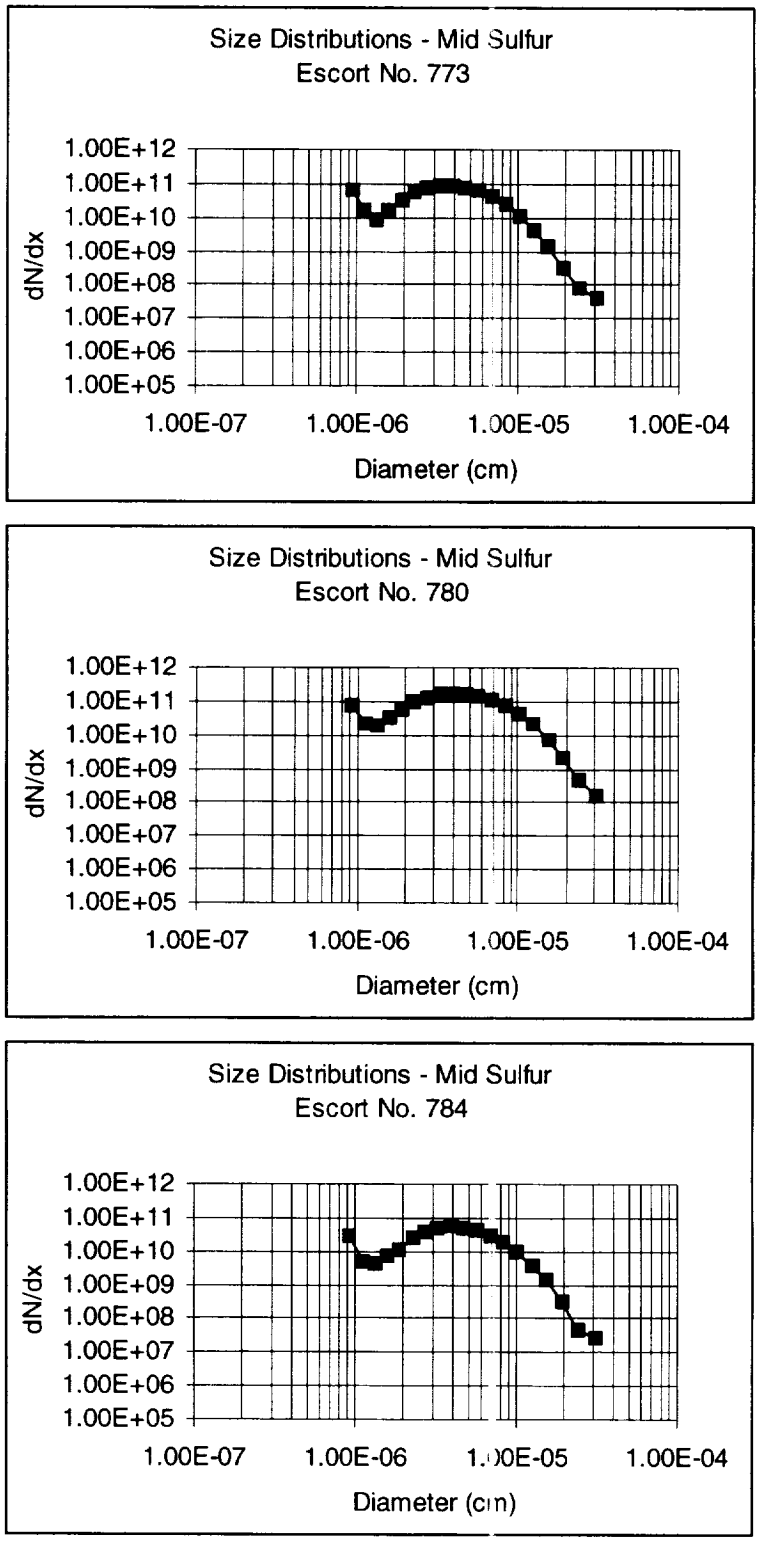

Figure D-29: Size distributions for escort numbers 773, 780, 784

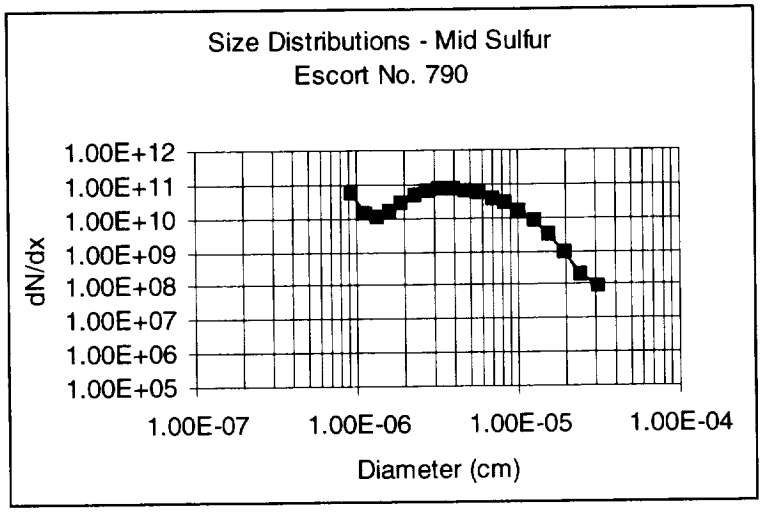

Figure D-30: Size distribution for escort number 790

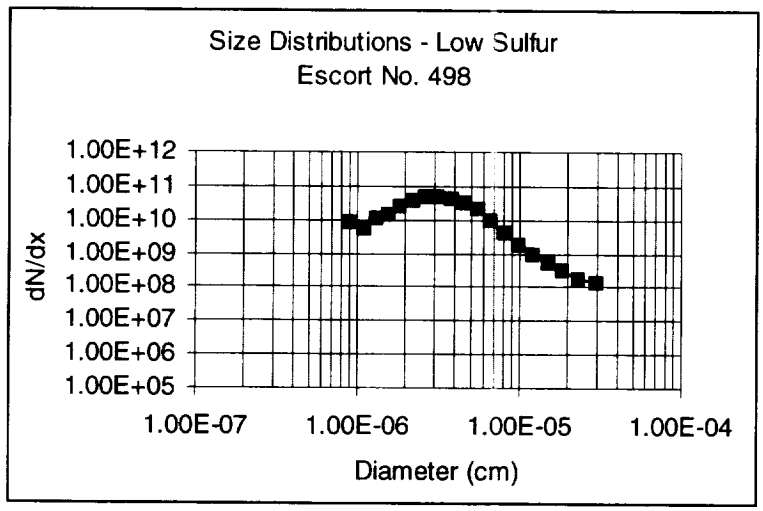

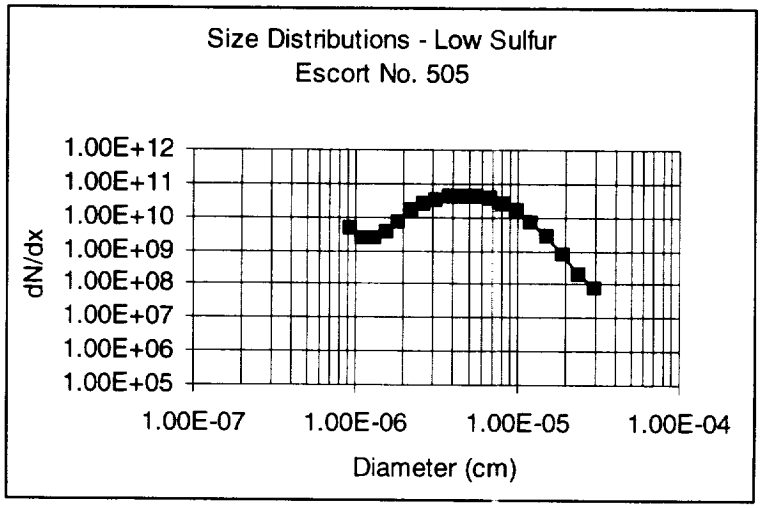

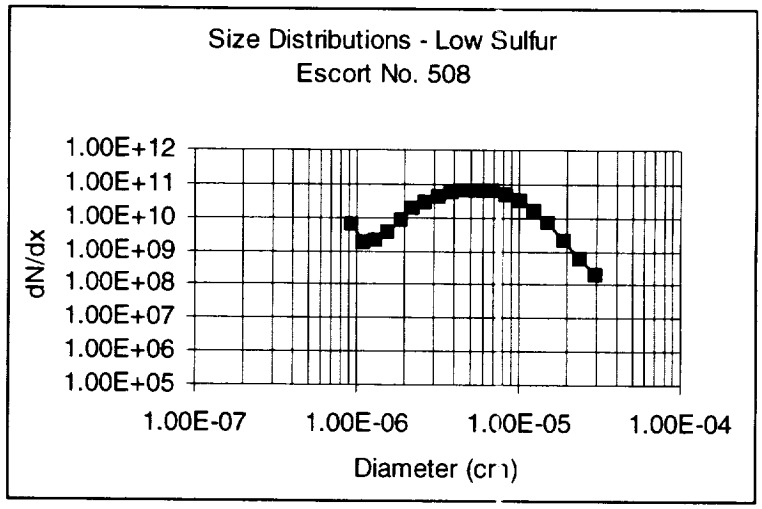

Figure D-31: Size distributions for escort numbers 498, 505, 508

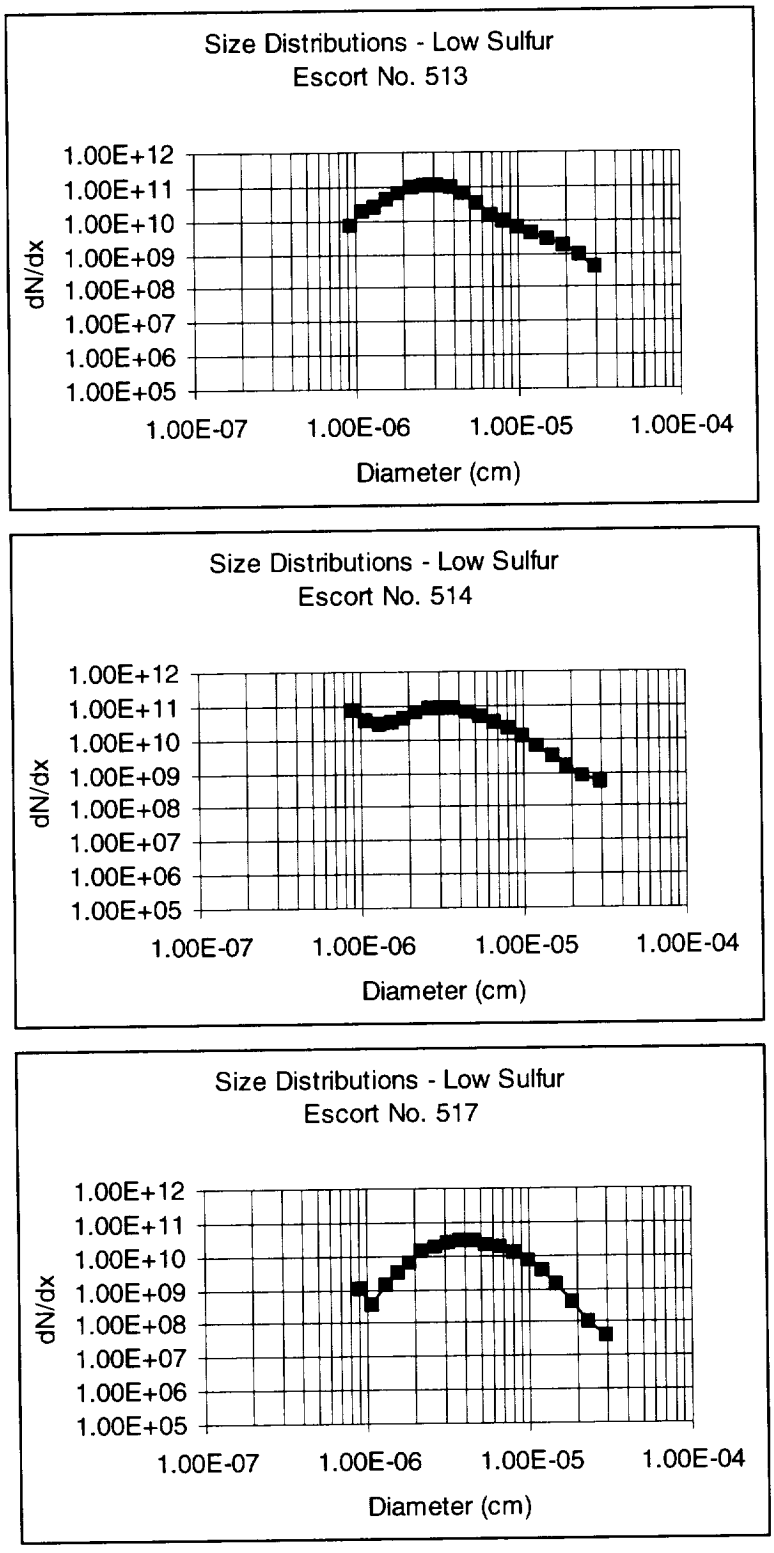

Figure D-32: Size distributions for escort numbers 513, 514, 517

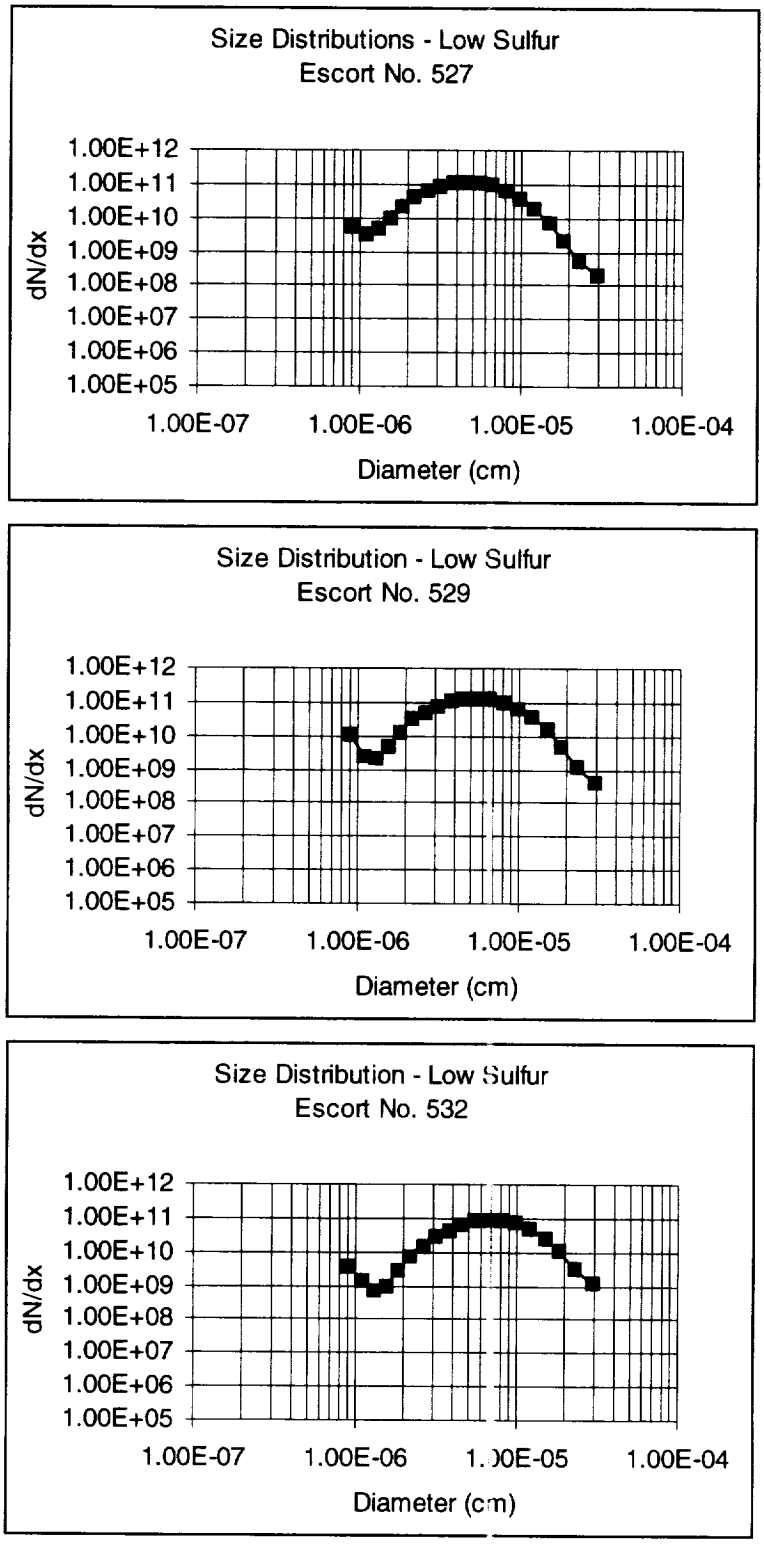

Figure D-33: Size distributions for escort numbers 527, 529, 532

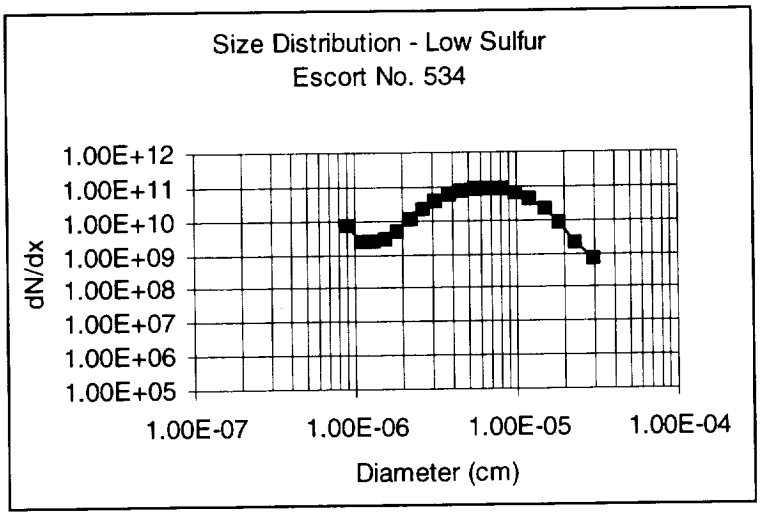

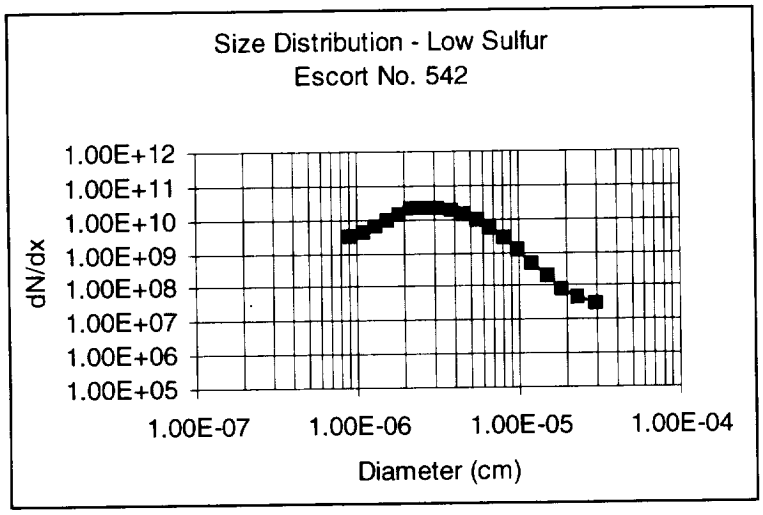

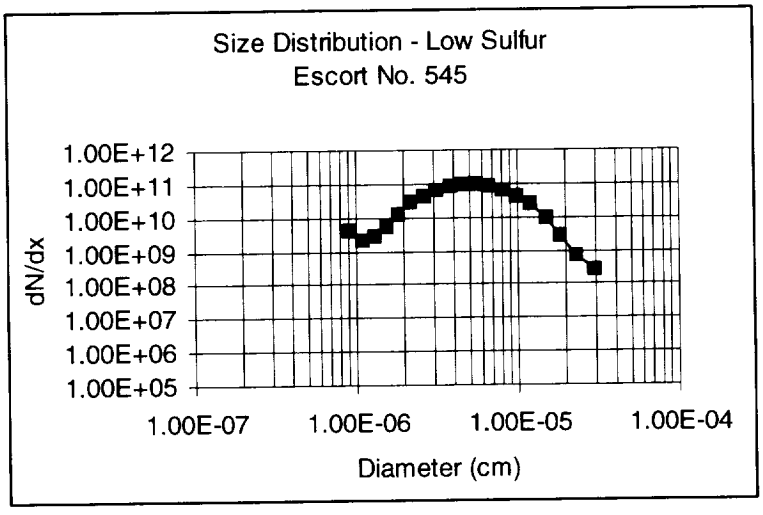

Figure D-34: Size distributions for escort numbers 534, 542, 545

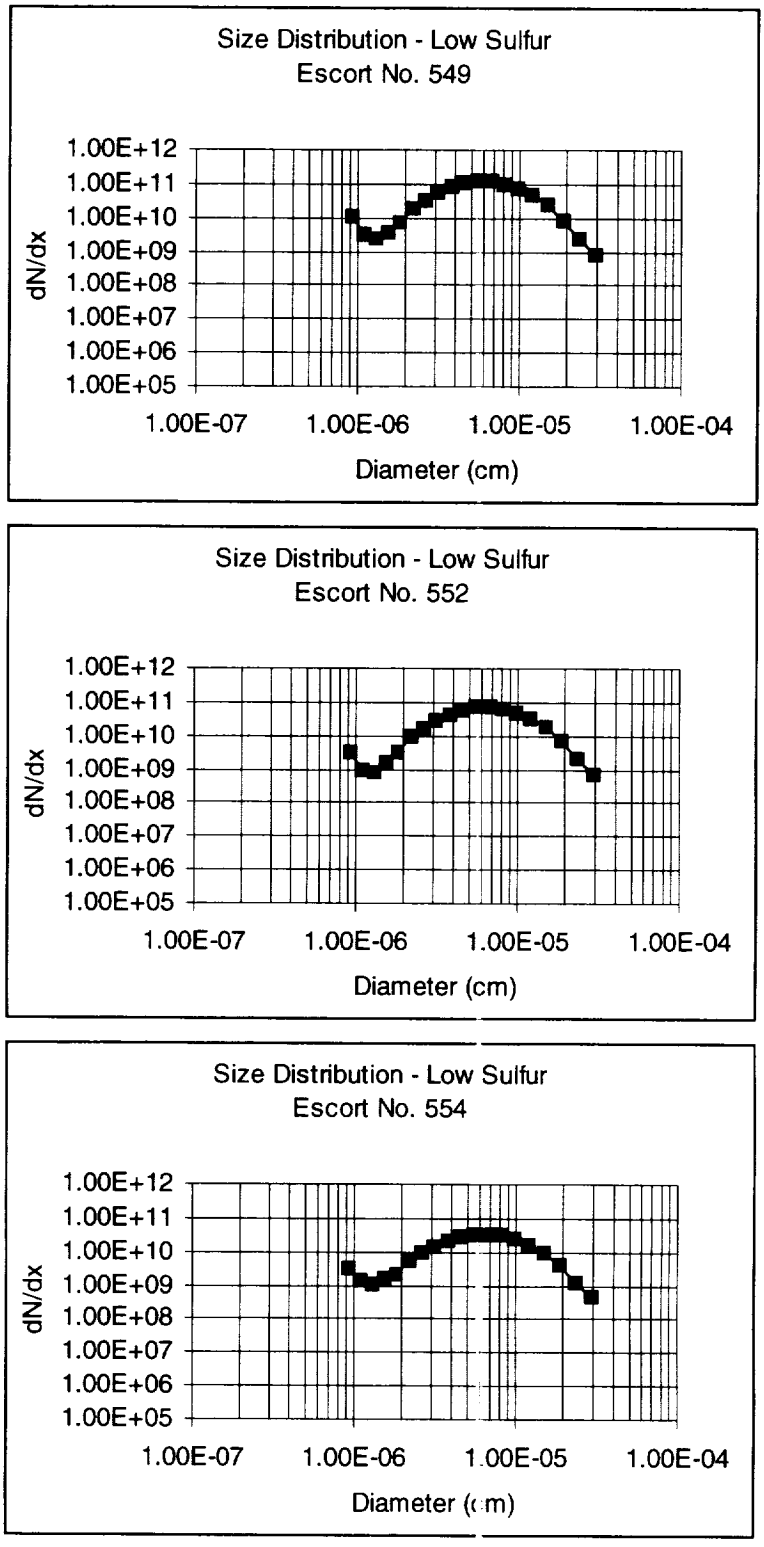

Figure D-35: Size distributions for escort numbers 549, 552, 554

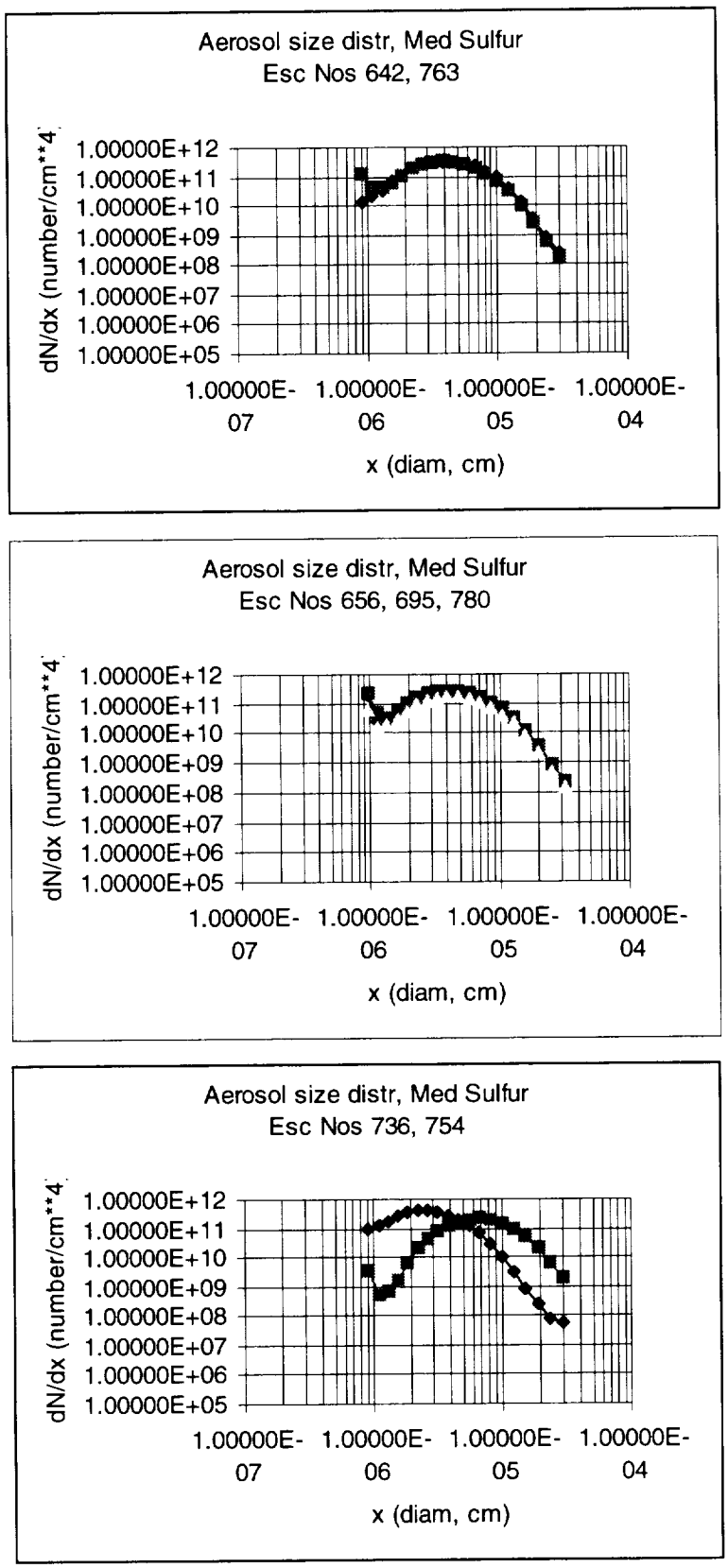

Figure D-36: Size distributions for the same operating conditions recorded at different times as referenced by escort number sets

APPENDIX E
Chemical Ionization Mass Spectrometry

John O. Ballenthin, Thomas M. Miller, and A.A. Viggiano
Air Force Research Laboratory

E.1. BACKGROUND

The chemical ionization mass spectrometer (CIMS) used in the jet engine tests at NASA-LeRC Research Center was developed and constructed at the Air Force Research Laboratory at Hanscom AFB, Bedford, Massachusetts. The instrument has been flown on board NASA T-39 and DC-8 aircraft to sample the exhaust gases of other aircraft in flights during the SNIF, SUCCESS, and SONEX programs (Ref. E-1). The SNIF program included flights behind F-16 fighters (using the F-100) jet engine. The same instrument, operated in its electron-bombardment ionization mode, has flown in the bomb bay of a NASA WB-57 to sample the exhaust in the stratosphere of space shuttle launches and Titan missile launches. An earlier version of the instrument, also in its electron-bombardment mode, has flown twice on the space shuttle in connection with the "shuttle glow" problem, and still earlier versions were flown on balloons, sounding rockets, and satellites.

Modeling of the results of the *in situ* aircraft exhaust measurements was complicated by lack of knowledge of exactly which trace gases are present at the exhaust plane of the jet engine—for example, if H_2SO_4 is observed, and surely is produced from SO_3 and H_2O, how much of the precursor SO_2 gas is oxidized into SO_3 inside the engine (by O atoms) as opposed to oxidation by OH in the wake? Similarly, how much NO_2 is converted into HNO_3 in the engine? Thus, the NASA-LeRC tests are important to, and complement, our other aircraft sampling data.

E.2. CIMS INSTRUMENT

The CIMS instrument consists of sampling lines, a flow reactor, an ion source, a drying region, a sampling orifice, a skimmer, ion lenses, an rf electric quadrupole mass spectrometer, and a electron multiplier, and is shown in Figure E-1. The electronics package includes dc and rf power supplies, pulse counting circuitry, and a microprocessor. The CIMS instrument weighs about 300 lb including pumps and electronics. The physical size is approximately 60 x 70 x 100 cm. A separate 100-cfm mechanical pump was installed at NASA-LeRC to pump the flow tube gas at a velocity (68 m/s) sufficient to keep the walls flushed, to reduce backgrounds signals, and to maintain a low pressure (37 Torr) in the flow tube. The 37-Torr flow tube pressure was chosen because the ion signal levels maximize in the 20-40 Torr range, and the low pressure allowed us to pump engine effluent through the sampling capillary at an acceptable rate over the entire simulated altitude range of the test cell.

Engine exhaust was sampled through three extractor probes on the lower half of the probe rake. The probes were located at 5.1 cm, 10.2 cm, and 15.2 cm below the engine axis. Siloxane-covered glass-lined stainless steel lines from the probes were joined after 1-m travel. From this point a single siloxane/glass-coated stainless steel line (0.64-cm OD, 7.3-m long), heated to 150 °C to inhibit condensation of exhaust gases, carried the engine effluent through the wall of the test cell to the CIMS instrument. The engine effluent passed through a siloxane-coated 0.32-cm OD stainless steel capillary into the flow tube of the CIMS. The purpose of the capillary was to confine the flow rate of engine effluent to <20 slm (std. liters per min.) to avoid saturating the CIMS signals. The flow tube gas consisted of 30 Torr N_2 flowing continuously at a rate of about 120 slm, 2 Torr of O_2 from the ion source and dryer region, and typically 5 Torr of engine effluent. The flow tube (3.5-cm OD) was maintained at 150 °C to avoid condensation of the effluent. A sampling orifice (100-μm diam.) for the CIMS was located 0.3 m downstream of the entry point for the engine effluent in the flow tube, near the wall of the flow tube. Directly opposite the sampling orifice was a source of CO_3^- ions. The CO_3^- was produced by a corona discharge in a small cup containing approximately 1 atm of O_2 gas mixed with about 0.05% CO_2. The corona produces O^- ions which rapidly associate with CO_2 to produce CO_3^- ions. The CO_3^- ions were injected into the flow tube through a 0.13-cm orifice, entrained in a jet of source gas (3 slm). The CO_3^- ions traveled across a diameter of the flow tube to the sampling orifice, reacting with the engine effluent along the way.

The primary reactions for detection of SO_2 and HNO_3 were given in Section 4.3. The precursor ion CO_3^- was chosen for the present work because it does not react appreciably with the major constituents of the flow tube gas, N_2 and O_2, but reacts with SO_2 and HNO_3. CO_3^- reacts with SO_2 to form SO_3^-, which immediately clusters with O_2 to yield SO_5^- ion signal at 112 amu (Ref. E-2). CO_3^- forms an adduct with HNO_3, at 123 amu (Ref. E-3). One complication is that CO_3^- associates with H_2O molecules, which are plentiful in the combustion exhaust. Even at 150 °C the concentration of $CO_3^-(H_2O)$ may be more intense than that of CO_3^-. The hydrated CO_3^- ions react with SO_2 and HNO_3 to produce the same product ions, but in some cases with different rate constants (Ref. E-4). The mechanism may be more complex as well; for example, CO_3^- reacting with SO_2 forms SO_3^-, and SO_3^- may become hydrated. A ligand-switching reaction with O_2 occurs, leading to the same SO_5^- product as found from unhydrated CO_3^-. Less important, but still significant, are adducts such as $CO_3^-(N_2)$ and $CO_3^-(CO_2)$ and higher-order clusters of H_2O, N_2, O_2, and CO_2. The hydration of ions, and clustering in general, tends to congest the mass spectrum at higher mass numbers. The detection sensitivity that our CIMS technique is capable of (presently 10 pptv for 1 s integration time) is achievable only if the product ion does not fall at the same mass number as one of the undesirable cluster species. For SO_2, which leads to signal at 112 amu as described in Sect. 4.3, and HNO_3, which leads to signal at 123 amu, there is no competing signal.

In contrast, consider our search for SO_3 in the engine exhaust. SO_3 may be detected by the reaction (Ref. E-5):

$$CO_3^- + SO_3 \rightarrow SO_4 + CO_2,$$

which gives ion signal at 96 amu, the same mass as $CO_3^-(H_2O)_2$. Since both SO_3 and H_2O are exhaust products, it isn't possible to separate contributions at 96 amu. A different precursor ion such as (possibly) NO_3^- is needed. Many species, such as N_2O, simply do not react with CO_3^-, or with extremely low efficiency, and are undetectable with this precursor ion. We also searched for H_2SO_4, which yields ion signal at 97 amu (HSO_4^-), but found that it could all be accounted for by HSO_4^- produced in the flow tube by SO_3^- (from SO_2), or SO_5^- interacting with H_2O. It is likely that neither SO_3 nor H_2SO_4 can survive the 8.3-m length of sampling line. In future engine tests, we would like to place the CIMS instrument directly inside the test cell, with an orifice or a very short sampling line of a few centimeters.

Ions entering the CIMS sampling orifice first passed through a "drying region" about 0.3-cm long, where hot, dry O_2 gas (3 slm) replaced the flow tube gas and allowed H_2O molecules to evaporate from the core ions. The evaporation is not complete, but greatly reduces congestion of the mass spectrum at high mass numbers. Between the sampling orifice and a skimmer (0.13-cm diam. orifice), two 350-l/s turbomolecular pumps removed most of the gas that passed through the sampling orifice. (An oil-free diaphragm pump was used to back up the turbomolecular pumps.) An electric potential of 100 V on the skimmer tended to keep ions in the central jet of gas that passed through the skimmer. The ion beam next passed through electrostatic lenses and entered an rf quadrupole mass spectrometer. A third turbomolecular pump kept the quadrupole region at high vacuum (typically 10^{-5} Torr). Ions exiting the mass spectrometer were detected with a electron multiplier. A fourth turbomolecular pump maintained the multiplier region at about 10^{-6} Torr vacuum. Pulses denoting ion detection were passed through shaping and counting circuitry and then to a computer for data storage and display.

Capacitance manometers were used to monitor the flow tube pressure, the pressure on the input side of the sampling capillary, and the differential pressure on a pitot tube mounted in the flow tube. Thermocouples or RTD devices were used to monitor temperatures of the flow tube and of the reservoir housing the HNO_3 calibration source.

N_2 purge gas could be introduced into the sampling line inside the test cell, to clear engine effluent out of the sampling line. The purge gas was useful as a diagnostic to identify the source of certain ion signals—that is, to show that a particular peak in the mass spectrum was due to flow tube gases instead of engine effluent.

Normally, only high-purity (99.999% pure) O_2 is used in the CIMS ion source, drying region, and as the calibration carrier gas. But the high-purity O_2 ordered by NASA-LeRC for these tests did not arrive until the low-sulfur Jet A fuel runs were completed, meaning that higher background signals resulted during the early days of the tests.

E.3. CALIBRATION SOURCES

The calibration source for SO_2 consisted of a 0.5-l cylinder filled to 6 atm of He gas with 1% SO_2 and a flow controller delivering the mixture to the flow tube at the same port through which engine effluent entered the flow tube. Tests at the AFRL lab and at NASA-LeRC (with the 7.3-m long, heated siloxane sampling line) showed no loss of SO_2 gas in the sampling line. The flow controller was set for 1.454 sccm (std. cm^3 per min.) of the 1% SO_2 mixture for the NASA-LeRC engine tests. Converting to slm and putting in the 1% factor gives an SO_2 flow rate of 1.454×10^{-5} slm.

The HNO_3 calibration source consisted of three HNO_3 permeation tubes which emitted approximately 5,000 ng/min of HNO_3 each at 60 °C. The HNO_3 calibrant vapor was carried from the 60 °C reservoir by 400 sccm of O_2 flush gas passing over the permeation tubes. The total flow rate of HNO_3 was approximately 15,000 ng/min or 5.333×10^{-6} slm. The word "approximately" is used because the HNO_3 emission rate depends somewhat on the equilibration time of the permeation tube; a correction has been applied to the data based on calibration measurements carried out at Aerodyne Research, Inc., in April of 1998. Tests at NASA-LeRC showed about 15% loss of HNO_3 over the entire length of the sampling line, as illustrated in Figure E-2. A caveat is that we assume there is no loss of HNO_3 in the siloxane/glass-coated, 0.32-cm OD stainless steel tubing used to deliver the calibration gas to the inside of the test cell. The He/HNO_3 flow (400 sccm) was maintained in the delivery line at all times to ensure that the HNO_3 was in equilibrium with surfaces of the delivery line, so that there was no loss of HNO_3 up to the points of entry into the sampling line. During a calibration event, a Teflon solenoid valve was actuated to divert the flow into the sample line. At other times the calibrant gas flowed into the vacuum chamber. Corrections for HNO_3 loss in the sampling lines were made as outlined above.

E.4. DATA PROTOCOL

The data protocol included mass scans from 45-127 amu with purge gas "on" and "off". Single-mass integrations with calibration gases "on" and "off" and purge gas "on" and "off" were carried out for masses 96 amu [$CO_3^-(H_2O)_2$ and SO_4^-], 97 amu (HSO_4^-), 112 amu (SO_5^-), and 123 amu [$CO_3^-(HNO_3)$]. [Because the purge gas greatly reduced the amount of water vapor in the flow tube, thus affecting the distribution of $CO_3^-(H_2O)_n$ precursor ions in the reaction zone, the calibration signal obtained with purge gas "on" is only of diagnostic value.] Next, data for a number of notable masses (46, 60, 62, 64, 78, 80, 87, 88, 94, 96, 97, 98, 105, 107, 109, 112, 115, 116, 123, and 125 amu) were integrated for at least 2.5 s, with the purge gas "on" and "off." Ion signal at most of these masses allow us to monitor the degree of H_2O, N_2, and O_2 clustering, as a diagnostic. Only the single-mass integrations (over time periods of 10-30 s) were used to arrive at the final results for emission indexes, for SO_2 and HNO_3.

E.5. DATA ANALYSIS

The CIMS data analysis for obtaining the emission index (EI) for a trace gas will be illustrated using SO_2 as an example. EI(SO_2) is defined as the number of grams of SO_2 in the engine exhaust per kilogram of fuel burned. We measure the mixing ratio of SO_2 in the exhaust effluent and use NASA measurements of combustion-related CO_2 to obtain EI(SO_2). Specifically, EI(SO_2) = (64/12)(0.87)(10^{-4})[ppbv(SO_2)] / (%CO_2). The factors 64 and 12 are the molecular mass of SO_2 and atomic mass of C, respectively; the factor 0.87 is the fraction of C in the fuel; the factor 10^{-4} is the product of a factor of 10^3 which converts g into kg and a factor of 10^{-7} which puts the ppbv(SO_2) and %CO_2 on the same scale; ppbv(SO_2) is our measured mixing ratio; and %CO_2 is the NASA-LeRC contribution. EI(HNO_3) is obtained similarly, except that it is conventional to report EI(HNO_3) in terms of the equivalent number of grams of NO_2 produced in the exhaust; hence, the corresponding formula for EI(HNO_3) contains a leading factor of (46/12), where 46 is the molecular mass of NO_2.

The CIMS mixing ratio (in ppbv) for SO_2 is determined from ion signals ["counts(eng-SO_2)" and "counts(cal-SO_2)"] due to engine-related SO_2 and calibrant SO_2, respectively, and from flow rates of calibrant SO_2 and engine effluent ["Q(cal-SO_2)" and "Q(effluent)" as follows:

ppbv(eng-SO_2) = 10^9*Q(cal-SO_2)*counts(eng-SO_2) / [counts(cal-SO_2)*Q(effluent)].

The count rate for SO_5^- (due to SO_2) was typically 75 per 10 ms sampling time. The count rate for $CO_3^-HNO_3$ (due to HNO_3) was typically 25 per 10 ms sampling time. The results reported here were based on integration times of about 10 s, so the total number of ion counts in an SO_2 measurement was typically 75,000, and for HNO_3, 25,000. SO_2 count rates for low-sulfur fuel were smaller than given above, and those for high-sulfur fuel were greater. The factor of 10^9 in the formula above puts the result in ppbv. The factor Q(cal-SO_2) is set by a flow controller that injects SO_2 calibrant into the flow tube.

The flow rate of engine effluent through the sampling capillary was measured both at NASA-LeRC and in our laboratory, as a function of the pressure across the capillary (which ranged from 175-1500 Torr during engine tests, depending on the simulated altitude and engine power setting). In this differential pressure (ΔP) range, we found Q(effluent) = 0.9434 + 0.021153 * ΔP, in slm for ΔP in Torr, at a temperature of approximately 60 C. During each test condition, the pressure on both sides of the capillary were monitored with capacitance manometers and recorded in the data stream.

Before the start of the NASA-LeRC engine tests, we had only a rough idea of the ion signal levels we could expect from the engine exhaust, and therefore what dilution of the effluent in the flow tube would be required to avoid saturating the CIMS. Early in the engine tests, during low-sulfur fuel runs, our procedures and ion signals were still being optimized for the NASA-LeRC conditions and these data carry larger error bars than later data. (The CO_3^- signal strength was ten times larger during the final week than during the first week.) The final data runs, for JP-8 fuel, consistently yielded large signal levels and

routine, reliable background and calibration measurements, and hence are the most accurate. The CIMS method is inherently very accurate as applied here, if the flow rates of calibration gases and engine effluent are known, because the count rates with and without the calibration gas may be accurately (<1%) measured by integrating over 10-30 s. The flow rates of calibration gas and engine effluent can be measured with flow meters to within 5%. In practice, however, we found larger hour-to-hour variations in the results, as great as 20%, indicating a systematic error associated with the sampling and/or calibration system (but not with the CIMS itself). The systematic error (for example, a leak in the sampling line or in the calibration line) cannot be traced now that the tests have ended. Considerable effort has gone into tracking down the source of the problem, unsuccessfully. However, it is clear for several reasons that future tests should be conducted with the CIMS mounted inside the test cell, with short sampling lines. Because of the systematic error, the present results are only accurate to ±30%. Averages for EI(SO_2) over many days of data are estimated accurate within 15% for JP-8 fuel, 20% for medium-sulfur Jet A fuel, and 25% for low-sulfur Jet A fuel. There is greater variation in EI(HNO_3) because of sampling line losses and associated time constants.

E.6. RESULTS

E.6.1. Nitric Acid Production In the Engine

NO_2 and OH, produced in the combustion process, combine to produce HNO_3. In this section we will examine the efficiency of that process. While we do not have a measurement of OH concentration, the NASA-LeRC measurements of NO and NO_x concentration allow us to deduce the NO_2 concentration. The emission indexes for NO, NO_x, and HNO_3 are, by convention, all expressed in terms of grams of NO_2 per kilograms of fuel. Therefore, we may calculate EI(NO_2) = EI(NO_x) - EI(NO), and compare this value to our EI(HNO_3) measured under the same engine conditions. Figure E-3 shows EI(NO_2) plotted versus combustor inlet temperature (T_3) for all fuels and all altitudes for which we have corresponding EI(HNO_3) data (i.e., not *all* of the NASA-LeRC NO_2 data are represented). Much of the dispersion in the data shown in Figure E-3 is due to an altitude dependence in EI(NO_2); there is little dependence on fuel type.

In Figure E-4 are shown the fraction of NO_2 conversion into HNO_3, calculated from EI(HNO_3) / [EI(NO_2) + EI(HNO_3)]. The dispersion in the data now includes the scatter in our measurements of EI(HNO_3). The most striking feature of Figure E-4 is the rapid decline in the production of HNO_3 as the combustor inlet temperature increases. The $NO_2 \rightarrow HNO_3$ conversion rate decreases a factor of 5 between 600-700 °K, and drops at least a decade between 700-800 °K. This decline is not due to a corresponding change in the concentration of NO_2; indeed, EI(NO_2) *increases* by perhaps a factor of 3 in the 600-800 °K range (Figure E-3). We attribute the decrease in the $NO_2 \rightarrow HNO_3$ conversion rate to the thermal instability of HNO_3.

In Figures E-5 and E-6 we examine the altitude dependence in these results, for one fuel type (#2). In Figure E-5, the $NO_2 \rightarrow HNO_3$ conversion rate is seen to depend on altitude. We shall show in the following sections that there is no significant altitude dependence in

the $EI(HNO_3)$ measurements. Figure E-6 shows that the altitude dependence in the calculation of the $NO_2 \rightarrow HNO_3$ conversion rate is a consequence of division by $EI(NO_2)$], which is altitude dependent. If $EI(HNO_3)$ does not track $EI(NO_2)$ precisely, it indicates that some other aspects of the conversion reaction are changing with altitude, e.g., EI(OH), the temperature profile in the combustor, and the residence time in the combustor.

Figures E-7 through E-13 give the $NO_2 \rightarrow HNO_3$ conversion rate for each altitude for all fuel types for which we obtained data on $EI(HNO_3)$. A linear fit to each data set is indicated on the figures to facilitate intercomparisons. $NO_2 \rightarrow HNO_3$ conversion rates for each fuel type will be given in the following sections. Overall averages are 8% at 500 °K, 6% at 600 °K, 1.5% at 700 °K, and <0.1% at 800 °K.

E.6.2. JP-8 FUEL

We will first focus on the JP-8 results because our procedures and signal strengths were well optimized during the final week of the test series. The emission indexes for SO_2 production, $EI(SO_2)$, are presented in Figs E-14 through E-20, as a function of combustor inlet temperature (T_3). $EI(SO_2)$ is judged to be independent of combustor inlet temperature at all altitudes, within the scatter in the data. Complementary plots vs combustor inlet pressure (P_3) are not given because there is a similar lack of dependence on P_3. The value of $EI(SO_2)$ averaged over combustor inlet temperature is somewhat different at different altitudes; it is our opinion that these variations are artifacts of the measurement system, as outlined in the previous section. Thus, it is best to consider the average (over altitude and combustor inlet temperature) of all measurements of $EI(SO_2)$ for JP-8 fuel, $\langle EI(SO_2) \rangle = 0.573 \pm 0.086$ g/kg.

Fuel sulfur analyses were obtained from Wright-Patterson AFB (336 ppmm for JP-8). If all the sulfur (32 g/mol) were converted to SO_2 (64 g/mol), the fuel would yield an SO_2 emission index 0.672 g/kg. Assuming the fuel sulfur analyses are correct, we find an overall average of (85 ± 15)% for the amount of sulfur appearing as gas phase SO_2. The remaining sulfur, if any, is most likely in the form of SO_3 or is incorporated into particulates.

The HNO_3 emission indexes (expressed, by convention, in terms of grams of NO_2 produced) are given in Figures E-21 through E-27. The amount of HNO_3 produced is found to be independent of the sulfur level in the fuel, and decreases with combustor inlet temperature as outlined in the previous section. For JP-8, we find $EI(HNO_3)$ = 0.20 $g(NO_2)$/kg fuel at 500 °K. This figure drops to 0.17 $g(NO_2)$/kg at 600 °K, and decreases still further to about 0.05 $g(NO_2)$/kg at 700 °K.

E.6.3. MEDIUM-SULFUR JET A FUEL

As with the other fuels, there is no significant dependence of $EI(SO_2)$ on combustor inlet temperature for the medium-sulfur (152 ppmm) Jet A fuel. The results are given in Figures E-14 through E-20. $EI(SO_2)$ is similarly independent of combustor inlet pressure

(P_3) within the scatter in the data. The overall average EI(SO_2) for the medium-sulfur Jet A fuel is 0.337 ± 0.067 g/kg. The fractional uncertainty for the medium-sulfur fuel results is somewhat larger than for the JP-8 because signal levels were lower and the SO_2 calibration is less certain (the calibration mixture is no longer available to verify). The fuel sulfur analysis from WPAFB implies that the maximum EI(SO_2) is 0.304 g/kg. Assuming this latter figure is accurate, the correct EI(SO_2) must be in the range 0.270-0.304 g/kg. Thus, our best estimate is that 88-100 percent of the fuel sulfur appears in the form of SO_2 in the engine.

EI(HNO_3) behaves as with the other fuels: EI(HNO_3) = 0.12 ± 0.05 g(NO_2) per kg fuel at 500 °K. This number drops by 10% at 600 °K, then drops a further factor of 10 by 750 °K. The data are presented in Figures E-21 through E-27.

E.6.4. HIGH-SULFUR JET A FUEL

Again, EI(SO_2) does not appear to vary with engine combustor inlet temperature (T_3) within the scatter in the data, here for the high-sulfur (1113 ppmm) Jet A fuel. The results are given in Figures E-14 through E-20. EI(SO_2) is likewise independent of combustor inlet pressure (P_3) within the scatter in the data. The overall average EI(SO_2) for the medium-sulfur Jet A fuel is 2.49 ± 0.62 g/kg. The fractional uncertainty is still larger for this fuel because, at that point in the test series, we were just settling on routine operation—with flow tube oxygen quality, flow tube heating, and calibrant gas delivery system all being modified between data runs. The fuel sulfur analysis from WPAFB implies that the maximum EI(SO_2) is 2.226 g/kg. If so, the correct EI(SO_2) must be in the range 1.87-2.23 g/kg. Thus, our best estimate is that 84-100 percent of the fuel sulfur appears in the form of SO_2 in the engine exhaust.

The EI(HNO_3) data for the high-sulfur fuel show greater statistical variation than for the fuels discussed above, but the gross behavior is the same. EI(HNO_3) = 0.15 ± 0.05 g(NO_2) per kg fuel at 500 K. This number drops to 0.13 at 600 °K, then drops a decade by 750 K. The data are presented in Figures E-21 through E-27.

E.6.5. LOW-SULFUR JET A FUELS

The pre-test analyses of the two batches of low-sulfur Jet A fuel at WPAFB yielded "<1 ppmm" sulfur content. Our data for the mixing ratios of SO_2 in the engine exhaust for all fuels indicate that the first batch of low-sulfur fuel was actually 3.5 ppmm sulfur, and the second batch was 7.4 ppmm sulfur. These results represent extrapolations of our measurements of mixing ratios versus the WPAFB analyses for the two medium-sulfur fuels (one Jet A and one JP-8) and for the high-sulfur fuel. The sulfur concentrations given here, 3.5 and 7.4 ppmm, respectively, are technically lower limits because in deriving these values we are assuming that the percentage of fuel sulfur appearing as SO_2 in the exhaust was the same for the low-sulfur fuels as measured (85-100%) for the higher-sulfur fuels. (It would seem unreasonable, to us, for the low sulfur fuels to have a lower conversion rate.)

Results for $EI(SO_2)$ are given in Figures E-14 through E-20. There is no dependence on combustor inlet temperature (or pressure, P_3) within the scatter in the data. Because these data are from the first week of the test series, when signal strengths were low, other parameters had not been optimized, and the data protocol was still being developed, the uncertainties in even the average values for $EI(SO_2)$ are relatively large (25%). The first batch of low-sulfur fuel yielded $\langle EI(SO_2)\rangle = 0.007 \pm 0.002$ g/kg. The second batch of low-sulfur fuel yielded $\langle EI(SO_2)\rangle = 0.015 \pm 0.004$ g/kg.

$EI(HNO_3)$ follows the pattern seen with the other fuels, though the data for the low-sulfur fuels have the greatest scatter, again due to the lower signal levels in the earlier data runs. We find $EI(HNO_3) = 0.12 \pm 0.06$ g(NO_2) per kg fuel at 500 °K, dropping to about 0.10 at 600 °K, and then declining more than a decade by 750 °K (see Figures E-21 through E-27).

E.7. CONCLUSIONS

We monitored SO_2 and HNO_3 emissions in the F-100 engine exhaust with the CIMS instrument, and measured mixing ratios for these compounds. Comparing to NASA-LeRC measurements of CO_2 production by the engine, the mixing ratios were given as emission indexes in Figures E-14 through E-20, for the various fuels (Jet A with low-sulfur, medium-sulfur, and high-sulfur, and JP-8) and altitudes ranging from 3-17 km, as functions of engine combustor inlet temperature.

The emission indexes for SO_2 are essentially independent of altitude and of combustor inlet temperature and pressure. Combining our measurements of SO_2 mixing ratios, NASA-LeRC data on CO_2 emissions, and sulfur analyses of the fuels carried out at Wright-Patterson AFB, we find that 85-100% of the fuel sulfur appears as gaseous SO_2 in the engine exhaust. Within our experimental uncertainty, this conversion level is independent of fuel type, altitude, and power setting. The remaining fuel sulfur, if any, most likely appears as gas phase SO_3 or is incorporated into particulates.

The amount of HNO_3 produced is independent of the sulfur level in the fuel. The HNO_3 level decreases considerably with engine temperature, presumably because HNO_3 is not stable at high temperatures. Within the uncertainties in the data, there is no difference in HNO_3 production for the various fuels studied. Using NASA-LeRC measurements of $EI(NO_x)$ and EI(NO), and the AFRL measurements of $EI(HNO_3)$, we can calculate the $NO_2 \rightarrow HNO_3$ conversion rate in the engine. The $NO_2 \rightarrow HNO_3$ conversion rate is about 8% at 500 K, 6% at 600 K, 1.5% at 700 K, and drops at least a decade by 800 °K. (These figures are averages over all altitudes and all fuels studied.) We attribute this decrease in the $NO_2 \rightarrow HNO_3$ conversion rate to the thermal instability of HNO_3. There is a systematic altitude dependence in this conversion rate. A detailed examination of the data (Figures E-3 through E-13) leads us to conclude that the altitude dependence is due either to variations in EI(OH)—not measured in this test series—or due to altitude-dependent changes in combustor temperature profile and/or residence time affecting HNO_3 formation from OH and NO_2. The steepness of the $EI(HNO_3)$ curve versus T_3 will be a critical test for engine combustion models.

REFERENCES

E-1. R. C. Miake-Lye, B. E. Anderson, W. R. Cofer, H. A. Wallio, G. D. Nowicki, J. O. Ballenthin, D. E. Hunton, W. B. Knighton, T. M. Miller, J. V. Seeley, and A. A. Viggiano, "SO_x Oxidation and Volatile Aerosol in Aircraft Exhaust Plumes Depend on Fuel Sulfur Content," *Geophysical Research letters 25,* 1677 (1988).

E-2. O. Möhler, T. Reiner, and F. Arnold, "The Formation of SO_5^- by Gas Phase Ion-Molecule Reactions," *Journal of Chemical Physics*, Vol. 97, No. 11, 1992, pp. 8223-8229.

E-3. O. Möhler and F. Arnold, "Flow Reactor and Triple Quadrupole Mass Spectrometer Investigations of Negative Ion Reactions Involving Nitric Acid: Implications for Atmospheric HNO_3 Detection by Chemical Ionization Mass Spectrometry," *Journal of Atmospheric Chemistry*, Vol. 13, 1991, pp. 33-61.

E-4. J. V. Seeley, R. A. Morris, and A. A. Viggiano, "Rate Constants for the Reactions of $CO_3^-(H_2O)_{n=0-5}$ + SO_2: Implications for CIMS Detection of SO_2," *Geophysical Research Letters*, Vol. 24, No. 11, 1997, pp. 1379-1382.

E-5. S. T. Arnold, R. A. Morris, A. A. Viggiano, and J. T. Jayne, "Ion Chemistry Relevant for Chemical Ionization Detection of SO_3," *Journal of Geophysical Research*, Vol. 100, No. D7, 1995, pp. 14141-14146.

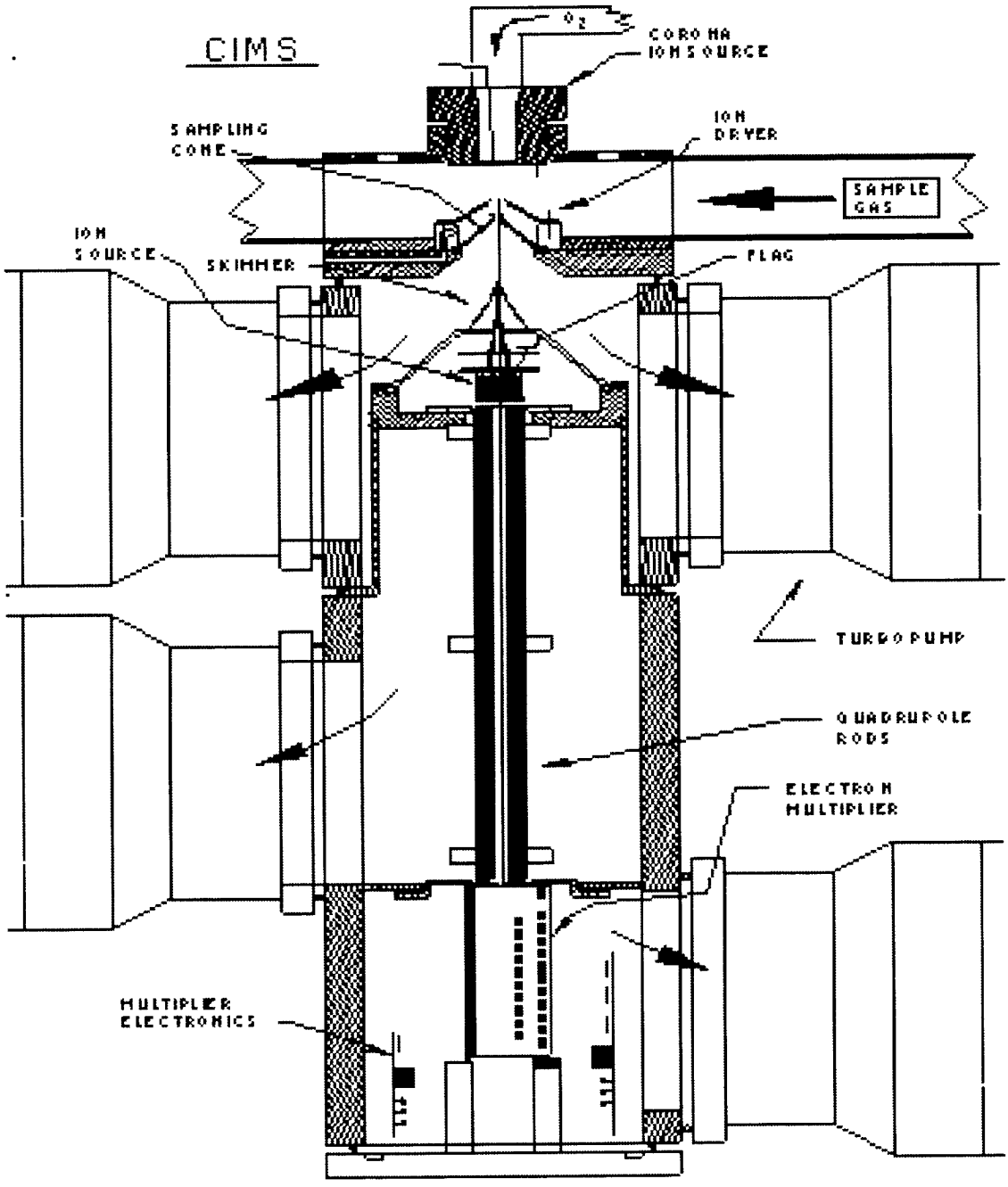

Figure E-1. AFRL chemical ionization mass spectrometer.

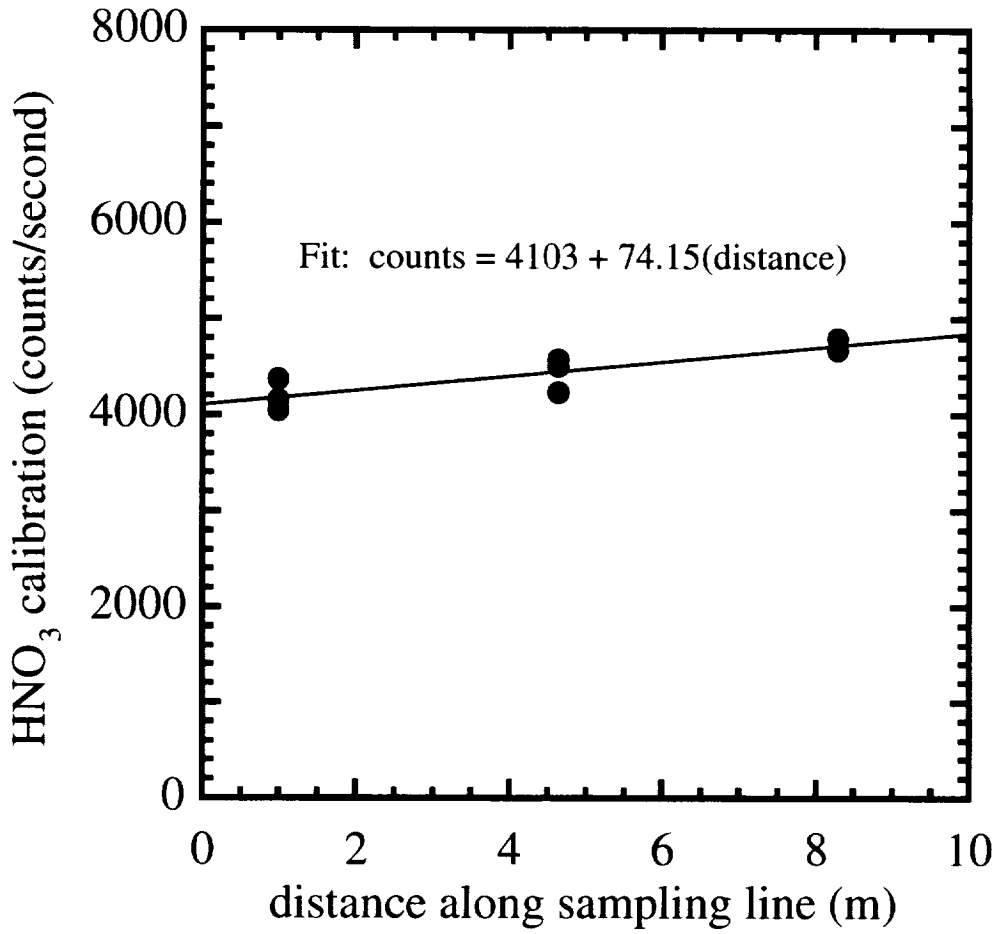

Figure E-2. Ion signal due to HNO_3 injected sequentially at three points along the sampling line. The data indicate that there is a 15% loss of HNO_3 over the full 8.3-m length of the sampling line.

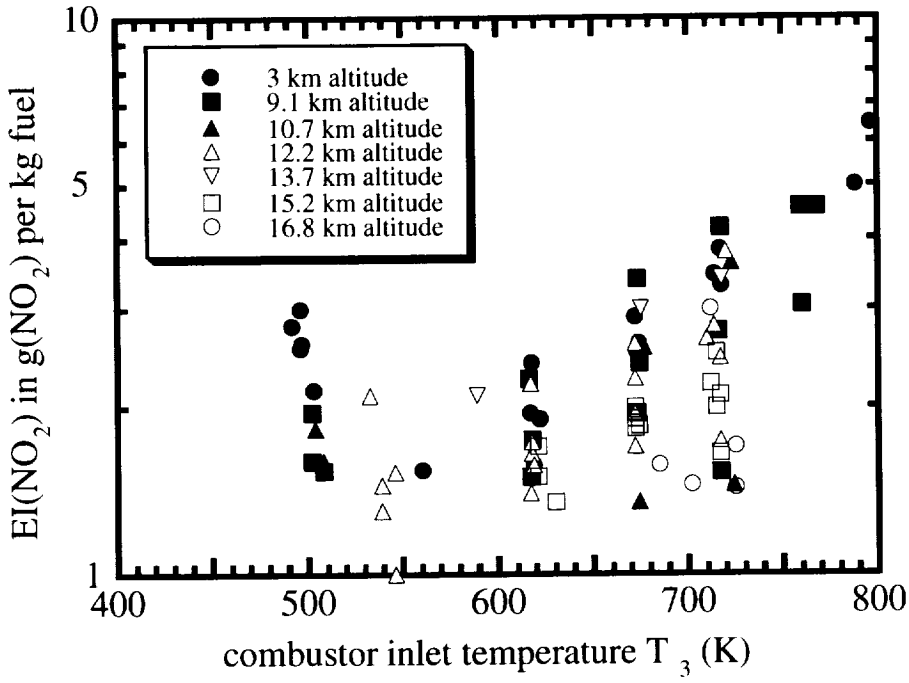

Figure E-3. $EI(NO_2)$ from $EI(NO_x)$ -EI(NO), for all fuels and altitudes.

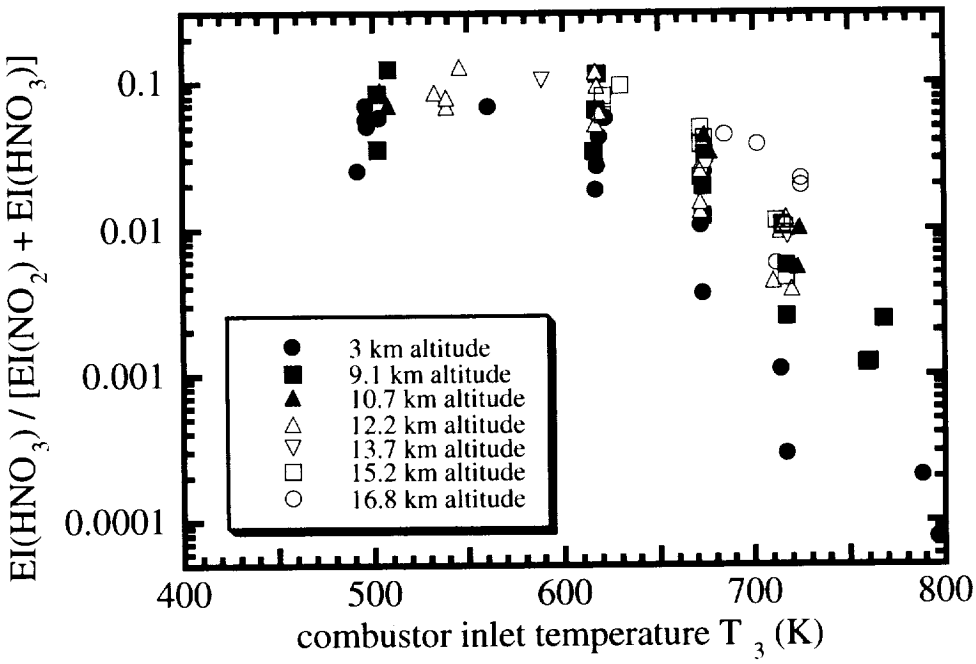

Figure E-4. Fraction of NO_2 converted into HNO_3, for all fuels and altitudes.

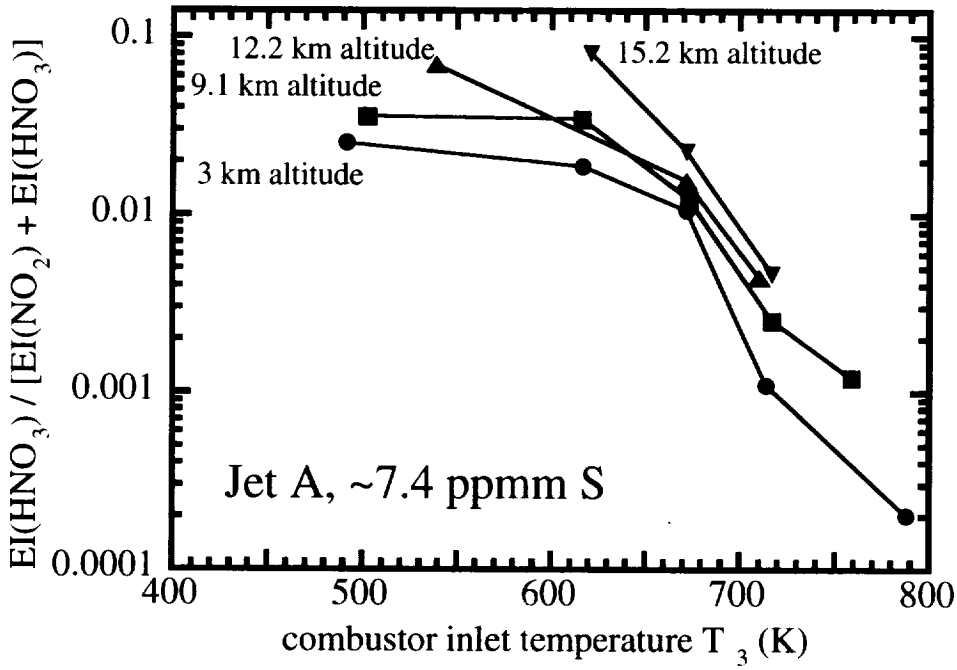

Figure E-5. Fraction of NO_2 converted into HNO_3 for fuel 2 at different altitudes.

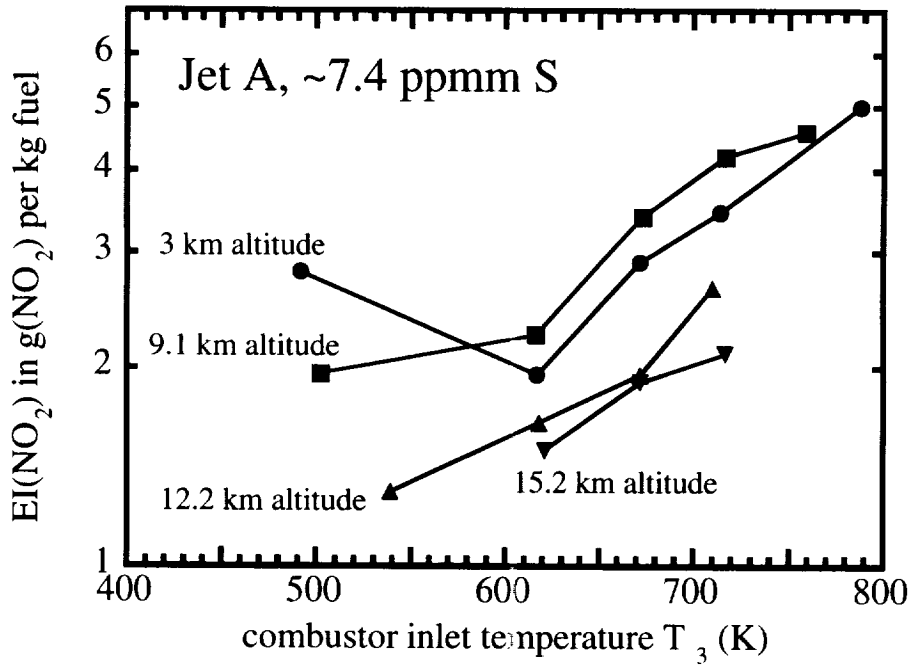

Figure E-6. EI(NO_2) for fuel 2 deduced from NASA-LeRC data for EI(NO_x) and EI(NO).

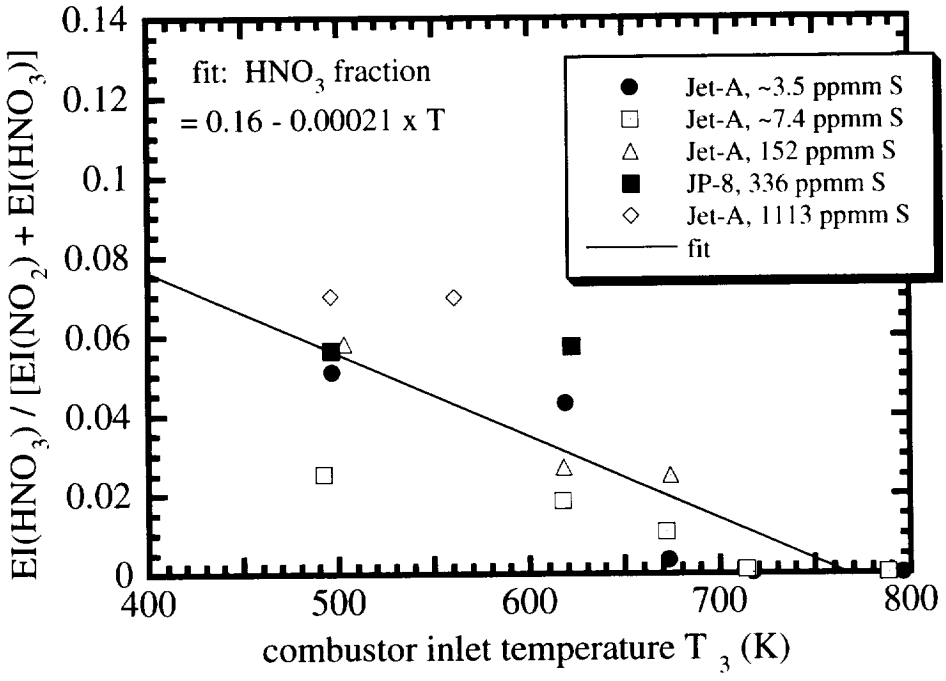

Figure E-7. Fraction of NO_2 converted into HNO_3 at 3 km altitude.

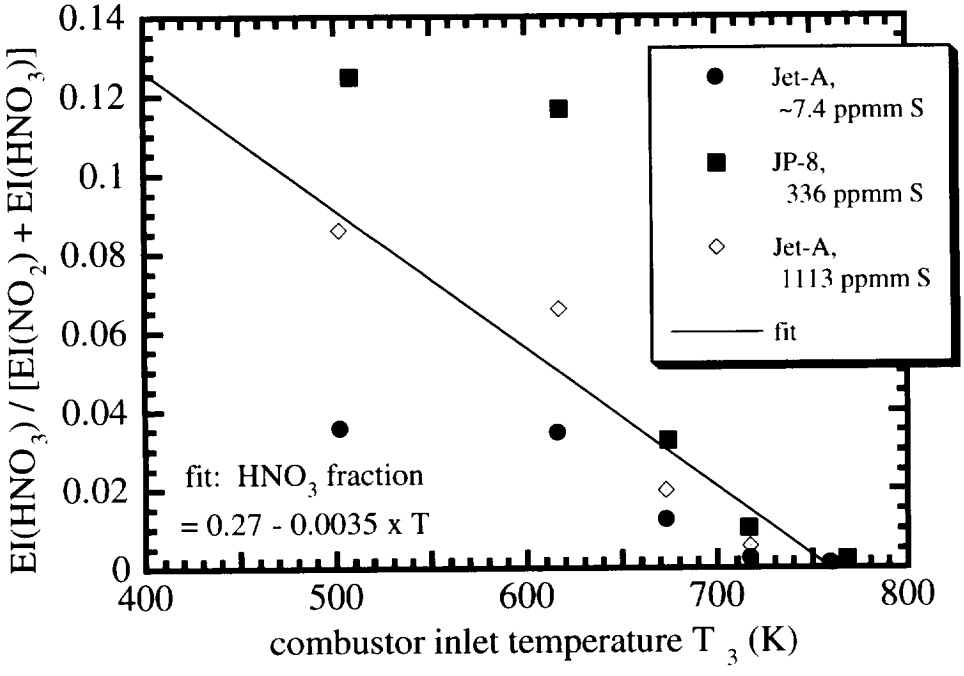

Figure E-8. Fraction of NO_2 converted into HNO_3 at 9.1 km altitude.

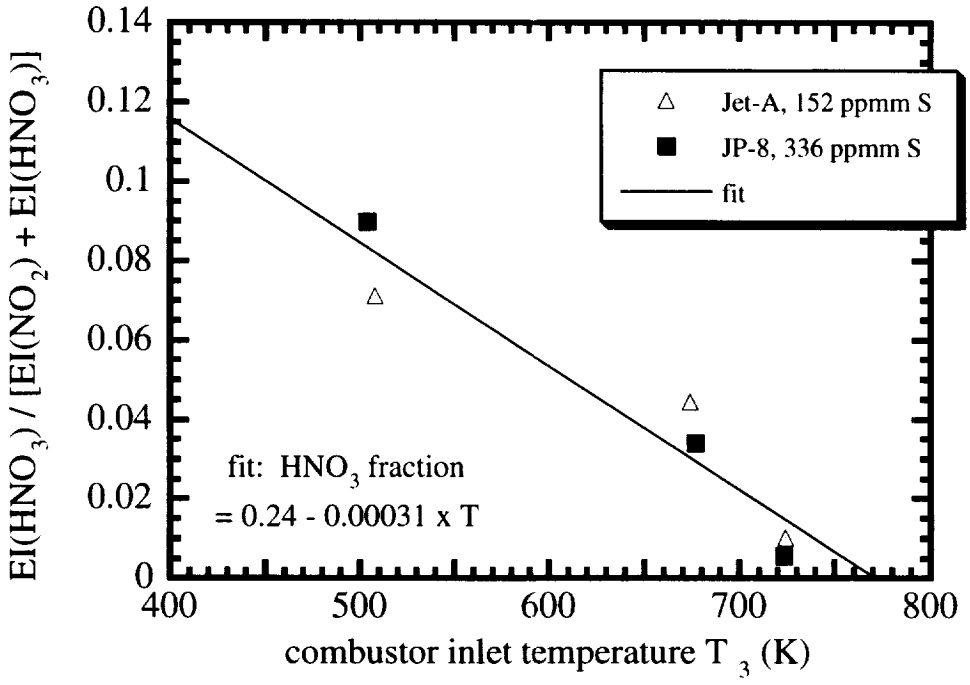

Figure E-9. Fraction of NO_2 converted into HNO_3 at 10.7 km altitude.

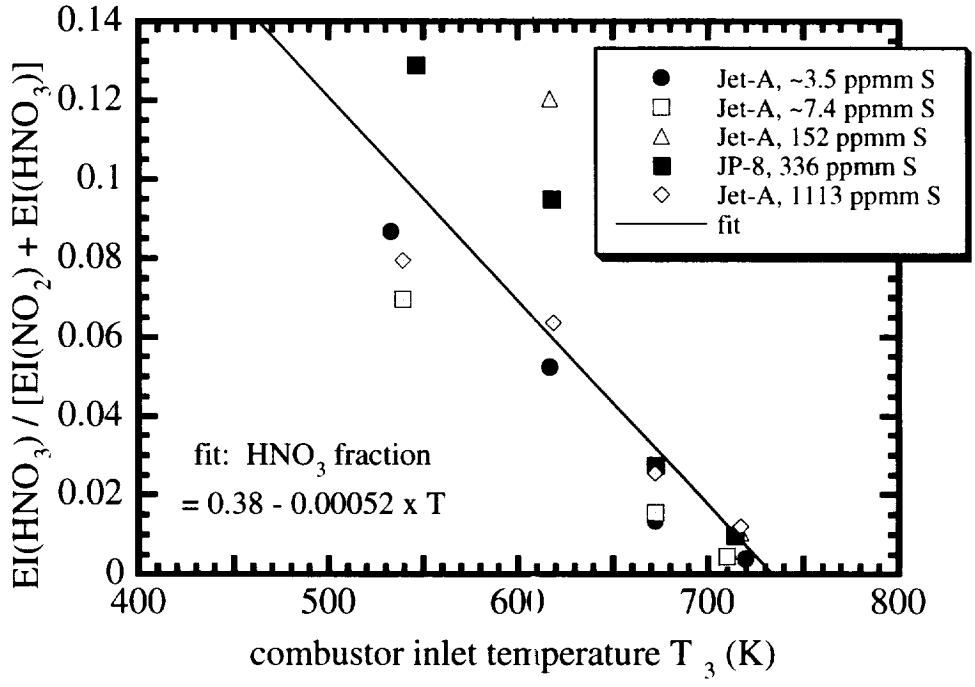

Figure E-10. Fraction of NO_2 converted into HNO_3 at 12.2 km altitude.

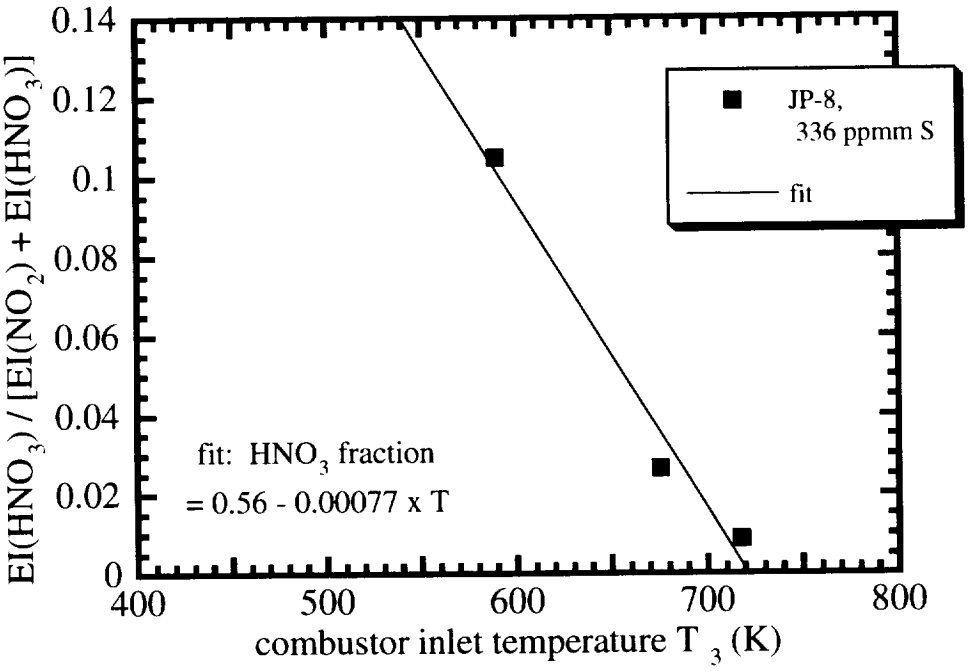

Figure E-11. Fraction of NO_2 converted into HNO_3 at 13.7 km altitude.

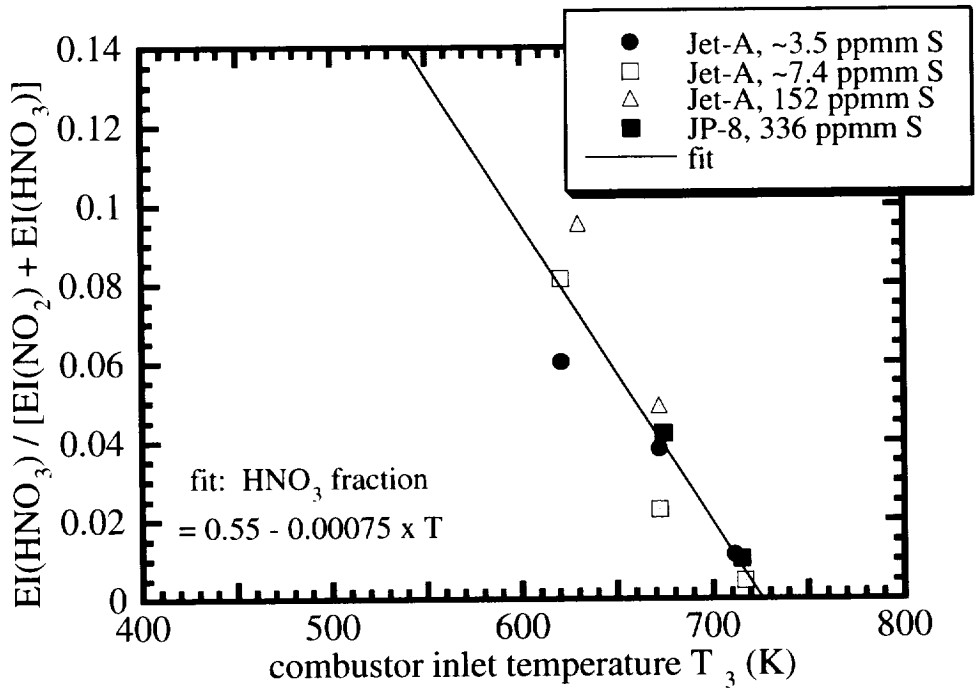

Figure E-12. Fraction of NO_2 converted into HNO_3 at 15.2 km altitude.

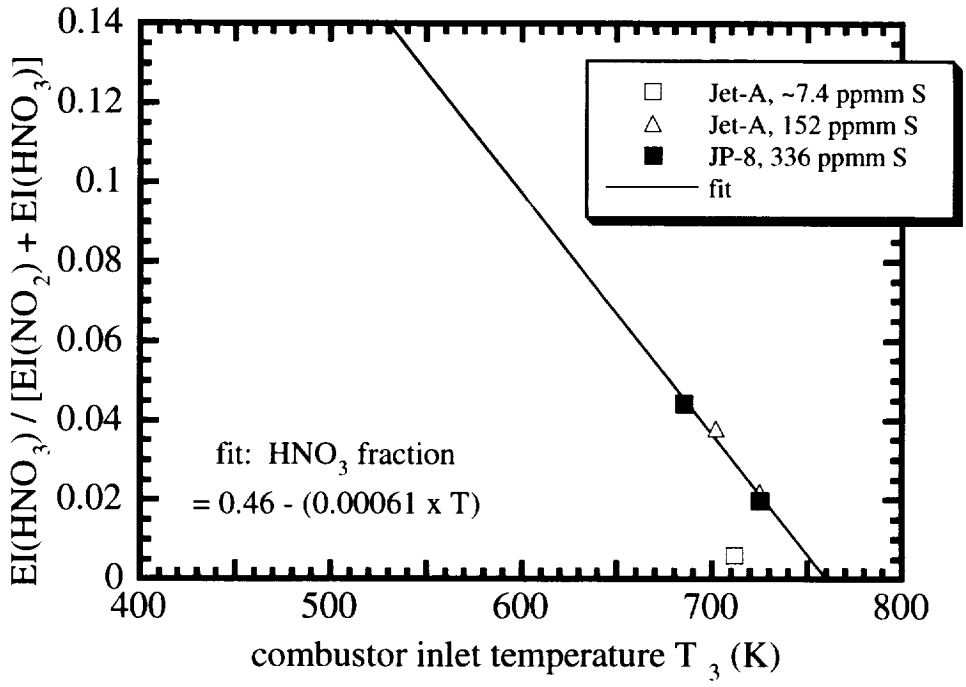

Figure E-13. Fraction of NO_2 converted into HNO_3 at 16.8 km altitude.

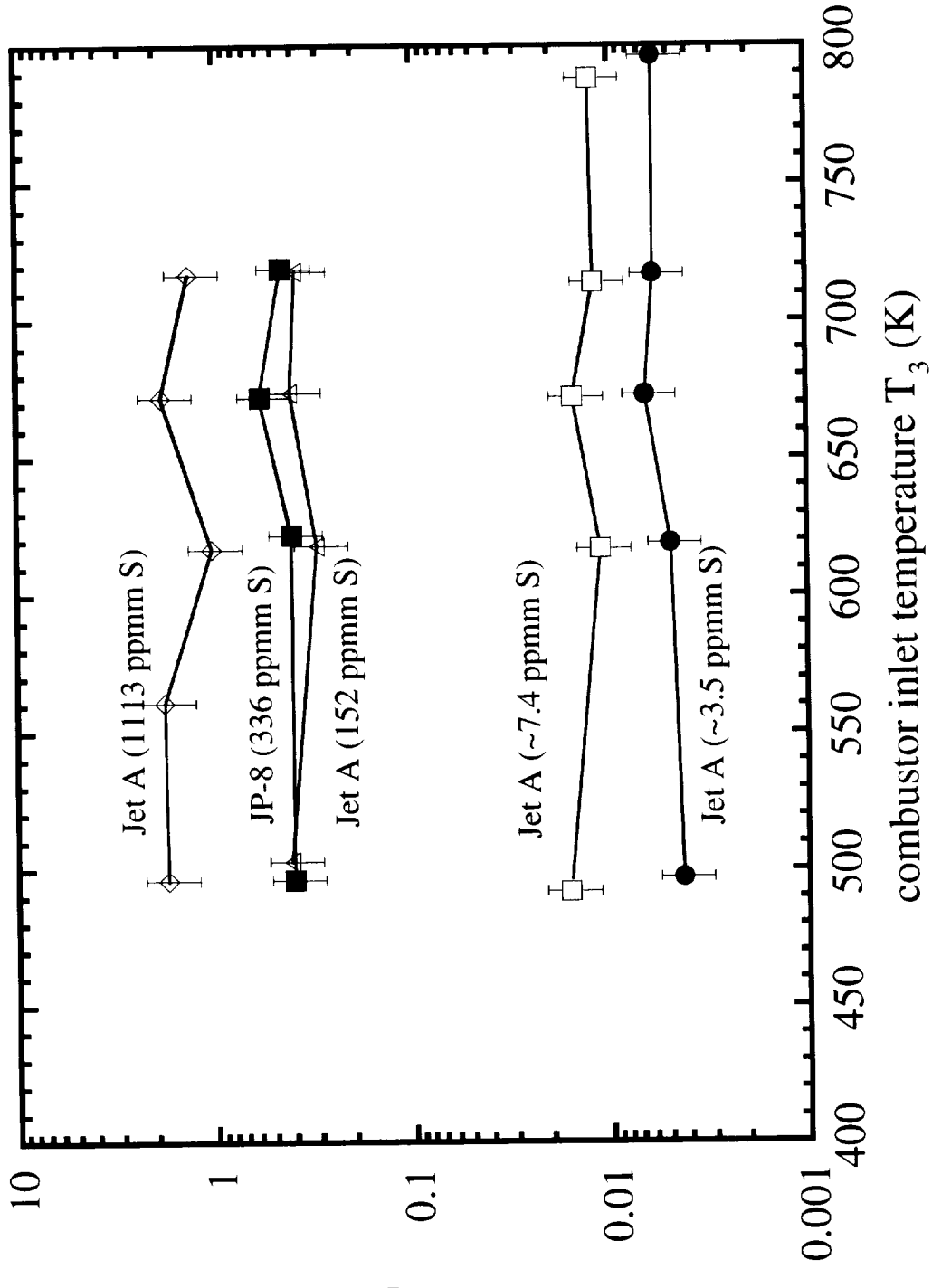

Figure E-14. EI(SO_2) at 3 km altitude (simulated sea level).

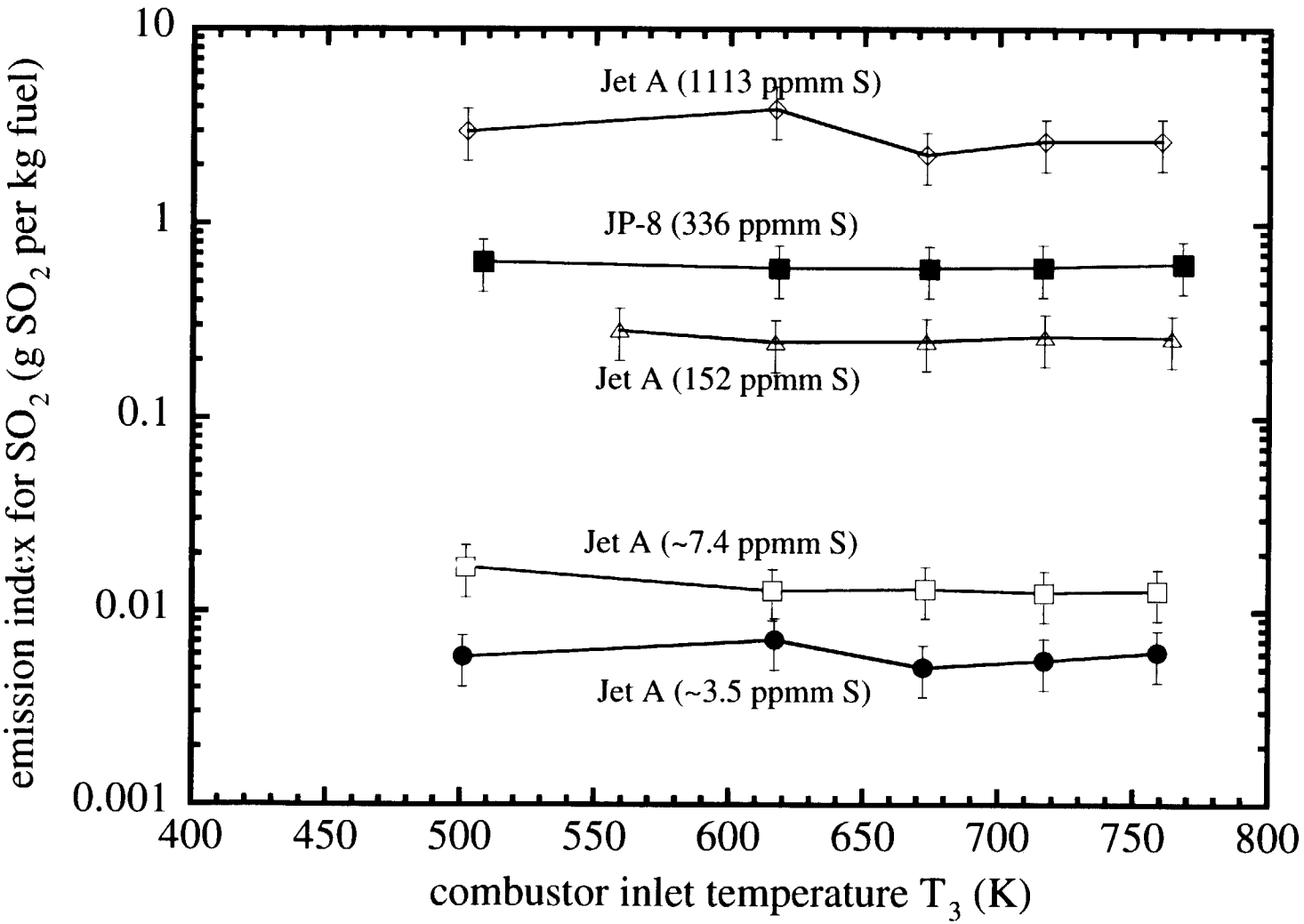

Figure E-15. EI(SO_2) at 9.1 km altitude.

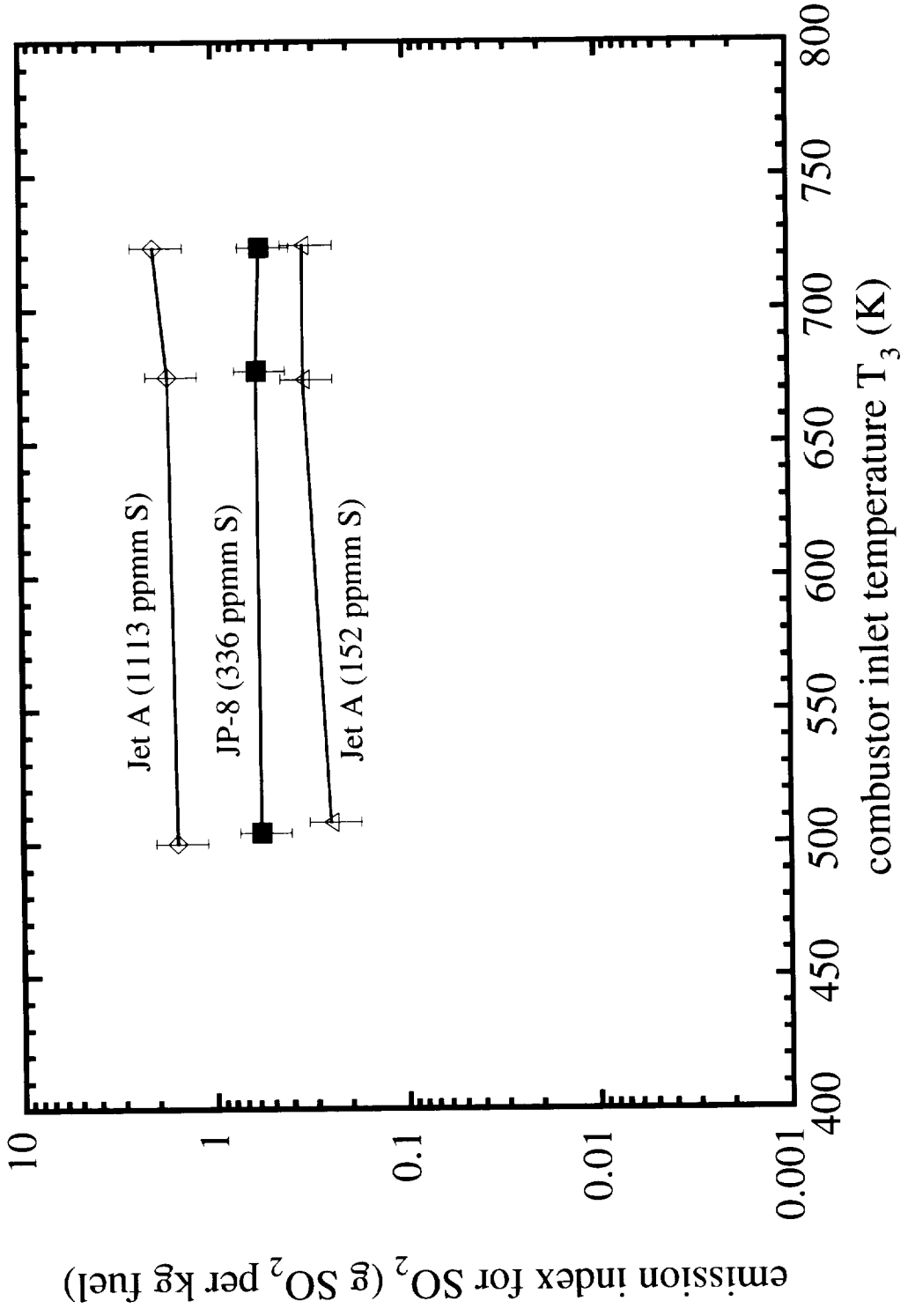

Figure E-16. EI(SO_2) at 10.7 km altitude.

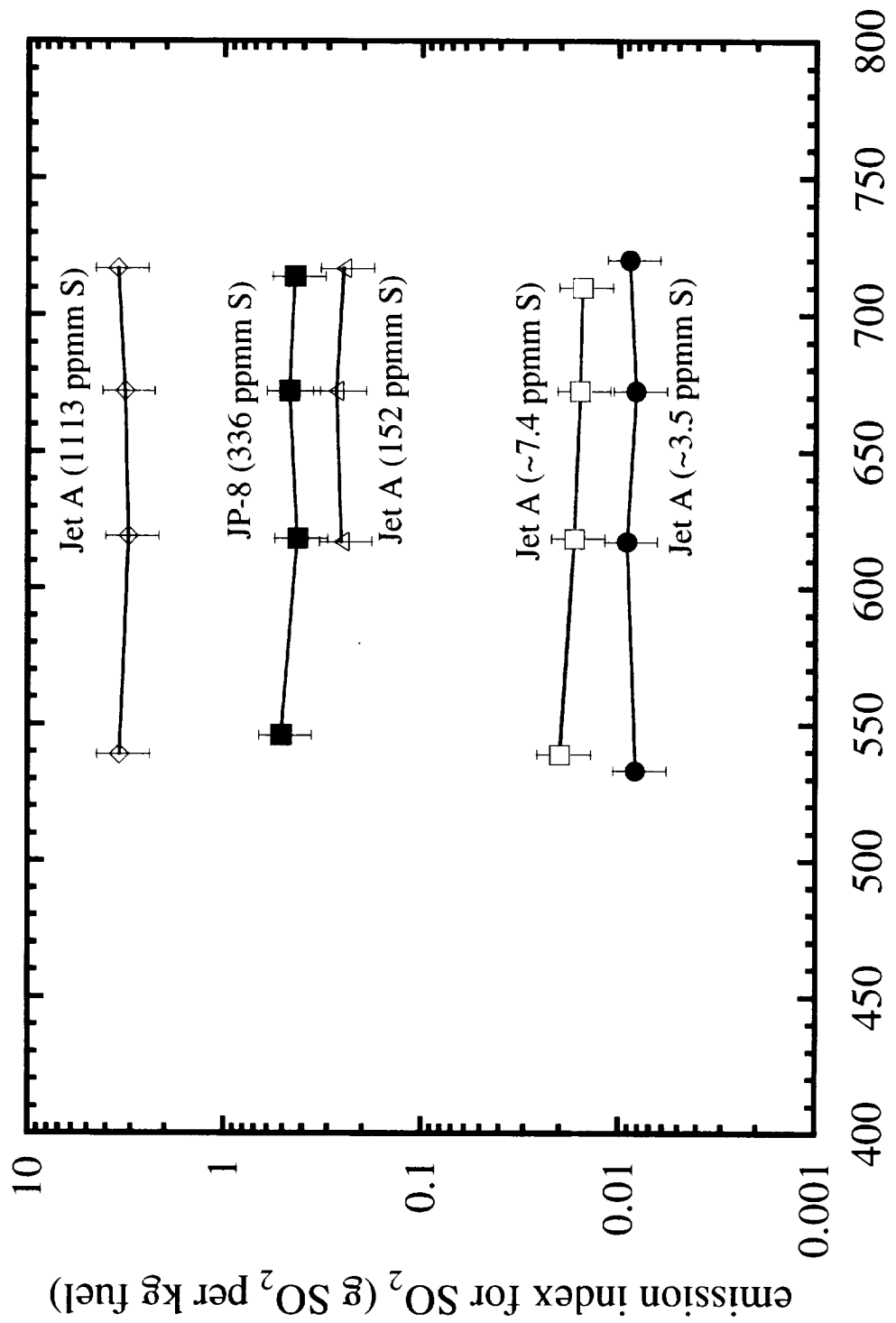

Figure E-17. EI(SO_2) at 12.2 km altitude.

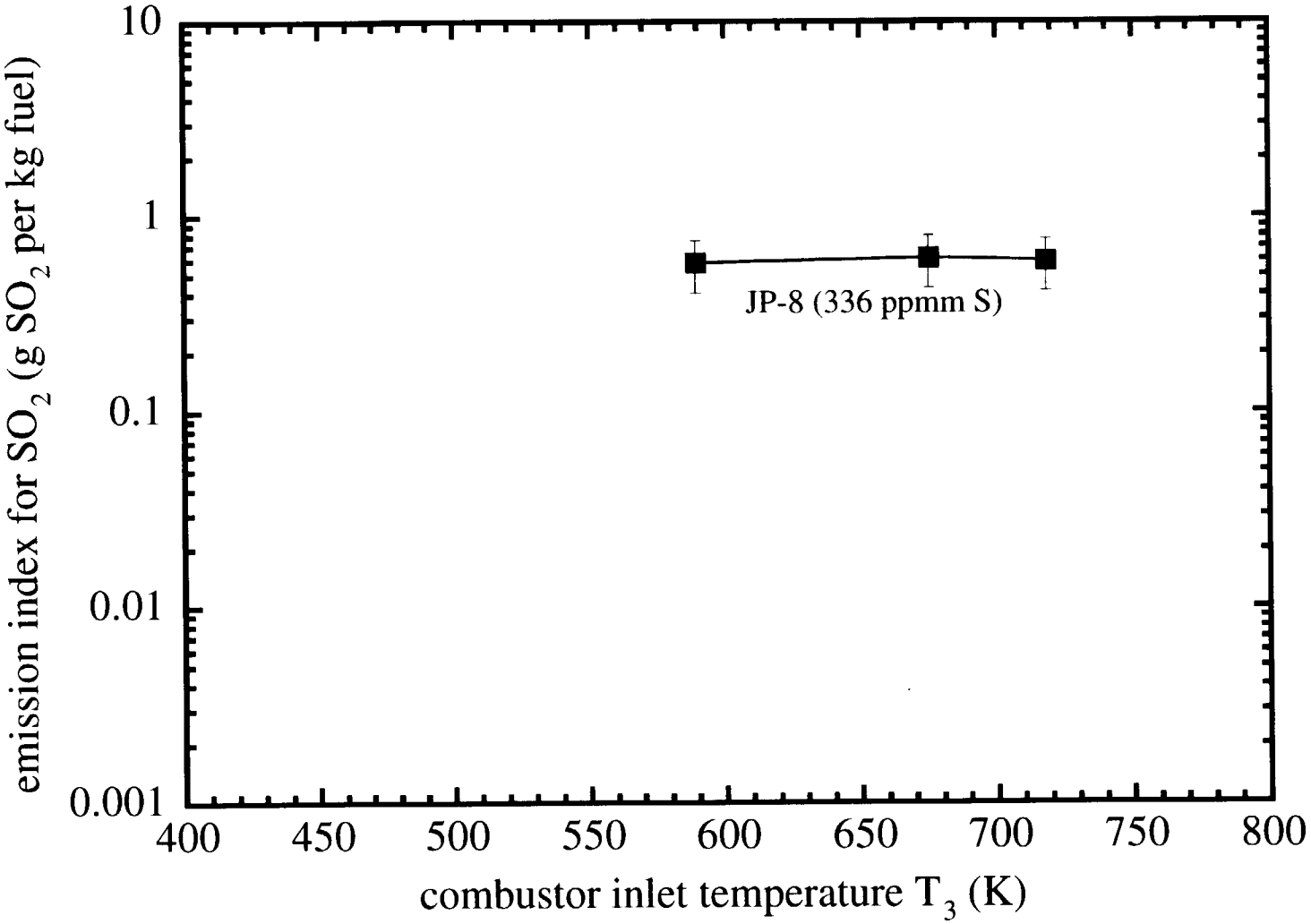

Figure E-18. EI(SO_2) at 13.7 km altitude.

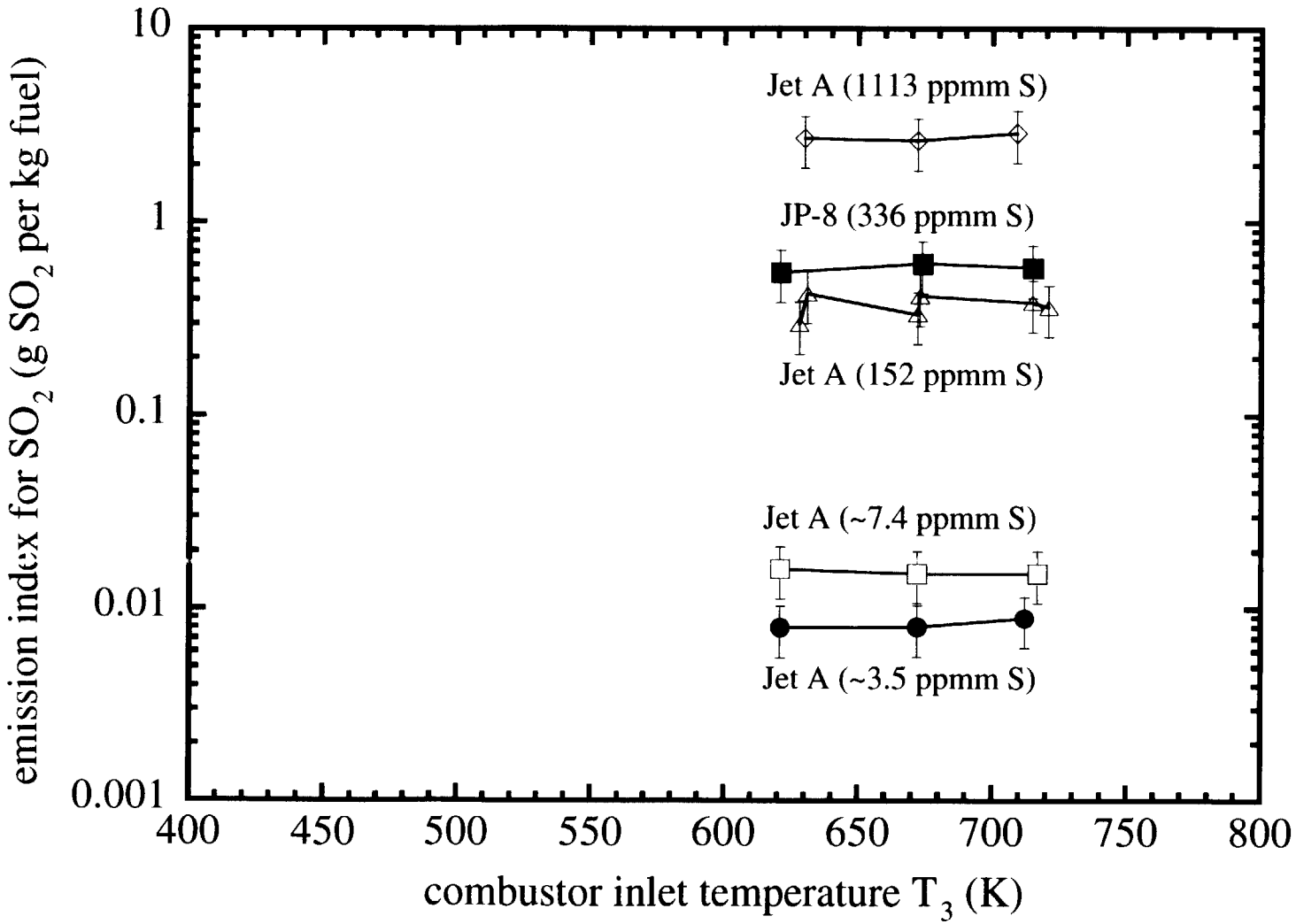

Figure E-19. EI(SO_2) at 15.2 km altitude.

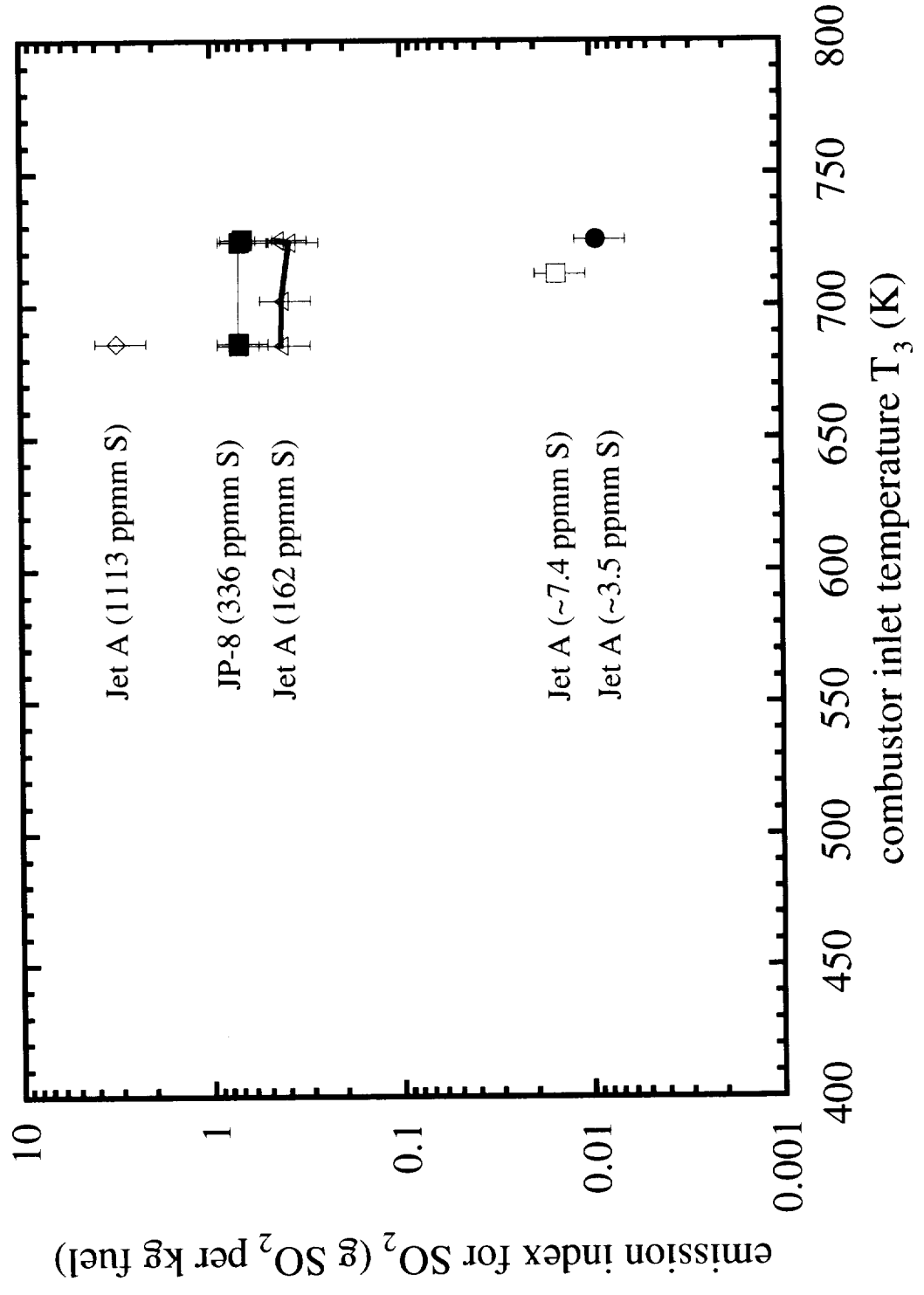

Figure E-20. EI(SO_2) at 16.8 km altitude.

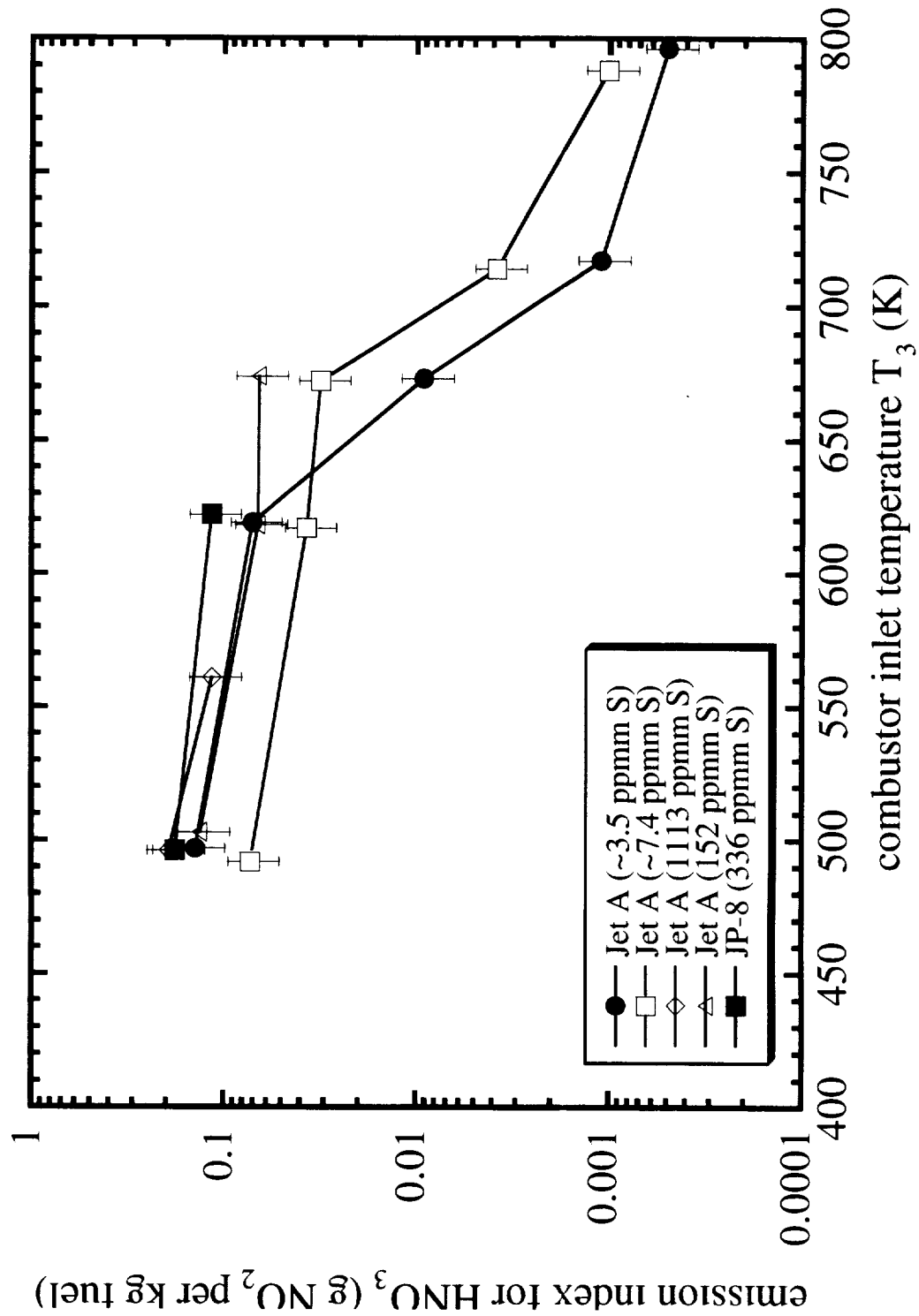

Figure E-21. EI(HNO_3) at 3 km altitude (simulated sea level).

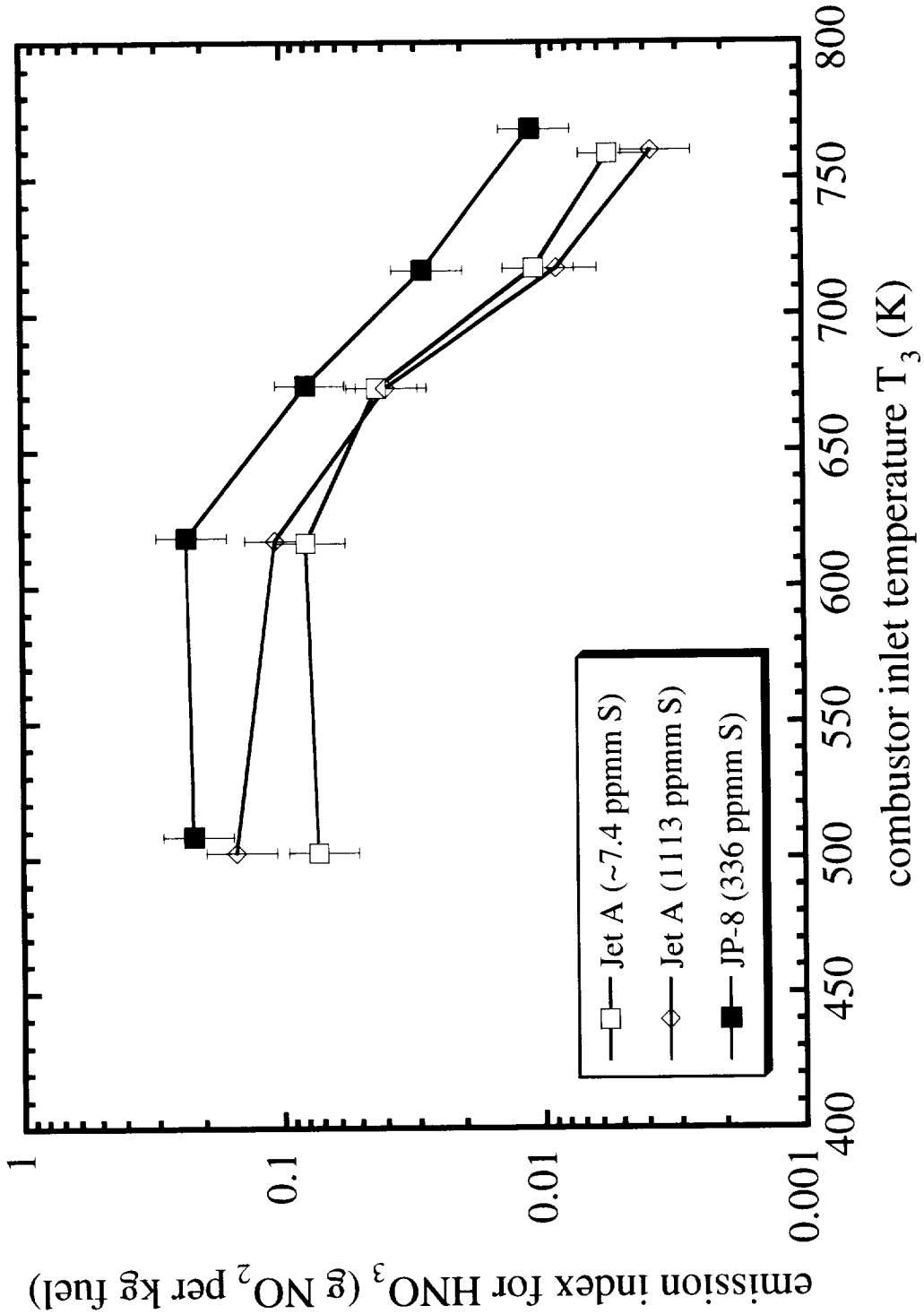

Figure E-22. EI(HNO_3) at 9.1 km altitude.

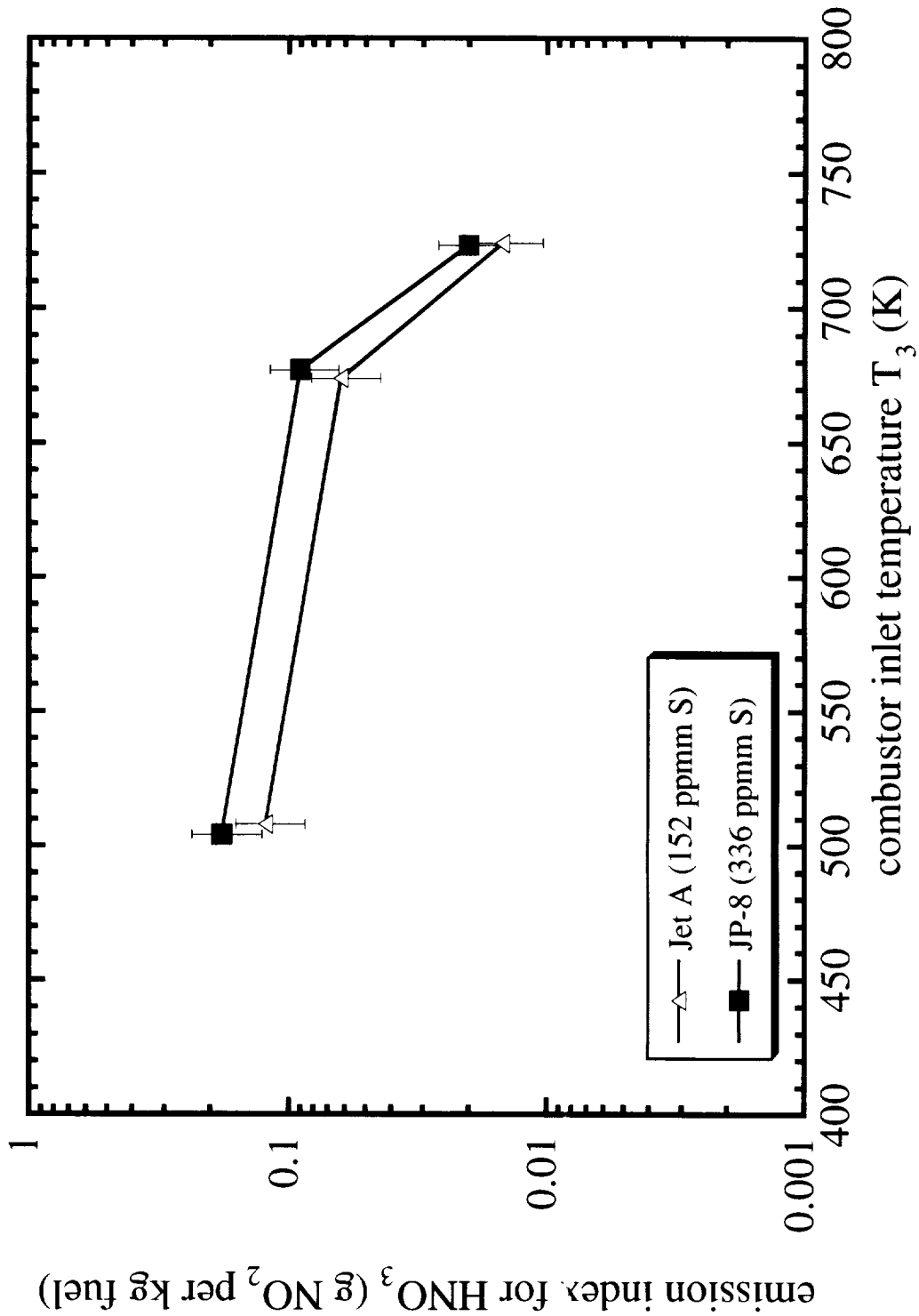

Figure E-23. EI(HNO_3) at 10.7 km altitude.

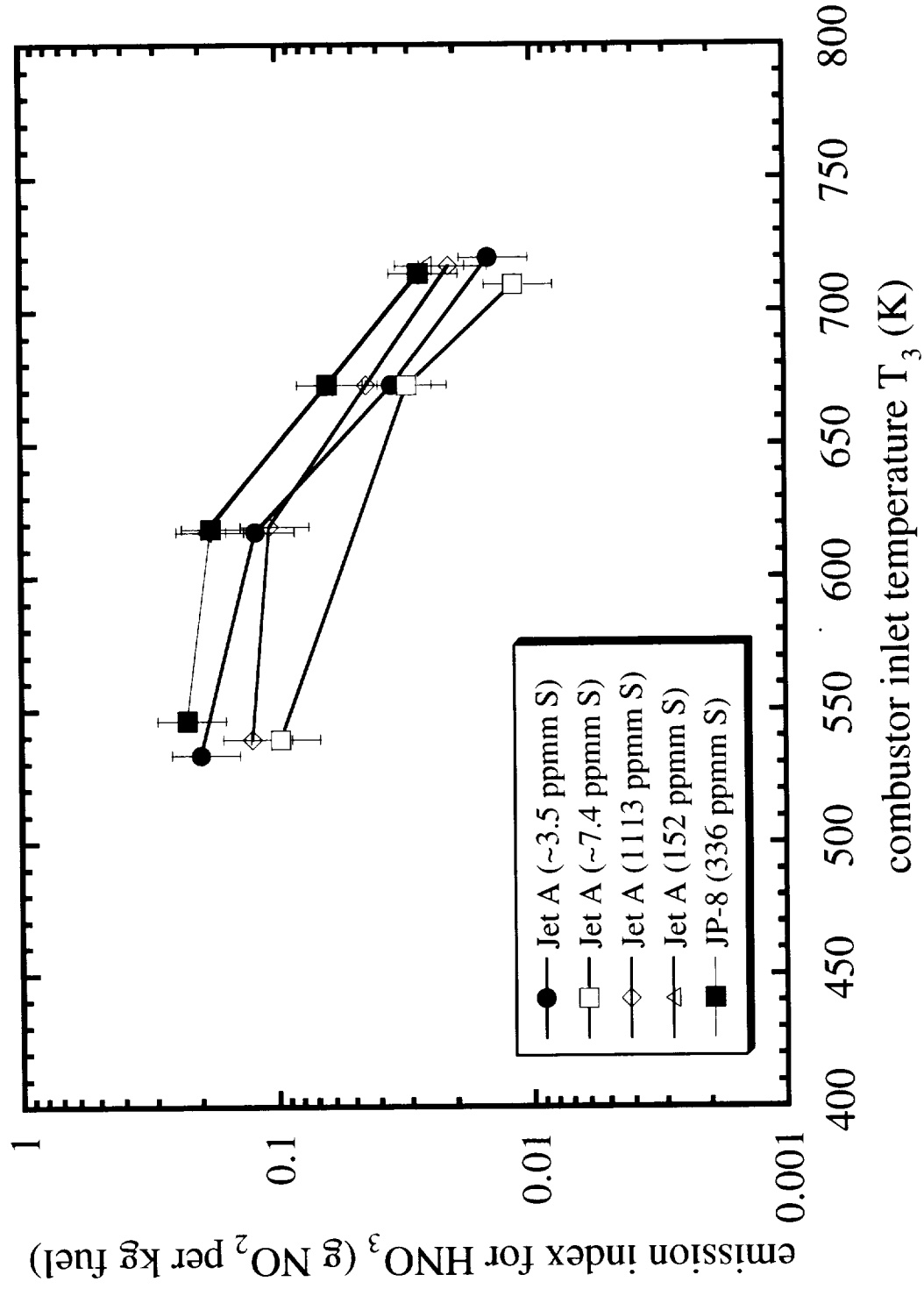

Figure E-24. EI(HNO_3) at 12.2 km altitude.

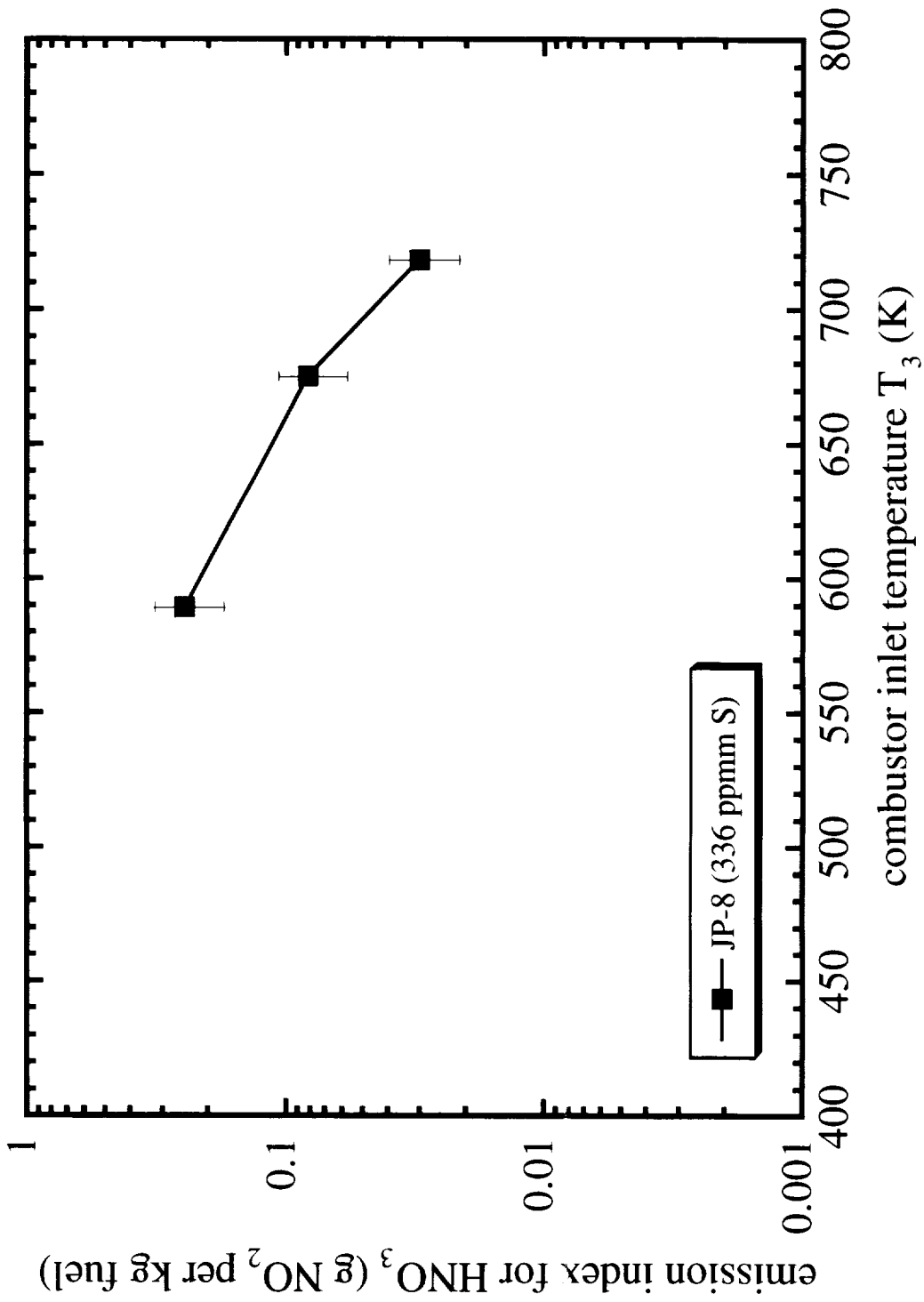

Figure E-25. EI(HNO_3) at 13.7 km altitude.

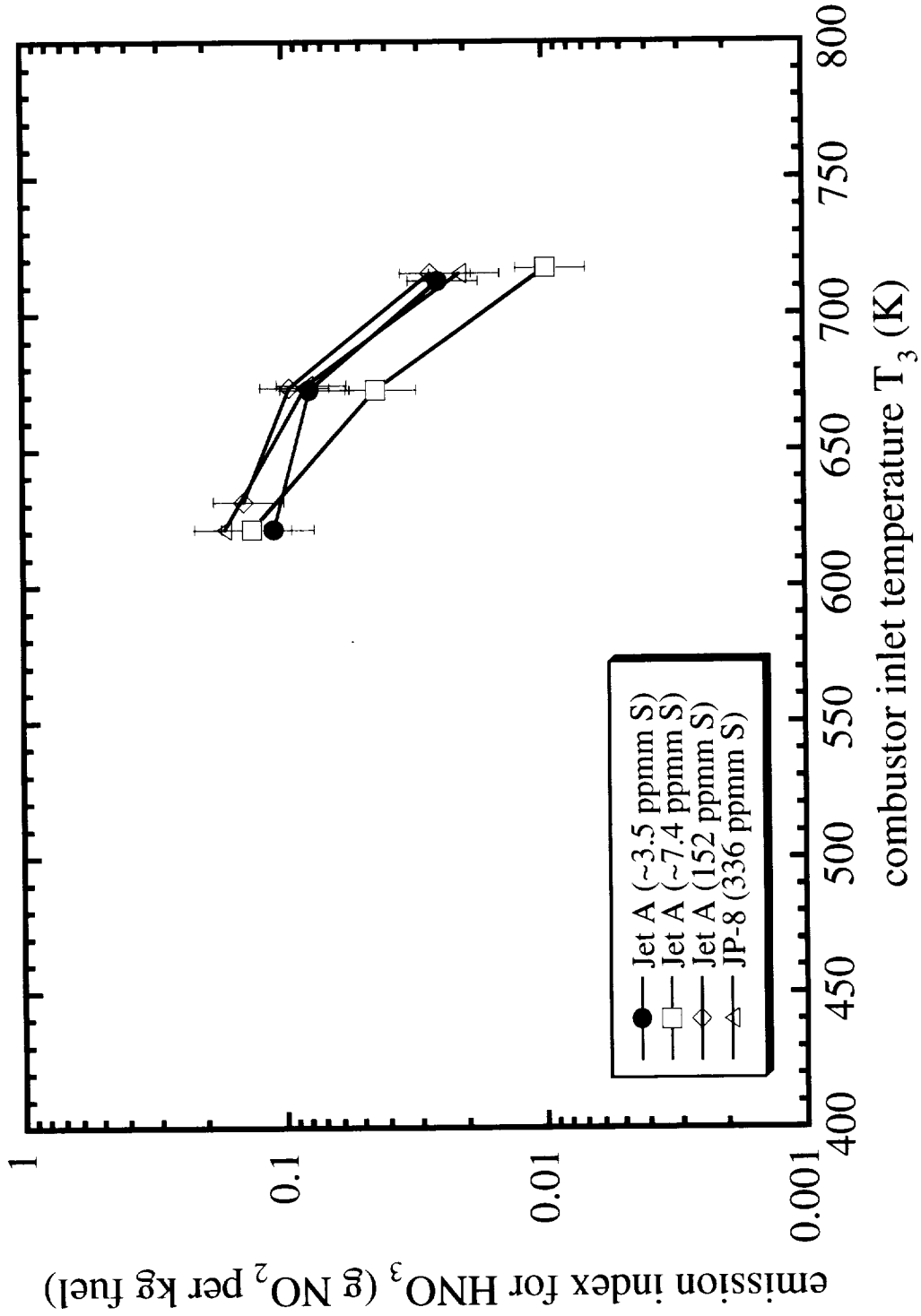

Figure E-26. EI(HNO_3) at 15.2 km altitude.

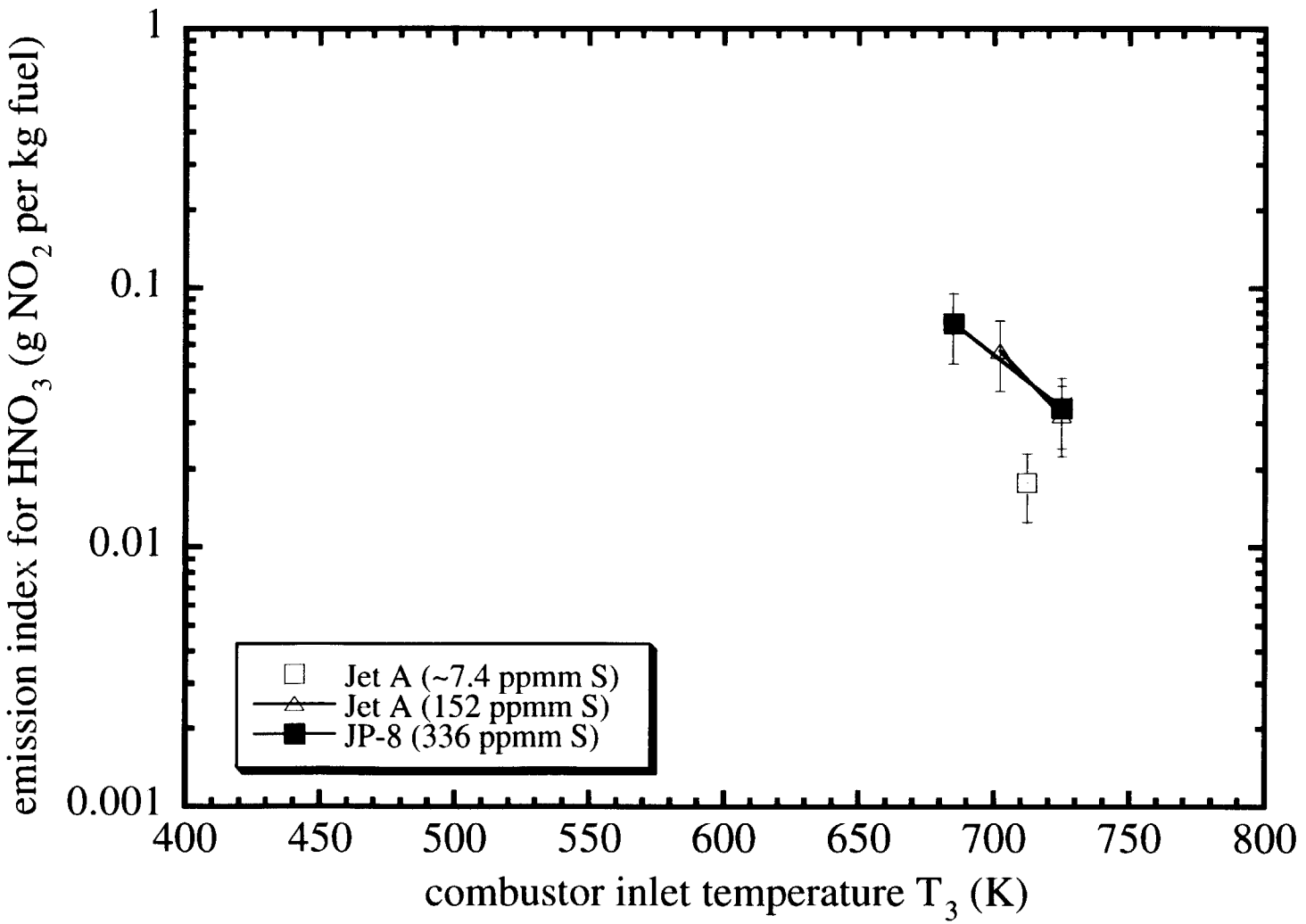

Figure E-27. EI(HNO_3) at 16.8 km altitude.

APPENDIX F
Infrared Tunable Diode Laser System

J. Wormhoudt, T. Berkoff and R. C. Miake-Lye
Center for Aero-Thermodynamics
Aerodyne Research, Inc., Billerica, MA 01821-3976

F.1. TDL INSTRUMENT

Tunable lead salt diode lasers have a long history of spectroscopic applications[1], and have recently been applied with considerable success to sensitive detection of atmospheric trace gases.[2] Our system had been applied to combustion gas flows in four previous field tests, first in a combustor simulator at NASA Lewis Research Center (LeRC)[3], then in two engine tests at the Air Force Arnold Engineering Development Center (AEDC)[4,5], and finally in a 1996 engine test in the Propulsion Systems Laboratory test cell PSL-4 which also supported the test reported here.

The laser diodes are housed in a liquid nitrogen dewar, with their nominal operating temperature controlled by a small resistance heater. Coarse frequency tuning is achieved by changing the diode temperature and thereby its refractive index and cavity mode frequencies. Fine tuning is done by scanning the injection current, which also has the effect of slightly changing the diode temperature. This current scanning can be done rapidly, allowing the averaging of many spectra whose spectral features are unperturbed by low-frequency fluctuations in the transmission. In the work reported here, the number of spectral points acquired was 500 and the scanning rate was 300 kHz (spectral points per second) so that 600 scans of each diode were accumulated each second.

A schematic drawing of the laser optical table is given in Figure F-1. The cryogenic dewar houses four laser diodes behind each of two infrared transmitting windows, with translation of the dewar or the collection optics serving to select which diode emits into the collecting optics and so through the entire optical train until laser light is focused onto a detector located in the same dewar. The optical system collects light from two laser diodes, sending two coincident, collimated beams to a either a retroreflector or multiple pass cell in the altitude test chamber, then collecting the return beams and focusing them onto the same detector element. Measurement time scales allow the use of a single detector, with discrimination between the two lasers achieved by alternating laser-on (frequency scanning) and laser-off periods. This design, allowing the simultaneous operation of two laser diodes, originated in a desire to collect data as efficiently as possible during engine tests. It can also be a key requirement for the line-ratio emission index measurement technique whose investigation was the focus of the previous test and several of the first days of the current test. In those cases, the two diodes were used to measure NO and CO_2 lines. The main focus of the present test series was the measurement of the sulfur oxide species SO_2 and SO_3. One diode was used to measure each species, with water lines present in each spectrum serving as reference lines for emission index calculations.

We begin a discussion of the details of the optical layout by tracing the paths of the main or diagnostic beams. Infrared light from the laser diodes is collected by reflective microscope objectives (15x) and focused onto 200 μm pinholes, which define input apertures. The pinholes are used only during alignment, so they are mounted on removable kinematically indexed bases. The microscope objectives are mounted on X-Y-Z translators to allow accurate focusing into the fixed apertures. Past the input aperture, curved mirrors create approximately collimated beams. The two

laser beams are then combined at the main beamsplitter and the co-aligned beams pass to a pair of flat mirrors and onto a large gimbal-mounted steering mirror which directs the beam off the table and into the engine test cell. An important development for this test was the replacement of the former main beamsplitter, a relatively thick (3 mm) sheet of ZnSe, with a very thin pellicle which eliminated one source of interference fringes which can be a major noise source in our spectra. The return beam is collected by the large steering mirror and a curved mirror of similar diameter, passed through several more flat mirrors and finally focused onto the main beam detector.

The remaining combined beam associated with the main beamsplitter goes into the reference optical path, where it may be sent through a gas calibration cell and/or passed through a grating monochromator, then focused onto the reference detector. Some calibration cells contain a sufficient pressure of the gases of interest that their strong absorption features fully absorb the laser light. This makes it easy to recognize that the laser is operating in the right wavelength region, and to check for the presence of other laser modes. These absorption lines are also used to set the frequency scale of the laser scan. In this case, we used cells containing NO and NO_2 as well as N_2O, to locate lines in the CO_2 region, and a cell of methane to determine frequency scales in the two sulfur oxide spectral regions. The monochromator is used to provide a coarse measurement of the laser frequency during setup of the instrument, and to determine whether the diode is emitting at different wavelengths (different modes). Since no monochromator is available in the main beam path, diode operating conditions must be chosen which allow single mode operation.

There is a parallel visible optical system for alignment and setup. A red HeNe "trace" laser beam passes through the dichroic beamsplitter downstream of each microscope objective, and is coaligned with each infrared beam. Coalignment is guaranteed by focusing the beam through the input aperture. The trace beam is an indispensable aid for alignment of the optical system. In addition, the trace beam is used for accurate calibration of the monochromator, via higher order diffraction. The fourth port of the dichroic beamsplitter can be used to observe the laser diode during alignment. An eyepiece mounted at the position conjugate to the pinhole forms an effective 150X microscope.

We found we had to make one addition to the optical system due to an effect which was presumably present in the previous PSL test but not noticed then due to the more forgiving nature of the retroreflector optical system. The effect was the motion of the test cell and the optics inside with respect to the laser table outside the cell which was firmly attached to the concrete floor. This motion first occurred as the test cell was brought to a simulated altitude, and seemed roughly proportional to the test cell static pressure. The maximum displacement was about 0.6 cm. Initially, we compensated for this by moving the entire laser table whenever there were major changes in the test cell pressure. Later, we installed a translation mount on the steering mirror on the laser table. This made recovery of a good transmitted signal relatively straightforward.

The temperature and current of each laser are controlled by a Laser Photonics controller. All inputs to this controller were made via a program running on the data acquisition and analysis computer. In a typical experiment, the laser temperature is held constant while the current through the laser is modulated with a computer generated sawtooth to sweep the output frequency across the infrared transition. The sawtooth was generated in 250 discrete steps for each laser by a digital to analog converter board. The total of 500 display points in the two laser spectra is swept at a rate of 300 kHz (display points per second). During approximately ten percent of the duty cycle the laser current is dropped below the lasing threshold to provide a precise measurement of zero light intensity.

The data acquisition techniques, involving a Scientific Solutions Lab Master analog to digital converter board and direct memory access transfer to the extended memory of the data acquisition computer, remain as described previously.[3] Although the TDL instrument could in principle produce real-time records of gas concentrations, this would require input of probe rake data (or assumptions about properties along the line of sight from other sources). Our data acquisition therefore consisted of the recording of a large number of spectral files covering segments of both the SO_2 and SO_3 regions (or the NO and CO_2 regions). These were recorded as averages over periods of 10 to 600 s.

F.2. DIAGNOSTIC IMPLEMENTATION IN ENGINE TEST CELL

The optical system used to propagate the laser beam through the engine exhaust in the altitude test cell was substantially modified from the one used in the previous test in PSL-4. The TDL instrument was again placed on a table directly in front of an optical access port into the test cell. However, this table rested on the concrete floor of the test cell building, where the earlier table had been on the mezzanine above it. Therefore, the TDL beams were directed into the test cell in the horizontal plane, rather than downward (at approximately a 45 degree angle) as in the 1996 test.

A change was necessitated by the larger size of the engine in the current test, and the ground level mounting seemed to offer fewer problems with vibration as well as a simpler optical layout. A 0.95 cm thick CaF_2 window with a 1° wedge (to suppress interference fringes) was mounted on the access port using a retaining plate with a 10 cm diameter clear area. The access port had a direct view of the engine exit plane location, so that the laser beam could pass through the exhaust, strike a corner cube retroreflector mounted on the test cell floor, and return, horizontally displaced by about 2 cm, to the test cell access port window and the steering mirror. The HeNe trace beam could be followed through the entire optical path, which allowed precise aiming of each steering mirror.

However, most of our observations in this test series were made not with the retroreflector but with a multipass cell which caused the laser beams to pass through the exhaust 14 times before being returned to the optical table. The multipass mirrors were 15 cm diameter, 91.4 cm focal length mirrors, with the mirror nearest the laser having a 1 cm hole in its center. They were contained inside heavy aluminum boxes equipped with nitrogen purge lines. The gaseous nitrogen purge was needed not only as a protection against recirculating exhaust but also to remove as much atmospheric water vapor and methane from the path as possible. The path between the access port and the back of the near box was contained inside a 10 cm diameter aluminum tube, also purged with gaseous nitrogen. Stainless steel tubes, 30 cm in length and 15 cm in diameter, were attached to the front of each protective box. This left a 122 cm gap between the two tubes. In the center of this gap was the exhaust flow, exiting from a nozzle with a diameter of about 65 cm. The separation between the outer two of four probe rake thermocouples which register the full core exhaust temperature was 30.48 cm, while the pair of thermocouples separated by 45.72 cm read temperatures more than half way to ambient values. The separation between the fronts of the protective boxes, where thermocouples were mounted, was 182 cm.

F.3. EXAMPLES OF OBSERVED SPECTRA

Figure F-2 presents an example of raw diode intensity spectra for the TDL diagnostic while the laser beam was passing through the exhaust. The vertical axis is simply intensity at the detector expressed in mV. The horizontal axis is in display points, or data acquisition points over the laser scan. The left hand side of the scan is the intensity of the SO_2 laser. After this laser is turned off at 250 display points and the intensity briefly drops to near the zero level, the SO_3 laser is turned on, and its intensity is recorded in the second half of the scan. The strongest absorption feature seen in the SO_2 laser scan, at display point 210, is a water absorption line at 1332.757 cm^{-1}.

In the SO_3 side of the laser scan, a diode mode break (abrupt transition in the laser frequency) occurs at 315 display points. The region between 250 and 315 display points, containing some very strong water lines, was not used in our analysis. Only the region between 315 and 490 display points was analyzed, and even there the absorption features seen in the figure are water lines. The smaller and more numerous SO_3 lines lie under and between the water lines. An analysis was carried out on the highest altitude spectra for the high sulfur loading, where SO_3 peaks should be most clearly distinguishable. By averaging absorbances in SO_3 peak and valley regions, we were able to determine that our detection limit for SO_3 was less than 2 ppm_v, and that the exhaust concentrations of SO_3, even under these most favorable conditions, were below that level.

F.4. DATA ANALYSIS PROCEDURES AND ERROR LIMIT ESTIMATES

F.4.1. Data Analysis Using the TDL Data Acquisition Program

Our technique in the data analysis reported here is to measure relative column densities of water and SO_2 and then use this ratio and the known emission index for water, derived from the fuel formula, to yield a direct measurement of SO_2 emission index without passing through the steps of quantifying absolute molecular mixing fractions and mass fluxes. To carry out the relative column density determination, the absorption features of water and SO_2 are quantified by least squares fits, using the TDL data acquisition program in data analysis mode. This is the routine which allows real-time fitting and concentration measurement, here applied to stored spectra. Lines are fit to a set of Voigt line profiles using a nonlinear least squares routine based on the Levenberg-Marquardt approach.[6]

A fit to the entire region seen on the left half of Figure F-2 is dominated by the strong water lines at the right hand side of the SO_2 scan. To quantify the water relative column density, we actually used a more restricted region, from 108 to 248 display points. The SO_2 determination was made using a fit to one of several even more restricted regions, detailed below. The baseline, varying from unit transmission due to diode laser power fluctuations and residual etalon fringes, was represented by a fourth order polynomial over each region in turn. The line parameters used in the least squares fits are taken from the HITRAN compilation[7] or from more recent measurements taken from the literature or communicated to us by the investigators prior to publication. The absorption line properties are evaluated at a single representative temperature and pressure derived from averages of probe rake values. The TDL analysis also uses an input path length (here taken as 500 cm) to derive an absolute density along this uniform absorption path. This path length, 14 times the distance through the hot region of the plume as estimated from probe rake data, will disappear when the column density ratios are formed, but it does in fact lead to absolute mixing fractions which agree well with sampling values.

Figure F-3 shows the entire spectral region which was analyzed. In this figure the solid line is the observed trace as converted to a transmission scale by the TDL data analysis program, through its fit of a polynomial baseline. The frequency scale is set using reference spectra of the methane reference cell, taken in between exhaust spectra. The dashed line is the actual least squares fit by the TDL data analysis program, evaluated at the same data acquisition points. This spectrum, for high sulfur loading, a 50 kft simulated altitude and a T_3 value of 629 °K, has lines which are fairly well separated from each other. As the altitude drops and the pressure rises, the lines become broader and overlap each other more, and it becomes more difficult to make an accurate estimate of the position of the unit transmission baseline. As described above a fit of the region from 1332.45 cm^{-1} to 1332.85 cm^{-1}, including the strong lines on the right hand side, is used to determine the water concentration.

Figure F-4 shows the spectral region containing the spectral features used to determine the SO_2 concentration. The circles show the positions of actual data acquisition points. The two strongest absorption lines in this spectrum, below 1332.1 cm^{-1} and above 1332.4 cm^{-1}, are due to methane in the test cell air in the regions between the exhaust and the purged boxes containing the optics. The smaller peak near 1332.3 cm^{-1} is due to water, which also has a few much smaller lines scattered through this region. Most of the remaining peaks, in particular those near 1332.2 cm^{-1} and between 1332.35 and 1332.4 cm^{-1}, are due to SO_2. This is seen in Figure F-5, which shows model spectra for the individual species SO_2 and H_2O as well as their sum and the observed spectrum of Figure F-4. When the SO_2 features are strong enough, it is possible to fit spectra of all three species to the entire spectral region in Figure F-5 to derive three species concentrations. When SO_2 features are weaker, it is necessary to concentrate on smaller spectral ranges in order to maximize the accuracy of the derived SO_2 concentration. Therefore, for most observations of the highest sulfur loading, the spectral region which was fit to determine SO_2 concentrations was from 1331.9 to 1332.45 cm^{-1}, (29 to 108 display points), while for the lower sulfur spectra, the most common range used was from about 1332.15 to 1332.35 cm^{-1} (51 to 88 display points). This latter range is seen to cover a spectral region including the single water line just below 1332.3 cm^{-1}, and the SO_2 feature (composed of several lines) around 1332.2 cm^{-1}.

F.4.2. Derivation of Emission Index Values

As noted above, the absolute concentration values resulting from TDL data analysis are not entirely measured quantities, but instead incorporate several approximations. These include the assumptions of an arbitrary absorption path length and of uniform pressures and temperatures along the line of sight. These pressures and temperatures are derived from averages of probe rake values for those sampling points fully in the exhaust core flow. For analysis of infrared data, the array of Mach numbers from probe measurements and an assumed specific heat ratio for the exhaust flow are used to convert probe rake observed total temperatures to static temperatures, while a similar conversion is applied to measured total pressures to yield an array of static pressures. Finally, ratios of total temperatures in the exhaust and the test cell free stream are used to estimate mixing ratio profiles, which are then used as weights in averages of the static pressure and temperature arrays derived from probe rake data to give single pressures and temperatures for input to the TDL program. After carrying out a few calculations using a multi-cylinder model whose properties are determined by individual probe values, we estimate the error levels associated with the assumption of uniform average properties as being on the order of a few per cent, when mixing ratio weighted averages are used.

Emission index is defined as the weight in grams of an exhaust component per kilogram of fuel burned. Thus, for the major exhaust species CO_2 and water, which are produced solely and quantitatively from the hydrogen and carbon in the fuel (combining with oxygen from the air), emission indices are determined once the chemical composition of the fuel is known. For the primary fuel, involved in sulfur loading variations, four analyses were made, with an average value for water emission index of 1240 (and a standard deviation of less than 5). For the alternate fuel (JP-8 +100) we used the first value we received of 1269, even though a second analysis yielded a value of 1253. Therefore, for the primary fuel case, the formula used is

$$1240\ (64/18)\ ([SO_2]/[H_2O])$$

where 64/18 converts from mass of H_2O to mass of SO_2. Since we know the weight fraction of sulfur in each fuel, we can calculate maximum theoretical SO_2 emission indices for the case when all fuel sulfur is present in the exhaust as SO_2. Since the molecular weight of SO_2 is twice that of atomic sulfur, these maximum theoretical SO_2 emission indices are simply twice the weight fraction of sulfur in the fuel (again, expressed as grams per kilogram). For the three fuels for which we could measure SO_2, these maximum emission indices were 2.226 for high sulfur, 0.672 for JP-8, and 0.304 for the mixture of high sulfur and low sulfur fuels.

F.4.3. Measured SO_2 Emission Index Values

We will present SO_2 emission index values in a series of six tables. More than one table is required because we want to examine not only the absolute values of SO_2 emission index for each observation condition, but also their ratios to theoretical maximum values (fractional conversion of fuel sulfur to SO_2) and their averages over one or two of the three observation parameters (sulfur loading, power setting, and altitude). The error limits in the tables have very different meanings, as well, again because there are several issues we want to examine.

One difference in the error limits in the various tables stems from the conventional division of error limit components into two types, random and systematic errors. Estimates of random errors are typically derived from the statistics of multiple measurements, while estimates of systematic errors involve bounding the effects of as many potential sources of bias or uncertainty as possible. Especially when small numbers of measurements are taken, estimates of random errors may vary widely from one measurement condition to another, while estimates of fractional systematic errors could either be made specific to each measurement condition or (our choice in the estimates described in the following section) could be assumed to apply equally to all measurements. The error limits in Tables F-2, F-4 and F-6 are total uncertainty limits which incorporate estimates of both types of error. Our work to date in making estimates of systematic errors is detailed in the following section. The result documented there was a decision to adopt a constant fractional error limit of 0.16 as an estimate of systematic errors. This value is added in quadrature to relative standard deviations in multiple measurements (derived from the absolute standard deviations in Table F-1 by dividing by the maximum theoretical emission index values) to form the error limits quoted in Table F-2.

The other difference in the error limits is related to the question of what one wishes to define as a single measurement of a quantity, such as SO_2 conversion fraction. The error limits in Table F-1 are simply the standard deviations in arrays of emission index measurements determined from individual spectra. In the cases where only one spectrum was obtained, no error limit is listed. Such error limits

provide useful information about the reproducibility of some measurements, and the variability of others, at the spectrum-to-spectrum level. Another point of view, however, is that the measurement of SO_2 conversion fraction is not complete until several spectra have been obtained and an average value has been formed. In that view, the averages in Table F-1 become the primary measured data, and it is then of interest to see what the random variations are in those values. In Tables F-3 and F-5, then, the error limits are standard deviations representing the distributions of emission index values in Table F-1.

We can now return to Table F-1, which presents SO_2 emission index values for all sulfur loadings, power settings, and altitudes for which we could make determinations with reasonable accuracy (we will comment below on the remaining cases, those involving the lowest sulfur loading and the lowest simulated altitude). For convenience, we also divide by the theoretical maximum emission index values and present, in Table F-2, the fraction of fuel sulfur in the exhaust in the form of SO_2. It can be seen that unity (all fuel sulfur existing as SO_2 in the exhaust) lies within or close to the range of variation for all cases.

The data in Tables F-1 and F-2 serve as the inputs to averages used to generate the remaining tables. In these tables, averages over one or more of the three variables are carried out in order to make clearer any possible trends with changes in the remaining variables. For instance, Tables F-3 and F-4 can be used to consider the possibility of a systematic trend with simulated altitude. In fact, they clearly demonstrate that within our uncertainty limits, we do not observe any trend with altitude.

In Tables F-5 and F-6, all data points with the same simulated altitude have been averaged, allowing consideration of trends with power setting and sulfur loading. It can be seen that in most cases, the emission indices at the lowest and highest power settings are smaller than those in the middle. It is entirely possible that this is an experimental artifact, due to two trends with engine power setting which make the measurements at the lowest and highest values the most difficult to perform. At idle, the species concentrations and line absorbances are smallest and least easily measured against baseline fluctuations. At maximum power, greater fluctuations in laser beam position on the detection optics reduced the intensity of transmitted laser light, again lowering the accuracy of the measurement.

The final trend to be considered, that with sulfur loading, is most easily considered using the final column in Table F-6. Although the SO_2 conversion fraction seems to increase substantially with decreasing fuel sulfur concentration, it can also be seen that it can be taken to be constant within the estimated error limits. For the three fuel types, the absolute values of SO_2 emission indices averaged over all engine conditions and altitudes are 1.64 ! 0.18, 0.55 ! 0.11 and 0.27 ! 0.05. The error limits here reflect only the standard deviations in individual data points. Dividing by theoretical upper limits to the emission indices, they yield fractional values of 0.08, 0.16 and 0.16 respectively. The overall average of all the individual data points of Table 2 yields the sulfur conversion fraction in the bottom right corner of Table F-6 of 0.82 ! 0.22. This value and its error limits (now reflecting systematic as well as random errors) encompass most of the individual values in Table F-2.

The data sets in which we have the most confidence are those at the highest altitudes. It can be seen that the sulfur conversion fractions are lowest for the higher altitude data sets. However, the fact that average values of SO_2 fraction are higher at the lowest altitudes is most likely not significant and simply an artifact of the greater difficulty of the measurements. Given the uncertainty estimates, in no case can we say that some fuel sulfur is definitely not in the form of SO_2 in the exhaust. Instead, the most we can say about the possibility of other sulfur species in the exhaust is that they could exist, but

only at levels of 30 per cent of total fuel sulfur at the very most. In the specific case of SO_3, this upper limit is consistent with our upper limit of less than 2 ppm_v: at high altitudes, this concentration level of SO_2 converts to an emission index increment of about 0.25. This increment is 11 per cent of the theoretical maximum for the high sulfur loading fuel. In other words, both our SO_2 and SO_3 measurements are consistent with the statements that at least the substantial majority, and quite possibly the overwhelming majority, of fuel sulfur exists in the form of SO_2.

Finally we turn to those components of the data set which are not reported in the tables. The lowest simulated altitude, leading to exhaust static pressure values in the 500 to 1000 Torr range, results in absorption lines so overlapped that an accurate determination of the baseline position has so far not been possible. The existence of SO_2 absorption features is discernible, and plausible baseline values can be seen to be consistent with SO_2 levels at the theoretical maximum. However, though we can show that these low altitude data subsets are consistent with values derived at higher altitudes, we cannot use them to derive independent measurements.

The low sulfur fuel was expected to be well below our SO_2 detection limit. However, we did perform an analysis of a subset of this data which led to an estimate of the minimum detectable SO_2 loading of less than 1 ppm_v. This minimum detectable concentration should be smaller than the random fluctuations in larger concentrations to be discussed in the following section, and indeed it will be seen that the random error component of the total error estimate is in the range of 1 to 3 ppm_v for high sulfur loading data points, and around 1 ppm_v for the mixed sulfur data points.

F.4.4. Estimates of the Errors in Measured SO_2 Emission Index Values

We almost always took at least two spectra for each engine power setting. The standard deviations in emission indices, when available, are taken to represent the random error component of our uncertainty levels. We observed, as we have in past tests, that reproducibility between parameters obtained from successive spectra is often very good. However, the spectral data analysis for SO_2 is a more demanding problem that was the case of NO, for example, and we do see more spectrum-to-spectrum variation in derived concentrations than in past tests. In several cases observations were made of the same nominal engine condition on two different days. We observed that while the engine parameters were very accurately reset, as seen in very similar probe rake data, the variation between our observed concentration values for different days was larger than the variations in a single day. Because the range of standard deviations was large and because systematic errors turned out to be the dominant contributors to overall error bounds in most cases, we did not include a random error component in the estimates when only one spectrum was used. The average standard deviations in Table F-1 are, for high sulfur data points, 0.16 or a fractional standard deviation of 0.07, 0.05 absolute or 0.08 relative for JP-8, and 0.07 absolute or 0.23 relative for mixed sulfur fuel. These random error limits could also be assigned to the two values in Table F-1 which represent single spectra. In Table F-5, in which standard deviations are now formed from the distributions in average values of Table F-1, a similar procedure could be followed for the highest power setting values, thus also raising the total error limits in this column of Table F-6.

The estimation of possible systematic errors was carried out by identifying those input parameters to the data analysis program which have significant uncertainties, perturbing them by that uncertainty limit, and carrying out a determination of SO_2 emission index. For some parameters, the issues

involved with choosing an uncertainty limit and determining the sensitivity of the emission index to such a variation are completely straightforward, while for others they are more complex. An example of the latter situation is the temperature along the absorption path. The data analysis program assumes a single temperature along the entire path. In fact, the temperature varies substantially through the exhaust. Because of this, a number of systematic errors can result from the assumption of a single temperature. As mentioned above, we carried out a few calculations in which we determined the SO_2 emission index using from a multi-cylinder model which incorporated all the measurements from the probe rake. We then found that this emission index was close to that derived from a single-cylinder, or uniform path, model whose temperature was derived from the array of probe rake temperatures by weighted averaging using a mixing ratio derived from ratios of total temperatures. The disagreement between detailed and single-temperature models is not the only potential systematic error we wish to estimate. For example, the finite spatial resolution of the probe rake could lead to uncertainties in temperature over significant segments of the total path.

As an easily available measure of the uncertainties associated with the temperature input to the analysis program, we examined the differences in temperatures derived from two different averaging procedures. One was the mixing ratio weighted technique mentioned above, while the other was a simple linear average of the four innermost temperatures. On the average, these two values differed by about 40 °K, a value we adopted as the uncertainty in the temperature input to the analysis program. The sensitivity of SO_2 and H_2O concentrations and the resulting emission index turns out to be quite variable, since this parameter can influence the spectral fit in a variety of ways. Averaging sensitivity calculations carried out using a half dozen spectra covering a range of altitudes, power settings and sulfur concentrations had the result that a 40 °K perturbation in the path temperature had a 9 per cent effect on the SO_2 emission index.

Two points should be made here. The first is that uncertainties in individual probe rake measurements undoubtedly are much smaller than the above !40 °K, which is intended to represent an entire complex of uncertainties associated with the analysis of absorption over a nonuniform path. In an earlier discussion of rake data uncertainty[5], a typical fractional uncertainty in a measured probe [total] temperature was said to be 0.0075, resulting in a an absolute uncertainty in this temperature regime of the order of !5 °K. The discussion goes on to say that the maximum fractional uncertainty in any of the derived thermodynamic parameters due to propagation of measurement uncertainties through the data reduction algorithms is about 0.02, and even when calibration uncertainties are included the total fractional uncertainty in any rake aerodynamic property is conservatively estimated to be no more than 0.05.

The second point to be made is that even a 9 per cent sensitivity to a 40 °K change in temperature could be substantially reduced if SO_2 and H_2O spectral features could be used whose strength variation with temperature was better matched than those used here. In this first measurement of SO_2 in an aircraft engine exhaust by infrared absorption, we were constrained by the laser diodes available to us at the time to the spectral regions reported here. In preparation for future observations, we plan to investigate other spectral regions. There is the possibility that the estimated sensitivity to uncertainties in the characterization of the temperature along the absorption could be reduced to a negligible contribution to the overall error limit estimate, through the use of different spectral features.

If the same type of estimate is made for an uncertainty in the pressure input to the analysis program, using the differences between the two types of averaging, we find an average fractional uncertainty

of about 0.05. If we examine the variation of static pressure values across the flow, we find average fluctuations closer to a fraction of 0.10, even though the true static pressure should be close to constant. However, even this larger uncertainty level leads to an uncertainty in SO_2 emission index of only 5 per cent, which when added in quadrature with several larger contributions has only a small effect on the total uncertainty estimate. An even more negligible source of error turned out to be uncertainty in the diode tuning rate. Calibration spectra were taken every few minutes, and the tuning rate derived from the closest one is normally used to analyze each spectrum. Taking the tuning rate from the next-closest reference spectrum resulted in changes in SO_2 emission index which were at most 1 per cent, and usually much less.

Our fitting procedure in analyzing this data set involved keeping the model for the zero absorption baseline fixed at a fourth order polynomial, then varying the beginning and ending points of the fitted region and the exact position (in display points) of a reference point for the absolute frequency scale (in the SO_2 region, the water peak at 1332.29 cm^{-1} is used) until a good visual fit is obtained to the SO_2 peak at 1332.2 cm^{-1}. The height of this absorption peak is typically only about twice the size of the minimum absorption on either side of it. In other words, in this spectral region we cannot directly determine the position of the baseline. In analyses of earlier data sets in which the baseline position was better determined (and so the above procedure of varying input parameters until a good visual fit was obtained was not used), we estimated the error due to this uncertainty by varying the polynomial order. In the data set of Reference 5, this was done for all NO spectra, with typical variations being in the range of a few per cent. For the current SO_2 data set, we only performed this set of analyses on one representative spectrum, finding about a 5 per cent effect for reasonable variations of polynomial order. Again, this level of sensitivity makes it a relatively small contributor to the overall uncertainty estimate.

Finally, we consider uncertainties in spectroscopic parameters, whose effects on the emission index turn out to be straightforward, giving very similar sensitivities in all spectra studied. Our SO_2 line parameters were taken not from the HITRAN listing[7] but from a more recent reanalysis[8]. This work found that HITRAN line strength values were often 10 to 25 per cent stronger than their values, due to spectroscopic perturbations ignored in HITRAN and to differences in the band strengths used. We could take a substantial fraction of these differences as characterizing the remaining uncertainty in SO_2 line strengths. However, differences in our spectral region turn out to be only about 3 per cent, so we adopt this value, leading directly to a 3 per cent change in SO_2 emission index and thus only a modest contribution to the total systematic error limit. We assume that uncertainties in water line strengths are even smaller.

The water line width values we used are based on recent measurements communicated to us privately by R. A. Toth of the Jet Propulsion Laboratory, taking into account calculations of temperature dependence performed for us by R. R. Gamache of the Center for Atmospheric Research of the University of Massachusetts, Lowell. Perhaps the most useful estimate of uncertainty in these parameters is the observation that even when experimental errors are assessed by the groups that made them as being only a few per cent, comparisons between different measurements suggest that true error limits (including systematic errors which are harder to assess) are closer to 10 per cent.[9] Using this value leads consistently to variations of about 6 per cent in SO_2 emission index. We should point out that the 10 per cent real error limit referred to room temperature, measured values, while we must use values extrapolated to the 500 K range, if anything adding to their uncertainty.

The SO_2 room temperature line width values we used were all 0.10 cm^{-1}, reduced from the HITRAN value of 0.12 to achieve better fits with our observed spectra. Independently, Sumpf, Schoene and Kronfeldt[10] measured a number of nearby lines (though none of the lines we used) and reported an average line width for our band of 0.10 ± 0.011 cm^{-1}. Again, because we must take into account the further uncertainty of the line width value at elevated temperatures, we use this entire error limit in our sensitivity calculations, arriving at an average 9 per cent change in SO_2 emission index for SO_2 line widths perturbed by 11 per cent from the nominal value.

In Table F-7, we summarize the above discussion of possible systematic errors, and show that the overall estimate for fractional systematic errors is 0.19. This is comparable, and if anything somewhat smaller, than estimates for previous data sets. Furthermore, it is clear that with additional work it can be reduced. Ratioing SO_2 and water lines with more comparable temperature dependences has already been mentioned as a way of lowering the sensitivity to probe rake temperatures. Additional measurements of spectroscopic parameters could also help. In addition, the random error component measured by standard deviations in multiple measurements could be reduced through better understanding of the fluctuations in the baseline, both those due to turbulence which are very strong for short averaging times, and those due to interference fringes which remain even after averaging for many minutes. This leads us to the conclusion that measurements with total error limits under 10 per cent are well within the realm of possibility. Even the total error limits shown in the tables, in the range of 17 to 25 per cent, allow useful conclusions to be drawn from the current data set.

F.5. SUMMARY AND CONCLUSIONS

In this section we wish to address, quantitatively, the key issues involved in understanding our data set of SO_2 emission indices or SO_2 conversion fractions. One set of issues involves the fact that SO_2 conversion fraction essentially has both an upper and a lower bound. The upper bound is definite: the sulfur in the exhaust cannot exceed the sulfur in the fuel. The lower bound comes from our upper limit on SO_3 concentration and the assumption that other sulfur species are similarly small components of the total sulfur in the exhaust. Our goal in this area is to demonstrate that the absolute values in our data set and our estimates of error limits are consistent, so that none of these bounds are exceeded by more than our estimated uncertainties. A second set of issues involves the assumption that systematic errors can be reduced as the measurement technique is further developed, so that it is of interest to examine the precision, as opposed to the accuracy, of the SO_2 conversion fractions determined by our data set. We will discuss each area in turn.

Our consistency with the upper limit constraint on SO_2 conversion fraction has already been discussed. Table F-2 shows a few values which exceed 1, but none by more than our error estimates. The consistency with a lower limit constraint is also easily demonstrated. We recall that our examination of the SO_3 detection limit in the high sulfur, highest altitude spectra yielded an upper limit of 2 ppm_v which was equivalent to an SO_2 emission index of about 0.25, or an SO_2 conversion fraction of 0.11. It happens that these high altitude, high sulfur spectra also give the lowest values of SO_2 conversion fraction. This can be seen in Table F-4, which also lists the appropriate total error

limits. If we take the 55 kft data point, the sum of SO_2 conversion fraction plus total uncertainty limit plus upper limit for SO_3 is

$$0.72 + 0.19 + 0.11 = 1.02$$

so that our SO_2 and SO_3 measurements and error limits are indeed consistent.

We can estimate the ultimate precision inherent in a data set of the size discussed here by computing the standard deviation of the mean of SO_2 conversion fraction. This is not the standard deviation of the distribution, which should remain roughly constant as more samples are considered, but is obtained from it by dividing by the square root of the number of samples, so that as the number of samples increases, the precision of the mean value increases (even though, due to systematic errors, the measured value may not be the true value). If we consider each spectrum to be an independent, equivalent measurement of SO_2 conversion fraction, then we have 130 samples, and while the standard deviation in SO_2 conversion fraction for this entire array is 0.23, the standard deviation in the mean is only 0.020. If we choose to consider the three fuels as three different data sets, there are still 30 to more than 50 samples in each, and standard deviations in the mean are 0.14 for high sulfur, 0.026 for JP-8 and 0.036 for the mixed sulfur fuel.

These levels of precision are of considerable interest because, as discussed above, we believe it is possible with additional work to reduce the sytematic errors present in our first SO_2 data set. The importance of better understanding of these systematic errors can be understood by considering the average values for sulfur conversion fraction for the three fuels, shown in the last column in Table F-6. These values, 0.74, 0.82 and 0.89 going from highest to lowest sulfur, clearly differ by much more than the precisions in mean values quoted above. There are, of course, two extreme possibilities: there is a real change in sulfur conversion fraction with fuel sulfur loading, or there are systematic effects on our measurements resulting in three different values when in fact there is only one. There could also be both a real dependence on sulfur loading and systematic errors as well. Our exercise in estimating possible systematic errors turns out not to allow a choice between these possibilities, since it only shows that systematic errors *could* be as large as the differences between sulfur loading data sets. Another possible reason for rejecting a systematic error would be that the trend does not logically follow from a change in the spectra with sulfur loading. However, it is not impossible that as the SO_2 peaks become comparable to incompletely characterized background peaks of water and methane, more of the intensity in some background peaks is taken by the least squares fit to be due to SO_2, thus giving rise, on the average, to the apparent trend quoted above.

In summary, tunable diode laser measurements in the SO_2 and SO_3 spectral regions were carried out for the first time in an aircraft engine exhaust and give the same result: fuel sulfur is converted largely to SO_2 at the exhaust exit plane, with SO_2 forming at least 70 per cent of the total sulfur species under all conditions, with typical fractions in the 80 to 90 per cent range.

REFERENCES

1. J. Wormhoudt A. C. Stanton and J. Silver, "Techniques for Characterization of Gas Phase Species in Plasma Etching and Deposition Processes," in *Spectroscopic Characterization Techniques for Semiconductor Technology*, F. H. Pollak, Editor, Proc. SPIE 452, 88 (1983).

2. C. E. Kolb, J. C. Wormhoudt and M. S. Zahniser, "Recent Advances in Spectroscopic Instrumentation for Measuring Stable Gases in the Natural Environment", in *Biogenic Trace Gases: Measuring Emissions from Soil and Water*, P. A. Matson and R. C. Harriss, Editors, pp. 259-290, Blackwell Science Ltd, Oxford, UK, 1995.

3. J. Wormhoudt, M.S. Zahniser, D.D. Nelson, J.B. McManus, R.C. Miake-Lye, and C.E. Kolb, "Infrared Tunable Diode Laser Diagnostics for Aircraft Exhaust Emissions Characterization", in *Laser Applications in Combustion and Combustion Diagnostics II*, Randy J. Locke, Editor, Proc. SPIE 2122, 49 (1994).

4. J. Wormhoudt, M.S. Zahniser, D.D. Nelson, J.B. McManus, R.C. Miake-Lye, and C.E. Kolb, "Infrared Tunable Diode Laser Measurements of Nitrogen Oxide Species in An Aircraft Engine Exhaust," in *Optical Techniques in Fluid, Thermal and Combustion Flows*, Proc. SPIE 2546, 552 (1995).

5. R. P. Howard, R. S. Hiers, Jr., P. D. Whitefield, D. E. Hagen, J. C. Wormhoudt, R. C. Miake-Lye and R. Strange, *Experimental Characterization of Gas Turbine Emissions at Simulated Flight Altitude Conditions,* Air Force Arnold Engineering Development Center Report AEDC-TR-96-3, September 1996.

6. W.H. Press, B.P. Flannery, S.A. Teukolsky, and W.T. Vetterling, "Numerical Recipes," Cambridge Univ. Press, Cambridge, 523-528, 1986.

7. L. S. Rothman, R. R. Gamache, R. H. Tipping, C. P. Rinsland, M. A. H. Smith, D. C. Benner, V. Malathy Devi, J.-M. Flaud, C. Camy-Peyret, A. Perrin, A. Goldman, S. T. Massie, L. R. Brown and R. A. Toth, "The HITRAN Molecular Database: Editions of 1991 and 1992". J. Quant. Spectrosc. Radiat. Transf. 48, 469, 1992.

8. P. M. Chu, S. J. Wetzel, W. J. Lafferty, A. Perrin, J.-M. Flaud, P. Arcas and G. Guelachvili, "Line Intensities for the μ-Bands of SO_2", J. Mol. Spec. 189, 55 (1998).

9. R. R. Gamache, J.-M. Hartmann and L. Rosenmann, "Collisonal Broadening of Water Vapor Lines- I. A Survey of Experimental Results", J. Quant. Spectrosc. Radiat. Transf. 52, 481, 1994.

10. B. Sumpf, M. Schoene and H.-D. Kronfeldt, "Self- and Air-Broadening in the n_3-Band of SO_2", J. Mol. Spec. 179, 137 (1996).

Table F-1. SO_2 Emission Index Values for Individual Engine Power Settings, Fuel Sulfur Loadings and Simulated Altitudes, with Standard Deviations in Multiple Measurements

	Power Setting, T_3, K	Altitude, m 16,764	15,240	13,716	12,192	10,668	9144
High S	500-538				1.41±0.14	1.31±0.06	1.60±0.11
	572						1.85
	616-630		1.81±0.12		1.87±0.25		1.58±0.05
	672-686	1.76±0.22	1.62±0.20		1.58±0.04	2.02±0.27	1.63±0.13
	714-720	1.44±0.09	1.54±0.17		1.51±0.21	1.76±0.32	1.71±0.13
	783						1.49±0.12
JP-8	505-506					0.48±0.09	0.34±0.16
	583-619			0.54±0.04			0.65±0.02
	673-691	0.61±0.04		0.51±0.01		0.64±0.02	0.73±0.04
	716-725	0.52±0.04				0.50±0.05	0.66±0.12
	770						0.45±0.01
Mixed S	502-543				0.27±0.15	0.34±0.09	0.21±0.07
	559						0.27±0.04
	615-628		0.22±0.04		0.29±0.09		0.33±0.05
	671-689	0.24±0.09	0.26±0.07		0.31±0.03	0.36±0.08	0.33
	716-726	0.26±0.02	0.23±0.07		0.20±0.05	0.30±0.07	0.26±0.07
	765						0.20±0.10

Table F-2. Ratios of SO_2 Emission Index Values to Theoretical Limits for Individual Engine Power Settings, Fuel Sulfur Loadings and Simulated Altitudes (Error Limits Formed from Standard Deviations and an Estimate of Fractional Systematic Error of 0.16)

	Power Setting, T_3, K	Altitude, m 16,764	15,240	13,716	12,192	10,668	9144
High S	500-538				0.63±0.17	0.59±0.16	0.72±0.17
	572						0.83±0.16
	616-630		0.81±0.17		0.84±0.20		0.71±0.16
	672-686	0.79±0.19	0.73±0.18		0.71±0.16	0.91±0.20	0.73±0.17
	714-720	0.65±0.17	0.69±0.18		0.68±0.19	0.79±0.22	0.77±0.17
	783						0.67±0.16
JP-8	505-506					0.72±0.21	0.51±0.16
	583-619			0.80±0.17			0.97±0.16
	673-691	0.91±0.17		0.75±0.16		0.95±0.16	1.08±0.17
	716-725	0.77±0.17				0.74±0.18	0.98±0.24
	770						0.68±0.16
Mixed S	502-543				0.88±0.51	1.10±0.34	0.70±0.27
	559						0.88±0.20
	615-628		0.71±0.21		0.97±0.33		1.09±0.24
	671-689	0.79±0.34	0.86±0.28		1.03±0.19	1.17±0.31	1.10±0.16
	716-726	0.84±0.17	0.77±0.28		0.63±0.22	0.98±0.28	0.85±0.29
	765						0.66±0.38

Table F-3. SO_2 Emission Index Values Averaged Over Engine Power Setting, for a Range of Fuel Sulfur Loadings and Simulated Altitudes, with Standard Deviations in Averaged Values from Table F-1.

	Theoretical Limit	Altitude, m 16,764	15,240	13,716	12,192	10,668	9144
High S	2.226	1.60±0.23	1.66±0.14		1.59±0.20	1.71±0.34	1.64±0.12
JP-8	0.672	0.57±0.06		0.53±0.02		0.54±0.09	0.57±0.16
Mixed S	0.304	0.25±0.01	0.24±0.02		0.27±0.05	0.33±0.03	0.27±0.06

Table F-4. Values of SO_2 Fraction of Total Sulfur in Exhaust Averaged Over Engine Power Setting, for a Range of Fuel Sulfur Loadings and Simulated Altitudes, with Error Limits from Table F-3 Standard Deviations and a 0.16 Estimate of Fractional Systematic Errors

	Altitude, m					
Fuel	16,764	15,240	13,716	12,192	10,668	9144
High S	0.72±0.19	0.74±0.17		0.72±0.18	0.76±0.23	0.74±0.17
JP-8	0.82±0.19		0.74±0.16		0.78±0.21	0.86±0.32
Mixed S	0.82±0.17	0.78±0.17		0.88±0.23	1.10±0.19	0.88±0.24
Overall Average	0.79±0.18	0.76±0.17	0.74±0.16	0.80±0.23	0.88±0.25	0.82±0.23

Table F-5. Values of SO_2 Emission Index Averaged Over Simulated Altitudes, for a Range of Engine Power Settings and Fuel Sulfur Loadings, with Standard Deviations in Averaged Values from Table F-1.

		Engine Power Setting Range, T_3 in °K					
	Theoretical Limit	500-545	560-620	615-630	670-690	710-730	765-785
Fuel							
High S	2.226	1.44±0.15	1.85	1.75±0.15	1.72±0.18	1.59±0.14	1.49
JP-8	0.672	0.41±0.10	0.60±0.08		0.62±0.09	0.63±0.11	0.45
Mixed S	0.304	0.27±0.07	0.27	0.28±0.06	0.30±0.05	0.33±0.05	0.20

Table F-6. Values of SO_2 Fraction of Total Sulfur in Exhaust Averaged Over Simulated Altitudes, for a Range of Engine Power Settings and Fuel Sulfur Loadings, with Error Limits from Table F-3 Standard Deviations and a 0.16 Estimate of Fractional Systematic Errors.

	Engine Power Setting Range, T_3 in °K						
Fuel	442-517	547-654	648-675	749-784	825-850	917-950	Overall Average
High S	0.65±0.17	0.83±0.16	0.79±0.16	0.77±0.18	0.72±0.17	0.67±0.16	0.74±0.18
JP-8	0.62±0.22	0.89±0.20		0.92±0.21	0.83±0.21	0.68±0.16	0.82±0.23
Mixed S	0.89±0.26	0.88±0.16	0.92±0.25	0.99±0.23	0.81±0.20	0.66±0.16	0.89±0.23
Overall Average	0.73±0.18	0.87±0.18	0.86±0.22	0.89±0.22	0.72±0.17	0.67±0.16	0.82±0.22

Table F-7. Bases for Systematic Uncertainty Estimates

Estimated Error Limit in Data Analysis Input Parameter	Fractional Uncertainty in SO_2 Emission Index
Exhaust temperature ±40 K from average change in temperature from simple average to mixing fraction weighted average	0.09
Exhaust pressure ±10 per cent from standard deviations in values that should be the same across exit plane (compared to ±5 per cent from two averages as above)	0.05
Using next-nearest instead of nearest set of tuning coefficients	0.01
Error in baseline, from changing polynomial order	0.05
Water line widths ±10 per cent from review article which notes that despite average error bars from individual studies of 5 per cent, comparing studies yields a real uncertainty of 10 per cent or more	0.06
Sulfur dioxide line widths ±11 per cent from literature value of average linewidth for observed band of 0.1 ± 0.011 wavenumbers (again, average uncertainty in individual measured width values in this source is ±0.007 wavenumbers)	0.09
Sulfur dioxide band strength ±3.2 per cent, by comparing adjusted values from NIST/Orsay with HITRAN values	0.032
The above, added in quadrature, result in an estimate of fractional systematic error of	0.16

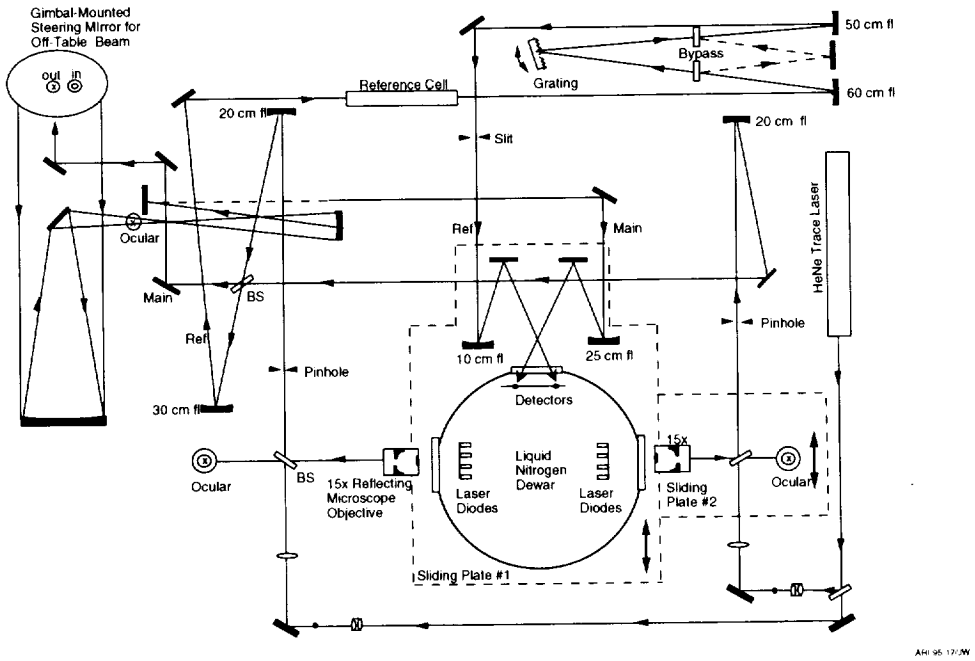

Figure F-1. Optical Layout of Tunable Infrared Diode Laser System.

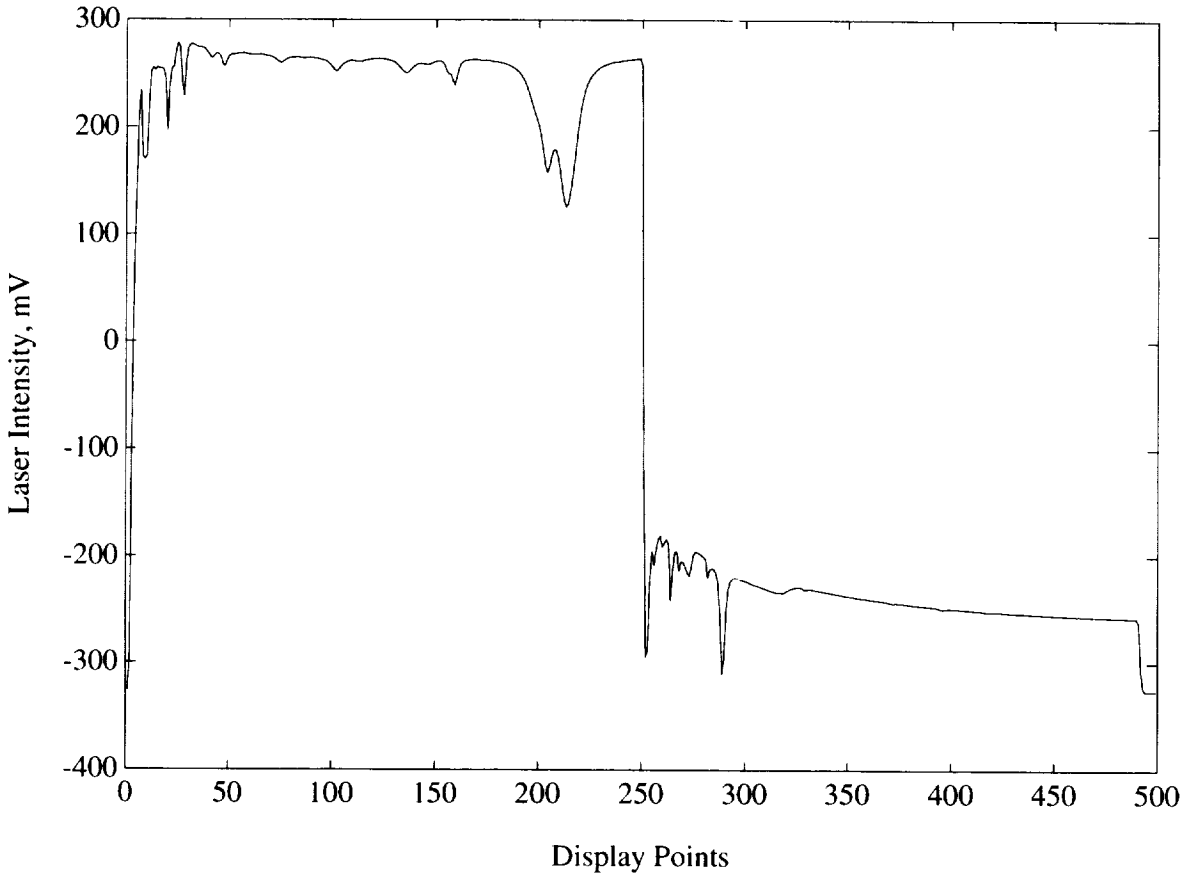

Figure F-2. Example Intensity Scans for SO_2 and SO_3 Lasers for Beam Passing Through Exhaust.

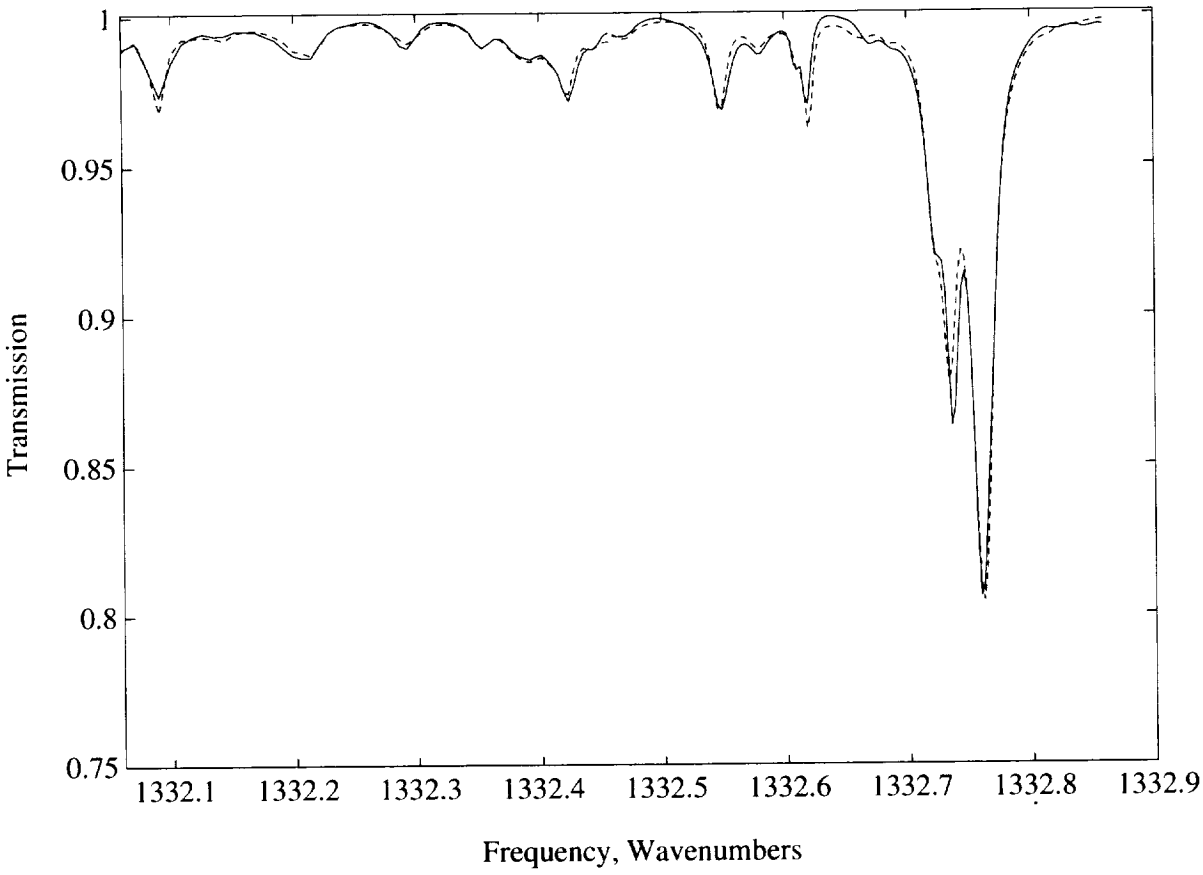

Figure F-3. Observed Transmission Spectrum (Solid Line) and Single Temperature and Pressure Model Fit (Dotted Line).

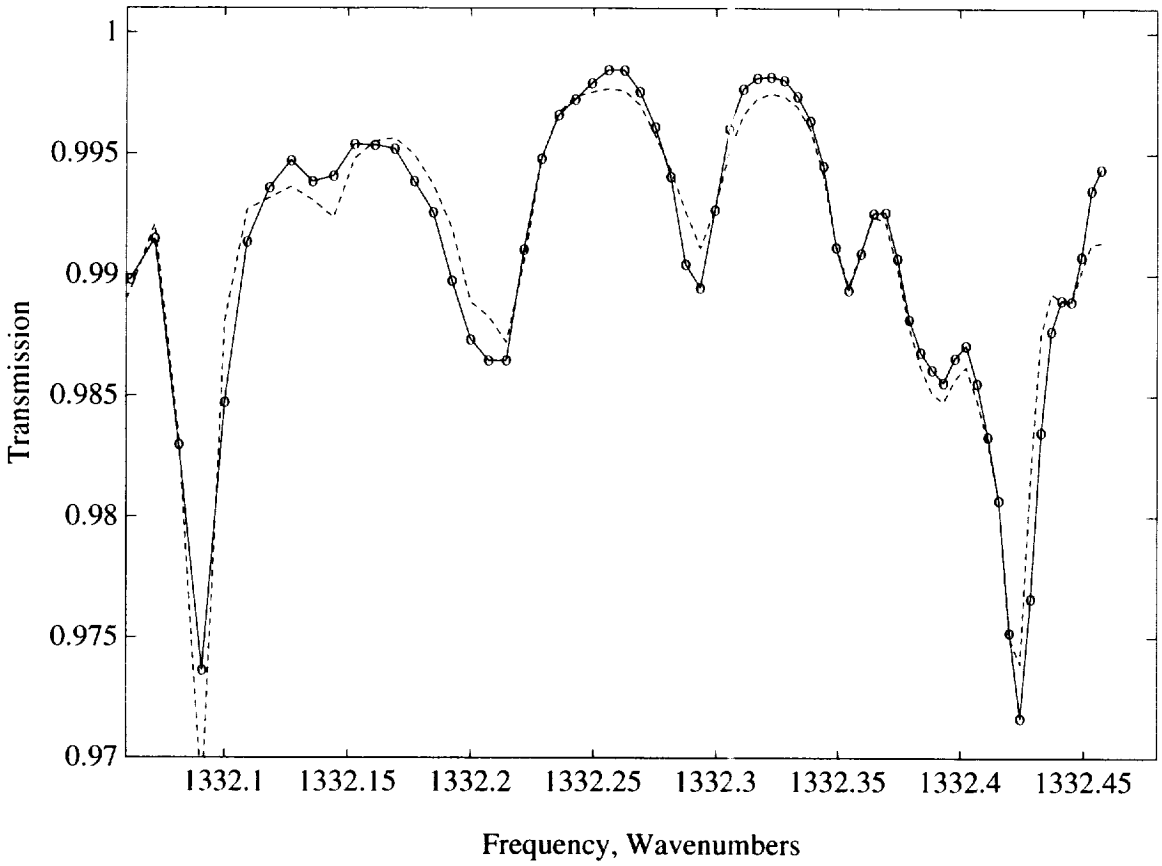

Figure F-4. SO_2 Region Observed Transmission Spectrum (Solid Line and Circles) and Uniform Path (Single Temperature and Pressure) Model Fit By Data Analysis Program (Dotted Line). The fit in this spectral region is used to determine the relative SO_2 column density.

REPORT DOCUMENTATION PAGE

Form Approved
OMB No. 0704-0188

1. AGENCY USE ONLY (*Leave blank*)	2. REPORT DATE	3. REPORT TYPE AND DATES COVERED
	October 1998	Technical Memorandum

4. TITLE AND SUBTITLE

Engine Gaseous, Aerosol Precursor and Particulated Emissions at Simulated Flight Altitude Conditions

5. FUNDING NUMBERS

WU–538–08–12–00
1L161102AH45

6. AUTHOR(S)

C.C. Wey

7. PERFORMING ORGANIZATION NAME(S) AND ADDRESS(ES)

NASA Lewis Research Center
Cleveland, Ohio 44135–3191
and
U.S. Army Research Laboratory
Cleveland, Ohio 44135–3191

8. PERFORMING ORGANIZATION REPORT NUMBER

E–11360

9. SPONSORING/MONITORING AGENCY NAME(S) AND ADDRESS(ES)

National Aeronautics and Space Administration
Washington, DC 20546–0001
and
U.S. Army Research Laboratory
Adelphi, Maryland 20783–1145

10. SPONSORING/MONITORING AGENCY REPORT NUMBER

NASA TM—1998-208509
ARL–TR–1804

11. SUPPLEMENTARY NOTES

The work reported herein was sponsored by National Aeronautics and Space Administration (NASA) Atmospheric Effects of Aviation Project (AEAP), and managed through the sub-element Emission Characterization at NASA Lewis Research Center (LeRC) by Mr. Richard Niedzwiecki, NASA, and Dr. Chowen Chou Wey, Army Research Laboratory (ARL). The engine test was conducted at NASA LeRC, Cleveland, OH. It was accomplished by the team efforts of many engineers and scientists from government and private organizations including NASA LeRC, Dynacs Engineering Company, Inc. (Dynacs), Pratt & Whitney (P&W), Aerodyne Research Inc. (ARI), Air Force Research Laboratory (AFRL), and University of Missouri-Rolla (UMR). Responsible person, C.C. Wey, organization code 0300, (216) 433–8357.

12a. DISTRIBUTION/AVAILABILITY STATEMENT

Unclassified - Unlimited
Subject Category: 45 Distribution: Nonstandard

This publication is available from the NASA Center for AeroSpace Information, (301) 621–0390.

12b. DISTRIBUTION CODE

13. ABSTRACT ***(Maximum 200 words)***

The overall objective of the NASA Atmospheric Effects of Aviation Project (AEAP) is to develop scientific bases for assessing atmospheric impacts of the exhaust emissions by both current and future fleets of subsonic and supersonic aircraft. Among the six primary elements of the AEAP is Emissions Characterization. The objective of the Emission Characterization effort is to determine the exhaust emission constituents and concentrations at the engine exit plane. The specific objective of this engine test is to obtain a database of gaseous and particulate emissions as a function of fuel sulfur and engine operating conditions. The database of the particulate emission properties is to be used as a comparative baseline with subsequent flight measurement. The engine used in this test was a Pratt & Whitney F100-200E turbofan engine. Aviation fuel (Jet A) with a range of fuel sulfur was used. Low and high sulfur values are limited by commercially available fuels and by fuel specification limits of 0.3% by weight. Test matrix was set by parametrically varying the combustor inlet temperature (T_3) between idle and maximum power setting at simulated SLS and up to five other altitudes for each fuel. Four diagnostic systems, extractive and non-intrusive, were assembled for the gaseous and particulate emissions characterization measurements study. NASA extractive system includes smoke meter and analyzers for measurement of CO, CO_2, NO, NO_x, O_2, total unburnt hydrocarbons (THC), and SO_2. Particulate emissions were characterized by University of Missouri-Rolla Mobile Aerosol Sampling System. A chemical ionization mass spectrometer from the Air Force Research Laboratory at Hanscom AFB was used to measure SO_2 and HNO_3. Aerodyne Research, Inc. used infrared tunable diode laser absorption to measure SO_2, SO_3, NO, H_2O and CO_2.

14. SUBJECT TERMS	15. NUMBER OF PAGES
Aircraft Emissions; Particulate; Aerosol; Attitude Chamber Engine Test	176
	16. PRICE CODE: A09

17. SECURITY CLASSIFICATION OF REPORT	18. SECURITY CLASSIFICATION OF THIS PAGE	19. SECURITY CLASSIFICATION OF ABSTRACT	20. LIMITATION OF ABSTRACT
Unclassified	Unclassified	Unclassified	

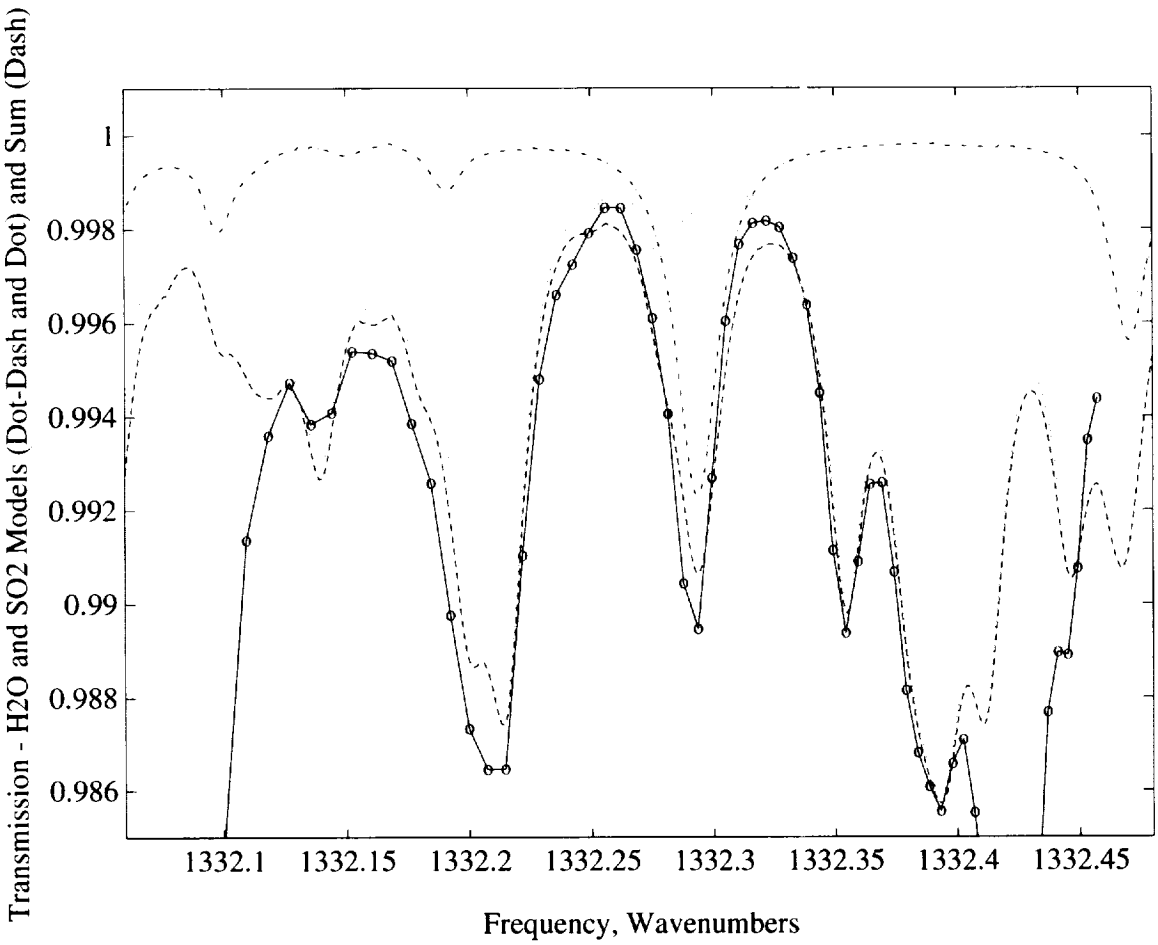

Figure F-5. SO_2 Region Observed Transmission Spectrum (Solid Line and Circles) and Uniform Path (Single Temperature and Pressure) Model Spectra for the Individual Species SO_2 (Dotted Line) and Water (Dot-Dash Line) as well as Sum of the Two Model Spectra (Dashed Line).